UILU-ENG-72-2020

CIVIL ENGINEERING STUDIES
STRUCTURAL RESEARCH SERIES NO. 390

THICK WALLED MULTIPLE OPENING REINFORCED CONCRETE CONDUITS

By
M. O. RYAN
M. H. SALEM
W. L. GAMBLE
B. MOHRAZ

An Interim Progress Report on the Study
"Investigation of Multiple Opening Concrete Conduits"

Sponsored by the
Department of the Army
Corps of Engineers
Engineering Division
Civil Works
Contract No. DACW-73-70-C-0037

Conducted by
THE STRUCTURAL RESEARCH LABORATORY
DEPARTMENT OF CIVIL ENGINEERING
ENGINEERING EXPERIMENT STATION
UNIVERSITY OF ILLINOIS AT URBANA-CHAMPAIGN

UNIVERSITY OF ILLINOIS
URBANA, ILLINOIS
DECEMBER 1972

UILU-ENG-72-2020

THICK WALLED MULTIPLE OPENING REINFORCED CONCRETE CONDUITS

by

M. O. Ryan
M. H. Salem
W. L. Gamble
B. Mohraz

An Interim Report on the Study

"Investigation of Multiple Opening Concrete Conduits"

Sponsored by the

Department of the Army
Corps of Engineers
Engineering Division
Civil Works
Under Contract No. DACW-73-70-C-0037

Conducted by

THE STRUCTURAL RESEARCH LABORATORY
DEPARTMENT OF CIVIL ENGINEERING
ENGINEERING EXPERIMENT STATION
UNIVERSITY OF ILLINOIS AT URBANA-CHAMPAIGN

UNIVERSITY OF ILLINOIS
URBANA, ILLINOIS

DECEMBER 1972

TABLE OF CONTENTS

LIST OF TABLES

LIST OF FIGURES

Page

Page

Page

1. INTRODUCTION

1.1 General Comments and Background

The "Investigation of Multiple Opening Concrete Conduits" was initiated in 1970 with the purpose of providing information needed for the rational design of conduits or "box culverts" suitable for use under earth dams and other embankments with fill heights ranging up to about 250 ft.

At this fill height the average earth pressure is about 30 k/ft^2, although consideration of the relative compressibilities of the conduit and the surrounding earth leads to the conclusion that the maximum pressure acting vertically on the structure may be as much as 50 percent greater than average, or up to 45 k/ft^2.

The currently used design guides, such as the Corps of Engineers Engineering Manual 1110-2-2902 (1)*, were prepared assuming fill depths of no more than 60 to 70 ft, and maximum earth pressures of 8 to 10 k/ft^2. Attempts to use this information has led to designs in which it appears that the member thicknesses are considerably greater than are necessary, at least when they are compared with the thicknesses used in some of the test specimens from this investigation. As an example, the cross-section of a conduit built as part of the dam at Fall Creek Reservoir, Oregon, and shown in Fig. 1.1, gives wall thicknesses of up to 39 in. with spans of 5.5 ft for the horizontal members. This was subjected to a maximum fill height of about 165 ft. By comparison, on a scaled basis, the members of specimens R2 and R3 described in this report were 2 ft

---

* Numbers in parentheses indicate entry in the List of References.

thick with 6.5 ft spans, and both resisted loads of at least 90 k/ft^2; and R1 resisted 150 k/ft^2 with scaled member thicknesses of 3 ft.

Such a discrepancy should not be expected, however, since the present state of knowledge about the strength and behavior of deep reinforced members is relatively incomplete. The shear strength provisions in Ref. 1, which control member depth, are based on a study by Diaz de Cossio and Siess (2,3) and are consequently based on member span-depth ratios of 5 or more, rather than 2 to 3.

While there are many unknown factors about the behavior of isolated deep members, there are even more uncertainties about the behavior of frames made of a group of deep members. A survey of the literature on the behavior of deep reinforced concrete members, information developed largely in response to various questions about the design of structures to resist the effects of nuclear weapons, shows that most of the tests reported have been on simply supported beams subjected to one or two concentrated loads. Albritton (4) presents a review of the literature published through 1965.

Only a very small number of investigators have conducted tests on specimens subjected to approximating distributed loads (5,6,7,9) and only one series of tests of two-span specimens has been found, as reported in Ref. 8. In all cases, the beams were supported on some kind of steel bearing system with steel rollers, and no cases of frames, where the beams are supported by being made monolithic with concrete "columns" have been found in the literature although one specimen reported in Ref. 7 was supported on stub columns extending a few inches

below the bottom of the beam. The support stress conditions may be much different near a steel bearing plate than the stress conditions near a reinforced concrete supporting column, and this problem apparently has not been either addressed or answered.

The test specimens described in this report are three-span frames representing models of thin slices of a three opening conduit similar to that shown in Fig. 1.1. Each span was loaded by three or four concentrated loads, which is not the same as a distributed load, although the approximation must be reasonably good since the loading plates cover about 40 percent of the surface of the specimen.

In the case of the buried conduit, there are significant forces in both the vertical and horizontal directions. For purposes of design, following the Corps of Engineers practice, the loading combinations considered include the case in which the vertical pressure is 1.5 times the overburden while the horizontal pressure is 0.5 times the overburden and the case in which the vertical and horizontal pressures are both equal to the weight of the overburden. Consequently every member in the conduit is subjected to large axial compression forces in addition to the moments and shears caused by the loads acting on the surface of the conduit.

Since the test specimens used in this investigation were thin slices of a long, linear structure, the question of the effects of forces perpendicular to the plane of the test specimen, or parallel with the longitudinal axis of the prototype structure, must be briefly considered. It appears that there are no major forces acting parallel to the axis of the structure because of the way in which the conduits built to date have been constructed. Typically, the conduit is built as a

series of separated 20 ft long boxes. The joint between adjacent boxes is not capable of transferring tension forces, although it is fitted with an extensive system of waterstops. The structural separation between elements effectively prevents development of the forces which might occur in a long monolithic structure because of differential settlement of the material above and below the conduit, and axial length changes due to temperature changes, shrinkage of the concrete, and slight horizontal movements in the fill above the structure.

The literature on deep beam behavior does not appear to include any information on tests in which known axial compression forces were imposed on test specimens. However, it seems reasonable to assume that in many cases there were substantial axial forces existing simply because there was no way to provide reactions having very low coefficients of friction. In other cases (5) the bearings were essentially pinned (free to rotate but not to slide or roll) at both ends of the specimens. As a result of these practical problems, most of the deep beam test data probably include some unknown influence of axial compressive forces even though this has not been a variable in any of the test programs.

The intent of the work described in this report is to fill some of the gaps in the existing information by providing new experimental data on the behavior of more nearly complete concrete structures, and to interpret this data in view of information gained from theoretical studies which are made taking into account as many variables as possible, including cracking of the concrete and the non-linear stress-strain characteristics of the materials. This is expected to lead to the development of a design procedure directly applicable to the conduit problem.

1.2 Object and Scope

This report is intended as a progress report at the middle of a four-year research program, and as such is concerned primarily with the presentation of the work accomplished during the first two year interval. It is expected that at least two additional reports will be issued. One of these will present, in complete detail, the results of the analytical phase of the investigation. It will include all the information developed on the use of the finite-element method of analysis, taking into account the progression of cracking with increasing load and the non-linear stress-strain response of the materials. A second report will cover the results of the tests of the reinforced concrete models in complete detail, and discuss the relationship between observed and predicted behavior. Design recommendations will be included in this report, unless it appears desirable to prepare a third, smaller report specifically directed twoard the design aspects of the thick-walled conduit problem.

Chapters 2 through 6 of this report describe the fabrication, instrumentation, and testing of the first three specimens. The procedures will be approximately the same for the remaining specimens. Chapter 7 describes the behavior of these three specimens as they were loaded to failure under externally applied compressive forces approximating uniformly distributed loads.

Chapter 8 describes the analytical work completed to date, and compares predicted and theoretical behavior for a few specific cases. Chapter 9 contains a summary and recommendations for the continuation of the work.

1.3 Administrative Organization and Acknowledgements

The administration of the contract for the Corps of Engineers has been under the supervision of Wendell E. Johnson and Joseph M. Caldwell, who have served successively as Chief, Engineering Division, Civil Works, Office of the Chief of Engineers. Direct contact between the Engineering Division and the University has been through Howard Goodhue and Keith O'Donnell, and appreciation is expressed for their continued interest and many helpful suggestions.

At the University of Illinois, Urbana-Champaign Campus, the work has been under the administrative direction of D. C. Drucker, Dean of the College of Engineering, Ross J. Martin, Director of the Engineering Experiment Station, and N. M. Newmark, Head of the Department of Civil Engineering. Professor W. L. Gamble has provided overall supervision of the project and of the experimental phase of the investigation, and Professor Bijan Mohraz has directed the analytical phase of the work.

Acknowledgements are due to A. E. Aktan, Graduate Student in Civil Engineering, and J. L. Hoebel, Research Assistant in Civil Engineering, for their parts in the experimental and analytical phases, respectively, of the program. Thanks are also due to L. G. Pleimann, Graduate Student in Civil Engineering.

2. DESCRIPTION OF TEST SPECIMENS

The test specimens were designed to represent a "slice" of a multiple-opening reinforced concrete conduit. The opening sizes are scaled from a prototype opening size of 6.5 by 9.0 ft. Considerations of the capacity of the loading equipment led to the adoption of specimen dimensions which are 3/8 scale of the prototype dimensions, and a "slice" thickness of 10 inches (see Figs. 2.1 and 2.2).

Preliminary approximate calculations of the forces due to 250 ft of overburden, and a literature review of research on deep beam behavior, provided a basis for the selection of the member sizes and the reinforcement ratios. It is current practice with this type of structure to provide 4 in. clear cover over all reinforcement, and the test specimens were reinforced with this in mind.

For test specimen R1, the external members were 13.5 in. thick, and the internal members were 9 in. thick, based on prototype dimensions of 3 ft and 2 ft, respectively (see Fig. 2.1). Four #7 deformed bars were used in each member, with two bars at each face, with details as shown in Fig. 2.3 and 2.4.

Test specimens R2 and R3 were identical, with internal and external member thickness of 9 in., based on a prototype dimension of 2 ft (see Fig. 2.2). Four #6 deformed bars were used, with 2 bars at each face, as shown in Figs. 2.5 and 2.6.

In accordance with the practice of providing longitudinal crack-control steel on the internal surfaces of conduits, an inner layer of #3 bars was provided, perpendicular to the main reinforcement, in all three specimens (see Figs. 2.3 and 2.5). This steel was provided in the

models mainly because of its possible influence on crack development and had been included in prototype for control of erosion of the concrete by hydraulic forces.

Table 2.1 lists reinforcement ratios and member thicknesses for each specimen.

Photographs of some of the reinforcement details are shown in Figs. 2.7 to 2.9.

3. MATERIALS AND CONSTRUCTION

3.1 Reinforcement

The #7 bars for specimen R1, the #6 bars for specimens R2 and R3, and the #3 bars used to represent the longitudinal steel were all ASTM A-615, Grade 60 material. Typical stress-strain curves are shown in Fig. 3.1, and average values of yield and ultimate stress, and ultimate elongation are given in Table 3.1. All values are substantially above specification minimum values.

3.2 Steel Assembly and Placement

All of the reinforcement was tied into a cage before being placed in the pre-assembled timber form. The #3 bars acted as spacers for positioning the main reinforcement in the members. The reinforcement at the external faces was attached to the ends of the reinforcing bars used for the internal faces, and in the internal vertical members. This helped in locating the main reinforcement with a cover of 1 1/2 in. clear.

At those locations where strain gages were attached, the bar deformations were ground and filed off. A sufficient area was prepared and the strain gage and leads were attached.

The cage was then lowered into the form and further minor adjustments were made to position the reinforcement as accurately as possible.

Photographs of the reinforcement in specimen R1 are shown in Figs. 2.7 to 2.9.

3.3 Concrete

a. Mix Proportions

For specimen R1, the mix proportions (by weight) used were 1:4:4 (cement:sand:aggregate) with a water/cement ratio of 0.85. For specimens R2 and R3, the mix proportions were 1:4:4 (cement:sand:aggregate) with a water/cement ratio of 0.9. Representative stress-strain curves for these concrete mixes are shown in Fig. 3.2.

Type III, high-early strength, cement was used for all specimens. Crushed limestone aggregate, with a maximum size of 1 in., and Wabash River sand were used in the mix. The concrete was mixed in a 1/2 cu yd horizontal pan type mixer.

Twelve full cylinders and eight half-cylinders were cast with specimen R1. Nine full cylinders and six half-cylinders were cast with each specimen R2 and R3. The full cylinders were used for compression tests and the half-cylinders were used for split-cylinder tests. All cylinder tests were conducted at about the time of the final test of the specimen.

Table 3.2 lists the slump, age of the specimen at the time of testing, average compressive strength, average tensile strength from split-cylinder tests and modulus of elasticity of concrete.

3.4 Formwork, Casting and Curing

The test specimens were cast in timber forms with plastic-coated plywood surfaces. The form was designed so that the member widths in the specimen could be easily adjusted. The member widths of a test specimen correspond to the wall thicknesses in a prototype conduit.

Holes for the rods used to support the specimen during the test were provided by casting in pieces of hollow aluminum tubing through the thickness of the specimen.

The reinforcement cage was placed and positioned in the form using temporary timber pieces wedged between the reinforcement and the sides of the form. The reinforcement cage rested on the ends of the #3 bars. The #3 bars were used to accurately locate the main reinforcement to which they were tied. The temporary timber pieces were withdrawn at the time of casting. Inserts for four lifting hooks were embedded in the concrete before final setting.

Specimen R1 was cast in four batches, with three full cylinders and two-half cylinders being cast from each batch. Specimens R2 and R3 were cast in three batches.

Casting was almost continuous with only a short delay of about 10 minutes between the placing of each batch. The concrete was vibrated with an electric internal vibrator. The concrete surface was first smoothed with a wooden screed and then finished with a steel trowel.

About twenty-four hours after casting, the side forms were removed, and the specimen and the control cylinders were covered with wet burlap and plastic sheeting. The wet burlap was removed after seven days. The control cylinders and the specimens were then cured under laboratory conditions until the time of the tests.

4. LOADING SYSTEM

4.1 Test Set-up

The test specimens, which were three-eighth scale models of a slice of a prtotype conduit, were hung in a horizontal position on four steel rods suspended from a supporting frame as shown in Figs. 4.1 to 4.3. The vertical and horizontal load directions correspond to the north-south, and east-west directions, respectively.

The soil pressures are simulated by a series of independent loading units. A loading unit consisted of two tie-rods, two steel beam "yokes", and two hydraulic rams. Each loading unit formed a closed loading system (see Fig. 4.4). Consequently, no external reaction system was required, other than the frame supporting the weight of the specimen and the loading units, which rested on the specimen.

Supplementary supports, from the laboratory floor, had to be provided under the hydraulic rams of part of the loading system for specimen R1 to prevent excessive bending of the tie-rods on which the hydraulic rams and beams rested. All tie-rods for the loading system for R2 and R3 were 1 in. diameter and the supplementary supports were required only under the 60-ton hydraulic rams. These supports were necessary only when the system was unloaded.

A photograph of the loading system assembled on specimen R1 is shown in Fig. 4.5.

4.2 The Loading System

The uniform soil pressures were approximated by a series of loads applied to the specimen by independent loading units. The system was

designed so that for given pressure conditions, the axial load and shear force at the critical sections could be accurately simulated. The bending moments produced approximated those for the ideal uniform load. The loading units were divided into two main groups: (i) those providing axial load only and (ii) those acting as span loads. A span was considered to be the clear distance between the faces of opposite members. The load on a span was provided by three equally spaced loading units for the short spans, and by four equally spaced loading units on the long spans. One loading unit applied axial load directly to each member with the loading units spaced as shown in Figs. 4.6 and 4.7.

The load applied by each loading unit was that required by its "tributory width." As an example, the width for a span unit applying the vertical load to specimen R1, Fig. 4.6, is 9.75 in., while the width for an adjacent unit applying axial load directly to an interior wall is 9.0 in. Consequently, the load on the span unit had to be maintained at about eight percent higher than in the axial unit.

A loading unit consisted of two round high-strength steel tie-rods threaded at each end, two steel beams "yokes," and two hydraulic jacks, as shown in Fig. 4.4. The rods in the north-south direction were 10 ft long, 1 in. in diameter, and were in horizontal planes 6 in. from the centroidal plane of the specimen. The tie-rods in the east-west direction were made up of two lengths, 3 ft and 12 ft, spliced together, and were in planes 9 in. from the centroidal plane of the specimen. For specimen R1, 3/4 in. diameter tie-rods were used in the east-west direction. The 3/4 in. diameter tie-rods were replaced by 1 in. diameter rods for specimens

R2 and R3. All tie-rods had yield stress values in excess of 100 k/in.^{2} ASTM A-194 Grade 2H nuts were used on all tie-rods.

The steel "yokes" in the north-south direction were short beams cut from standard 8 by 4 in. rectangular tubing. The "yokes" had holes near each end of both 4 in. faces, through which the tie-rods passed, and internal stiffneers adjacent to the holes.

The steel "yokes" in the east-west direction were made up of two short beam lengths cut from standard 7 by 2 in. channel section, placed back to back. They were held 2.5 in. apart by three special pins, fitted through holes in the channels and secured with nuts at each end. The tie-rods passed through holes drilled through the two outermost pins. The pins at one end of each loading unit acted as a bearing for the tensioned tie rods.

Center-hole rams, mounted on one end of each tie-rod, applied the tension force to the tie-rod. Each rod was equipped with an electrical load-cell. Thirteen loading units were required in the north-south direction, and six loading units were required in the east-west direction.

4.3 The Hydraulic System

The basic parts of the hydraulic system were: thirty-four 30-ton and four 60-ton, center-hole, double-acting hydraulic rams; three electric pumps; one air-powered pump; and two hand pumps.

The hydraulic system for each specimen was divided into five groups. Each group contained either a set of span-loading units only, or a set of axially-loading units only. For the test on specimen R1, four groups

required one pump each, and the fifth group was further divided between two pumps. The test on specimen R2 required one pump for each of the five groups. Only the three electrical pumps and the air-pressure powered pump were utilized for the test on specimen R3, two of the groups having been connected to the same pump.

A feature of the hydraulic system was that each ram had an associated load-cell, and could be connected to or disconnected from the hydraulic system by an independent valve. Consequently, load could be applied or released in any ram independently of the other rams in the system. Load could also be applied or released simultaneously in all the rams connected to a particular pump.

5. INSTRUMENTATION

5.1 Strain Gage Measurements

Foil type electrical strain gages, type EA-06-500BH-120 (manufactured by Micro-Measurements), were used to measure the reinforcement strains at the locations shown in Figs. 5.1, 5.2, and 5.3 for the three test specimens.

Special care had to be taken in mounting the gages on the reinforcement. The bar deformations were first ground off and an area made round and smooth. The surface was thoroughly cleaned with acetone, before cementing the gage and a lead-tab to the rebar with Eastman 910 adhesive. The lead-tab and the gage were originally mounted on backing tape. When the adhesive had matured, the backing tape was removed with the aid of acetone. The electrical leads were then soldered to the lead-tab and the gage. The leads were secured to the bar with tape, and a layer of waterproofing also provides a protection against damage to the gage during the casting of the specimen. Waterproofing was accomplished by applying a piece of an 1/8-in. sheet of Scotch No. 2200 E-Z Seal electrical insulation over the gage area, and pressing firmly to the bar. The material is a semi-cured neoprene compound.

The strain measurements were monitored on a 100-channel Pivan strain gage indicator panel. One strain gage reading can be visually displayed on the Pivan panel at any particular time. The strain gage readings were automatically displayed consecutively and recorded on an attached teleprinter at the rate of about one reading per second. The teleprinter provided an immediate print-out of the strain gage readings and also recorded the data on punched paper tape. The punched-tape records were later converted into IBM punched cards which were used as input data for a

computer program. The computer program compiled and reduced the data and provided a print-out of the strain measurements at each location at each specific load level.

5.2 Load Measurements

A total of 38 load cells were used to measure the applied loads. The load cells were axially loaded thick-walled cylinders machined from 6061-T651 aluminum rods. Each load cell was 6 in. long with an outside diameter of 2 in. and an inside diameter of 1 1/8 in. The four strain gages mounted on the external surface of each load cell were wired to form a four arm bridge measuring circuit.

The load cell capacity was computed to be 57 kips at a stress of 30 $k/in.^2$ The load cells were calibrated to a maximum load of 50 kips. Twenty-eight load cells, which had been used in an earlier study, had sensitivites between 80 and 87 lb per dial division. The ten new load cells had sensitivities between 78 and 80 lbs per dial division. Before the tests on specimens R2 and R3, load cells were chosen at random and re-calibrated. The sensitivities showed variations of less than 0.5 percent.

As with the strain gages, the load cells were monitored on the Pivan strain system. Load cell reading could be automatically displayed, and were recorded by the teleprinter. In this way immediate inspection of the load state could be carried out at any particular time, and permanent records made as desired. The computer program converted the load cell readings to applied loads, gave average load values for the rams in each group and provided a comparison between the desired and the actual loadings.

5.3 Dial-Gage Measurements

In order to monitor the change in length of the members, dial gages were mounted at one end of each typical member. Steel 1/4 in. diameter rods were mounted along the member, one end being fixed to a piece of steel angle glued to the face, the other end on a sliding support, as shown in Fig. 5.4. The dial gage was mounted in contact with this end of the rod. In this way, the change in length of the member, between the points of fixed support for the rod and the gage was measured.

The relative displacement at mid-span of each member was also recorded by dial gages. Light metal frames were erected off the center of both of the interior members and the gages were mounted on the metal frame and located as shown in Fig. 5.5.

The deflections reported are changes in height or width of frame openings due to all deformations, including shortening of the "columns" and, in the case of the vertical deformations, were obtained by adding the deflections from two different gages, such as 2 plus 3 or 7 plus 8.

6. TESTING PROCEDURE AND TEST DESCRIPTION

Before testing each specimen to failure, a short preliminary test was performed to check the instrumentation and leaks in the hydraulic loading system. The load level achieved during this test was equivalent to 30 k/ft^2, for specimen R1 and 25 k/ft^2 for R2 and R3. The specimen was then unloaded. This procedure was generally successful, and the readings obtained provide useful data for lower loading range. The load of 30 k/ft^2 was reached in six equal increments of 5 k/ft^2, with readings taken after each load increment was applied. A careful examination of the instrumentation and the hydraulic loading system (a careful checking of the hydraulic system was necessary to insure the performance of the system, since pressures as high as 8,000 $lb/in.^2$ were reached in some of the failure tests) were carried out during this preliminary loading.

For the full-scale test, a load equivalent to 30 k/ft^2 in the vertical direction and the load corresponding to horizontal direction were achieved in two equal increments of 15 k/ft^2. Thereafter load increments of 7.5 k/ft^2 were applied. A set of readings was taken, and an examination of the specimen was carried out after application of each load increment.

The loading units were divided into two main groups: (i) those providing axial load only and (ii) those acting as span loads. A further subdivision separated those acting vertically from those acting horizontally, Fig. 4.6. The loading condition for specimens R1 and R2, where the load in vertical direction was three times that in the horizontal direction, indicated that the horizontal members were the most critically stressed

in shear. This observation dictated how each load increment should be applied. Each group of loading units, controlled by a different pump, were loaded separately. For each increment the loads were applied in the following sequence:

1. Axial loads in both directions.
2. Span load in the horizontal direction.
3. Span load in the vertical direction.

Modifications to this loading procedure had to be devised for specimens R1 and R3. During the test on specimen R1 a load level corresponding to 82.5 k/ft^2 was reached by the above procedure when the test had to be aborted due to a failure of one of the loading units. When the test was re-initiated, the load level of 82.5 k/ft^2 was reached in three increments corresponding to 30, 60, and 82.5 k/ft^2, respectively. Load increments of 7.5 k/ft^2 were then applied until a load level of 105 k/ft^2 was reached. This was considered the safe limit of the loading units acting in the horizontal direction. The load level in the vertical direction was increased to 112.5 k/ft^2. Then load was reduced incrementally to zero in the horizontal direction while the vertical load level of 112.5 k/ft^2 was maintained. The specimen was then unloaded in the vertical direction. A further test was carried out with the horizontal load held constant at a load of 10 k/ft^2. This corresponds to 30 k/ft^2 in the vertical direction for the 3:1 load ratio condition. The vertical load was then increased to the equivalent of 60, 90, 112.5, 120, 127.5, 135, 142.5, 150 k/ft^2, in that order. The horizontal load was then removed and failure immediately occurred in one end span of a horizontal

member. Further efforts to increase the load level on the other spans led to immediate failure.

Because of time limitations, specimen R2 had to be tested in two stages. In the first stage, vertical loads of 15, 30, 37.5, 45, 52.5, 60, 67.5, 75, 82.5, 90 k/ft^2, with corresponding horizontal loads of 1/3 of the vertical load intensity, were applied. The specimen was then unloaded gradually. In the second stage, vertical loads of 15, 60, 75, 90, 97.5, and 105 k/ft^2 with corresponding horizontal loads of 1/3 the vertical were applied.

Failure occurred in an end span of a horizontal member. The load was then reduced gradually to zero.

Specimen R3 was tested under a load condition which corresponded to a 1:1 ratio of vertical to horizontal load intensity. For this loading condition, the vertical side members had the smallest axial and the largest shear stresses. The procedure of applying each load increment was different from those for specimens R1 and R2. First the axial loads in both directions were applied, and the span loads in the vertical direction were applied next. The span loads in the horizontal direction were then applied, causing the critical shear force in the vertical side members. Loads corresponding to 15, 30, 37.5, 45, 52.5, 60, and 67.5 k/ft^2 were applied. Failure occurred in a vertical side span while bringing the horizontal span load to the 67.5 k/ft^2 load level. The loads in the horizontal direction were then reduced to zero. All the vertical loads on the undamaged portion were increased to 67.5 k/ft^2. The span loads in the vertical direction where then increased to 75,

82.5, and 90 k/ft^2, while all other loads were maintained constant. While attempting to reach a load level of 97.5 k/ft^2, an end span of a horizontal member failed. The loads were then reduced to zero.

7. BEHAVIOR OF THE TEST SPECIMENS

7.1 Specimen R1

Specimen R1 was subjected to a number of tests, and eventually failed under a vertical applied load of 150 k/ft^2 and zero horizontal load. The tests are described in detail in the following sections, and photographs of the specimen, after testing, are shown in Figs. 7.1 to 7.4.

In the discussion of the test results, a positive moment is defined as that producing tension on the inside of the conduit openings, and a negative moment as that causing tension on the outer surfaces.

7.1.1 Preliminary Test

A preliminary test was run to a load level of 30 k/ft^2, which is 2/3 of the design owrking load level of 45 k/ft^2 vertically and 15 k/ft^2 horizontally. No visible cracking occurred during this test, and the strain gage readings showed a generally linear response to load. All but three strain gages indicated compressive strains. The tensile strains were less than 30×10^{-6} at maximum load, and indicated some flexural response in the specimen. The load was then removed. During this preliminary test, the loading system was successfully operated, and a satisfactory loading procedure was worked out.

7.1.2 Test Number One

In the first test, a load level corresponding to 82.5 k/ft^2 in the vertical direction was achieved. The test was aborted at this stage because of failure of a loading unit during the application of the next increment. The first two load increments were each the equivalent of

15 k/ft^2, and all the succeeding increments were of 7.5 k/ft^2 (see Table 7.1). Although some strain gages exhibited tensile strains greater than 100 x 10^{-6} at lower load levels, cracking was not observed until the load reached 82.5 k/ft^2. These were flexural cracks occurring near mid-span of the end bays of the horizontal members. Also, a vertical crack, similar to a flexural crack, which existed on the interior face of an end span of a horizontal member showed slight propagation transversally across the member. This crack was observed prior to testing, and may have occurred due to shrinkage, or due to surface stresses caused at the time of the removal of the formwork. Some difficulty in removing the internal formwork was encountered with this particular specimen. The concrete was 5 to 6 hours old at this time, and slight damage was caused at three corners, with small pieces of concrete being dislodged. All loose concrete was removed, and a 3:1 sand-cement mix was used to repair the damaged portions. Slight cracking was observed where the forms had to be forceably removed due to tightness of fit and surface friction. These cracks apparently did not penetrate deeply and generally ran along the surface, parallel to the major reinforcement. The formwork was modified to eliminate the problem.

The load was being increased above 82.5 k/ft^2 on the first group of load units when one tie-rod was inadvertently over-loaded. It fractured suddenly, exhibiting a brittle type failure. The "cupping" which occurred at the bearing point of the rod on the "yoke" beam, indicated a high overload prior to the failure of the tie-rod. At the load point of the loading unit slight local damage was caused to the

specimen. After the failure of the loading unit, all existing loads were removed. During this unloading procedure, the existing cracks propagated slightly and a small flexural crack appeared on a vertical side member. This occurred because of the unbalanced load removal pattern. However this cracking had little influence on the behavior of the specimen as data from the subsequent tests revealed.

The specimen responded linearly to load increase in general. At zero load, residual tensile strains up to 200 x 10^{-6} were recorded at some crack locations (see Figs. 7.5 to 7.13). Dial gages monitoring deflections and axial shortening showed a linear load-deflection behavior (see Figs. 7.14 to 7.23). The cracking pattern indicated a definite flexural behavior.

The loading unit was repaired and precautions were taken to reduce the probability of overloading accidentally. The precautions taken were the attachment of an independent monitor, in addition to the recording unit, to each loading group as it was being loaded. A protective barrier of wood and plywood sheeting was erected around the specimen directly in front of the loading units.

7.1.3 Test Number Two

Table 7.2 indicates the loading pattern adopted upon re-initiation of the test. The load level attained in the previous test was reached in three load increments. Three increments corresponding to 7.5 k/ft^2 were then applied. The load was at this stage at the equivalent of 105 k/ft^2 vertically and 35 k/ft^2 horizontally. The flexural cracking

initiated in the previous test propagated further, with some new cracks appearing in regions of positive and negative moment. This cracking was in general slight and did not indicate that any member was nearing failure. The vertical load was increased to the equivalent of 112.5 k/ft^2 while the horizontal load was maintained at its previous level of 35 k/ft^2. No significant crack propagation occurred. The horizontal load was reduced to the equivalent of 30 k/ft^2 while the vertical load was maintained at 112.5 k/ft^2 load level. Small shear cracks were observed propagating from the support ends in the horizontal spans. The horizontal load was further reduced in 3 increments to load levels equivalent to 22.5, 12.5, and zero k/ft^2, respectively, while maintaining the vertical load level. The propagation of existing shear cracks continued with new shear cracks appearing. The flexural cracks in the positive moment regions began to develop diagonally towards the center of the span, while the flexural cracks in the negative moment regions developed diagonally towards the supports. The span loads in the vertical direction were then increased to the equivalent of 120 k/ft^2. Further crack propagation occurred. Some cracks penetrated well into the upper half of the members, reducing the compressive zone.

This phenomenon is borne out by the gradual reduction of compressive strain and change to tensile strains in the gages which are nominally in the "compressive zones" of the horizontal members. At the end of the test, all these gages showed tensile strains (See Figs. 7.5 to 7.13). The gages on the "compressive" faces of the horizontal members at the

supports (Figs. 7.6, 7.8, 7.9) indicated tensile strains up to 1,500 x 10^{-6} when the vertical load was 112.5 k/ft^2 with zero horizontal load. The gages on the "compressive" face at mid-span of the horizontal members had shown gradual reductions of compressive strain from 400 x 10^{-6} to 500 x 10^{-6} down to 350 x 10^{-6} to 50 x 10^{-6}. The gages in nominally "tension" zones indicated maximum tensile strains from 1,000 x 10^{-6} to 2,000 x 10^{-6}. At zero load all gages on the horizontal members showed residual tensile strains.

The tension which developed was concurrent with the development of shear cracks crossing the reinforcement at or near the support. It is also possible that at this stage bond had broken down and tension in nominally "tension" zones of positive moment was being transmitted along the reinforcement to the support regions. The tension at mid-span on the nominally "compressive" faces could be explained by the encroachment of cracking towards the compressive face. Cracking had reached within one inch of the compressive face in some spans. The reinforcement was located with 1 1/2 in. clear cover from the compressive face. From the rather slow crack development and high shear resistance of the specimen, and the cracking pattern, an "arch action" behavior was apparent. The maximum mid-span deflection relative to the supports was about 0.05 in. for the end span, and about 0.025 in. for the central span, (see Figs. 7.14 to 7.23). The nominal shear stresses were about 1000 psi at the support. Due to time limitations, the test had to be stopped and all loads were gradually reduced to zero.

Except for one strain gage, the strain measurements showed a repeat and continuation of the behavior of previous tests. Gage 22, at the center of the interior span of a horizontal member, Fig. 7.10, was an exception to this rule. At the end of the previous test a sizeable residual tensile strain of 250×10^{-6} was recorded there. Upon reloading, the strain readings reduced at first and then showed an increase toward tensile strains. A residual tensile strain might explain this phenomenon. In general the strains indicating tension showed a continuation of the "softening" pattern with increasing load portrayed in the previous test. (See Figs. 7.5 to 7.13).

Up to the point of digression from the 3:1 loading ratio of horizontal to vertical, the dial-gages monitoring deflections and axial shortening reflected a continuation of the generally linear response observed during previous tests. Residual deformations were recorded at most locations (Figs. 7.14 to 7.23).

7.1.4 Test Number Three

Table 7.3 describes the loading pattern during the next test. The load in the horizontal direction was brought to the equivalent of 10 k/ft^2. While maintaining this load level, the vertical load was increased to 60, 90, and 112.5 k/ft^2. Because of the capacity limitation of the axial loading units on the vertical side members, it was decided not to increase the load level there above the equivalent of 112.5 k/ft^2. The remainder of the loading units in the vertical direction were then brought to load levels of 120, 127.5, 135, 142.5, and 150 k/ft^2. The horizontal load

had been maintained at the equivalent of 10 k/ft^2. By this time extensive cracking had occurred in all horizontal members. The shear and flexural cracks had developed deep into the compression zones of the members, in some cases to within 1 to 1 1/2 inches of the surface. Shear cracks had also developed well towards the supports, some having penetrated through the haunch. The angle of the shear cracks near the supports was about 45°, corresponding to the slope of the haunch. Cracking in the negative moment region had penetrated deeply into the support. From the pattern of cracking the arching action of the members in resisting the span loads was very apparent. The development of this type of behavior could be seen from the crack pattern which existed at the end of the previous test. Failure seemed imminent as some cracks seemed to have developed right across the member.

As the span load in the horizontal direction was being removed, a sudden shear failure occurred in an end span of a horizontal member. The horizontal load was brought to zero. Efforst were made to regain the load level of 150 k/ft^2 on other spans of the horizontal members, but failure occurred on a central span, and then in the other end span when the test was brought to an end. All loads were reduced to zero.

The failures were sudden and complete separation of the concrete at the supports occurred. The "arch" had been broken, consequently the members had lost almost all their resistance. The failure planes cut across the spans from the springing of the haunch, and were at an angle of approximately 45 degrees. The effective depth of the member in resisting

shear was increased at internal supports, as the failure plane cut through the haunch. At the external support, the failure plane did not cut through the haunch, but initiated along a line from the point at which the haunch ends. Thus at this point the effective span was reduced. Consequently it can be concluded that the total ultimate span load was increased by the haunch (see Figs. 7.1 to 7.4).

The strains measured indicated that during loading there was a strong tendency to retrace the unloading path of the previous test. Where compressive strains were recorded, the slopes of unloading and loading correspond fairly closely. Where tension was induced, a stiffer response is observed in general. This may be due to the existence of horizontal load. A definite "softening" of the strain versus load curve occurs at the higher load regions prior to failure. (See Figs. 7.5 to 7.13).

Large compressive strains were induced in the vertical interval members (see Figs. 7.12 and 7.13). Compressive strains of the order of 800×10^{-6} to $1{,}400 \times 10^{-6}$ were reached in the final test just prior to the initial failure. These members did not appear to be under distress. However, a slight flaking tendency was noticeable at the springing of the haunch, where a large stress concentration occurred.

The dial gages also reflect a strong tendency to retrace the unloading path of the previous test and then exhibit a continuation of the pattern established during the earlier loading test-stage (see Figs. 7.14 to 7.23). "Softening" of the deformation versus load plot is noticeable in the higher load regions.

7.2 Specimen R2

Following a preliminary test, full-scale testing was commenced on R2. Full scale testing was performed in two test stages, with a 3:1 ratio of vertical to horizontal load being adhered to throughout. Detailed discussion is given to each test in the following sections. A load of 105 k/ft^2 was just reached during the second test-stage when a horizontal member failed, and photographs are shown in Figs. 7.24 and 7.25. The failure, which was a sudden fracture, is similar to that which occurred in R1.

7.2.1 Preliminary Test

A preliminary test was run on specimen R2 for the purposes of checking out the system. As with specimen R1, specimen R2 was tested for a 3:1 ratio of vertical to horizontal load. However, in the preliminary test the load ratio was kept at 3:2. Comparison of data indicates a significant difference in response, especially of the end spans of the horizontal members. The maximum load reached during this test was 25 k/ft^2, vertically, and 16.7 k/ft^2 horizontally.

Some technical difficulties of a minor nature were encountered during this test. The load was reduced to zero by first reducing the span loads in the vertical direction followed by the span loads in the horizontal direction, and then all the axially loading units. A small flexural crack offurred at midspan in one of the vertical side members following the removal of the span loads on the horizontal members. No further cracking occurred. Tensile strains occurred at this location

during the test, reaching a maximum of 120 x 10^{-6} at maximum load. In all subsequent tests compressive strains were monitored in this location. In general the data indicated a linear response to load, although a scatter in the results occurred at some locations. However, at these locations the indicated strains were very small -- less than 20 x 10^{-6}. The dial-gages also indicated a general linear load versus deflection response, the slopes being steeper for the horizontal members. Compared to the deflections in later tests, the deflection direction was reversed in the vertical side members. This is due to the larger amount of horizontal load in proportion to the vertical load.

7.2.2 Test Number One

In the first test, the specimen was loaded in a 3:1 ratio of vertical to horizontal load. During this test a load of 90 k/ft^2 in the vertical direction was reached. The first two load increments were of 15 k/ft^2 each and thereafter load increments were applied as indicated in Table 7.4. Positive moment cracking was observed in all end spans of the horizontal members, and negative moment cracking was observed at the interior support points, at a load level of 30 k/ft^2. The load deflection plots (Figs. 7.35 to 7.44) indicate that cracking may have initiated at a load level of 15 k/ft^2. When initially observed, the positive moment cracks extended 1 to 2 in. into the member, and the negative moment cracks extended about 4 in. into the member. The plots of strain versus load at these locations also show a change in slope at 15 k/ft^2 (Figs. 7.26 to 7.34). With increasing load the flexural cracking

extended slowly into the members. Positive moment cracking was observed in the interior spans of the horizontal members at a load of 37.5 k/ft^2. This cracking continued to extend slowly as the load increased. At a load level of 82.5 k/ft^2, inclined cracks were observed near the interior supports of the end spans of the horizontal members. These cracks were located at about mid-depth of the beams. At a load level of 90 k/ft^2, these cracks showed development towards the supports and towards mid-span. Inclined cracking also appeared near the supports of the interior spans of the horizontal members. Because of time limitations, the test had to be concluded, and the loads removed.

The dial-gage readings indicate a gradual "softening" in response to load once cracking had occurred (see Figs. 7.35 to 7.44). However this was in general a slight effect. After unloading, residual deformations were recorded at most locations. Strain gages showed a change in slope at cracking where tensile strains were recorded and a gradual "softening" of the load-strain plots is noticeable. Where compressive strains occurred there was a linear response to load increase. Tensile strains occurred at the positive moment locations and also at the negative moment locations of the horizontal spans. Cracking occurred at about 100×10^{-6} tensile strain. The onset of inclined shear cracks did not seem to alter the load versus strain response.

Tensile strains developed in the steel in the nominally "compressive" zone at the end supports of the horizontal members following initial cracking. Also, at the internal supports, the "compression" steel began

to show a reduction in compression with increasing load as soon as shear cracking occurred. At corresponding vertical load levels, lower compressive strains than those of the preliminary test were recorded in this test. During the preliminary test, the strains in these areas were always compressive and increased linearly with load. Where tension occurred residual tensile strains were recorded at zero load.

7.2.3 Test Number Two

A load level 105 k/ft^2 was almost reached during the second test when a sudden failure occurred in an end span of a horizontal member. The load increments applied are listed in Table 7.5.

Existing cracks showed progression at 75 k/ft^2 loading, and some new flexural cracks appeared. This pattern of development continued up to failure. The shear cracks which had developed were at angles of approximately 45 degrees. The failure occurred in an end span of a horizontal member, as can be seen in the photos in Figs. 7.24 and 7.25. Diagonal shear cracks, which had already reached the bottom of the member at each support, had developed across the member into the compression zone. The failure was sudden, and cracks ran along planes at approximately 45° from each support. At the outer support, the failure plane began at the junction of the fillet and the horizontal surface of the member. At the interior support the failure plane cut through the fillet. Specimen R1 exhibited a similar type of failure, indicating the influence of the fillet in increasing the strength of the member. Its effect can be considered either to increase the effective depth of the beam resisting shear, or to reduce the effective span, at failure.

In those parts of the specimen where shear cracking did not strongly affect the distribution of stresses, good correlation of data bewteen the first full scale test and the final test occurred. Sizeable shear cracks developed during the first full scale test and they apparently influenced the behavior of the specimen upon reloading.

Tensile strains developed at much lower load levels in the bottom steel at the outer supports of the horizontal members during the final test (see Figs. 7.26 to 7.34). Slightly less tension developed at mid-span in the final test, possibly indicating arching action with the vertical members acting as abutments. At the internal supports of the end span the pattern of exhibiting linearly increasing compressive strain with increasing load initially, and then a gradual fall off of compressive strain, was repeated in the final test. However the fall-off point occurred at a higher load level in the final test. It occurred at a load of 67.5 k/ft^2 in the first test and at 75 to 90 k/ft^2 in the final test. The cracking in the interior spans seemed to be mainly of a flexural character. The cracks near the supports in the negative moment region were only slightly inclined. Shear cracks had begun to develop near the supports at about mid-depth of the beam.

The strain gages indicate a definite flexural response. Those strain gages indicating compressive strains exhibited a generally linear response to load, as in the previous test, with the slopes of load versus strain being almost identical for both tests. Residual tensile strains had been recorded following the previous test, and in these locations the load versus strain curve is flatter than either the previous loading

or unloading plot. In the upper load regions a gradual "softening" of the curve is noticeable. In the end spans of the horizontal members tension developed in the nominally "compressive" zone at the end support. Only low compressive strains developed in this region at the interior support. Comparison of these strains with those at midspan indicate the possible break-down of bond between the reinforcement and the concrete, thus developing the "tie-action" characteristic of an arch-action behavior.

The dial gages consistently exhibit a continuation of the pattern of the previous test (Figs. 7.35 to 7.44). The slope of the load versus deformation curves corresponds closely to that of the unloading plot of the previous test in similar loading regions. In the higher load region the specimen stiffness decreased with increasing load.

7.3 Specimen R3

A loading ratio of 1:1 of vertical to horizontal load was maintained during tests on R3, up to initial failure. For a 1:1 loading ratio, the most critically loaded members, both in shear and flexure, are the vertical side members.

Failure occurred at a load of 67.5 k/ft^2. After this failure, the horizontal load was completely removed. The vertical load on two spans was then gradually increased until a sudden shear failure occurred at a load of 97.5 k/ft^2 in a horizontal member. Detailed descriptions of the tests are given in the following sections, and photographs of the specimen are shown in Figs. 7.45 to 7.47.

7.3.1 Full Scale Test

Table 7.5 tabulates the loading pattern adopted during the full-scale test of R3. The first load increment applied was 15 k/ft^2. Thereafter, the load level was increased in increments of 7.5 k/ft^2. At the load approached 67.5 k/ft^2, a shear failure occurred in one of the side spans. Efforst made to increase the load were abandoned as progressive failure of the side member was occurring, and the horizontal span loads were reduced to zero. The axial loads in the failed member and in the horizontal members were also reduced to zero.

One additional test was then conducted on the intact portions of the test specimen. The loads on two horizontal spans were then increased in increments of 7.5 k/ft^2. The load units on the span adjoining the failed member were left sealed, and the loads remaining or developed were measured. The purpose of this test was to determine the strength of the horizontal members when there was no axial load in these members. Shear failure occurred in the end span of one of these members just before a load level of 97.5 k/ft^2 was attained.

During the initial stage of this test, i.e., up to the failure of the vertical side member, loads were maintained at a loading ratio of 1:1 vertical to horizontal. Existing flexural cracking in the positive moment regions of the vertical members developed gradually as the load increased. Cracking was observed in the negative moment regions at the ends of the horizontal members at 30 k/ft^2, and this cracking also developed gradually with load. At a load of 60.0 k/ft^2 diagonal cracks were observed at the ends of both vertical side members. In general,

these cracks appeared near mid-depth of the members, inclined at an angle of about 45°, and were positioned either on or slightly behind (closer to the support) a line representing the continuation of the edge of the fillet. Failure occurred at a load level of 67.5 k/ft^2. The diagonal cracks had developed into the compressive region at the fillet ends and up and across the span into the compressive region near midspan. The cracks show a curving pattern, becoming less inclined as they developed into the span, and becoming steeper towards the supports.

The failure occurred at the end of the member where the first diagonal crack appeared. The failure plane initiated at the end of the fillet and cut across the span at approximately 45°. Curved cracks had also developed at the other end locations of the vertical side members. However, the shear cracks at these locations were developing through the fillet. The failure occurred at the location where an inclined crack first appeared at the relatively low load of 25 k/ft^2. It is to be noted that the shear cracks passed through the lifting hook positions. The holes formed by the cast-in sockets were, due to their positions, points of weakness. It is doubtful however, that these holes influenced the ultimate shear strength of the member to any appreciable extent.

During this stage of the test, prior to the failure, a linear response to load is indicated by the strain-gages and the dial gages (Figs. 7.48 to 7.67). Tensile strains were monitored at both the positive and negative moment regions of the vertical side members and at end supports of the horizontal members. Compressive strains occurred at all other locations. Initially a linear response is evident

from the load versus strain plots, but a "softening" effect occurred at many locations with increasing load, especially as the failure load was appraoched (Figs. 7.48 to 7.57). The dial gages (Figs. 7.58 to 7.67) behaved in a similar manner, with the load-deflection curve "softening" as the failure load was approcahed, and also indicating a stiffer structure than in the preliminary test. The strains and deflections measured on the interior vertical members indicate that sizeable moments were being applied at the ends, whereas with a loading ratio of 3:1 these moments were very small.

Following the failure of the vertical side member, the load in the horizontal direction was removed as described earlier. Flexural and shear cracks appeared immediately in all spans of the horizontal members. The span loads in the vertical direction were increased incrementally. As the load equivalent to 97.5 k/ft^2 was being applied, a shear failure occurred in one of the end spans of a horizontal member. There was no axial load being applied to the members at the time of failure. The flexural and shear cracks developed gradually as the load was being increased. Strain gages in the horizontal members indicated clearly the effect of the removal of the axial load in the member. Large reductions in the compressive strains which had existed there were recorded, and some strains became tensile. "Arching" action was evident since the strain gage (#12) in the nominally compressive region at the end of the interior span indicated high tensile strains. As the load was being increased the strains in general responded linearly, especially the gages indicating tension. The compressive strains in the

compression zone at mid-span only showed a slight increase in the end span where failure occurred. The corresponding strain in the center span in fact reduced slightly with increasing load. This occurred since the shear cracks had progressed to within 1.5 in. from the top of the member, i.e., the tensile zone at midspan had reached the steel location.

The failure exhibited a slightly different character than those of R1 and R2. As with the failures in R1 and R2, the end-span proved the weakest, probably due to the rotation of the ends. This rotation facilitated the development of the shear crack through the end of the member. The shear failure plane cut through the fillet at an angle of approximately 45° at the internal support in all three specimens. In R1 and R2 the failure plane at the external support intersected the member at the junction of the fillet and the bottom of the member and was inclined at an angle approximately 45°. However the failure plane at the external support of R3 cut through the fillet and was inclined at an angle greater than 45°. This may have occurred because of the flexural and partially inclined cracks which had developed at this location, either during the first stage of the test or just following the removal of the axial load.

7.4 Comparison of Test Results With Previous Tests

As was mentioned in Chapter 1, there have been tests of very few deep reinforced concrete members even remotely similar to those contained in the conduit specimens, so comparisons of strengths of the conduit specimens with the strengths found by other investigators must be filled with uncertainties.

The tests reported by Crist (6,9), de Pavia and Austin (7), and Albritton (5) are the only tests found in which there were more than two concentrated loads applied to one span, and in all these cases the specimens were simply supported beams. Only these tests appear to be particularly relevant to the current investigation because of the failure modes observed. In cases of one or two concentrated loads, shear failures are always accompanied by major shear cracks extending from near the reaction to near the closest load point. In the cases of distributed loads, the major shear cracks extend from near the reactions to near midspan of the beam. In this respect the cracking patterns ovserved in the conduits, subjected to three concentrated loads per span, closely resembled those in the simply supported beams subjected to distributed loads.

The general impression obtained from comparison of the shear stresses at failure in the conduits with stresses in deep beams is that the conduits are appreciably weaker in shear than the simple beams. To aid in the few comparisons which can be made, shear stresses at failure, the ratios of shear stress to compressive strength of the concrete, and average compressive stresses existing in the critical members of the conduits are listed in Table 7.7.

Specimen R1 had a span-depth ratio of 2.55, and resisted a nominal shear stress of 1,320 lb/in.^{2} at failure. The shear stress is computed at the face of the support, neglecting the fillets, and is taken as $v = V/bd$. The ratio of shear stress to compressive strength of concrete was 0.21. Four beams tested by Crist (6) had span depth ratios of 2.67,

and the shear stresses at failure ranged from 1,540 to 1,680 lb/in.^{2} In each case the concrete strength was much lower than that in R1. Only one of the four specimens failed in shear, at a shear stress level corresponding to 0.51 of the cylinder strength. The other specimens failed in flexure at comparable stress levels. The reinforcement ratios were 0.013, with f_y of about 45 k/in.^{2}, so that a steel index identified by pf_y is not greatly different than in the case of R1. If R1 had developed the same concrete stress, normalized in terms of f'_c, its capacity in shear would have been over 300 k/ft^2 rather than 150 k/ft^2.

In specimen R2 and the second stage of the test of R3, the span-depth ratios were 4.18 for the members that failed. R2 developed a shear stress of 1,520 lb/in.^{2}, in conjunction with an average compression stress of 790 lb/in.^{2}, while R3 developed, 1,300 lb/in.^{2}, with zero compression. Crist reported the tests of three beams with span-depth ratios of 3.72, and obtained shear stresses of 1,100 to 1,401 lb/in.^{2}, or 0.30 to 0.35 of the compressive strength of the concrete. The test of R2 mobilized a shear stress of 0.275 of the compressive strength, and that only with the aid of appreciable axial compression. The test of R3 developed only 0.235 of the cylinder strength in shear, rather than a value approaching or exceeding 0.3. Albritton (5) reported the tests of a number of specimens which had span-depth ratios of 4.0. The average shear stress developed in the few specimens which failed in shear was 1,200 psi, which was 0.3 of the cylinder strength of the concrete used. In this particular case, there was probably some unknown but appreciable axial compression force present, because of the types of bearing devices used.

The span-depth ratio of the vertical member in specimen R3 was 5.79, which is large enough that it is not properly classed as a deep beam, but rather is at the end of the range of shallow beams. This member developed a shear stress of 1,310 lb/in.^{2}, in conjunction with an average compression stress of approximately 510 lb/in.^{2} The shear stress was about 0.24 of the cylinder strength.

While the above information is not intended to suggest that the section at the face of the support is necessarily a suitable section for determining the design or controlling stresses, it is a suitable section for comparing the results of tests of various beams.

The tests of the conduits appear to indicate that the results of simple beam tests cannot be extrapolated to the case of the continuous frames. This may be due to the influence of the large negative moments existing at the sections of maximum shear, or due to other less readily defined factors. It is premature to try to determine the reasons for discrepancies on the basis of the tests of only three models, and it is expected that the five or more tests to be conducted in the next two years will add insights as the range of variables is broadened.

One of the limiting shear stress cases is that of a vertical shear crack at the face of the support, termed "shear proper" by some investigators. Laupa, et al, (10) has suggested that the average shear stress (computed as $v_c = V/bjd$) at failure could be expressed as

$$v_c = 200 + 0.188\ f'_c + 21{,}300\ p_t \quad (\text{lb/in.}^2)$$

where:

$$p_t = A_s/bD$$

A_s = total area of steel crossing section,

b = width of section, and

D = total depth of section.

This expression makes the shear strength of a very deep section a direct linear function of the compressive strength of the concrete, and of the amount of reinforcement in the cross section. In view of this expression, which has been applied by a number of investigators, it is obvious that the future test series should include the strength of the concrete and the amount of reinforcement as significant variables. The above expression applied to the current test specimens indicates limiting shear stresses of about 1,600 lb/in.^{2}, ignoring the axial compression stresses. Reducing the concrete strength to 4,000 lb/in.^{2} and the reinforcement to half that in the three specimens tested to date would reduce the limiting shear stress to about 1,150 lb/in.^{2} if the trends of the equation suggested by Laupa are valid.

In addition to the continuity in the conduits specimens, two other factors make these tests different than any others. The axial forces imposed on the specimens are either known exactly or determinable to reasonably close limits, which is not the case in any other tests. In all of the other tests, there must exist some uncertainity about the magnitude, and consequently the influence, of force acting along the member. The second factor is in the anchorage of the tension reinforcement. In virtually all tests of isolated members, the tension steel has been anchored against bond failure by welding the steel to some kind of an end plate or set of cross-bars. In the conduit specimens, the

steel was anchored by bond alone. The top (outside) bars were bent around the corners, and in fact were continuous across all members. The bottom (inside) bars extended through the vertical members at the ends of the specimens, and thus had a possible anchorage length of half a span plus most of the edge member thickness, and it must be noted that the anchorage within the supporting member is in a region of high compression perpendicular to the bars.

The influence of axial compression on the shear strength appears to still be an open question. The only direct comparison in this test series is between the strength of R2 and the second stage test of R3. The addition of about 800 lb/in.^{2} compression increased the shear strength by about 200 lb/in.^{2}, which is not a very impressive change. However, in the case of very deep beams subjected to distributed loads, failures due to inclined compression, generally described as web crushing, have occurred, and adding an axial compression can only make this problem more critical by increasing the principal compression as it reduces the principal tension. The influence of the axial load on the shear strength needs to be further studied, and it appears that additional insight can be obtained from the analytical techniques which are described in the following chapter, especially in those cases where principal compression is a limiting factor.

The sequence and patterns of cracking observed in the conduit specimens do not suggest that inclined compression is a primary cause of failure, but the possibility requires some further study. In some cases there was crushing of concrete near the face of the support, but

in these cases this is believed to have been secondary damage which occurred after the inclined cracks, caused by inclined tension stresses, had substantially reduced the available area for transfer of both shear and longitudinal compression forces to the supporting members.

From the questions posed in trying to interpret the results of the tests of the first three specimens, the most pressing questions to be resolved in the future work are those of the influence of the strength of the concrete and of the amount of tension reinforcement on the shear strengths of the structures. The effect of the span-depth ratio must not be ignored, but it is planned to hold the specimen dimensions to those of R2 and R3 for several additional specimens while the material property and quantity variables are investigated.

8. ANALYTICAL INVESTIGATION

8.1 General Remarks

In conduct of an experimental program it is desirable to develop an analytical method which can predict the behavior of the structure being investigated. If such a method is developed and good correlations between the experimental and analytical results are obtained, the analytical procedure can then be used to study the response of the structure to various parametric changes much more economically than one could by conducting a large number of experiments. In dealing with reinforced concrete conduits under high embankment dams, conventional methods of structural analysis are not applicable. The existing practice for the design of reinforced concrete box culverts under low embankments is to consider the culvert as a closed rectangular frame subjected to uniform loads on four sides. Various members of the frame are analyzed as beams subjected to a combination of axial load, shear, and bending. The behavior of multiple-celled box culverts of ordinary dimensions is not far from that of framed structures. Their analysis and design are given in Ref. 2.

Under high embankment dams the intensity of applied loads are high. This has two consequencies:

1. The magnitude of axial forces is large.
2. The span to depth ratios of the members are small.

Therefore, the assumption of linear variation of strain through the depth of the member is not valid. Moreover, the state of stress is biaxial as compared to the uniaxial state assumed in the members of culverts under low embankment.

For conduits under high embankments, like other complex reinforced concrete structures, the behavior of the structure after cracking and its ultimate load carrying capacity are of great importance. Therefore, an analytical model which is capable of providing the above needed information is desirable.

Several existing methods of analysis such as the finite difference, the lumped parameter, and the finite element methods can be used to obtain the desired information. Both the lumped parameter and the finite element methods have been used successfully to obtain solutions to various problems. However, the finite element method possesses certain characteristics that makes it more advantageous than the lumped parameter method. In particular, the method can be systematically programmed to accommodate such complex and difficult problems as non-homogeneous materials, non-linear stress-strain behavior, and complex boundary conditions. Another favorable aspect of the finite element method is that one can follow a physical or intuitive approach for the formulation and usage of the method. On the basis of past experience the finite element method has been selected for this study.

8.2 Object and Scope

The objective of the analytical phase of this study is to develop a procedure for predicting the behavior of conduits in both the linear and non-linear range of material behavior. A finite element program has been developed for the study of conduits in the elastic range and is being modified to include cracking and plasticity of concrete. The

modified program will include special elements to simulate the reinforcement and the bond between the concrete and the reinforcement. The external loads will be applied incrementally, so that the program will be able to provide stresses, strains, and displacements in the conduit at the successive levels of the external loads.

8.3 Nature of the Problem

Since the variation of load along the length of the structure is small, a plain strain condition prevails in the actual conduit. Therefore, the problem can be reduced to a two-dimensional problem. However, in order to simulate the test specimens, the case of plain stress is considered.

In determining the distribution of stresses in any structure subjected to external loads, the conditions of stress equilibrium, strain compatibility, and the constitutive relations for the materials used must be satisfied. The equilibrium equations for a plane stress problem are:

$$\begin{aligned} \frac{\partial \sigma_x}{\partial x} + \frac{\partial \tau_{xy}}{\partial y} - X = 0 \\ \frac{\partial \tau_{xy}}{\partial x} + \frac{\partial \sigma_{xy}}{\partial y} - Y = 0 \end{aligned} \qquad (1)$$

where X and Y are body forces. For small deformations the strain components are related to displacements u and v by the following relations:

$$\varepsilon_x = \frac{\partial u}{\partial x}$$

$$\varepsilon_y = \frac{\partial v}{\partial y}$$

$$\gamma_{xy} = \frac{\partial v}{\partial x} + \frac{\partial u}{\partial y} \tag{2}$$

from which the strain compatibility is obtained as:

$$\frac{\partial^2 \varepsilon_x}{\partial y^2} + \frac{\partial^2 \varepsilon_y}{\partial x^2} = \frac{\partial^2 \gamma_{xy}}{\partial x \partial y} \tag{3}$$

It is of interest to note that Eqs. 1 to 3 are independent of material properties.

For the problem in this study the solution of the governing differential equations complete with the satisfaction of boundary conditions is virtually impossible. This is due to several reasons:

1. Concrete is inherently a non-homogeneous and a nonlinear material for which no adequate failure theory under combined stresses exists.
2. The nature of bond between the steel reinforcement and concrete, the bond slip, the effect of dowel action of the reinforcing bars, and the aggregate interlocking are not well understood.
3. The structural topology continuously changes as cracks propagate further into the concrete.
4. Concrete deformations are influenced by creep and shrinkage.

8.4 The Finite Element Technique

In the finite element method the continuous body is subdivided into triangular or quadrilateral subregions called elements, Fig. 8.1. The corners of these elements are referred to as nodes or joints. Usually the displacements, and in some cases derivatives of the displacements, are specified at the nodes, Fig. 8.2. An equilibrium equation is obtained for each degree of freedom yielding a set of algebraic equations. This procedure reduces the problem from that of solving a system of differential equations to that of solving a set of linear algebraic equations. The method is described in detail in Ref. 11 or 12, therefore, only a general description of the method will be presented here.

Figure 8.1 shows an arbitrary structure, loaded in its own plane, which has been subdivided into small triangular finite elements. The elements are assumed to be connected at the nodal points only. The thickness of each element is taken as unity. The simplest configuration is to consider two nodal displacements, horizontal and vertical at every nodal point, Fig. 8.2.

The displacement within each element $u(x, y)$ and $v(x, y)$ is described in terms of the nodal displacement $\{\bar{u}\}$ by some interpolation function $[N(x, y)]$:

$$\begin{Bmatrix} u(x, y) \\ v(x, y) \end{Bmatrix} = [N(x, y)]\ \{\bar{u}\} \tag{4}$$

The strain-displacement relations, Eq. (2) become:

$$\{\varepsilon\} = [B]\ \{\bar{u}\} \tag{5}$$

where [B] can be obtained by the proper differentiation of the shape functions [N]. The stresses are related to strains through the material property matrix [D]:

$$\{\sigma\} = [D]\ \{\varepsilon\} \tag{6}$$

The stiffness matrix of an element is obtained by giving a virtual displacement $\delta\{\bar{u}\}$ to the nodal points and then equating the external and internal work of the system. The internal work is the product of stresses and virtual strains integrated over the volume of the element

$$\delta W_{int} = \int_V \delta\{\varepsilon\}^T\ \{\sigma\}\ dV = \delta\{\bar{u}\}^T\ [B]^T[D][B]\ \{\bar{u}\}\ dV.$$

The work done by the nodal forces is the product of the nodal forces and the virtual nodal displacements

$$\delta W_{ext} = \delta\{\bar{u}\}^T\ \{f\}$$

where {f} is a vector of the nodal forces. Equating the external and internal work, we obtain

$$\delta\{\bar{u}\}^T\ \{f\} = \delta\{\bar{u}\}^T\ \left(\int_V [B]^T[D][B]\ dV\right)\ \{\bar{u}\}$$

For any arbitrary virtual displacement the above expression reduces to

$$\{f\} = [k]\ \{\bar{u}\} \tag{7}$$

where [k] is the element stiffness matrix. The force-displacement

relations for the overall structure is given by proper summation of element stiffness

$$\{F\} = [K]\ \{U\} \tag{8}$$

where {F} and {U} are the generalized nodal forces and the nodal displacements, respectively, and [K] is the stiffness matrix. By solving the set of linear algebraic simultaneous equations, Eq. 8, one obtains the nodal displacements {U}, from which the stresses and strains are obtained according to Eq. 5 and 6, respectively.

8.5 Structure Idealization

The first application of the finite element method to reinforced concrete structures was made by Ngo and Scordelis (13), where a cracked reinforced concrete beam was analyzed assuming it to be linearly elastic. Nonlinear analysis of reinforced concrete beams has been carried out out by Nilson (14). Both investigators used separate elements for concrete and steel reinforcement, with link-elements in between. The link-elements have no dimensions and are to account for the bond slip and the dowel action of the longitudinal reinforcement. They attempted to propagate the crack through the model by continuously changing the topology of the model as the crack propagates from one element to the next. Such an approach has the disadvantage that either the crack direction is restricted to lines defining the edges of neighboring elements or a rezoning (a topological modification) is required when new cracks are formed. This presents a considerable difficulty in bookkeeping even with the present day generation of computers.

Another method of accounting for the presence of cracks was introduced by Mohraz, Schnobrich, and Echeveria (15), where the material property of the region containing cracks is modified in such a way that the element cannot sustain any load in the direction perpendicular to the crack. The cracked element is visualized as being made up of a series of bars that can carry the loads in one direction only. The new orthotropic material property matrix is obtained using an energy approach.

It was observed from the experimental results of reinforced concrete conduit models that the failure modes are flexure and shear. Therefore, before selecting a model for the problem in hand, one needs to consider the manner in which reinforced concrete beams carry external loads. Many tests were carried out to investigate the factors that influence the stress distribution within a reinforced concrete beam during its loading history. Several hypotheses based on test results were introduced. The bending moment in a reinforced concrete beam loaded by point loads, Fig. 8.4, can be obtained from the internal moment equilibrium equation,

$$M(x) = Vdx = Tjd = Cjd$$

The shear resistance mode can be obtained from the previous equation by differentiating with respect to x,

$$V = \frac{dM}{dx} = jd\,\frac{dT}{dx} + T\,\frac{d(jd)}{dx} \qquad (9)$$

The bond force $\frac{dT}{dx}$ represents a true beam action in which the force in the longitudinal reinforcement should change along the beam to reflect the distribution of the externally applied moment M(x), provided that the lever arm jd stays constant (a well known assumption in the analysis of reinforced concrete flexural members). If the bond force cannot develop over a section, then the tension force T cannot change and the external shear force should be resisted by inclined compression, which is the case of pure arch action expressed in the second term of Eq. 9.

Fenwick and Paulay (16) were able to demonostrate by carrying out several tests that in the beam action, about 60 percent of the shear force is carried by aggregate interlock between two cracked blocks of concrete (force G in Fig. 8.4a). Only 20 percent of the shear force is carried by dowel action of the flexural reinforcement (force V_d in Fig. 8.4a). The remaining shear force is resisted by what is called "flexural resistance of cracked concrete blocks", in which it is assumed that the blocks will act as cantilever beams supported in the concrete arch, Fig. 8.4b.

In normal beams ($L/d > 5$), the arch action is confined to two localities of the beam; one is near the point load and the other is in the vicinity of the support. The tied-arch behavior over the whole shear span can only occur if these two localities merge together.

For the present study, concrete is idealized by constant strain triangular finite elements, Fig. 8.2, whereas bar elements, Fig. 8.3, are used to represent the steel reinforcement. This implies that the

ends of the bar elements are rigidly connected to the adjacent triangular concrete elements and that perfect bond between steel and concrete is assumed. It also implies that the dowel action in the longitudinal reinforcement is neglected. The validity of these assumptions is questionable, but the distribution of bond stresses between concrete and steel, and the amount of dowel action have not yet been established. These two factors can be included by introducing a two-dimensional link-type element as was suggested by Ngo and Scordelis (13).

A large variety of elements exists in the finite element library at the present time. However, for applications that involve cracking and nonlinear material behavior, an element possessing homogeneous stress and strain conditions seems most desirable. This is best achieved by constant strain triangular element with deformations defined as linear displacement functions of the coordinates. Therefore, the elements of [B] in Eq. 5 are constant. On the other hand, the element has certain disadvantages. One disadvantage is that due to a constant stress or strain field in the element, the results frequently require interpretation. The calculated stresses can be assumed to represent the state of stress at the centroid of the element. However, a more accurate stress distribution normally results from averaging the stresses of the various elements connected at each node.

Another disadvantage of the constant strain triangular element is its directionality; i.e., the structure may behave in a certain way for one arrangement and in another way for a different arrangement. These directionality properties can be eliminated if a zigzag orienta-

tion of elements is used while generating the element incidences. This is demonstrated by using two different orientations of elements in the elastic solutions which will be discussed later.

8.6 Material Properties

For reinforced concrete, the constitutive relations between stresses and strains include both elastic and inelastic behavior due to the gradual cracking and plasticity of concrete. However, a linear relationship is assumed for a small stress change during an incremental solution, as will be shown later.

8.6.1 Elastic Material Properties

Uncracked concrete is considered as homogeneous and isotropic. The uniaxial stress-strain relationship for concrete is assumed to be elastic-perfectly plastic in compression, whereas it is assumed that concrete will behave as a brittle material in tension, Fig. 8.5. In the two-dimensional case the stress-strain relationships are:

$$\begin{Bmatrix} \sigma_x \\ \sigma_y \\ \tau_{xy} \end{Bmatrix} = \frac{E}{\alpha^2-\beta^2} \begin{bmatrix} \alpha & \beta & 0 \\ \beta & \alpha & 0 \\ 0 & 0 & \frac{\alpha^2 - \beta^2}{2(1+\nu)} \end{bmatrix} \begin{Bmatrix} \varepsilon_x \\ \varepsilon_y \\ \gamma_{xy} \end{Bmatrix}$$

where E and ν are Young's Modulus and Poisson's ratio of concrete, respectively.

For plane stress $\alpha = 1$; $\beta = \nu$

and for plane strain $\alpha = 1 - \nu^2$; $\beta = \nu\ (1 + \nu)$

Concrete is assumed to have a limited tensile strength σ_{cr}, and a crushing strain in compression equal to ε_{ult}. These two values can be determined from test results.

8.6.2 Cracked Concrete

It is assumed that cracking occurs in an element once the principal stress in any direction exceeds the limiting tensile stress of concrete σ_{cr}. Upon cracking, the material property of the uncracked element should be modified to reflect the fact that the element cannot sustain any stresses in a direction perpendicular to the crack and that a large proportion of the shear force is carried by aggregate interlock.

In this model a cracked element is conceived to be made up of several concrete bars parallel to the crack direction, Fig. 8.6. After cracking, an element releases part of the energy stored in it. This loss of energy is accompanied by mobilization of shear stresses alongside the concrete bars. That part of energy that cannot be stored in the element is converted into nodal forces and is applied back on the structure as external loads in order to make it deform further and carry the extra load. This point will be explained later in Section 8.7.

The orthotropic properties as established in the principal directions should be transformed back to the global or the original x-y coordinate system. The material property matrix $[\bar{D}]$, which corresponds to the cracked element as defined in the original coordinate system x-y axes in Fig. 8.6, can be obtained from the properties defined in the principal coordinate system using the principle of conservation

of energy. Thus, by equating the energy in the global coordinate to that in the principal coordinate (containing the direction of the crack), one obtains

$$\{\varepsilon\}^T \{\sigma\} = \{\varepsilon_c\}^T \{\sigma_c\} \tag{10}$$

where the subscript c refers to the coordinate system containing the principal or cracked directions. Accordingly one can write the following:

$$\{\sigma_c\} = [D]_c \{\varepsilon_c\}$$

$$\{\sigma\} = [D] \{\varepsilon\}$$

$$\{\varepsilon_c\} = [T_\varepsilon] \{\varepsilon\}$$

where $[T_\varepsilon]$ is a transformation matrix given as

$$[T_\varepsilon] = \begin{bmatrix} \cos^2\alpha & \sin^2 & \cos\alpha\sin\alpha \\ \sin^2\alpha & \cos^2 & -\cos\alpha\sin\alpha \\ -2\cos\alpha\sin\alpha & 2\cos\alpha\sin\alpha & \cos^2\alpha-\sin^2\alpha \end{bmatrix}$$

Substitution of the above expressions in Eq. 10 gives

$$\{\varepsilon\}^T [\bar{D}]\{\varepsilon\} = \{\varepsilon\}^T ([T_\varepsilon]^T [D]_c [T_\varepsilon]) \{\varepsilon\} \tag{11}$$

From the above equation the modified material property matrix is expressed as

$$[\bar{D}] = [T_\varepsilon]^T [D_c] [T_\varepsilon] \tag{12}$$

8.6.3 Plasticity of Concrete

The method of analysis, which will be discussed later, is an iterative incremental solution and follows what is known as the "initial stress method" (17). Therefore the constitutive relations in the plastic range need to be expressed in incremental forms.

The material property matrix within each load increment is considered to be linear. During a load increment, while some of the elements may be elastic, others may be in the plastic range or have modified stiffness due to cracking. Therefore, the resulting stiffness matrix will be a combination of both elastic and plastic material properties.

No unified failure criteria for concrete under biaxial stresses exists. However, a recent investigation for defining the failure envelope was carried out by Kupfer, Hilsdorf, and Rusch (18). In this study, the compressive yielding of concrete is assumed to follow Von Mises yield criterion. The maximum normal stress criterion as shwon in Fig. 8.7 will be used for other combinations of stress. The governing constitutive relations have been incorporated in the finite element analysis by Zienkiewicz and others (17). Only a short summary of the method will be presented here for clarity.

The Von Mises yield criterion is given by the following equation

$$F(\sigma) = \sigma_x^2 - \sigma_x\sigma_y + \sigma_y^2 + 3\tau_{xy}^2 - \sigma_o^2 = 0 \qquad (13)$$

where $F(\sigma)$ is a yield function that describes an ellipse in the σ_1, σ_2

plane, and σ_o is the value of the uniaxial compression stress at yield, which is given as 0.85 f'_c. The total incremental strain is composed of elastic and plastic parts

$$\{\delta\varepsilon\} = \{\delta\varepsilon\}_e + \{\delta\varepsilon\}_p \tag{14}$$

The elastic strain is related to the incremental stress by

$$\{\delta\varepsilon\}_e = [D]^{-1} \{\delta\sigma\} \tag{15}$$

whereas the plastic part is given by the normality rule as

$$\{\delta\varepsilon\}_p = \lambda \frac{\partial F(\sigma)}{\{\partial\sigma\}} = \lambda\{q\} \tag{16}$$

where λ is a proportionality constant and $\{q\}$ is the normal to the yield surface. From Eqs. 14, 15 and 16, the total strain could be written as

$$\{\delta\varepsilon\} = [D^{-1}] \{\delta\sigma\} + \lambda\{q\} \tag{17}$$

In the case of potential yielding of concrete the state of stress is represented by a point on the yield surface (point P in Fig. 8.8). In order for point P not to loose contact with the yield surface, the direction of the incremental stress vector $\{\delta\sigma\}$ should coincide with the tangent to the yield surface at point P, or

$$\{q\}^T\{\delta\sigma\} = 0 \tag{18}$$

Equations 17 and 18 can be written

$$\begin{Bmatrix} \delta\{\varepsilon\} \\ 0 \end{Bmatrix} = \begin{bmatrix} [D]^{-1} & \{q\} \\ \{q\}^T & 0 \end{bmatrix} \begin{Bmatrix} \delta\{\sigma\} \\ \lambda \end{Bmatrix}$$

Upon eliminating the parameter λ and after carrying out the inversion operation we obtain

$$[D]_{ep} = [D] \left((1 - \{q\}\{q\}^T [D]) \frac{1}{\{q\}^T [D] \{q\}} \right) \tag{19}$$

where $[D]_{ep}$ is the instantaneous elasto-plastic material property matrix which relates the incremental stresses to incremental strains

$$\delta\{\sigma\} = [D]_{ep} \delta\{\varepsilon\} \tag{20}$$

8.7 Method of Solution

As mentioned earlier, material nonlinearity occurs due to cracking, plasticity of concrete, and yielding of the reinforcement. When this is the case, the stiffness matrix [k] is no longer linear but instead it becomes a function of material property matrix $[D(\sigma)]$.

One of the common methods of solving a set of nonlinear algebraic simultaneous equations such as

$$[k]\{u\} = \{P\} \tag{21}$$

is the incremental procedure where the nonlinear problem is approximated as a series of linear problems, i.e., the nonlinearity is treated as a series of piecewise linear portions. This procedure has been applied

to various kinds of nonlinear problems. The method provides a complete description of the load-deflection curve and the stress or strain history of the structure. Nevertheless, the procedure is time consuming and requires the inverstion of the stiffness matrix at each load step. Another procedure, often employed in nonlinear problems, is the iterative scheme. In this procedure the structure is fully loaded in each iteration. Since the stiffness matrix of the structure is modified to account for material nonlinearities, the equilibrium is not necessarily satisfied. After each iteration, the portion of the total load that is not balanced is calculated and used in the next step to compute an additional increment of the displacement. This process is repeated until equilibrium is attained to the required degree of accuracy. An alternate scheme to this procedure is the "modified iterative scheme" in which the same stiffness is employed through the whole iterations in one load step. The iterative method of solution is easier to use and to program, especially for cases where the materials have different elastic properties in tension and compression. However, there is no assurance that the procedure converges to the right solution; moreover, the displacements, stresses, and strains are determined only for the total load.

The method that will be employed in this study combines the advantages of both procedures and is called "the initial stress method" (17). In this method of solution the load is applied incrementally but after each increment successive iterations are performed. The stiffness matrix is modified for each increment but it is not changed within the iteration increment. The iterative procedure for the ith increment is

$$[k]\ \{\delta U_i^{(j)}\} = \{\delta P_i\} \text{ for } j = 1, 2 \ldots M \tag{22}$$

where i denotes a load increment and j denotes a cycle of iterations. For a typical load increment $\{\delta P_i\}$, the displacements $\{\delta U_i^1\}$, strains $\{\delta \varepsilon_i^1\}$, and stresses $\{\delta \sigma_i^1\}$ are obtained in the first iteration. Due to material nonlinearity, the stress increment $\{\delta \sigma_i^{(j)}\}$ is not in general the correct stress to equilibrate the applied load $\{\delta P_i\}$. During any iteration the correct stress is calculated according to one of the following cases

(1) If plasticity of concrete has occurred then the stress is calculated from Eq. 20 as

$$\{\delta \sigma_{ci}\} = [D_{ep}]\ \{\delta \varepsilon_i^{(j)}\} \tag{20}$$

(2) In case of yielding of the reinforcement and with the assumption of elastic-perfectly plastic behavior the stress increment is zero.

$$\{\delta \sigma_{ci}\} = 0 \tag{23}$$

(3) If cracking has occurred in a number of elements during any iteration, then the stress is calculated from

$$\{\delta \sigma_{ci}\} = [\bar{D}]\ \{\delta \varepsilon_i^{(j)}\} \tag{24}$$

where $[\bar{D}]$ is the material property matrix of any cracked concrete element. These three types of nonlinearity may occur at the same time in different elements at higher levels of the applied load.

The difference between the computed and the correct stress, i.e., the difference between $\{\delta\sigma_i^j\}$ and $\{\delta\sigma_{ci}\}$ is treated as "the initial stress" and a correction load vector is calculated for each element as follows:

$$\{\delta P_i^{j+1}\} = \int_V [B]^T \left(\{\delta\sigma_i^{(j)}\} - \{\delta\sigma_{ci}\}\right) dV \tag{25}$$

The procedure is repeated until convergence is achieved where another load step i+1 will be applied to the structure.

In this procedure after the application of the ith increment the total load applied to the structure is given by

$$\{P_i\} = \Sigma_{k=1}^{i} \{\delta P_k\} \tag{26}$$

Similarly, the displacements are calculated as

$$\{U_i\} = \Sigma_{k=1}^{i} \{\delta U_k\} \tag{27}$$

In order to calculate the displacement increment at any iteration, a fixed value of the stiffness, evaluated at the end of the previous load increment, is used

$$[k_{i-1}]\ \{\delta U_i\} = \{\delta P_i\} \tag{28}$$

Figure 8.9 depicts schematically this procedure.

8.8 Elastic Solution of Test Model R1

A computer program for the elastic analysis of reinforced concrete conduits has been developed. The program has been modified and is

currently being code-checked for the nonlinear analysis. The elastic solution of a typical conduit, specimen R1, is given in this report.

Due to symmetry only one quarter of the test specimen is considered in the solution. The elastic response was obtained using two different finite element grids. Both grids have the same number of elements and joints but differ in element orientation. The finite element mesh is a fairly fine mesh with 900 elements, 517 nodes, and 1009 unknowns. The first grid with uniform orientation of the triangular elements is shown in Fig. 8.10. Figure 8.11 shows the same grid with zigzag orientation of the elements. The zigzag orientation is used in order to decrease the directionality of the elements. For the uniform orientation the horizontal equilibrium checked within 15 percent, which is a rather high error for a fairly fine grid. In the second grid the directionality property was reduced considerably and equilibrium checked within 1.8 percent. In both schemes a finer mesh was used in areas where stress concentration were believed to exist. The mesh generation is performed automatically by the computer. This saves time for feeding the required data to the computer and reduces the possibility for errors.

Boundary conditions are such that there is no shear on the lines of symmetry of the structure, nor is there any displacement in a direction perpendicular to these lines. This is achieved by specifying roller supports along the lines of symmetry. The interior surfaces are free of stress, whereas soil pressure acts on the exterior surfaces. One system of loading was obtained by considering the soil pressure

uniformly distributed on each side. Another solution was obtained using concentrated loads at locations where the loads from the jacks were applied. The solutions indicated that the difference between the two loading conditions is negligible. Therefore, the uniformly distributed pressure is considered in further solutions.

Plane stress condition was used to obtain the elastic solutions. An average value of 3800 $k/in.^2$ based on concrete cylinder tests was used for the modulus of elasticity of concrete. Two elastic solutions using Poisson ratios of 0 and 0.15, were obtained.

The deflected shape of the conduit obtained by the finite element solution for a Poisson's ratio of zero is shown in Fig. 8.12. Comparisons between the analytical and experimental results are shown in Figs. 8.13 and 8.14. The results are in excellent agreement with each other.

Figure 8.15 shows the direction and magnitude of principal strains at each node. An outward direction of arrows indicates tension whereas an inward direction indicates compression. The magnitude of strain is proportional to the arrow's length. This plot is for a Poisson's ratio equal to zero. It indicates that the first cracking is a flexural crack at the inner face of the horizontal spans. It also indicates the manner in which the loads are carried in various parts of the structure.

Figures 8.16 and 8.17 show comparisons between the strain gage readings from test results and the analytical solution. Strain gages reading compression agreed in general with the elastic solution, but those reading tension deviated from the elastic solution at an early load level. The behavior of strain gage 24 may be explained by the

fact that cracking might have occurred during the trial test performed earlier. Figures 8.18 to 8.23 show strain in horizontal and vertical sections in different parts of the structure as plotted by the computer.

It should be noted that no reinforcement is included in the elastic solutions because at lower load levels concrete behaves elastic and contribution of the reinforcement is very small. The results for a Poisson's ratio of zero agreed better with test results than those with a value of 0.15. In other test models, cracking occurred at lower load levels. The elastic solution makes a limited contribution to the understanding of the behavior of conduits at higher loads, and a solution taking into account cracking of specimens is essential to any broad understanding of their behavior.

9. CONCLUSIONS AND RECOMMENDATIONS

This report constitutes an interim progress report on the "Investigation of Multiple Opening Concrete Conduits" project, and as such it does not appear appropriate to make any firm recommendations for the design of such structures. However, there are a number of conclusions which have been reached.

Three specimens out of a projected series of eight have been tested, and on the basis of the results of these tests it must be concluded that the shear strength of a deep reinforced concrete beam forming part of a continuous frame will be substantially less than the shear strength of a simply supported beam having a similar span-depth ratio. This appears to be true even in cases where the beam used as a frame member is subjected to a significant axial compression in addition to the shear and flexural forces.

The remainder of the series of tests will be used to explore the effects of variables such as the concrete strength, reinforcement ratio, span-depth ratio, and axial stress level on the shear strength of deep reinforced concrete frame members.

The analytical work carried out on the problem includes the development of extensive finite element programs. The solutions reported in Chapter 8 are based on elastic behavior only, but they were successful in predicting the initial slopes of various load-strain curves for specimen R1.

Also described in Chapter 8 are the general techniques to be used in extending the finite element analysis to take into account the presence of cracking of the concrete in tension, the nonlinear stress-strain curve for concrete in compression, and the presence and eventual yielding of the reinforcement.

LIST OF REFERENCES

1. "Engineering and Design; Conduits, Culverts and Pipes," Engineering Manual EM 1110-2-2902, Headquarters, Department of the Army, Office of the Chief of Engineers, Washington, D.C., 1969.

2. Diaz de Cossio, R. and Siess, C. P., "Development of Design Criteria for Reinforced Concrete Box Culverts - Part I: Strength and Behavior of Reinforced Concrete Beams and Frames," Civil Engineering Studies, Structural Research Series No. 163, University of Illinois, Urbana, September 1958.

3. Diaz de Cossio, R. and Siess, C. P., "Development of Design Criteria for Reinforced Concrete Box Culverts - Part II: Recommendations for Design," Civil Engineering Studies, Structural Research Series No. 164, University of Illinois, Urbana, February 1959.

4. Albritton, G. E., "Review of the Literature Pertaining to the Analysis of Deep Beams," Technical Report No. 1-701, U. S. Army Engineers Waterways Experiment Station, Vicksburg, Mississippi, Nov. 1965, 80 pages.

5. Albritton, G. E., "Static Tests of Reinforced Concrete Deep Beams," Technical Report No. 1-676, U. S. Army Engineers Waterways Experiment Station, Vicksburg, Mississippi, June 1965, 125 pages.

6. Crist, R. A., "Shear Behavior of Deep Reinforced Concrete Deep Beams, Vol. II: Static Tests," AFWL-TR-67-61 Vol. II, Air Force Weapons Laboratory, Kirtland Air Force Base, New Mexico, October 1967, 182 pages.

7. de Paiva, H. A. R., and W. J. Austin, "Behavior and Design of Deep Structural Members -- Part 3: Tests of Reinforced Concrete Deep Beams," Civil Engineering Studies, Structural Research Series No. 194, University of Illinois, Urbana, March 1960, 126 pages.

8. Dill, A. F., "Strength and Behavior of Restrained Deep Reinforced Concrete Beams under Static Loading," RTD-TDR-63-3092, Air Force Weapons Laboratory, Kirtland Air Force Base, New Mexico, September 1963, 241 pages.

9. Crist, R. A., "Shear Behavior of Deep Reinforced Concrete Beams," R.I.L.E.M., Int. Symp. on the Effects of Repeated Loading of Materials and Structural Elements, Mexico City, 1966.

10. Laupa, A., C. P. Siess, and N. M. Newmark, "Strength in Shear of Reinforced Concrete Beams," University of Illinois Engineering Experiment Station Bulletin No. 428, Urbana, 1955.

11. Zienkiewicz, O. C., The Finite Element Method in Engineering Science, McGraw-Hill, 1971.

12. Desai and Abel, Introduction to the Finite Element Method, D. Van Nostrand, 1972.

13. Ngo, D. and A. C. Scordelis, "Finite Element Analysis of Reinforced Concrete Beams," ACI Journal, Proceedings Vol. 64, No. 3, Mar. 1967, pp. 152-163.

14. Nilson, A. H., "Nonlinear Analysis of Reinforced Concrete by Finite Element Method," ACI Journal, Proceedings Vol. 65, No. 9, Sept. 1968, pp. 757-766.

15. Mohraz, B., W. C. Schnobrich, and A. Echeverria Gomez, "Crack Development in a Prestressed Concrete Reactor Vessel," Nuclear Engineering and Design 11 (1970), pp. 286-294.

16. Fenwick, R. C., and T. Paulay, "Mechanism of Shear Resistance of Concrete Beams," Journal of the Structural Division, ASCE, Vol. 94 No. ST10, Oct. 1968, pp. 2325-2350.

17. Zienkiewicz, O. C., S. Valliapan and I. P. King, "Elastoplastic Solutions of Engineering Problems. Initial Stress Finite Element Approach," Int. J. Num. Method in Eng. Vol. 1, 1969, pp. 75-100.

18. Hilsdorf, H. K., Kupfer, H., and Rusch, H., "Behavior of Concrete Under Biaxial Stresses," ACI Journal, Proceedings Vol. 66, No. 8, Aug. 1969, pp. 656-666.

TABLE 2.1

Nominal Member Thicknesses and Steel Ratios

	Specimen	R1	R2	R3
External Members	Total Depth-in.	13.5	9.0	9.0
	Effective Depth-in.	11.6	7.1	7.1
	Tension* Steel %	1.0	1.2	1.2
Internal Members	Total Depth-in.	9.0	9.0	9.0
	Effective Depth-in.	7.1	7.1	7.1
	Tension* Steel %	1.7	1.2	1.2
Specimen Thickness-in.		10	10	10

*Tension Steel Area is Equal to Compression Steel Area

TABLE 3.1

Reinforcement Strength Properties

Bar No.	f_y - k/in.^{2}	f_{ult} - k/in.^{2}	ε_u - % in 8 in.
#3	78.0	124.0	12.2%
#6	72.7	118.9	14.7%
#7	69.8	112.2	13.6%

Each value average of three tests

TABLE 3.2

Concrete Strength Properties

Specimen	Slump in.	Age-days (cylinders)	f'_c - lb/in.^{2}	f_{sp} - lb/in.^{2}	E_c - lb/in.^{2} (initial Modulus)
R1	2 1/4	129	6,250	360	4.10×10^6
R2	2 3/4	66	5,520	338	3.92×10^6
R3	2	95	5,520	316	3.95×10^6

TABLE 7.1 TEST 1 R1
Nominal Equivalent Pressure k/ft.^{2}

Load No.	Vertical Load k/ft.^{2}			Horizontal Load k/ft.^{2}	
	Ext. Axial	Int. Axial	Span	Axial	Span
0	0	0	0	0	0
1	15	15	15	5	5
2	30	30	30	10	10
3	37.5	37.5	37.5	12.5	12.5
4	45	45	45	15	15
5	52.5	52.5	52.5	17.5	17.5
6	60	60	60	20	20
7	67.5	67.5	67.5	22.5	22.5
8	75	75	75	25	25
9	82.5	82.5	82.5	27.5	27.5
10	0	0	0	0	0

TABLE 7.2 TEST 2 R1
Nominal Equivalent Pressure k/ft.^{2}

Load No.	Vertical Load k/ft.^{2}			Horizontal Load k/ft.^{2}	
	Ext. Axial	Int. Axial	Span	Axial	Span
0	0	0	0	0	0
1	30.0	30.0	30.0	10.0	10.0
2	60.0	60.0	60.0	20.0	20.0
3	82.5	82.5	82.5	27.5	27.5
4	90.0	90.0	90.0	30.0	30.0
5	97.5	97.5	97.5	32.5	32.5
6	105.0	105.0	105.0	35.0	35.0
7	112.5	112.5	112.5	35.0	35.0
8	112.5	112.5	112.5	30.0	30.0
9	112.5	112.5	112.5	22.5	22.5
10	112.5	112.5	112.5	12.5	12.5
11	112.5	112.5	112.5	0	0
12	0	0	0	0	0

TABLE 7.3 TEST 3 R1
Nominal Equivalent Pressure k/ft.^{2}

Load No.	Vertical Load k/ft.^{2}			Horizontal Load k/ft.^{2}	
	Ext. Axial	Int. Axial	Span	Axial	Span
0	0	0	0	0	0
1	60.0	60.0	60.0	10	10
2	90.0	90.0	90.0	10	10
3	112.5	112.5	112.5	10	10
4	112.5	112.5	112.5	10	10
5	112.5	127.5	127.5	10	10
6	112.5	135.0	135.0	10	10
7	112.5	142.5	135.0	10	10
8	112.5	142.5	142.5	10	10
9	112.5	150.0	150.0	10	10
10	112.5	150.0	150.0	10	10
11	112.5	150.0	150.0	10	10
12	0	0	0	0	0

TABLE 7.4 TEST 1 R2
Nominal Equivalent Pressure k/ft.^{2}

Load No.	Vertical Load k/ft.^{2}			Horizontal Load k/ft.^{2}	
	Ext. Axial	Int. Axial	Span	Axial	Span
0	0	0	0	0	0
1	15	15	15	5	5
2	30	30	15	10	10
3	37.5	37.5	37.5	12.5	12.5
4	45	45	45	15	15
5	52.5	52.5	52.5	17.5	17.5
6	60	60	60	20	20
7	67.5	67.5	67.5	22.5	22.5
8	75	75	75	25	25
9	82.5	82.5	82.5	27.5	27.5
10	90	90	90	30	30
11	0	0	0	0	0

TABLE 7.5 TEST 2 R2
Nominal Equivalent Pressure k/ft.^{2}

Load No.	Vertical Load k/ft.^{2}			Horizontal Load k/ft.^{2}	
	Ext. Axial	Int. Axial	Span	Axial	Span
0	0	0	0	0	0
1	15.0	15.0	15.0	5.0	5.0
2	60.0	60.0	60.0	20.0	20.0
3	75.0	75.0	75.0	25.0	25.0
4	90.0	90.0	90.0	30.0	30.0
5	97.5	97.5	97.5	32.5	32.5
6	105.0	105.0	105.0	35.0	35.0
7	0	0	0	0	0

TABLE 7.6 TEST R3
Nominal Equivalent Pressure k/ft.^{2}

Load No.	Vertical Load k/ft.^{2}			Horizontal Load k/ft.^{2}	
	Ext. Axial	Int. Axial	Span	Axial	Span
0	0	0	0	0	0
1	15.0	15.0	15.0	15.0	15.0
2	30.0	30.0	30.0	30.0	30.0
3	37.5	37.5	37.5	37.5	37.5
4	45.0	45.0	45.0	45.0	45.0
5	52.5	52.5	52.5	52.5	52.5
6	60.0	60.0	60.0	60.0	60.0
7	67.5	67.5	67.5	67.5	67.5
8	67.5	67.5	67.5	0	0
9	75.0	75.0	75.0	0	0
10	82.5	82.5	82.5	0	0
11	90.0	90.0	90.0	0	0
12	97.5	97.5	97.5	0	0
13	0	0	0	0	0

TABLE 7.7 Loads and Stresses at Failure

Specimen	ℓ/d	f'_c lb/in.^{2}	P_v k/ft.^{2}	P_h k/ft.^{2}	$v^*_u = \frac{V_u}{bd}$ lb/in.^{2}	$\frac{v_u}{f'_c}$	$\frac{P_u}{Ag}$ lb/in.^{2}
R-1	2.55	6,250	150	< 10	1,320	0.211	< 170
R-2	4.18	5,520	105	35	1,520	0.275	790
R-3	5.79	5,520	67.5	67.5	1,310	0.237	510
R-3'**	4.18	5,520	97.5	0	1,300	0.235	0

* At face of support, neglecting fillets.

** Second test, after failure of end vertical member.

Note:

Construction Joints and Piping Locations not shown.

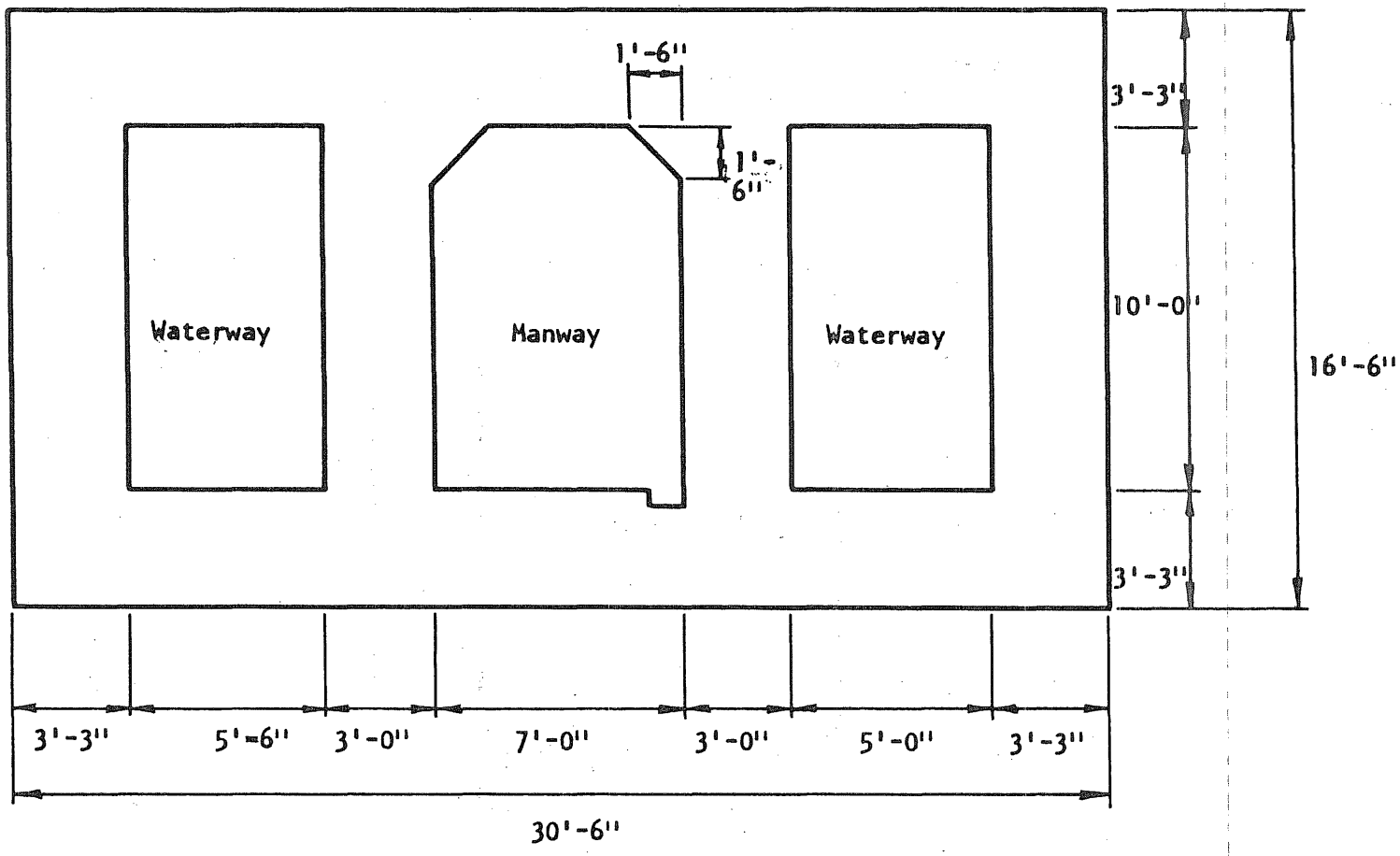

FIG. 1.1 CROSS-SECTION OF CONDUIT THROUGH DAM AT FALL CREEK RESERVOIR, OREGON

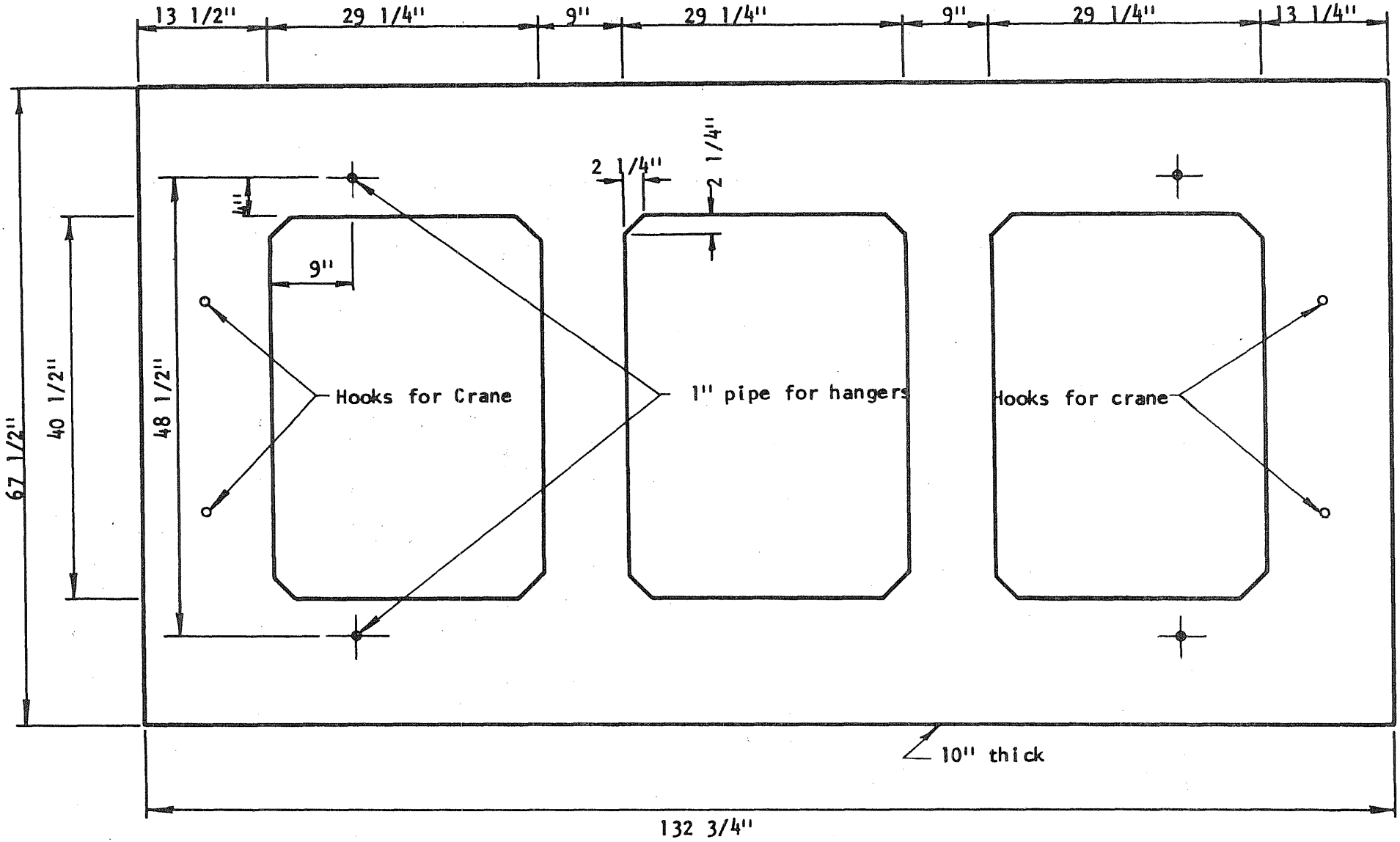

FIG. 2.1 DIMENSIONS OF CONDUIT SPECIMEN R1

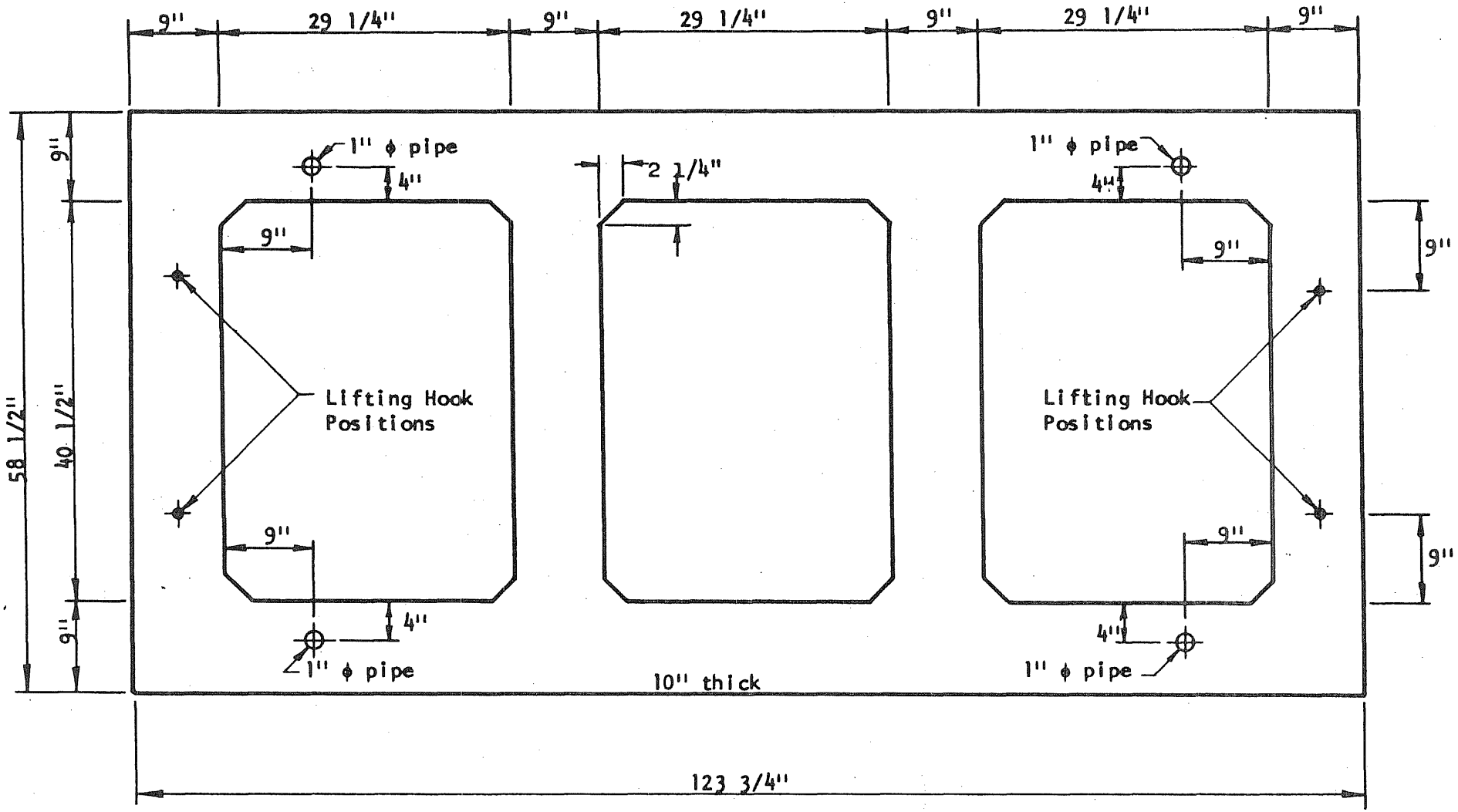

FIG. 2.2 DIMENSIONS OF SPECIMENS R2 AND R3

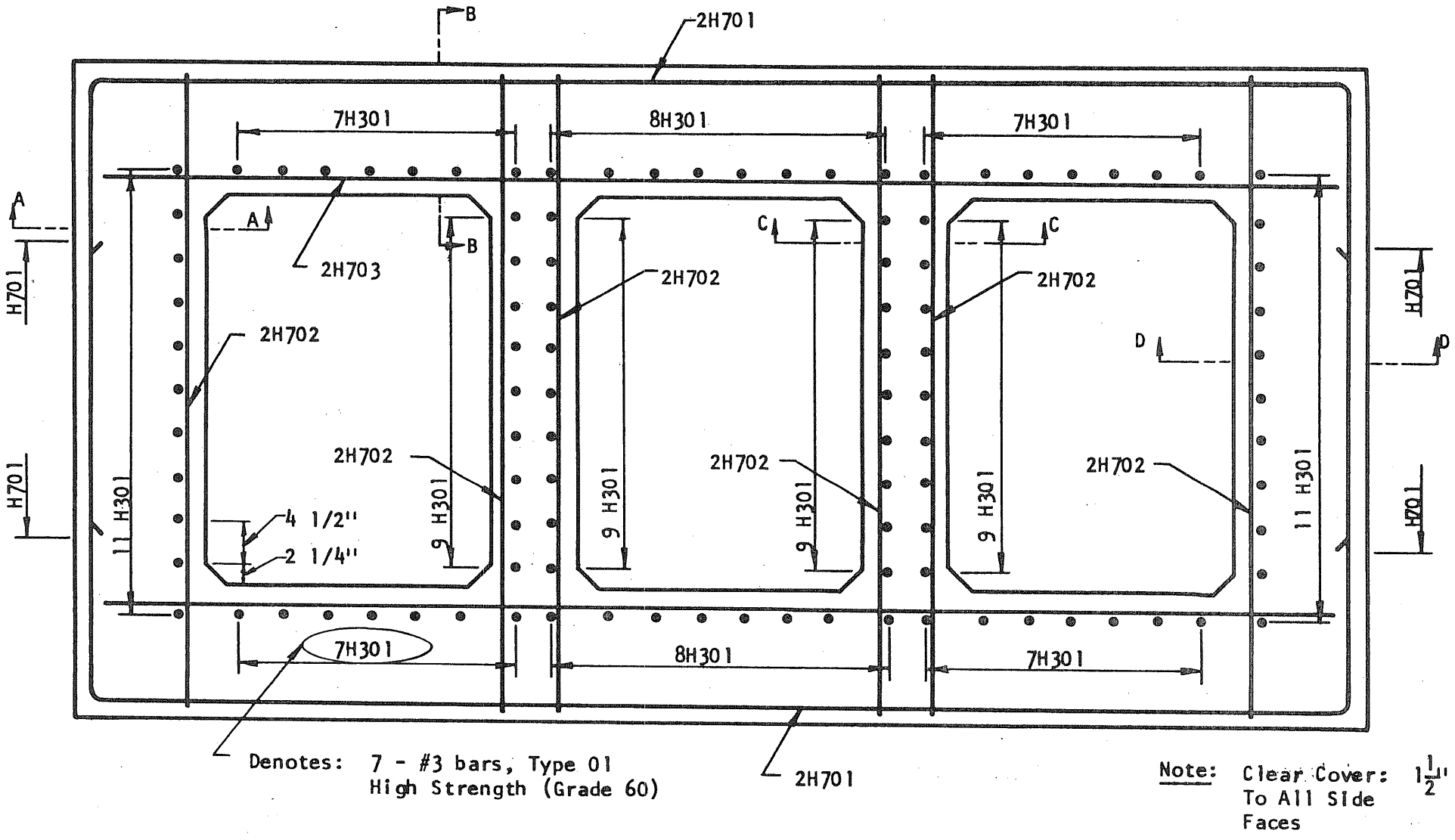

FIG. 2.3 ARRANGEMENT OF REINFORCEMENT IN SPECIMEN R1

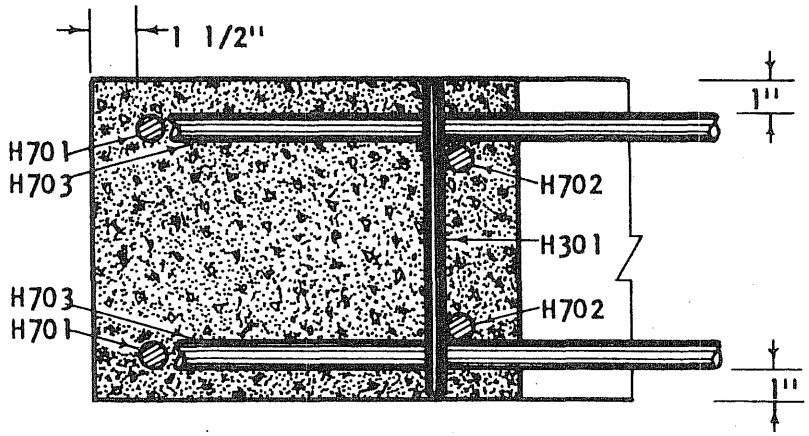

Section A-A

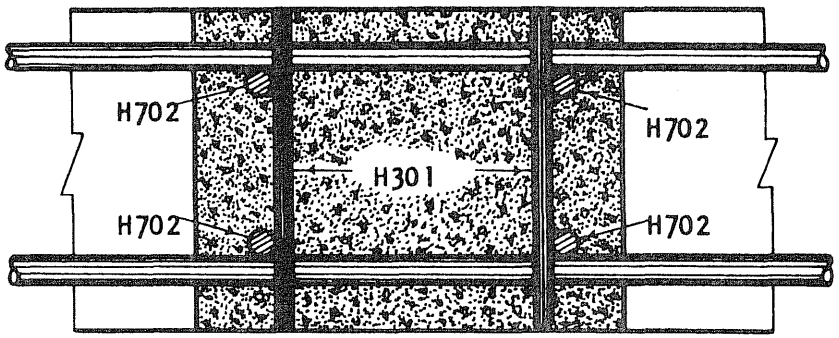

Section C-C

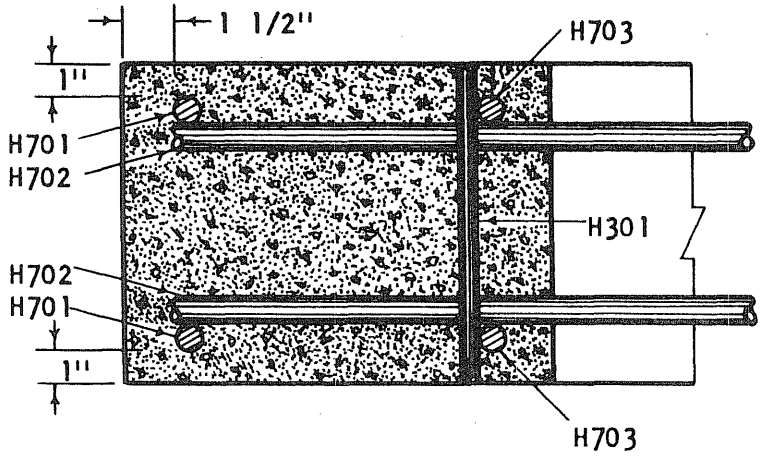

Section B-B

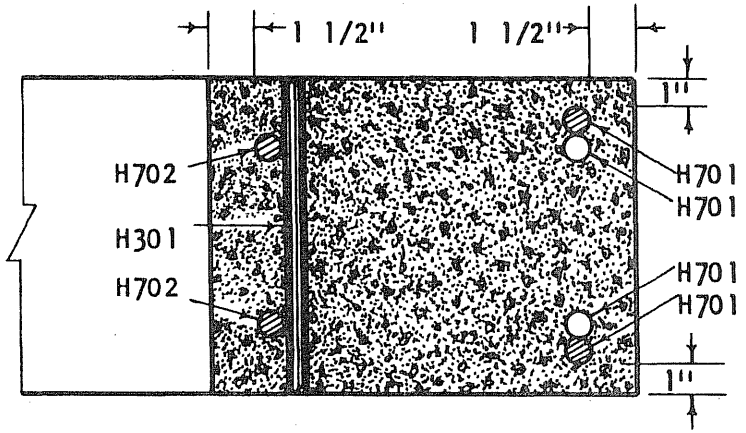

Section D-D

FIG. 2.4 DETAILS OF REINFORCEMENT, SPECIMEN R1

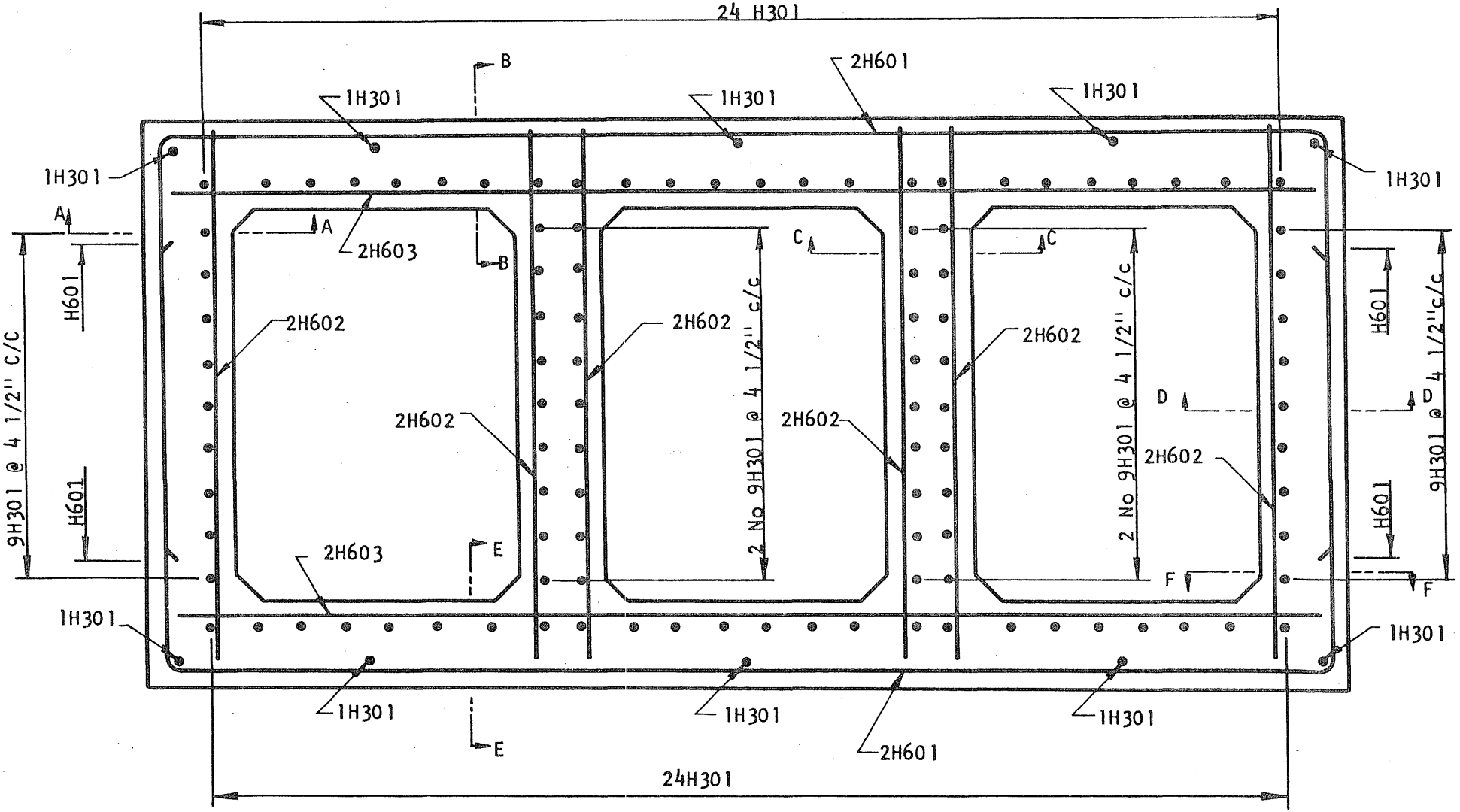

Note: Clear Cover: $1\frac{1}{2}$" To All Side Faces

FIG. 2.5 ARRANGEMENT OF REINFORCEMENT IN SPECIMENS R2 AND R3

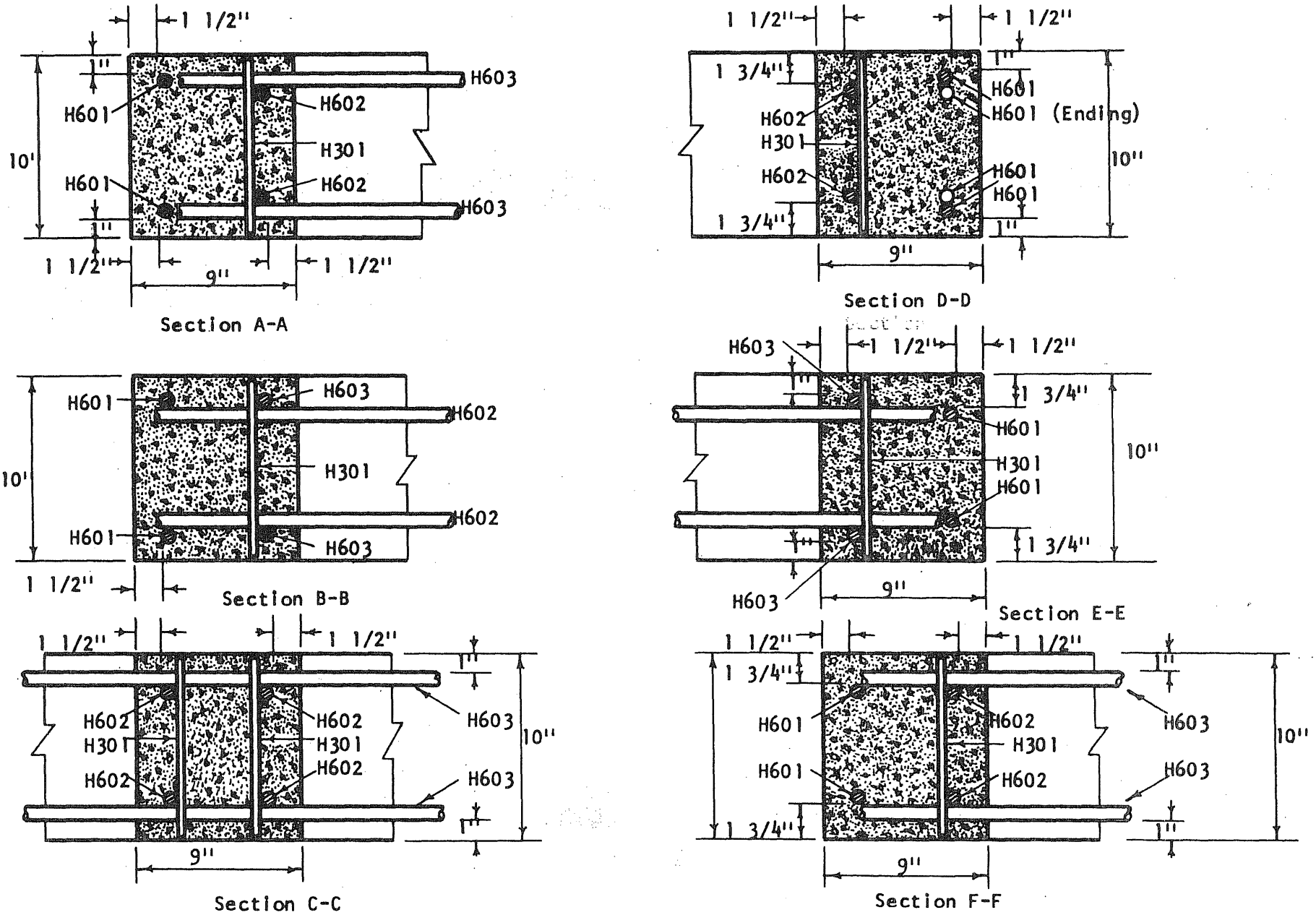

FIG. 2.6 DETAILS OF REINFORCEMENT, SPECIMENS R2 and R3

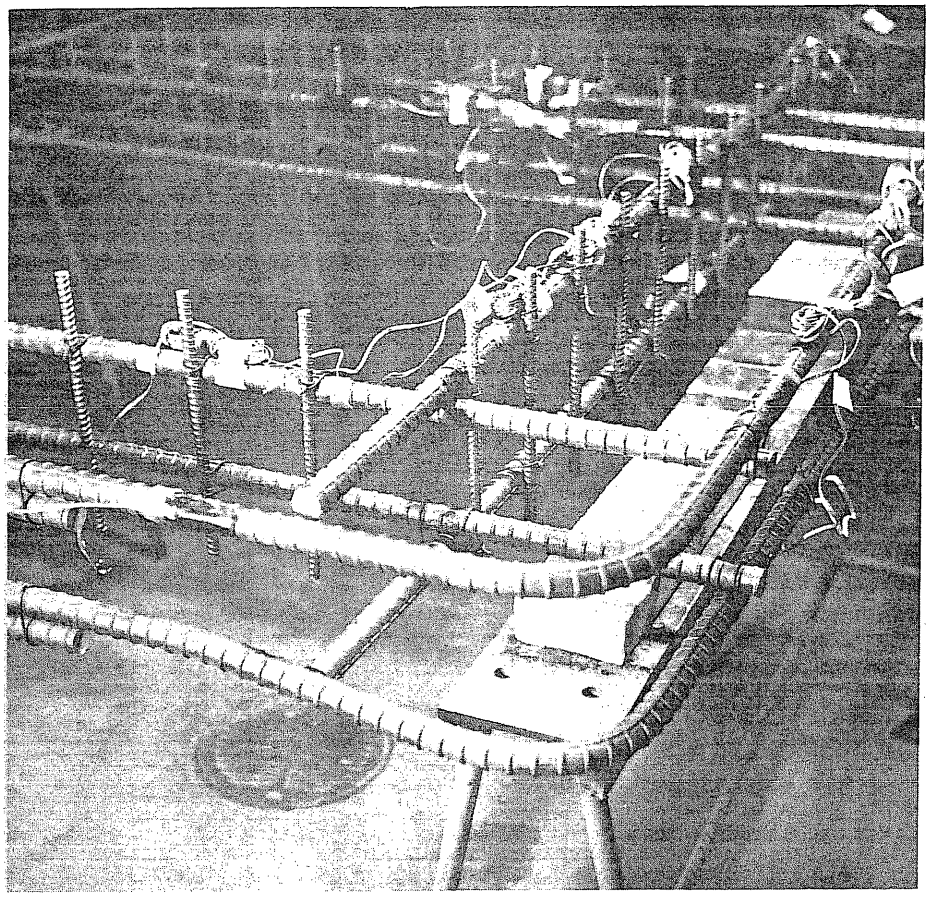

FIG. 2.7 PHOTOGRAPH OF CORNER REINFORCEMENT DETAIL, SPECIMEN R1

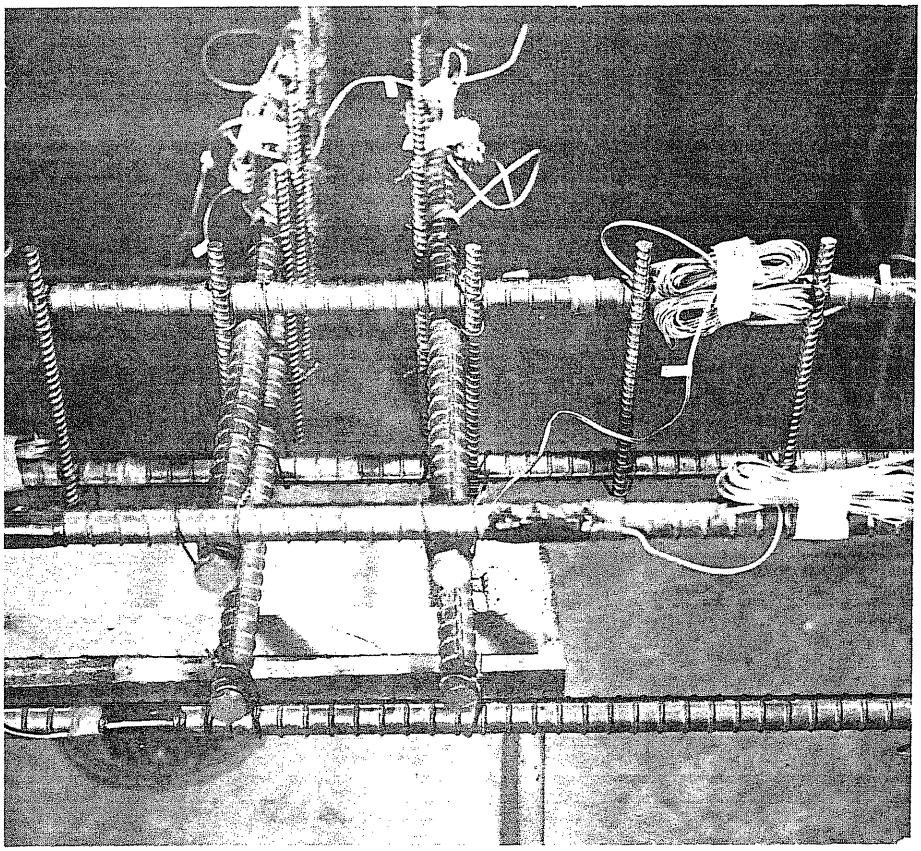

FIG. 2.8 PHOTOGRAPH OF REINFORCEMENT AT INTERIOR COLUMN-EDGE MEMBER JOINT, SPECIMEN R1

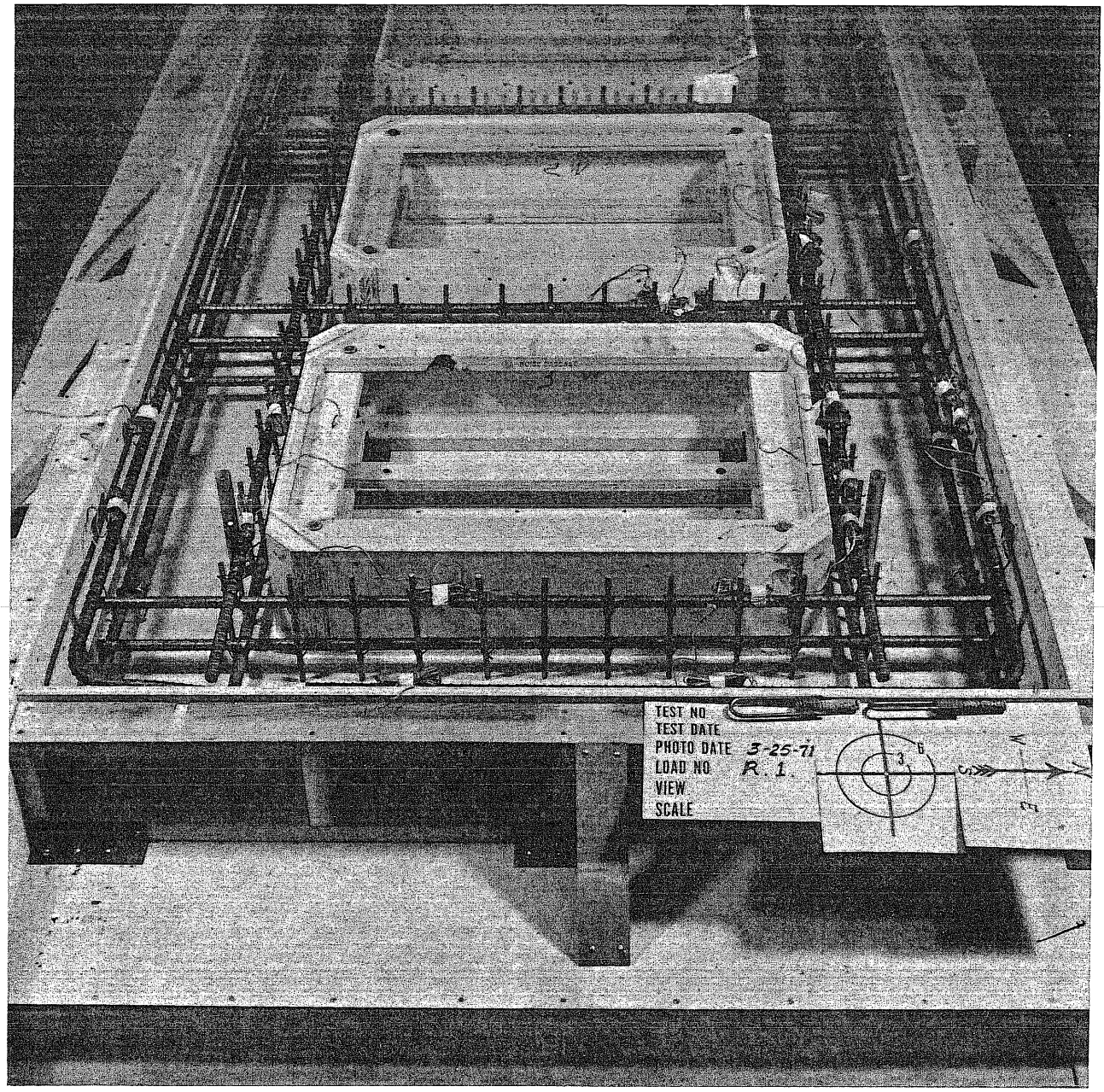

FIG. 2.9 PHOTOGRAPH OF SPECIMEN R1 REINFORCEMENT IN FORMWORK

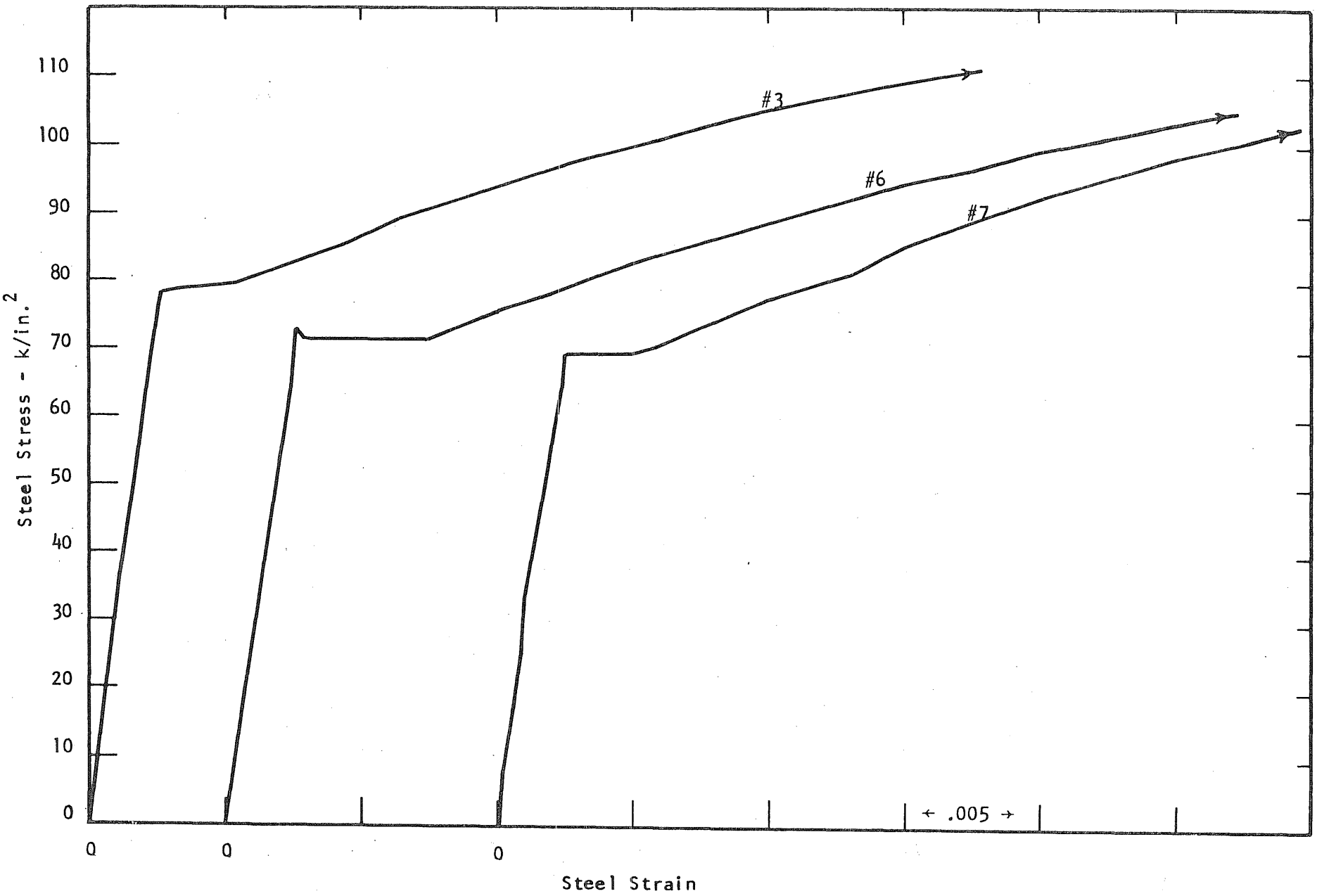

FIG. 3.1 TYPICAL STRESS-STRAIN RELATIONSHIPS FOR REINFORCING STEEL

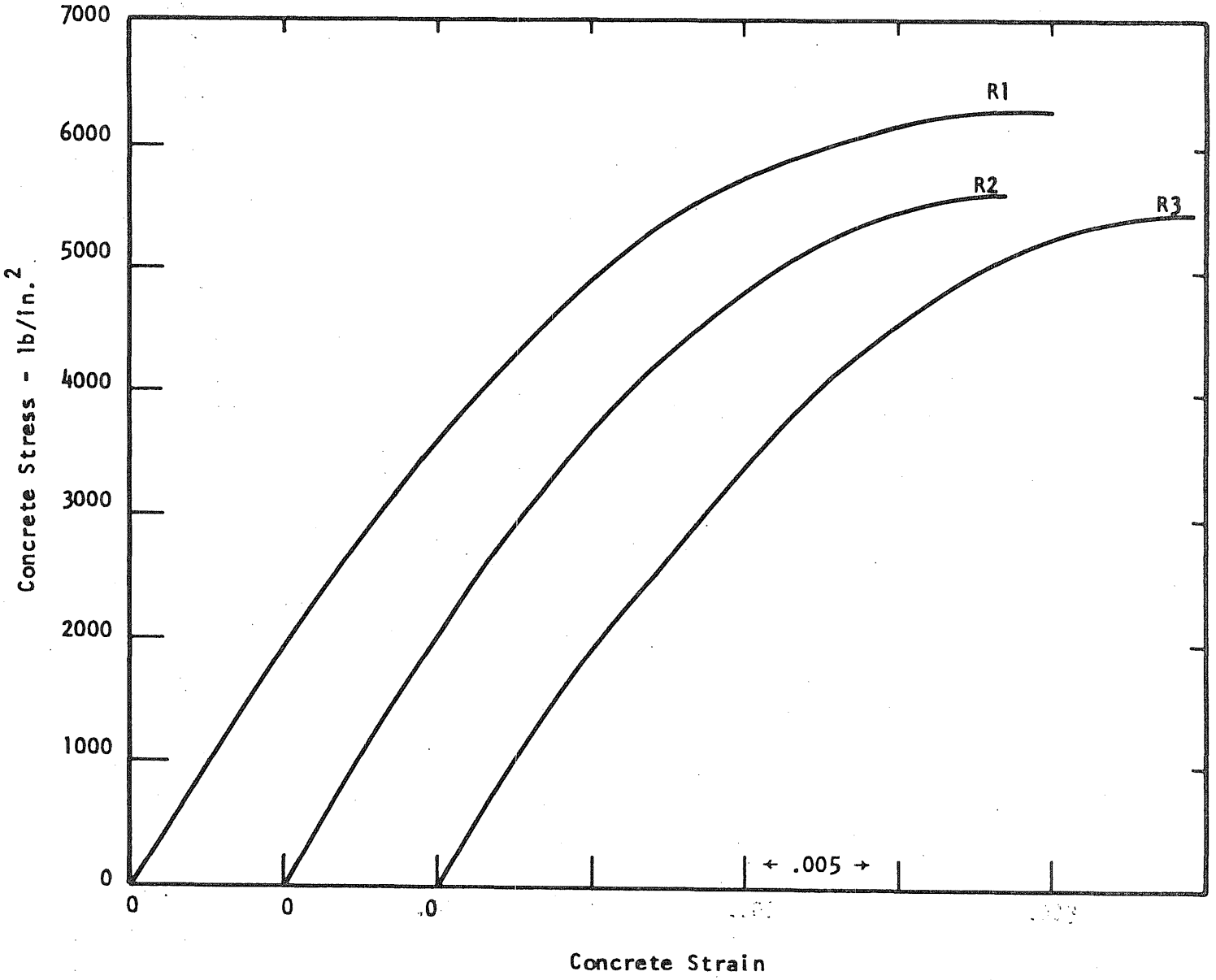

FIG. 3.2 REPRESENTATIVE STRESS-STRAIN CURVES FOR CONCRETE FROM TEST SPECIMENS

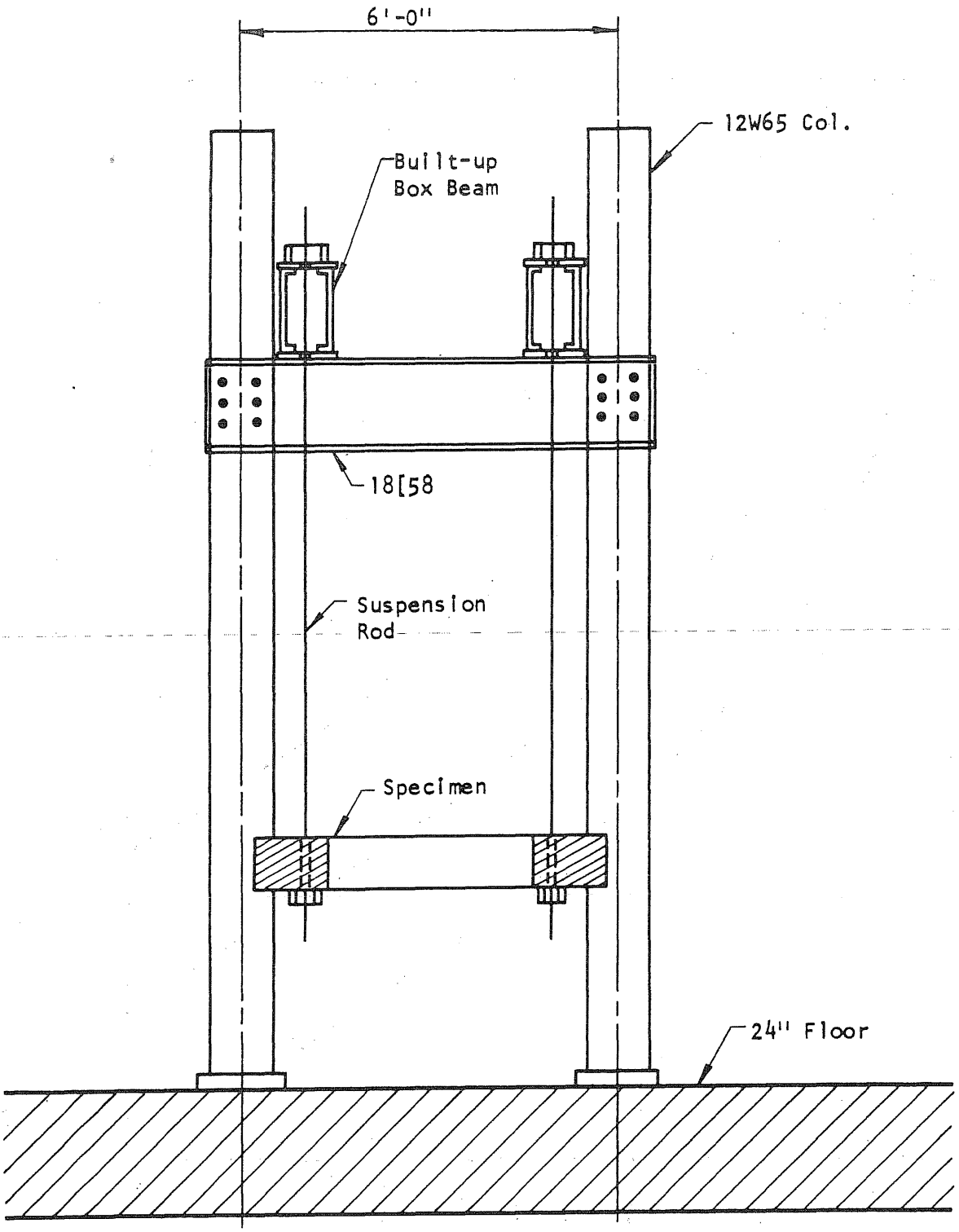

FIG. 4.1 END ELEVATION OF TEST FRAME WITH SPECIMEN IN PLACE

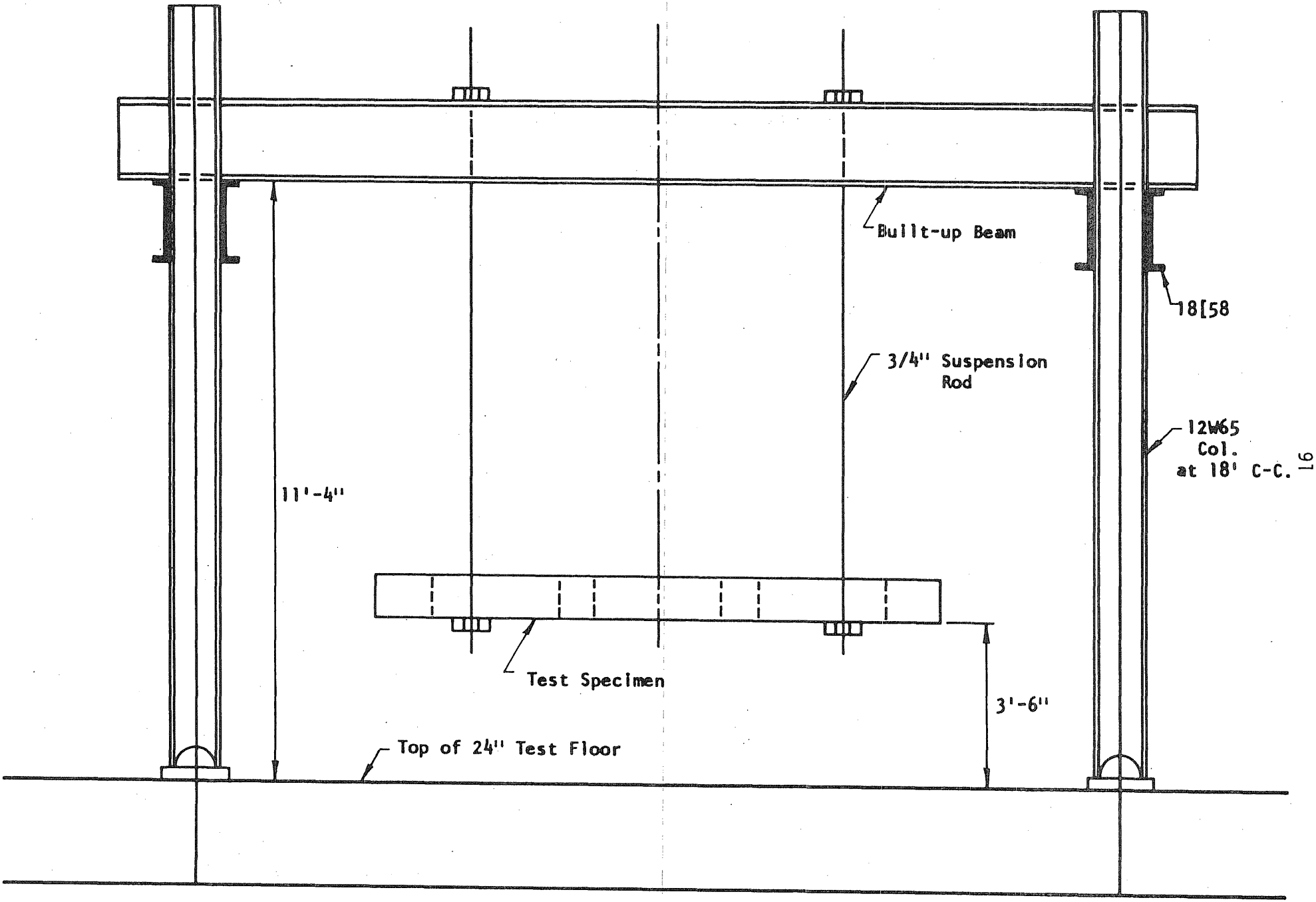

FIG. 4.2 SIDE ELEVATION OF TEST FRAME WITH SPECIMEN IN PLACE

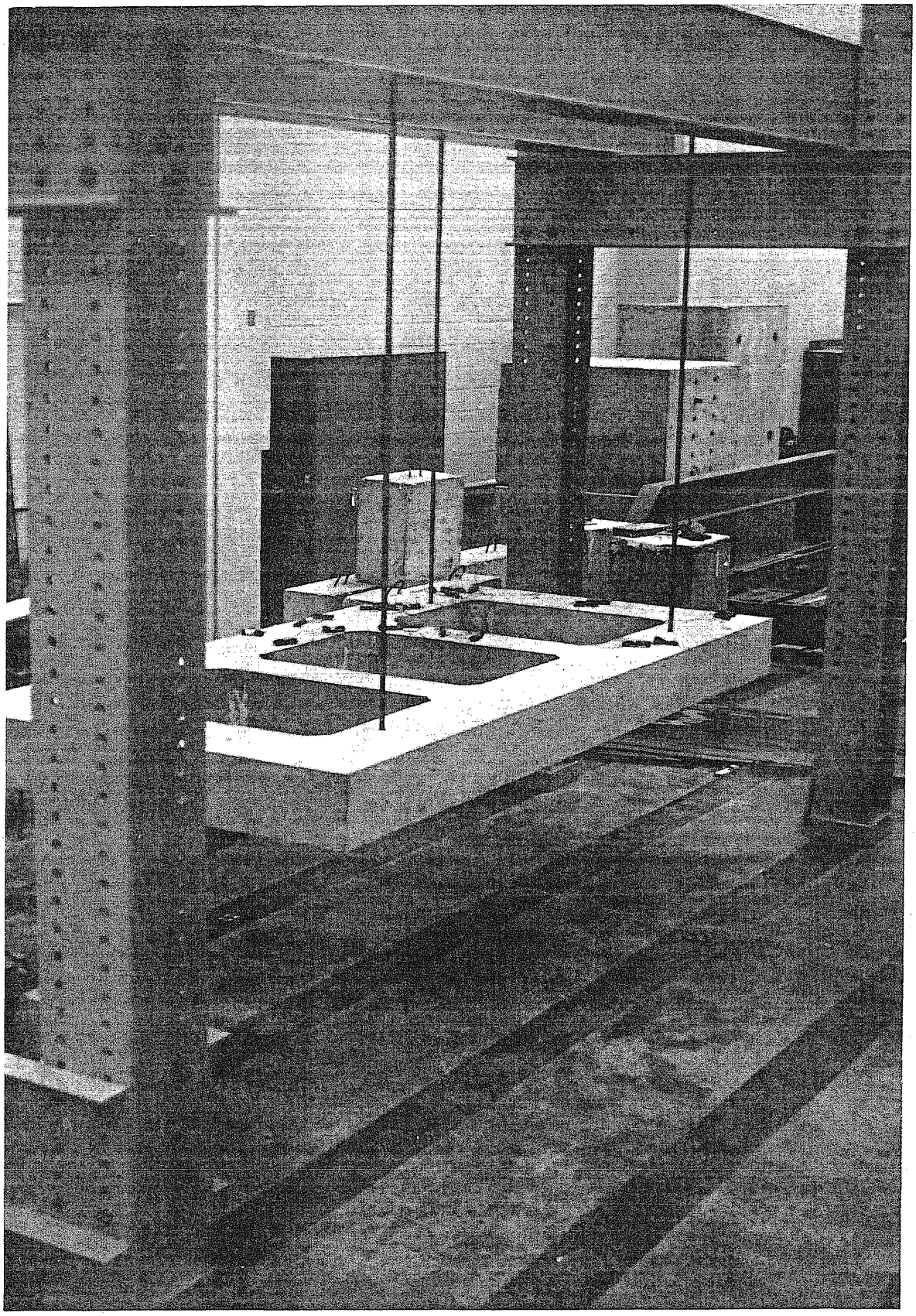

FIG. 4.3 PHOTOGRAPH OF SPECIMEN R1 IN TEST FRAME BEFORE ASSEMBLY OF LEADING EQUIPMENT

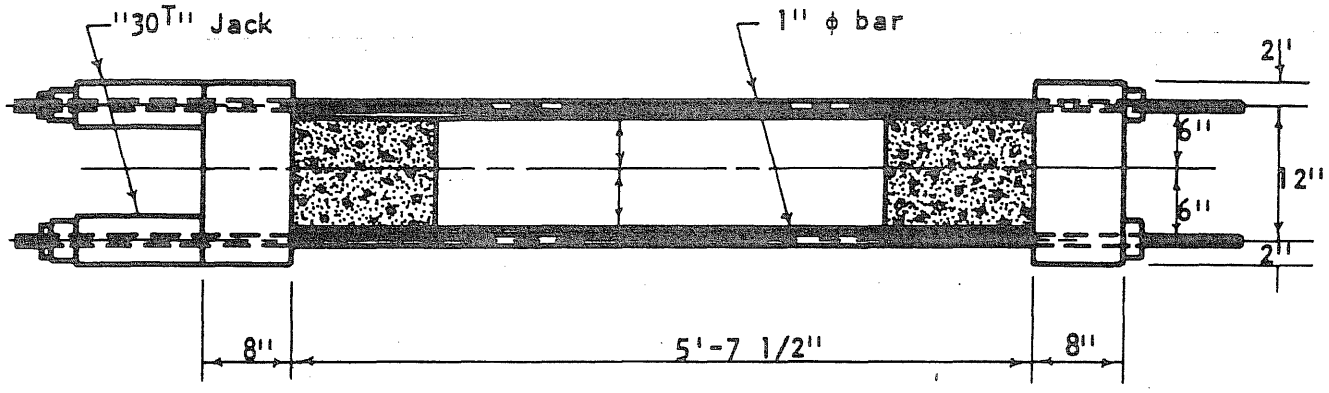

P_V DIRECTION

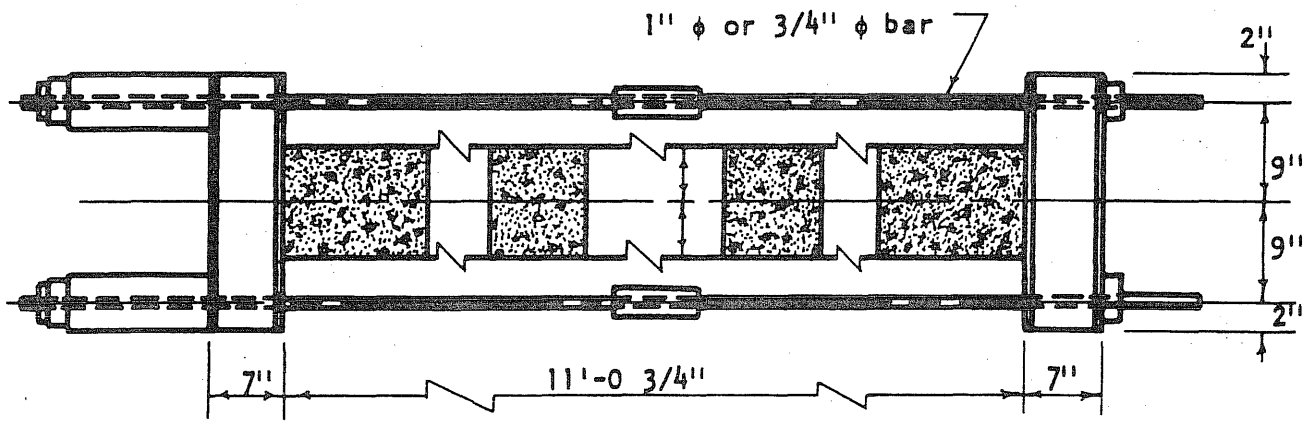

P_H DIRECTION

FIG. 4.4 ARRANGEMENT OF LOADING UNITS

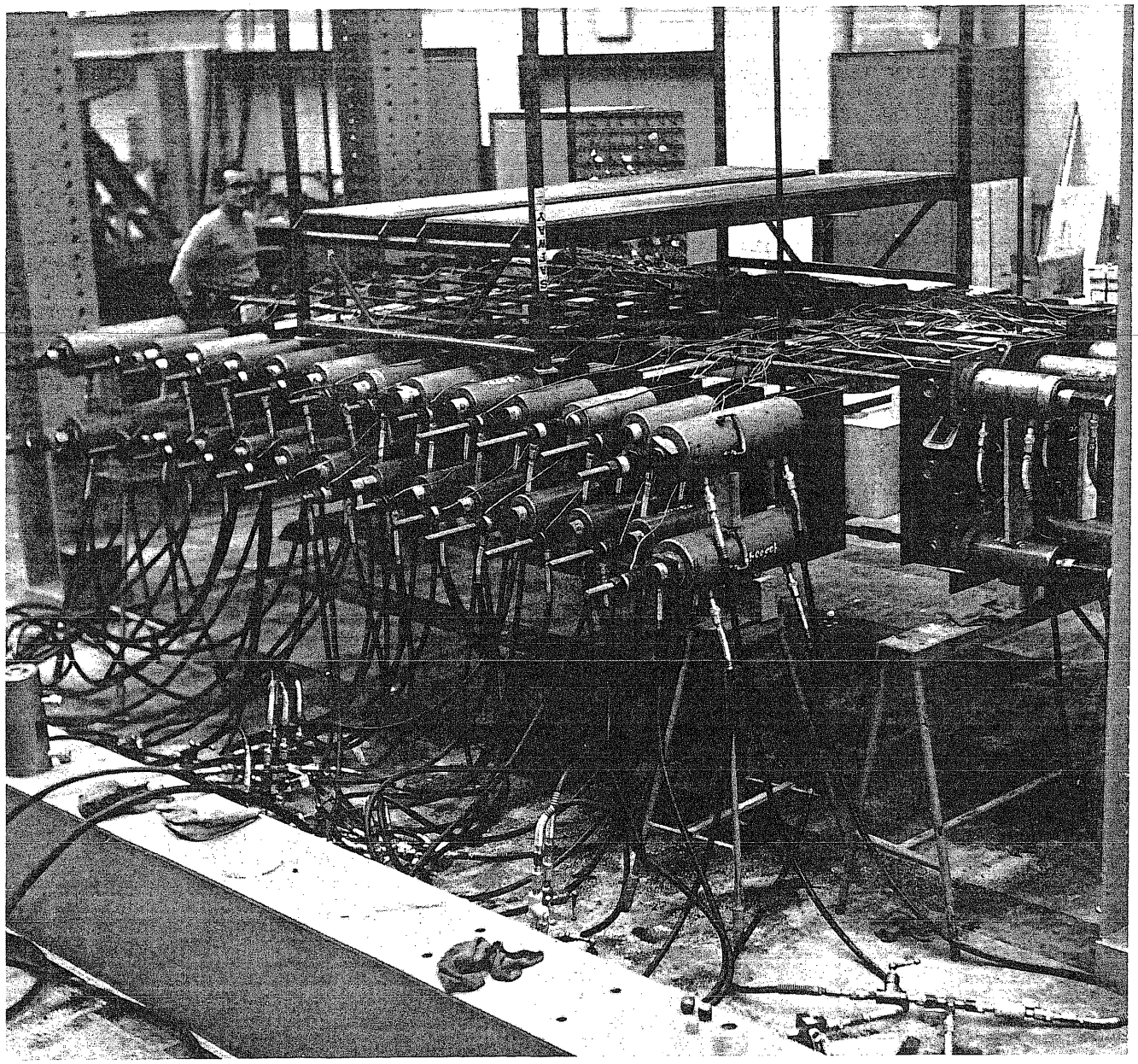

FIG. 4.5 PHOTOGRAPH OF SPECIMEN R1 WITH LOADING EQUIPMENT IN PLACE

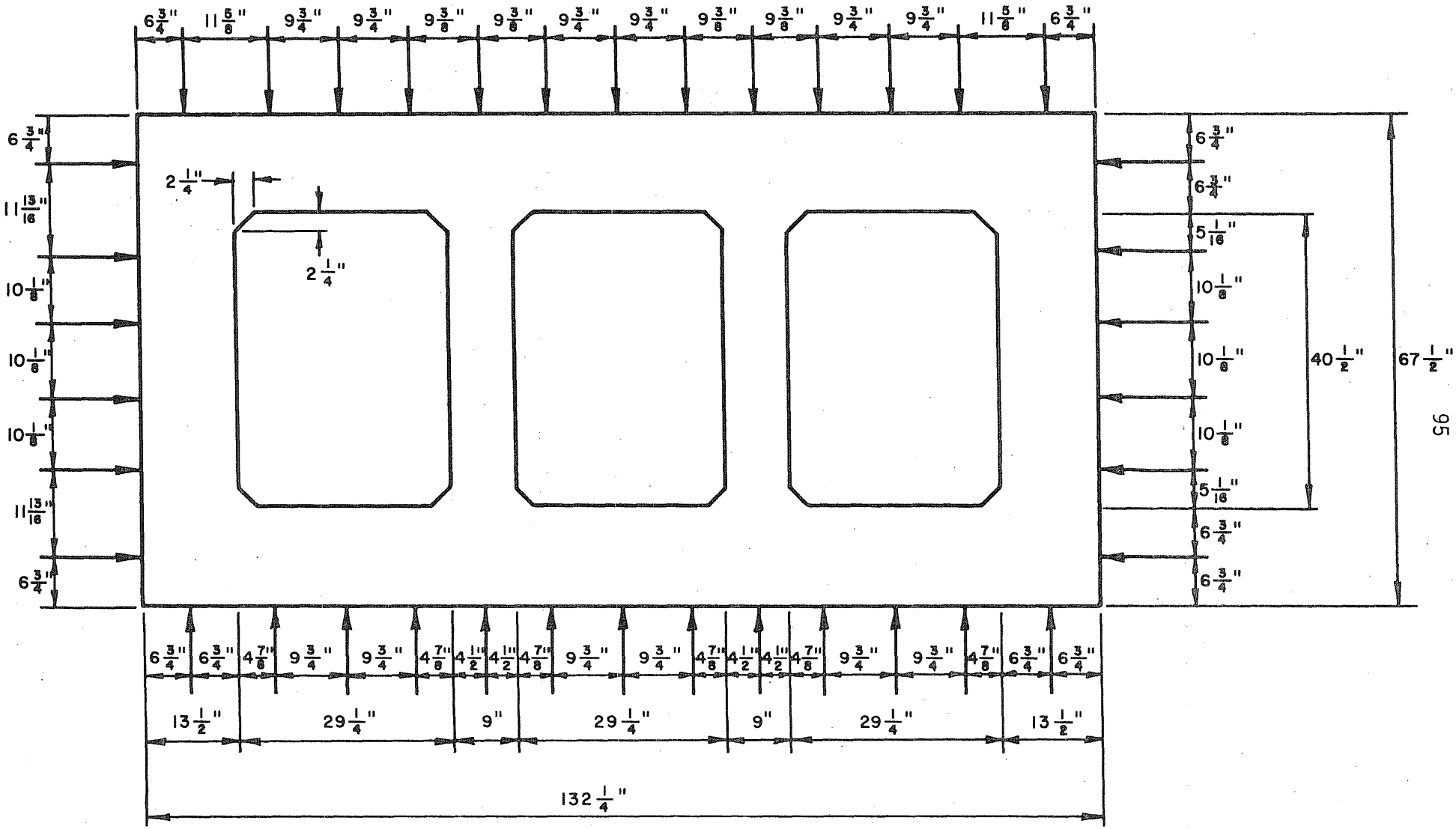

Note : All Jacks Are In Pairs

FIG. 4.6 SPACING OF LOADS FOR SPECIMEN R1

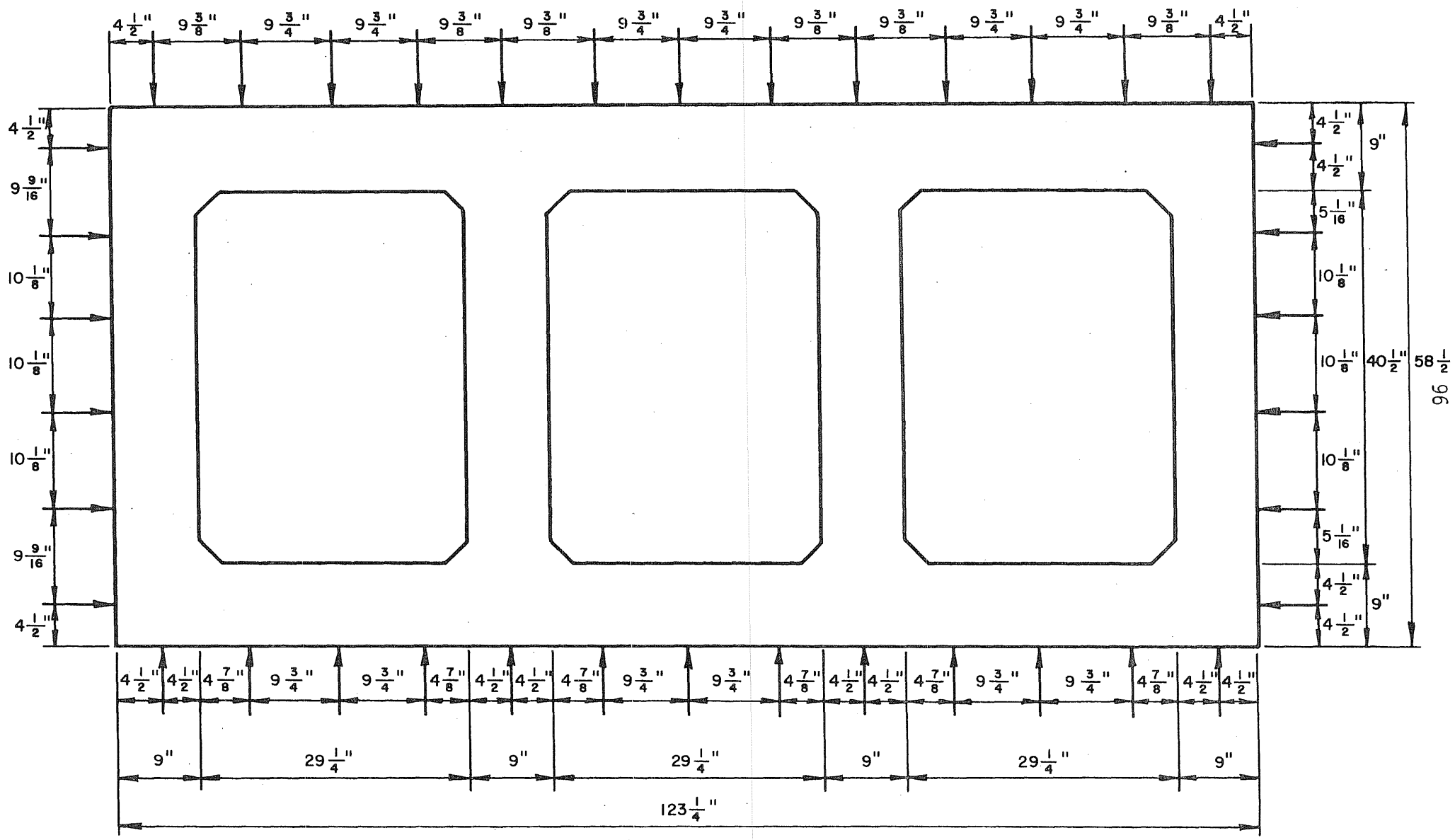

FIG. 4.7 LOCATIONS OF LOADING UNITS FOR SPECIMENS R2 and R3

Strain gages attached to top layer of steel unless noted otherwise.

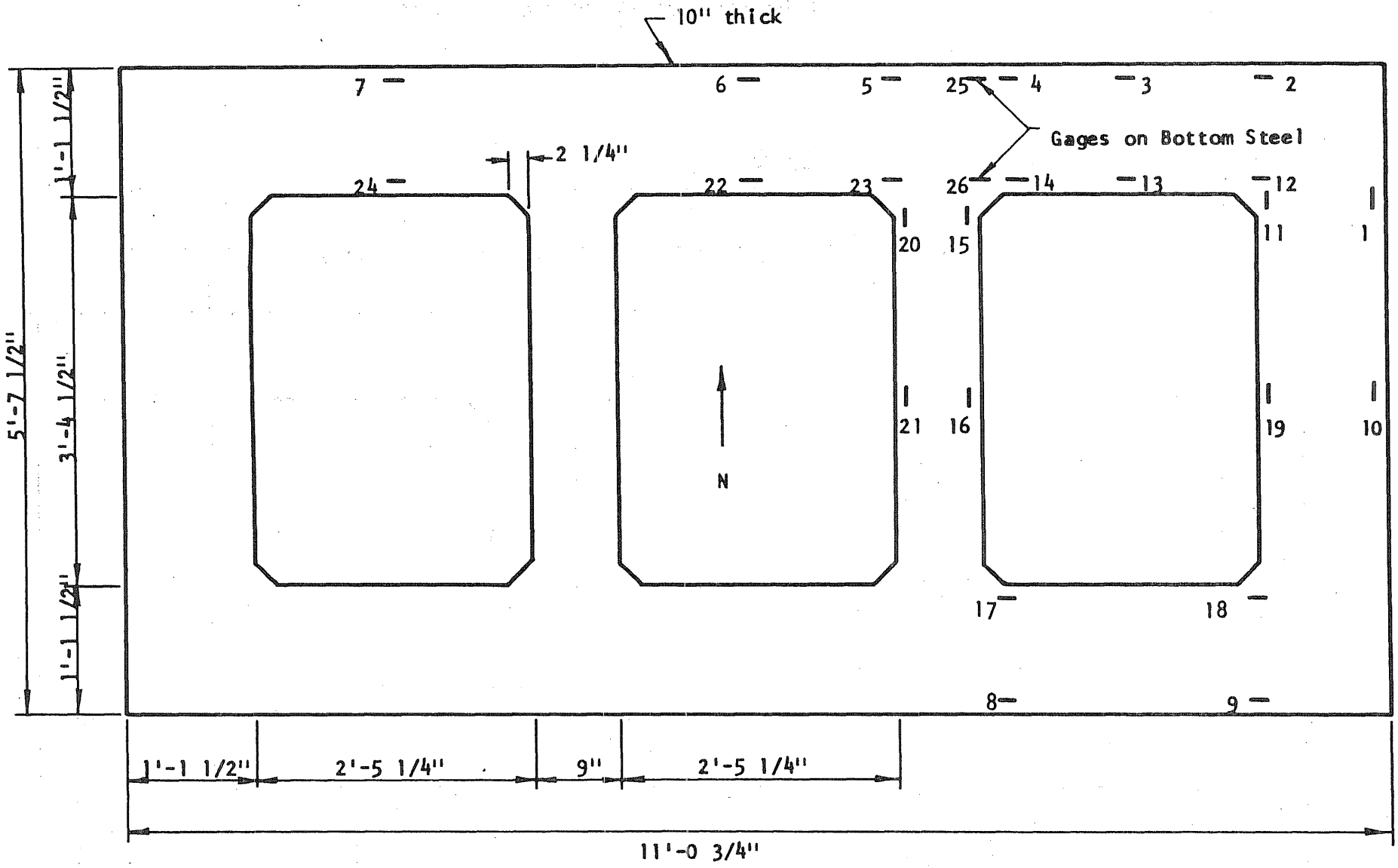

FIG. 5.1 LOCATIONS OF STRAIN GAGES IN SPECIMEN R1

Strain gages attached to upper layer of steel unless otherwise noted.

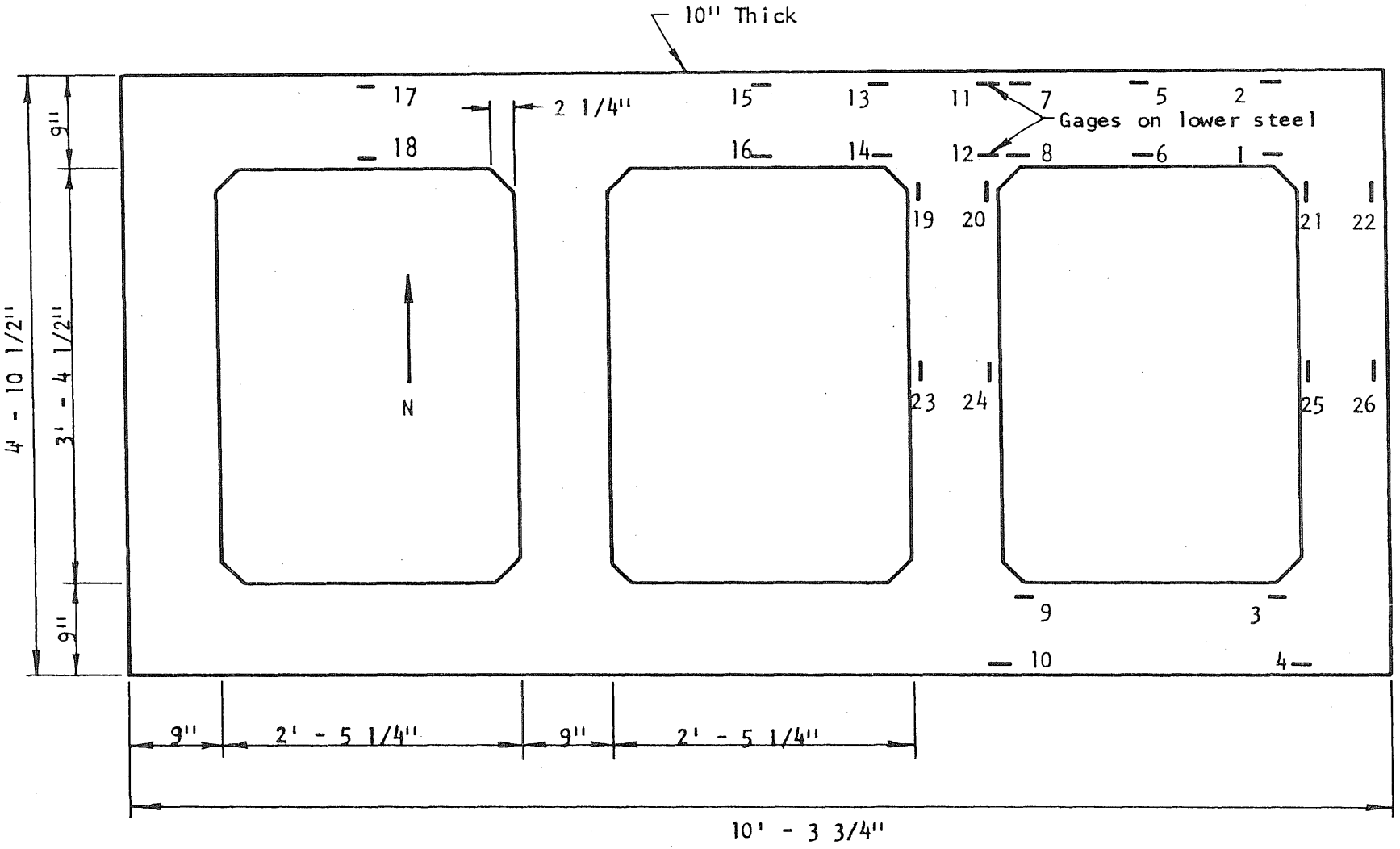

FIG. 5.2 LOCATIONS OF STRAIN GAGES IN SPECIMEN R2

Strain gages attached to upper layer of steel unless otherwise noted.

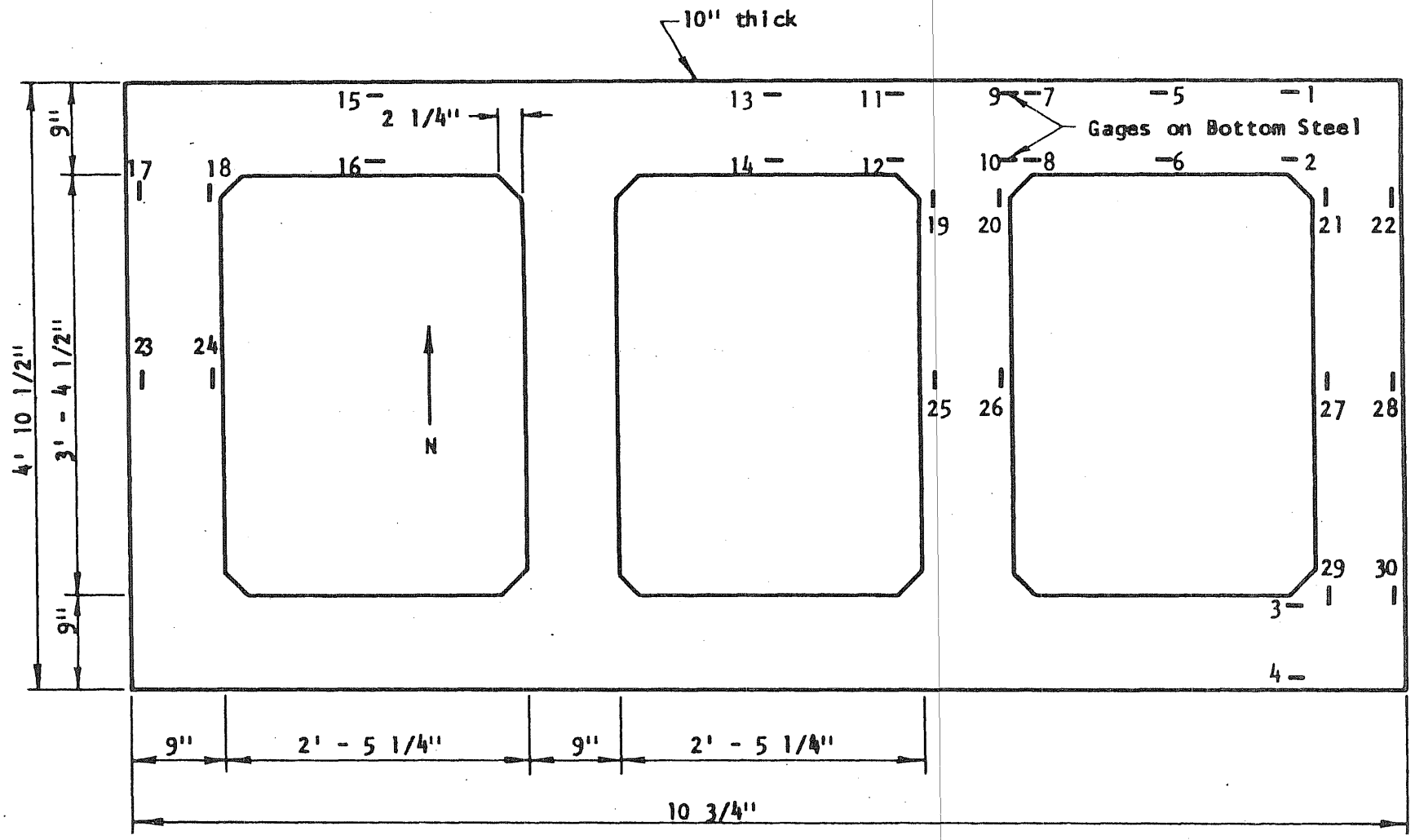

FIG. 5.3 LOCATIONS OF STRAIN GAGES IN SPECIMEN R3

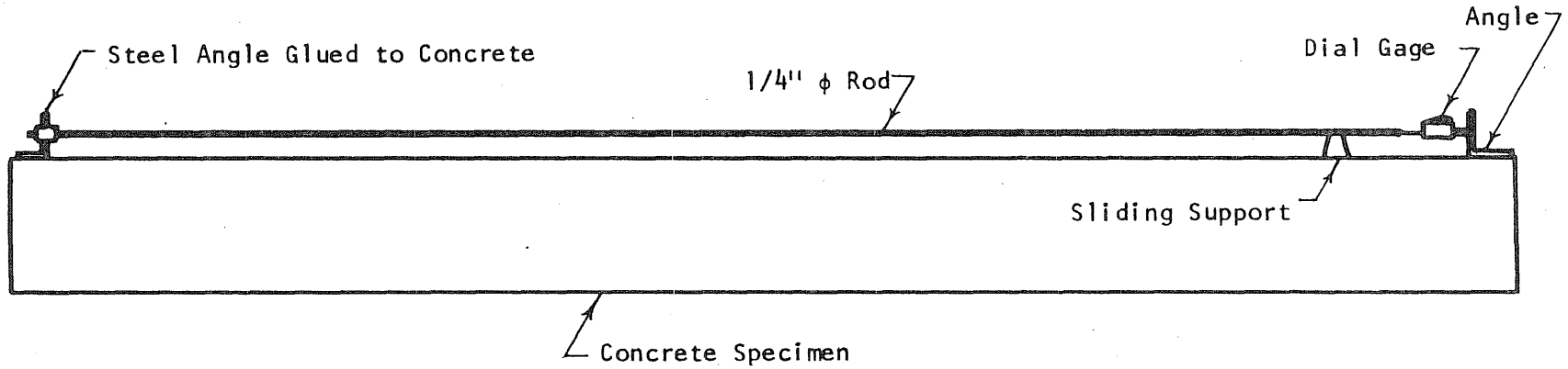

FIG. 5.4 ARRANGEMENT OF DIAL GAGE FOR MEASURING LENGTH CHANGE IN SPECIMEN

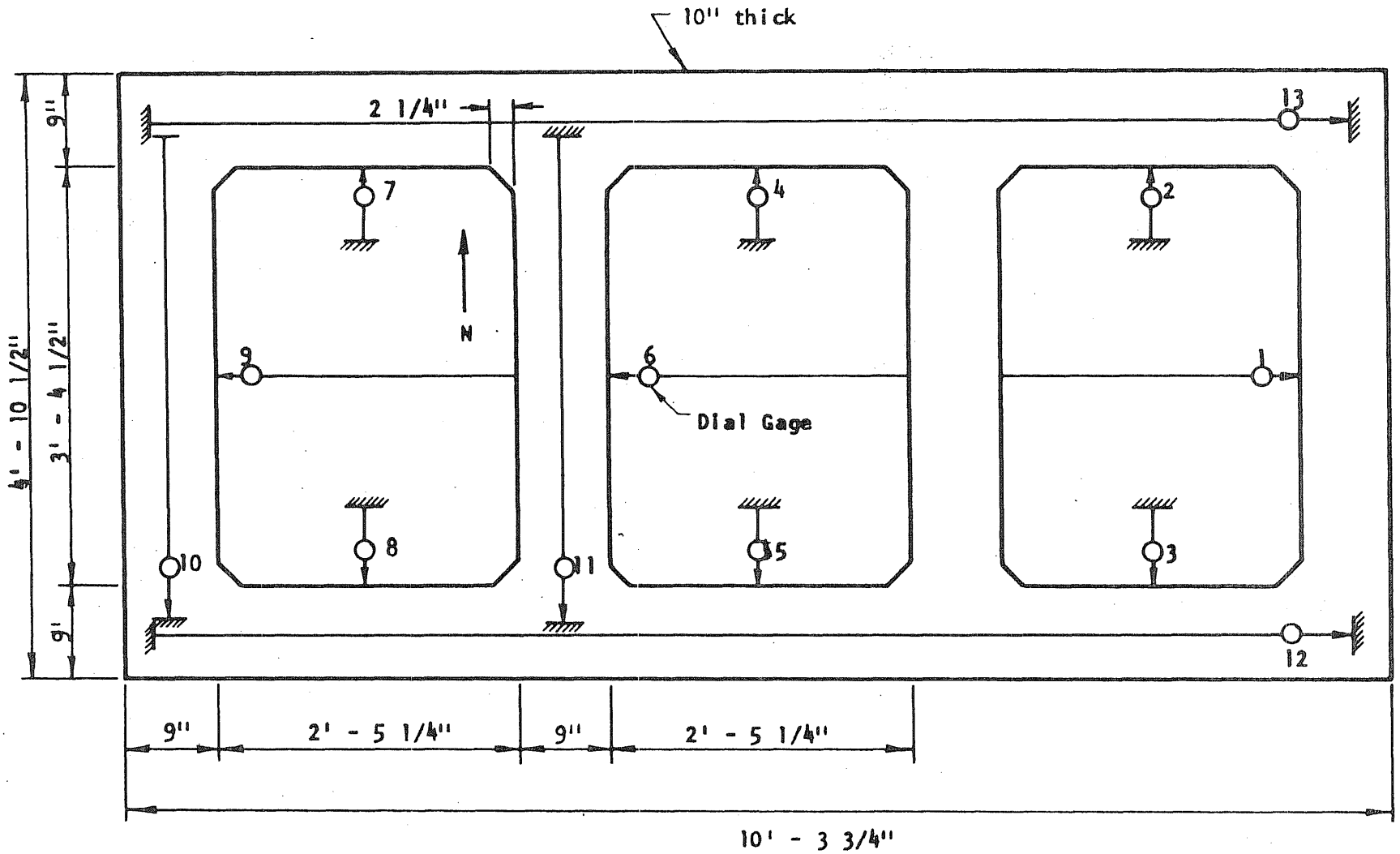

FIG. 5.5 LOCATIONS AND DESIGNATIONS OF DEFLECTION GAGES

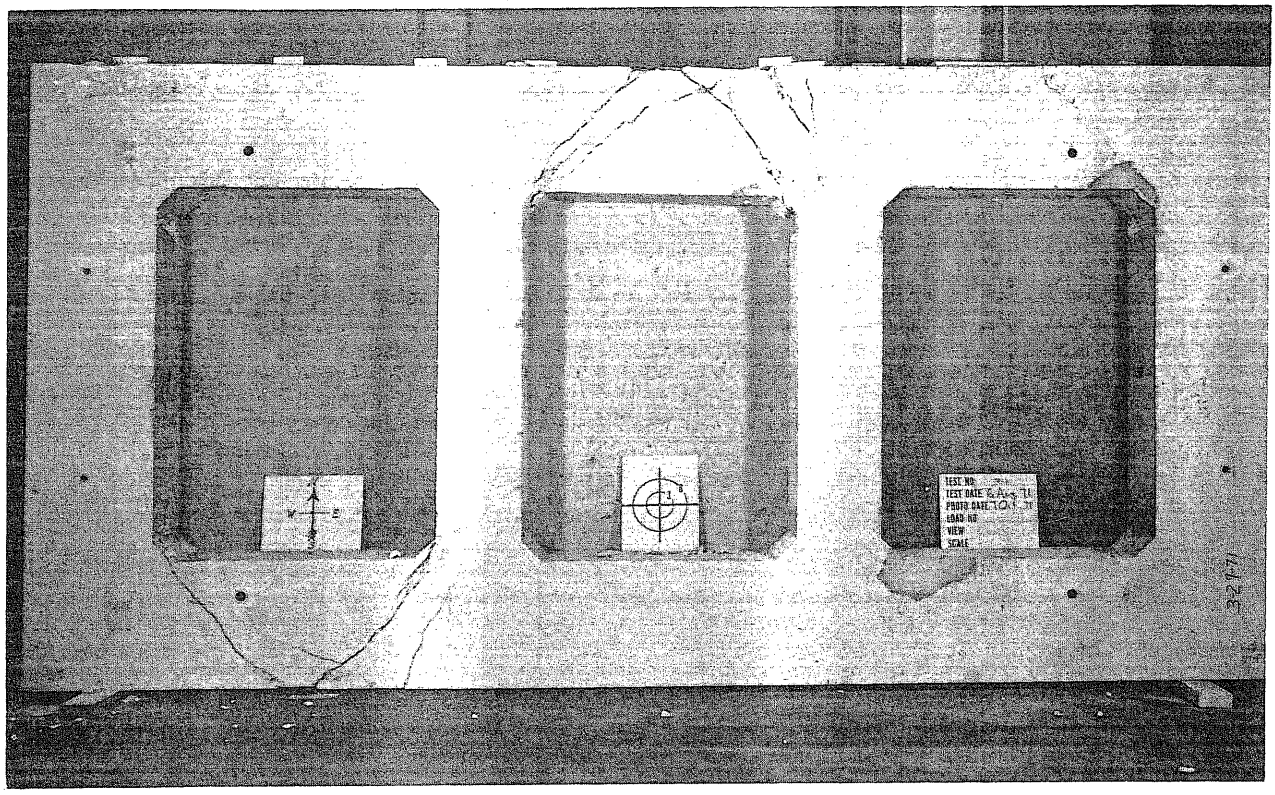

FIG. 7.1 SPECIMEN R1 AFTER TEST TO FAILURE

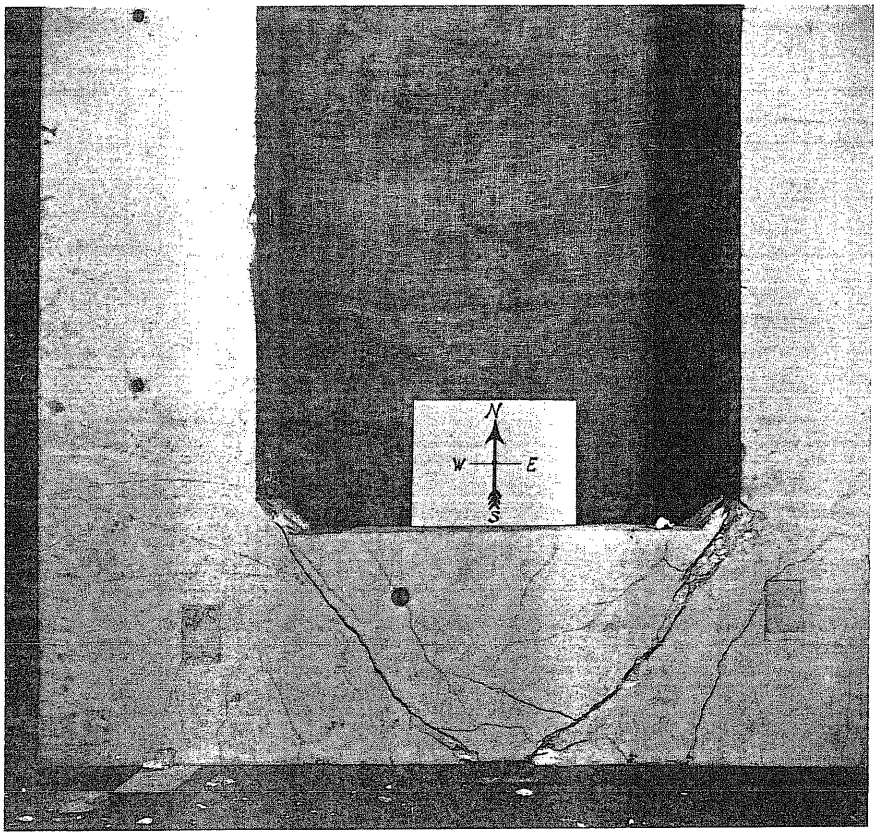

FIG. 7.2 FAILED END SPAN OF SPECIMEN R1

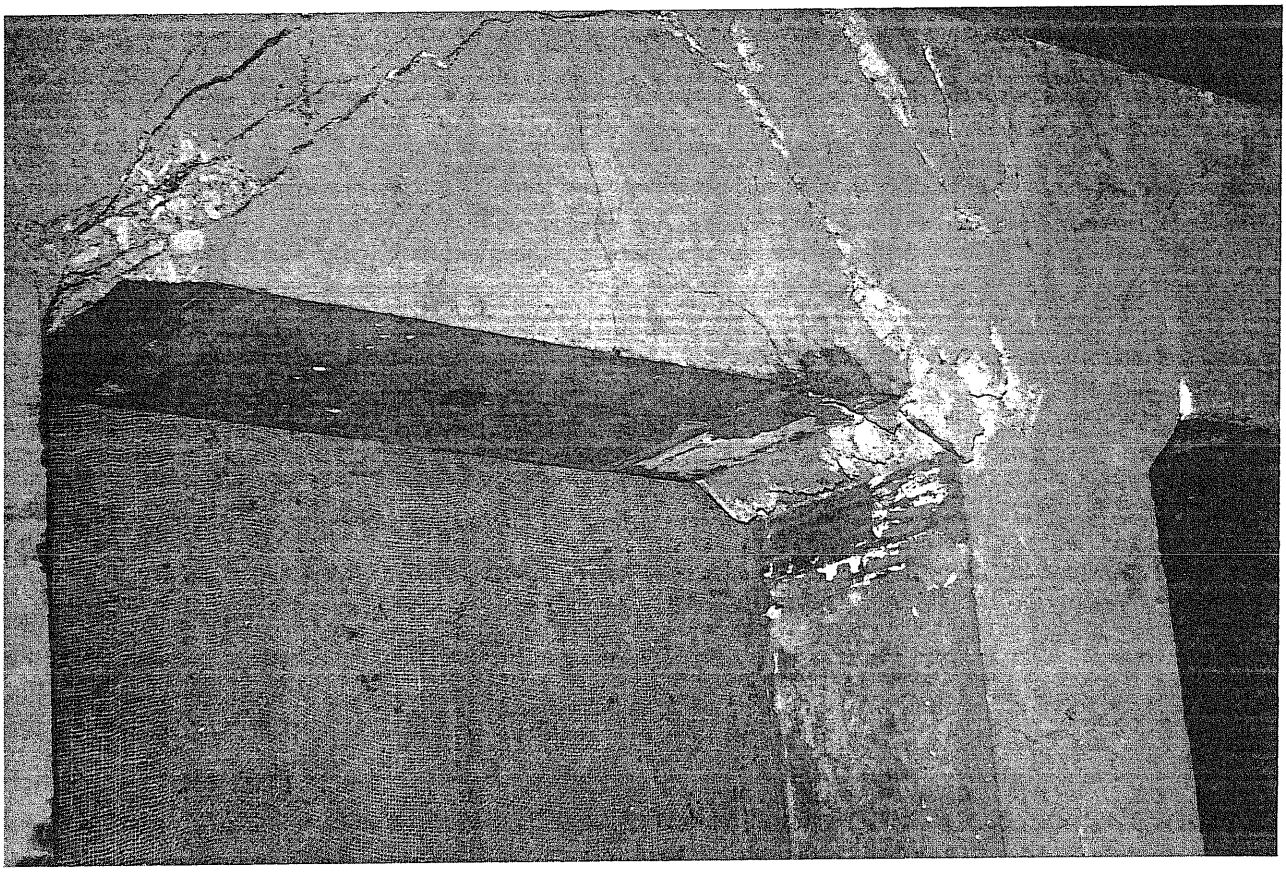

FIG. 7.3 INSIDE FACE OF INTERIOR SPAN, SPECIMEN R1

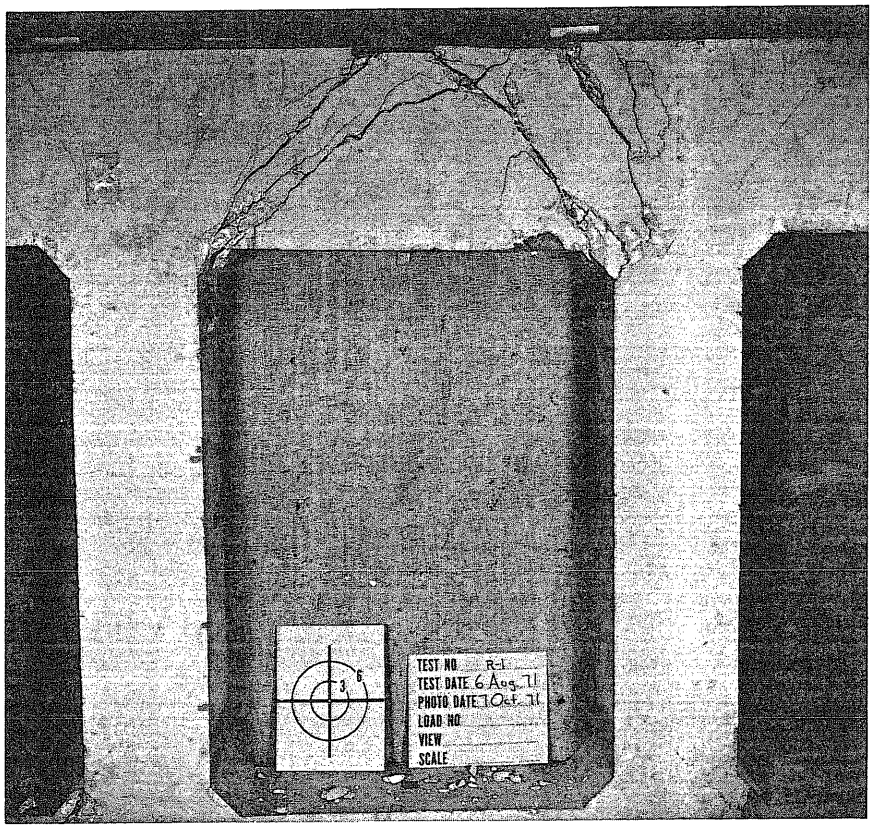

FIG. 7.4 FAILED INTERIOR SPAN OF SPECIMEN R1

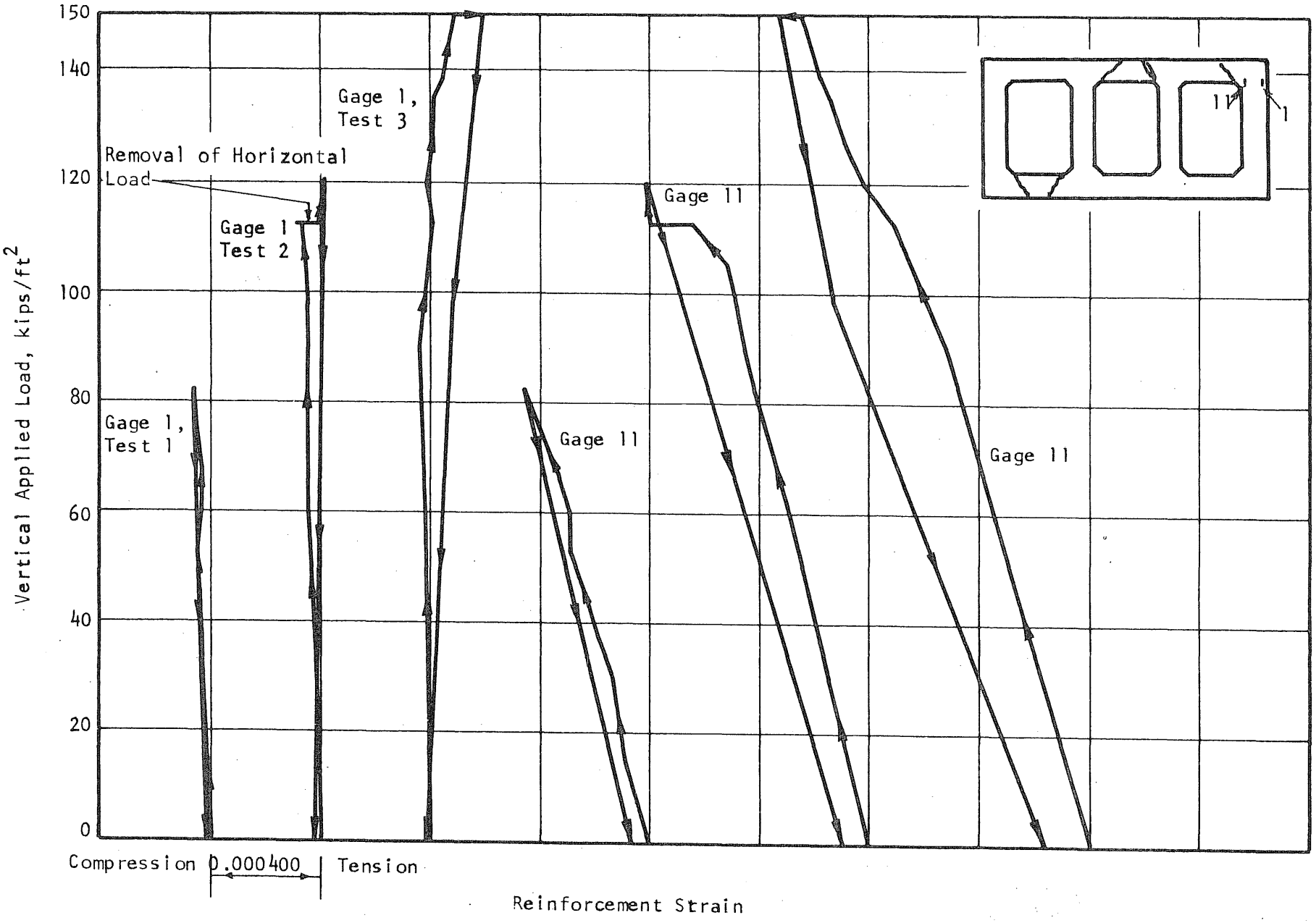

FIG. 7.5 LOAD-STRAIN CURVES, TOP OF END VERTICAL MEMBER, R1

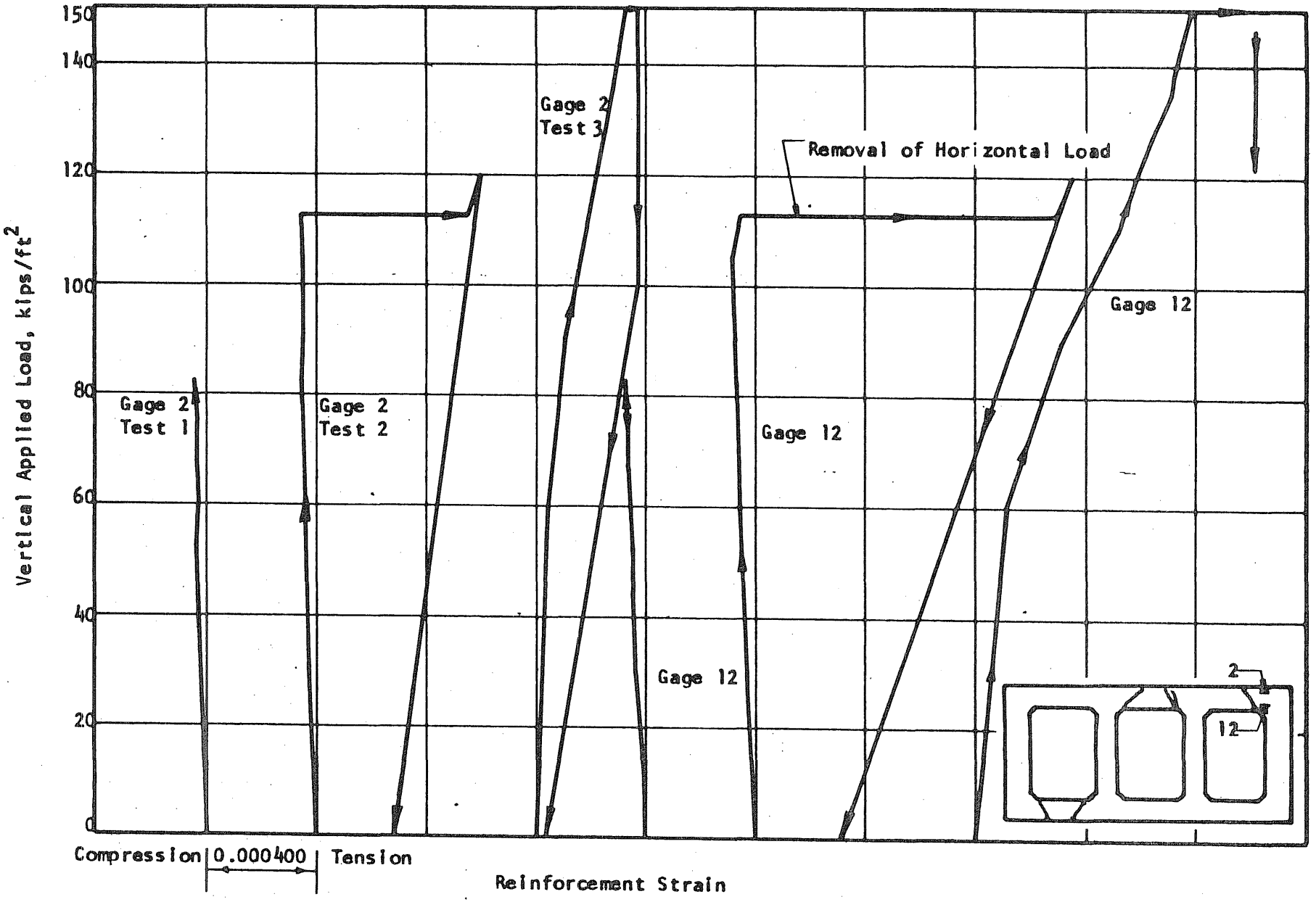

FIG. 7.6 LOAD-STRAIN CURVES, OUTER END OF END SPAN, R1

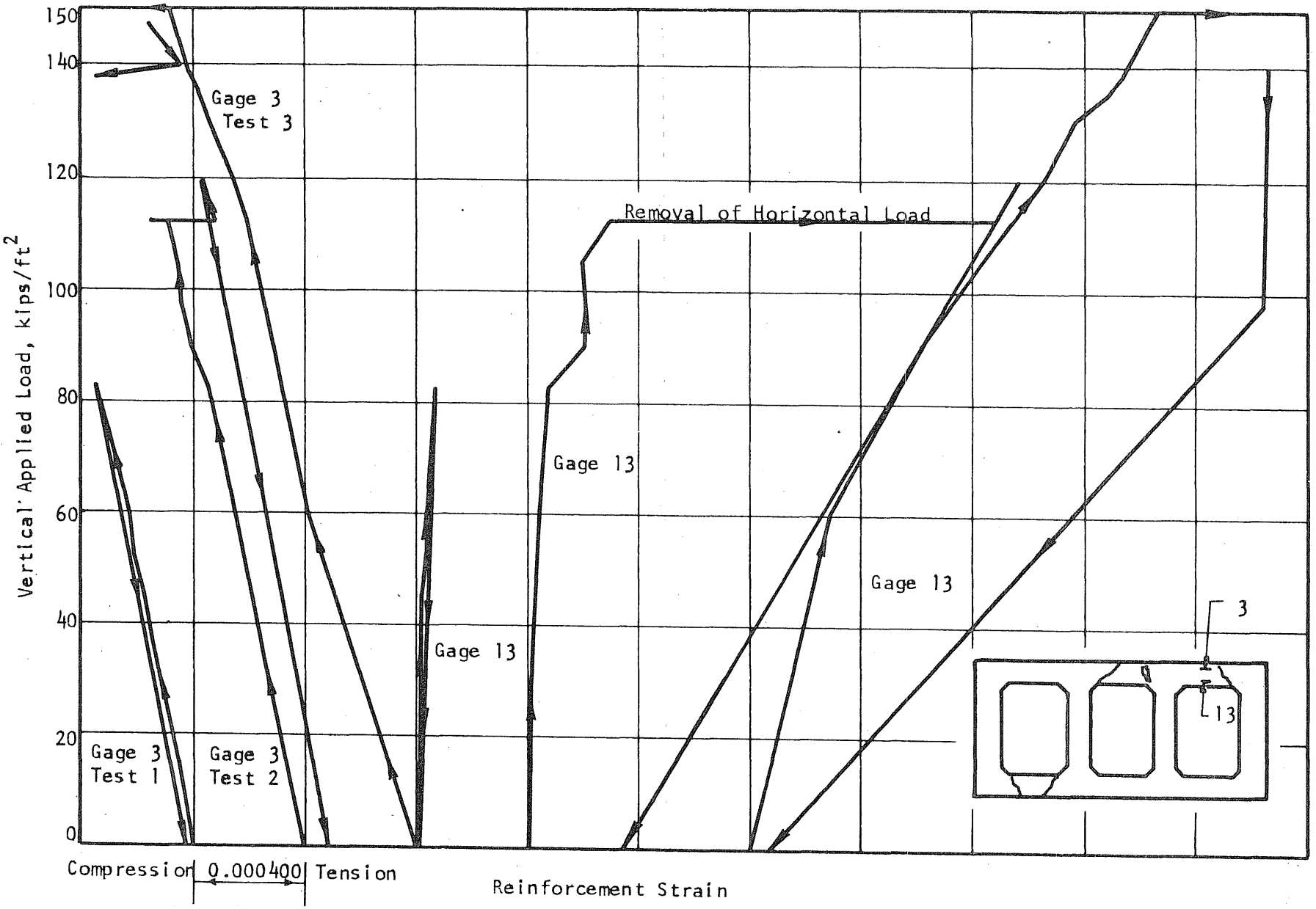

FIG. 7.7 LOAD-STRAIN CURVES, MIDSPAN OF END SPAN, R1

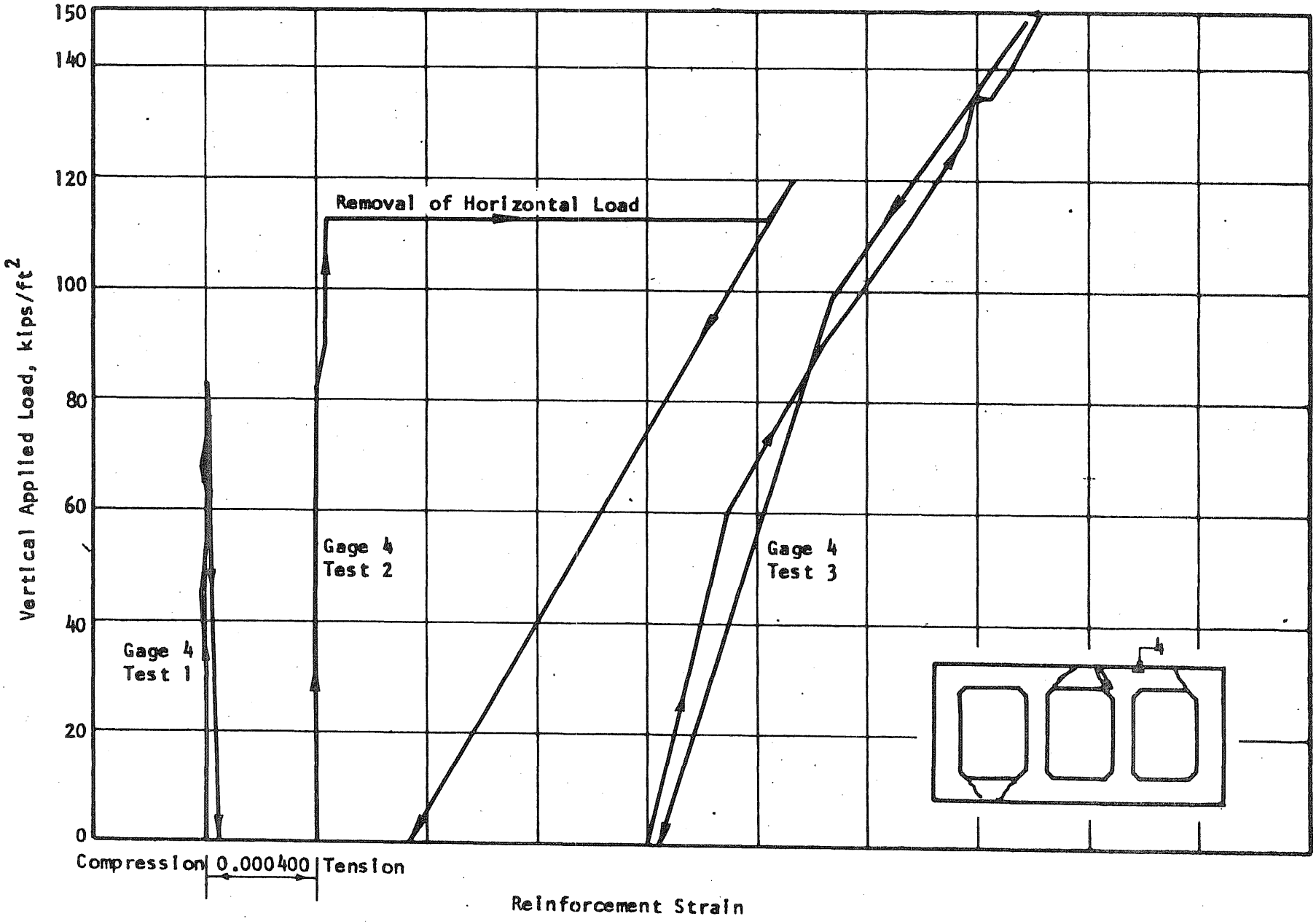

FIG. 7.8 LOAD-STRAIN CURVES, INTERIOR END OF END SPAN, R1

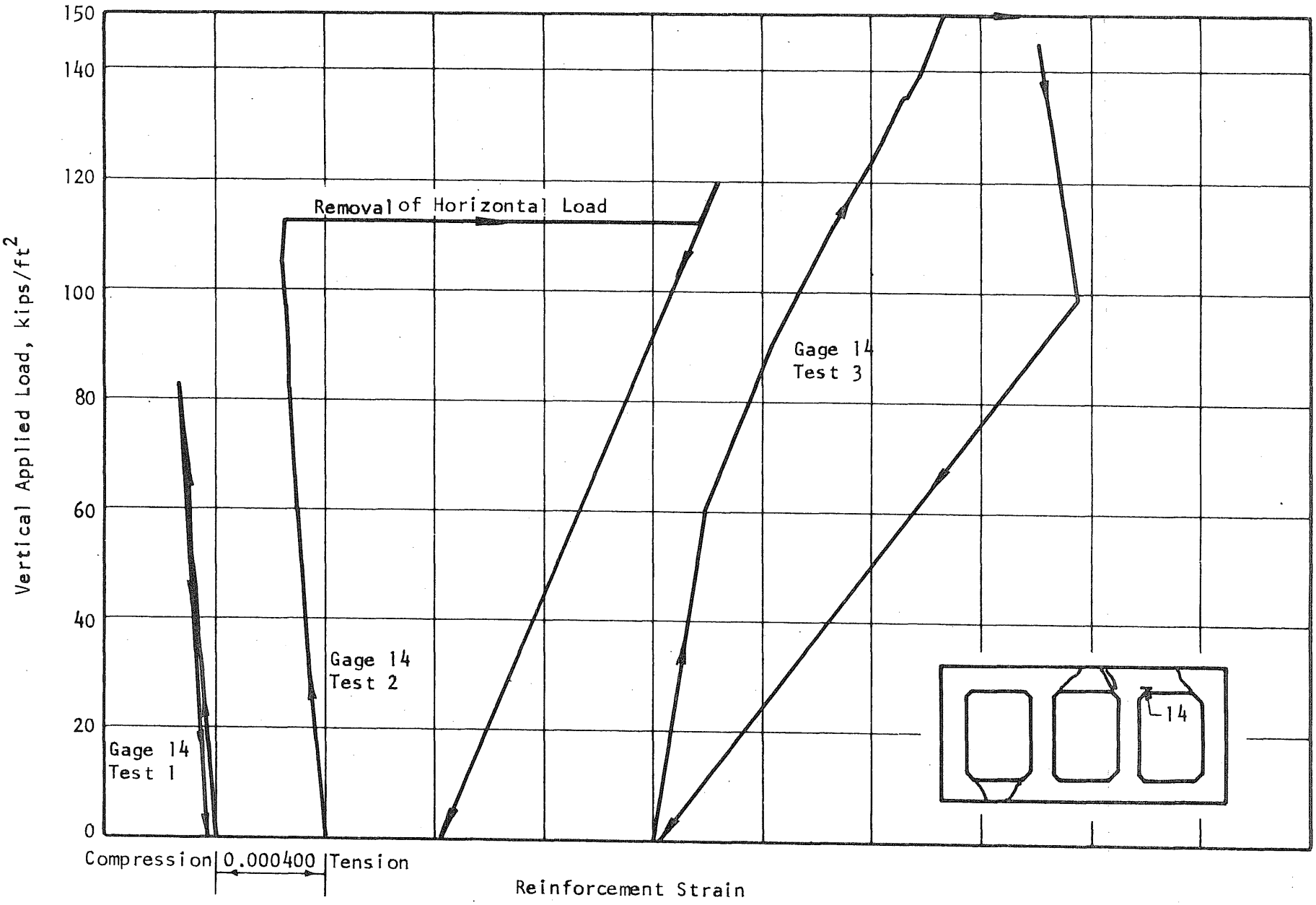
150
140
120
100
80
60
40
20
0
Vertical Applied Load, kips/ft²
Removal of Horizontal Load
Gage 14
Test 3
Gage 14
Test 2
Gage 14
Test 1
14
Compression
0.000400
Tension
Reinforcement Strain

FIG. 7.8 Cont.

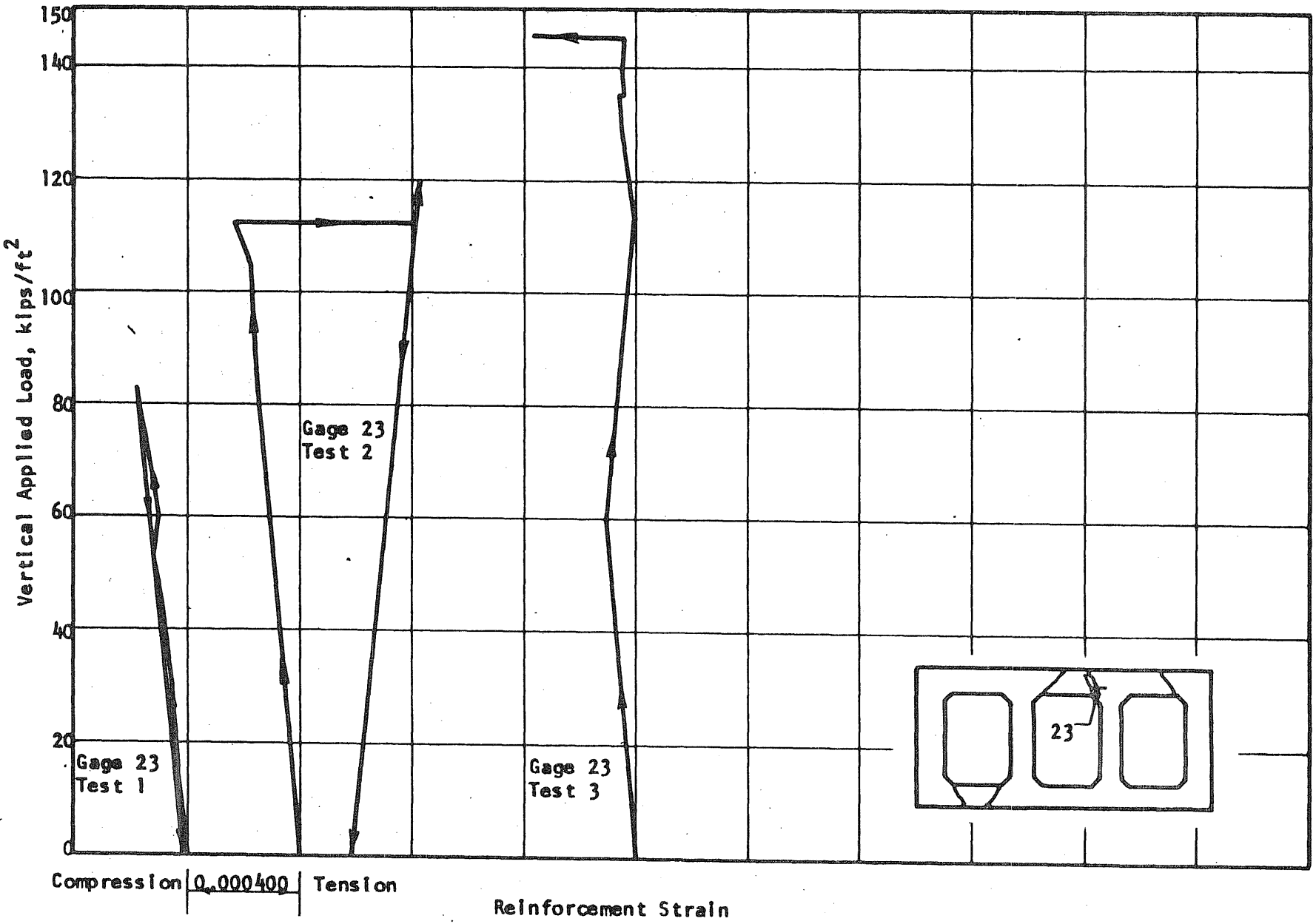

FIG. 7.9 LOAD-STRAIN CURVES, END OF INTERIOR SPAN, R1

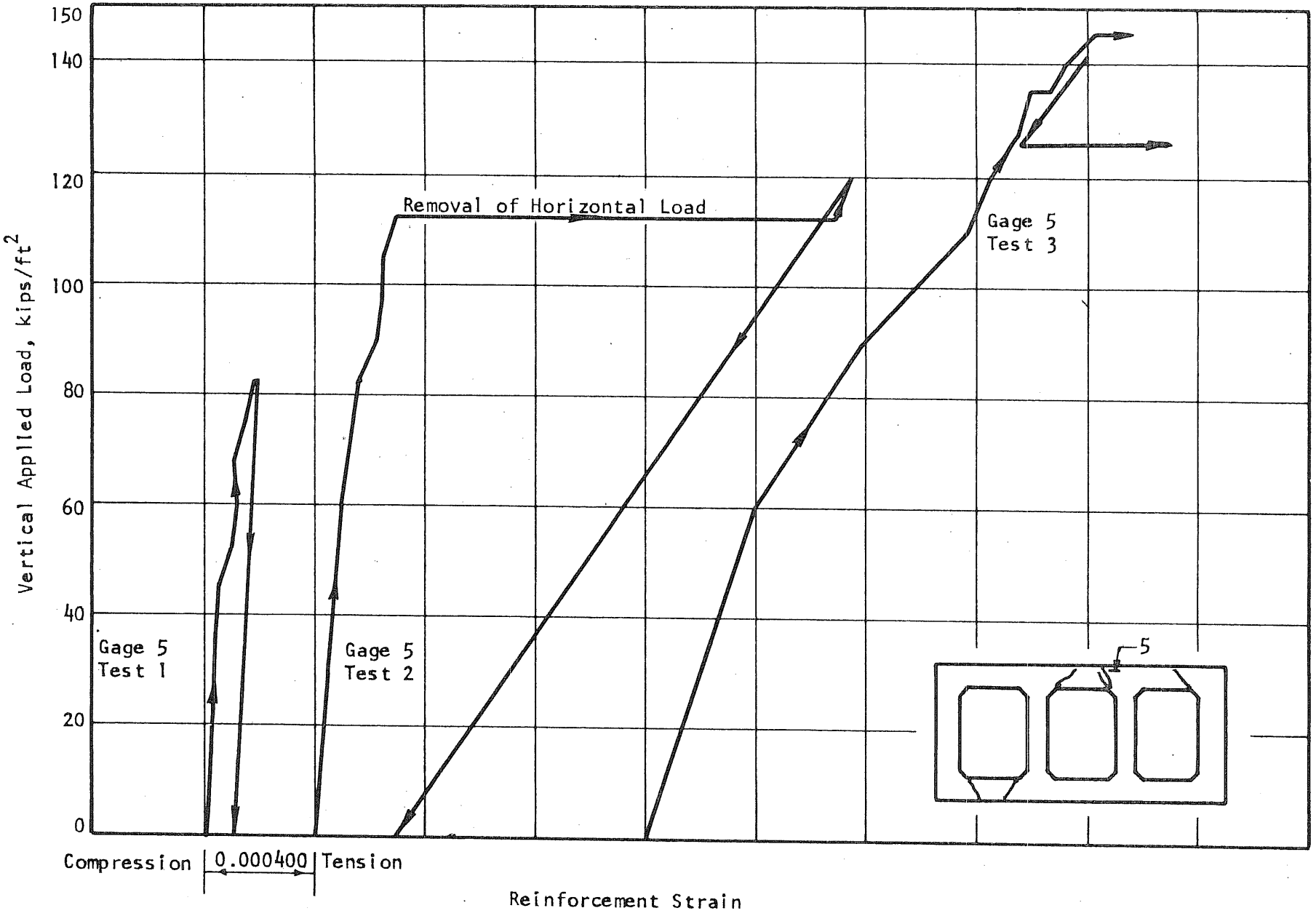
150
140
120
100
80
60
40
20
0
Vertical Applied Load, kips/ft^2
Removal of Horizontal Load
Gage 5
Test 1
Gage 5
Test 2
Gage 5
Test 3
5
Compression
0.000400
Tension
Reinforcement Strain

FIG. 7.9 Cont.

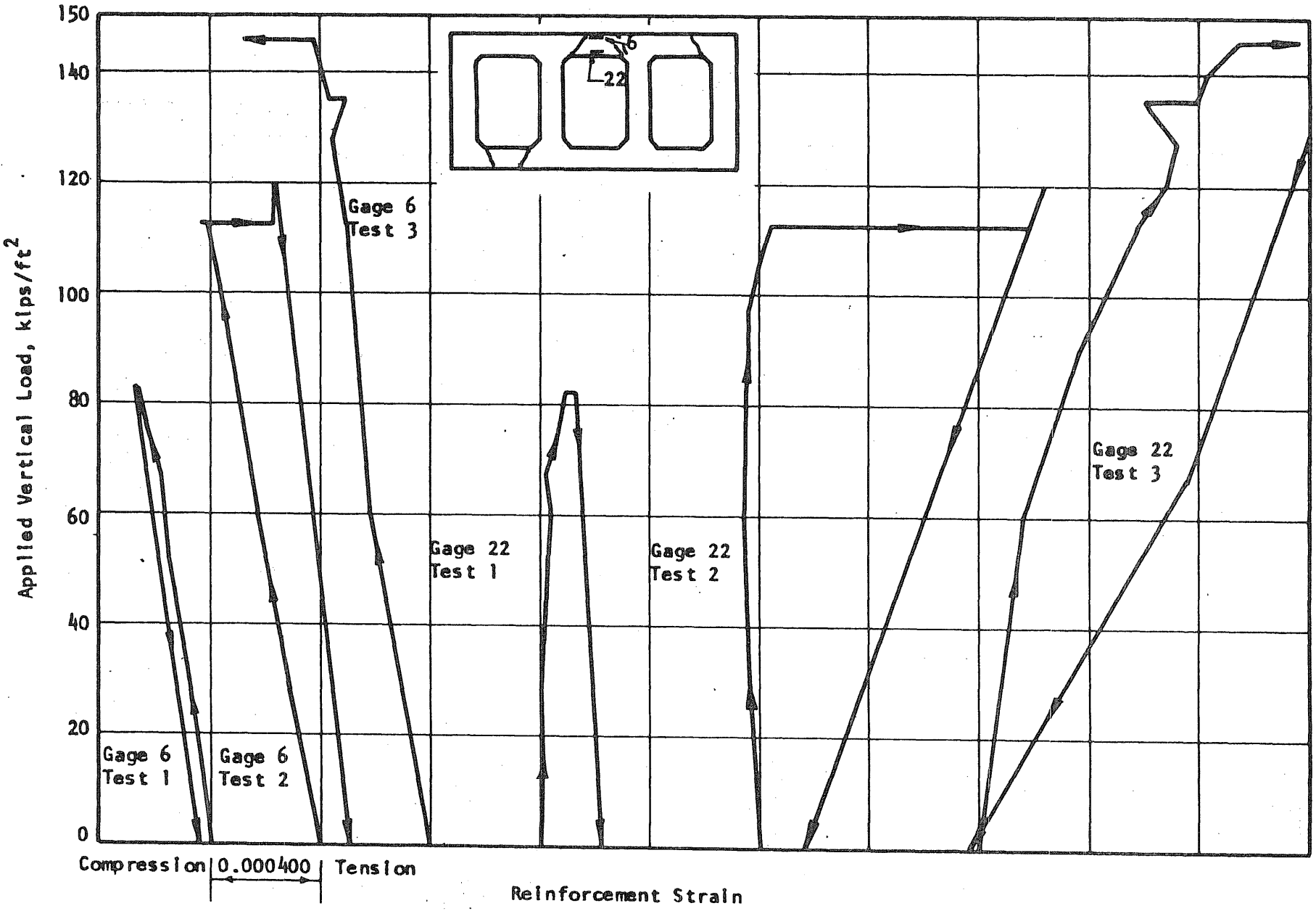

FIG. 7.10 LOAD-STRAIN CURVES, MIDSPAN OF INTERIOR SPAN, RI

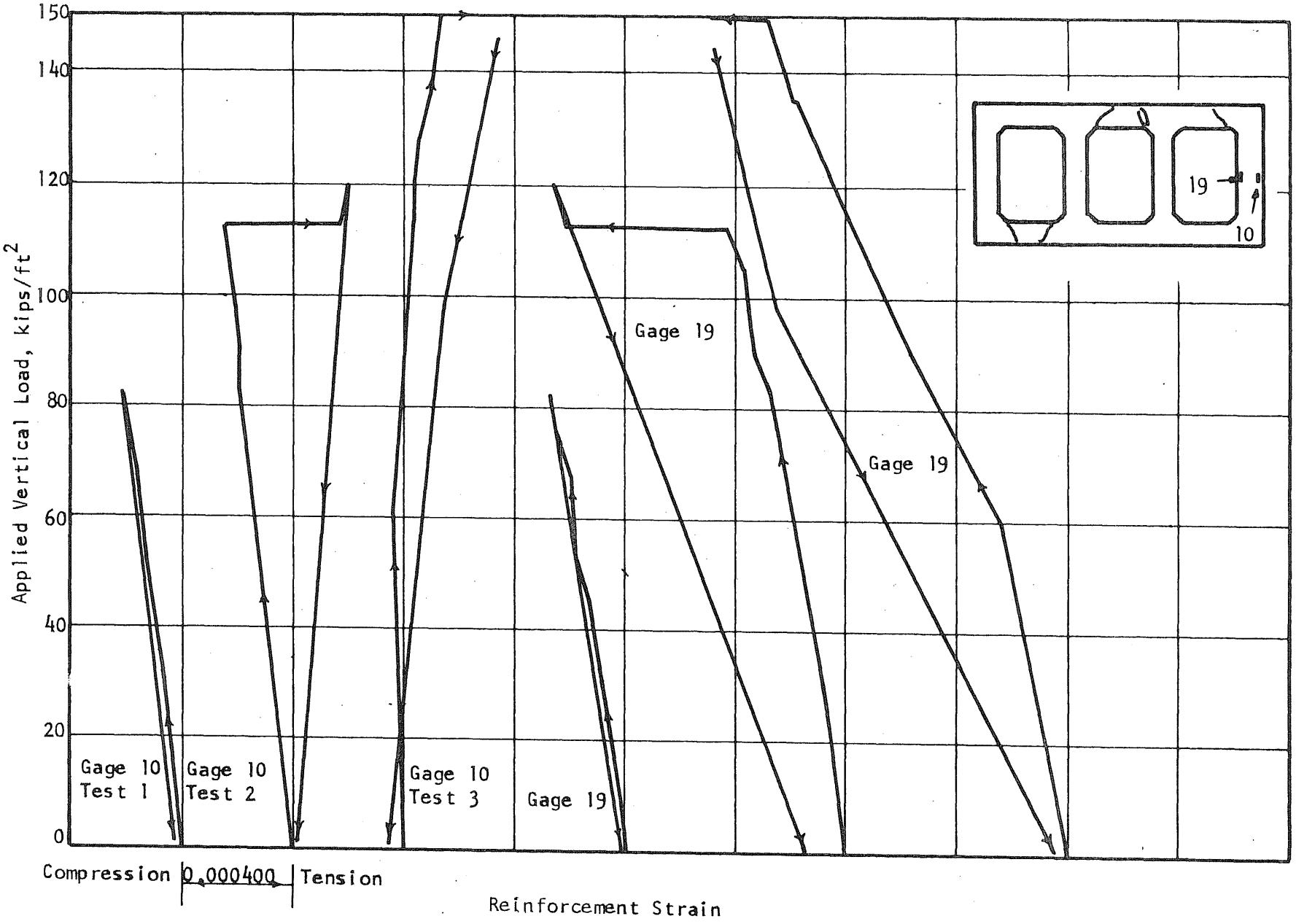

FIG. 7.11 LOAD-STRAIN CURVES, MIDHEIGHT OF END VERTICAL MEMBER, R1

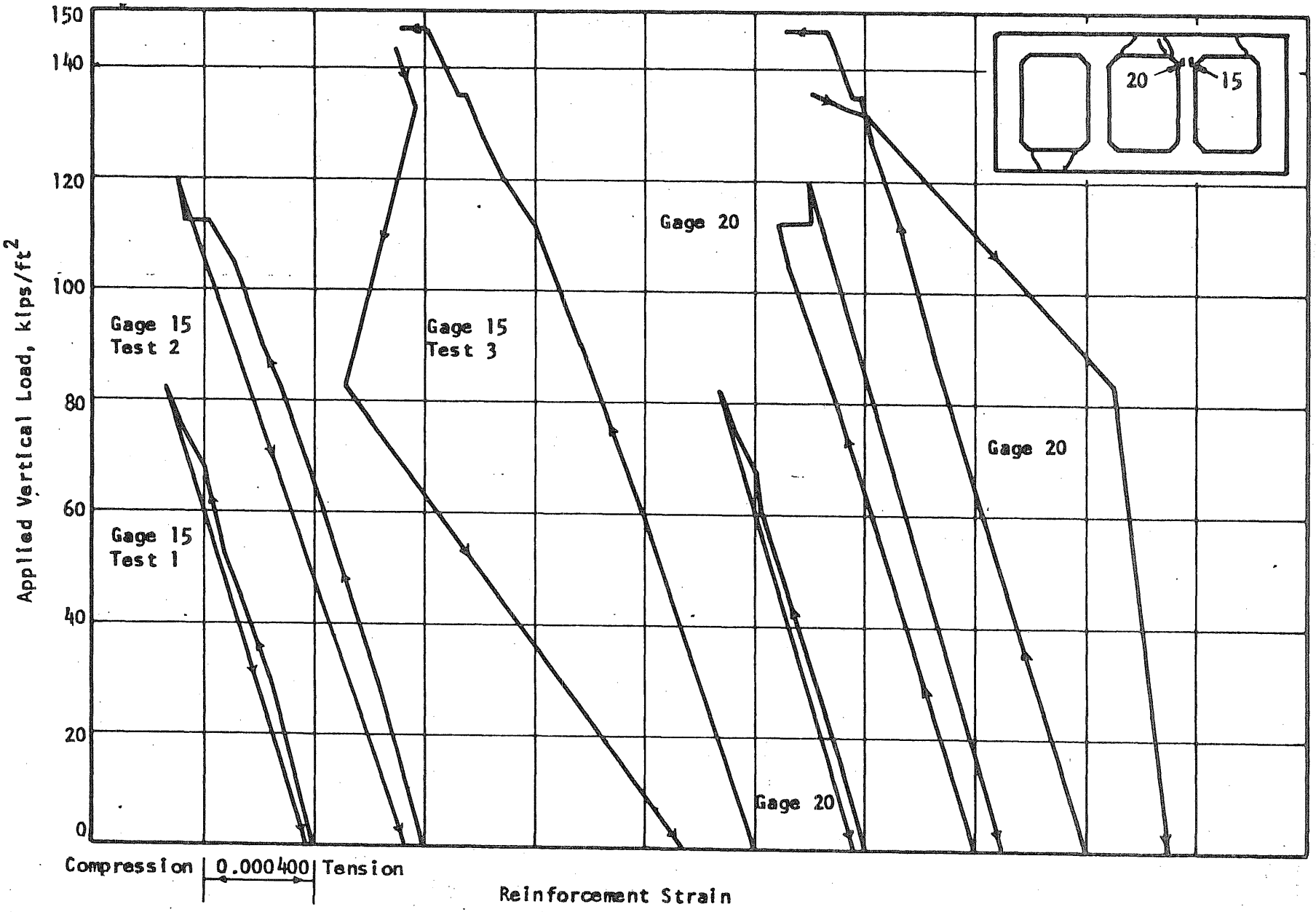

FIG. 7.12 LOAD-STRAIN CURVES, TOP OF INTERIOR VERTICAL MEMBER, R1

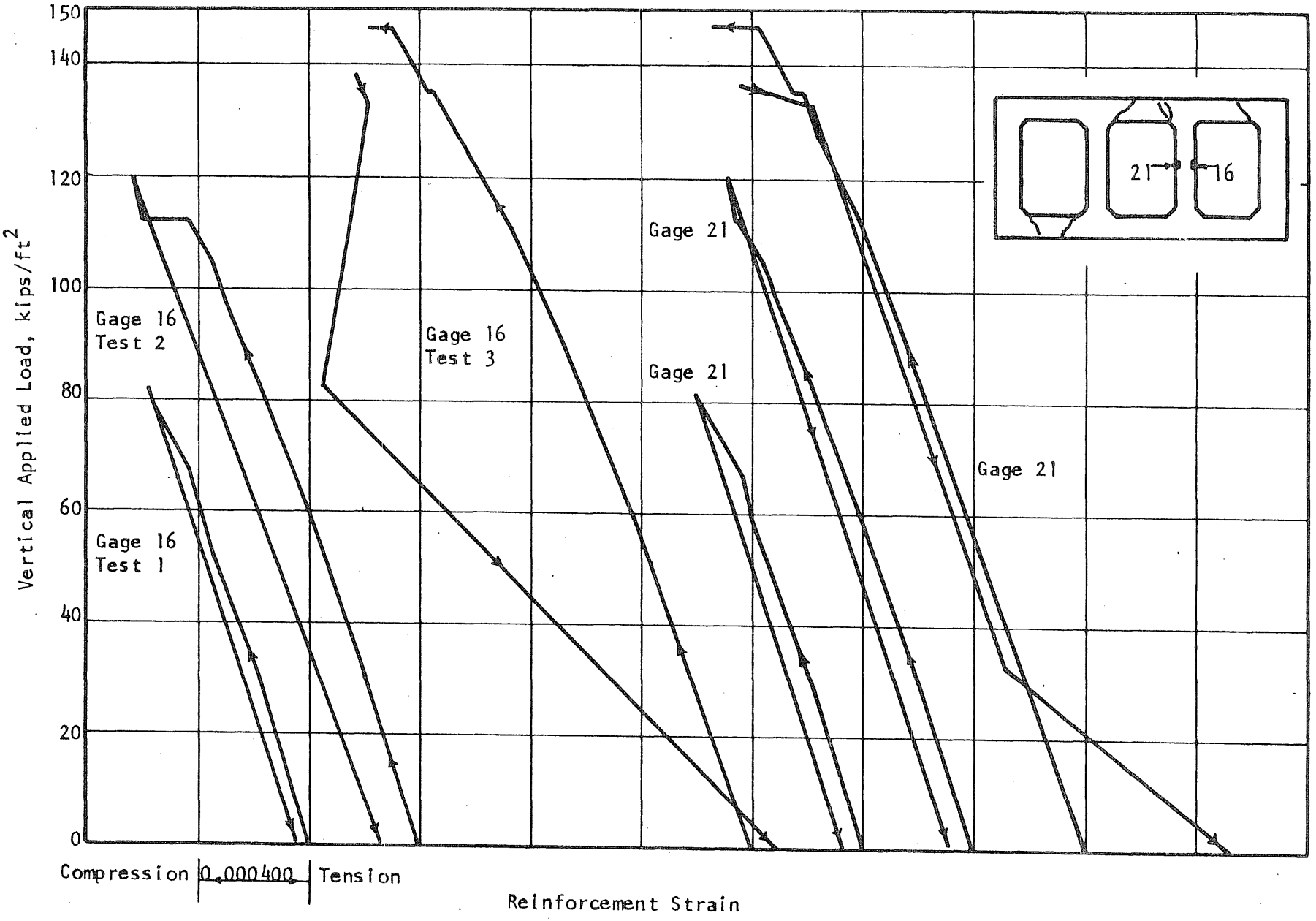

FIG. 7.13 LOAD-STRAIN CURVES, MIDHEIGHT OF INTERIOR VERTICAL MEMBER, R1

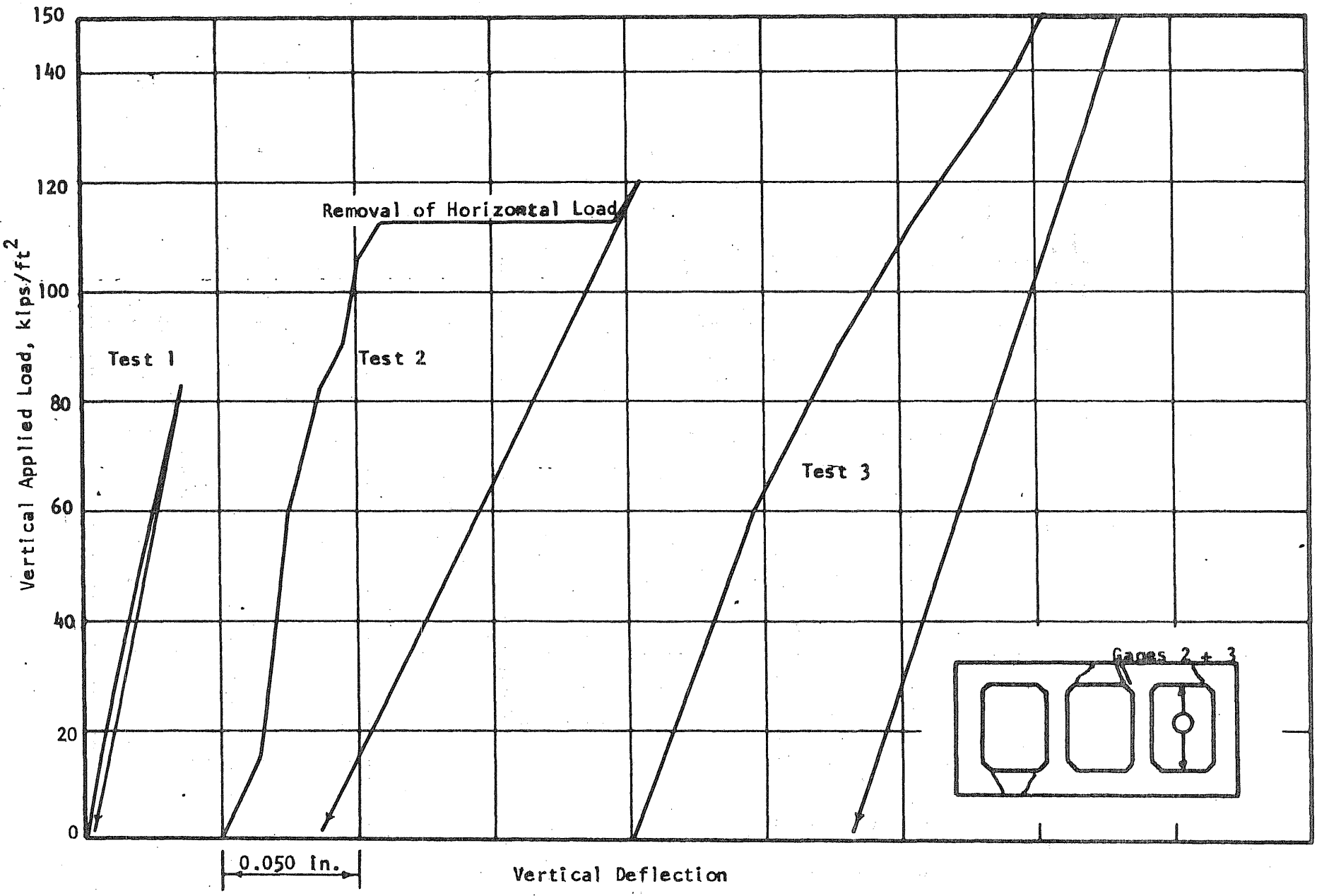

FIG. 7.14 LOAD-VERTICAL DEFLECTION CURVES, RIGHT END SPAN, R1

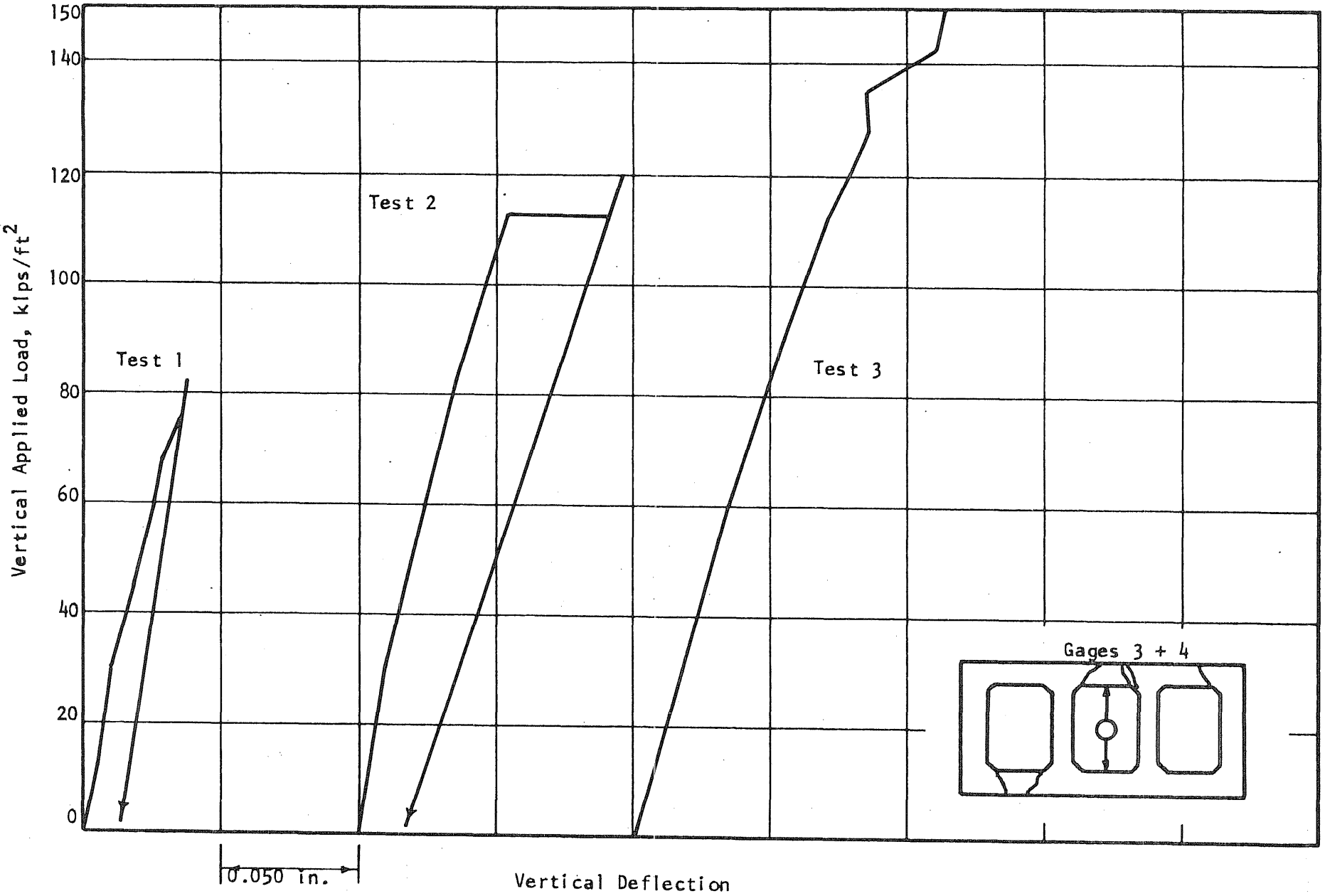

FIG. 7.15 LOAD-VERTICAL DEFLECTION CURVES, INTERIOR SPAN, R1

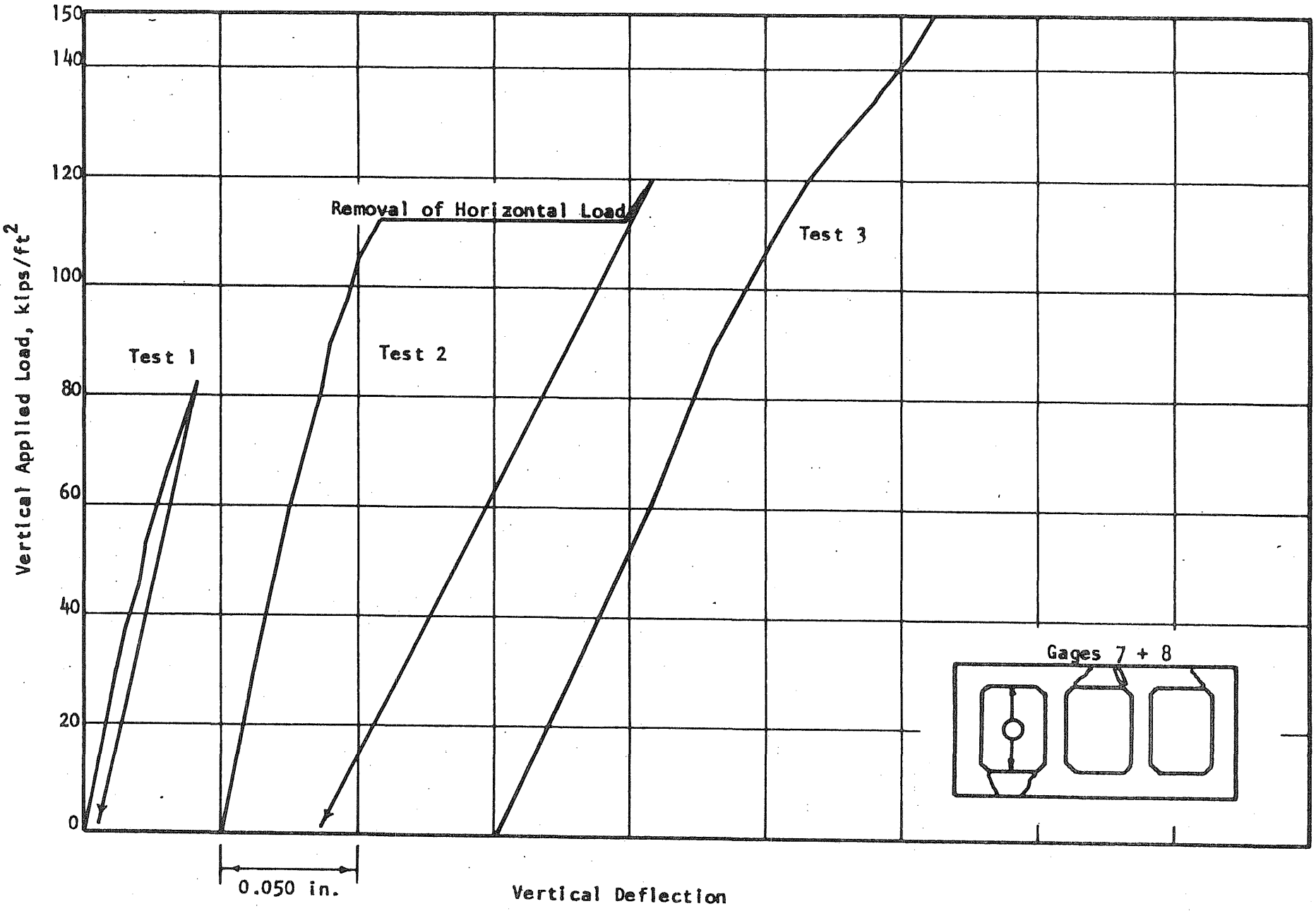

FIG. 7.16 LOAD-VERTICAL DEFLECTION CURVES, LEFT END SPAN, R1

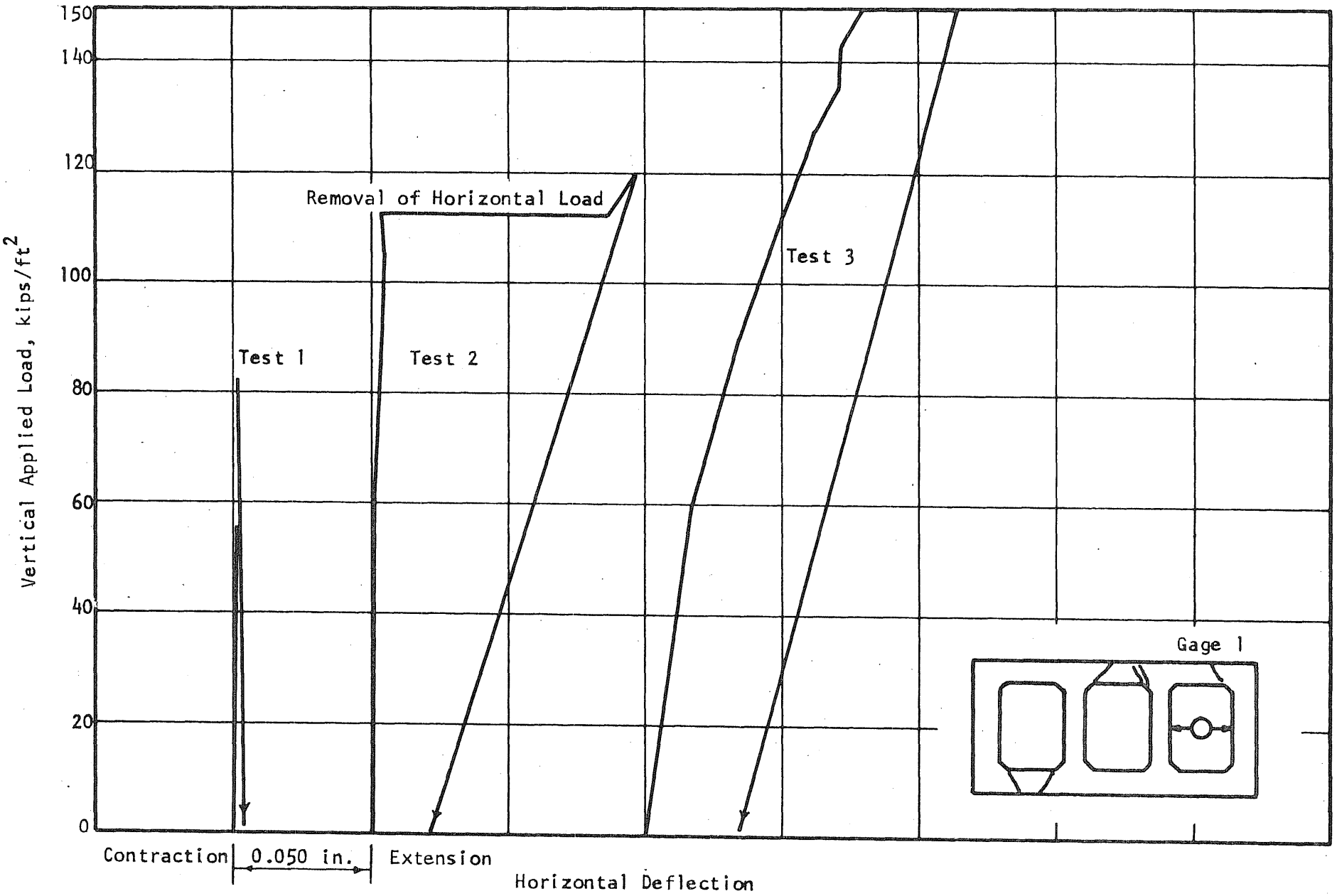

FIG. 7.17 LOAD-HORIZONTAL DEFLECTION CURVES, RIGHT END SPAN, R1

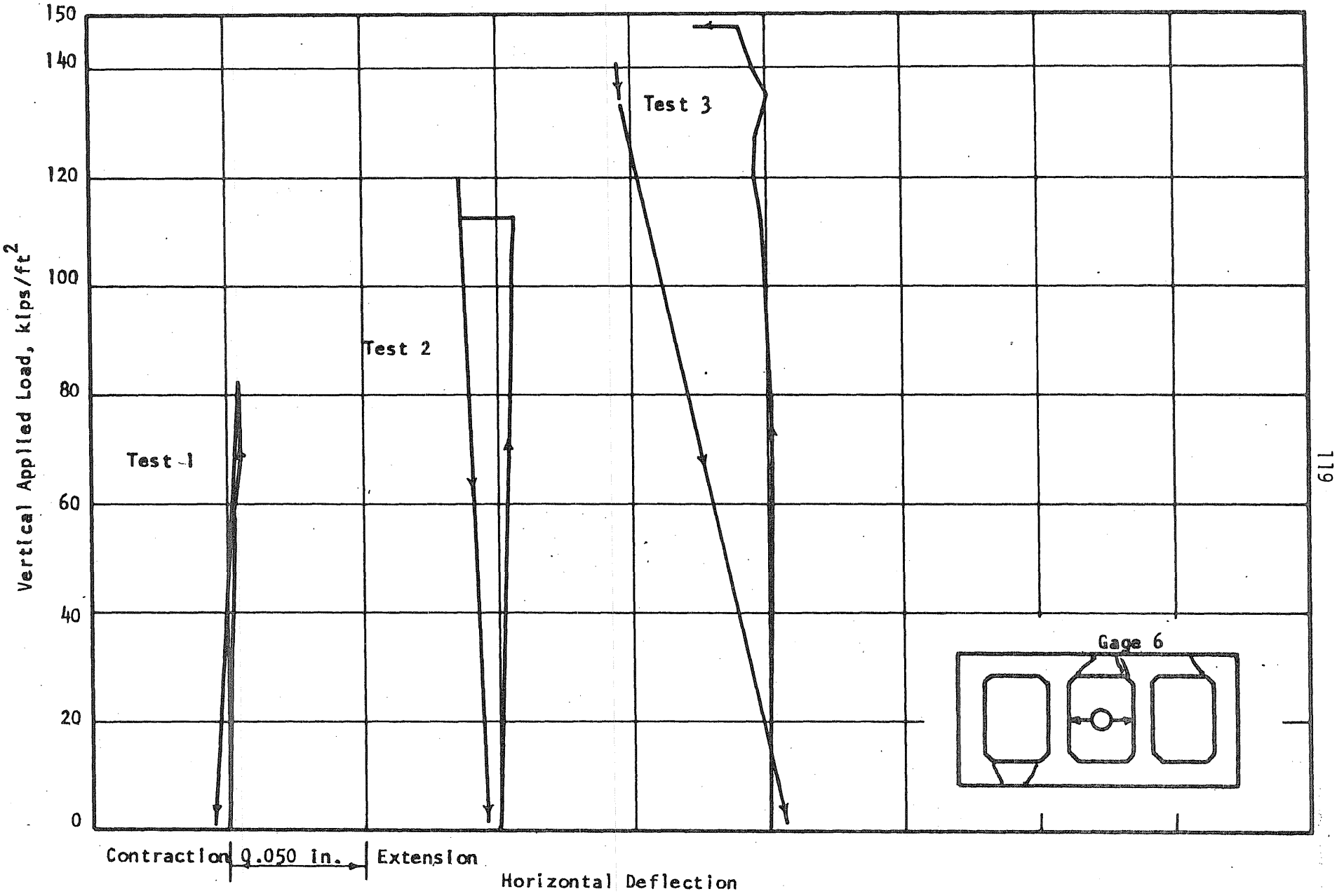

FIG. 7.18 LOAD-HORIZONTAL DEFLECTION CURVES, INTERIOR SPAN, RI

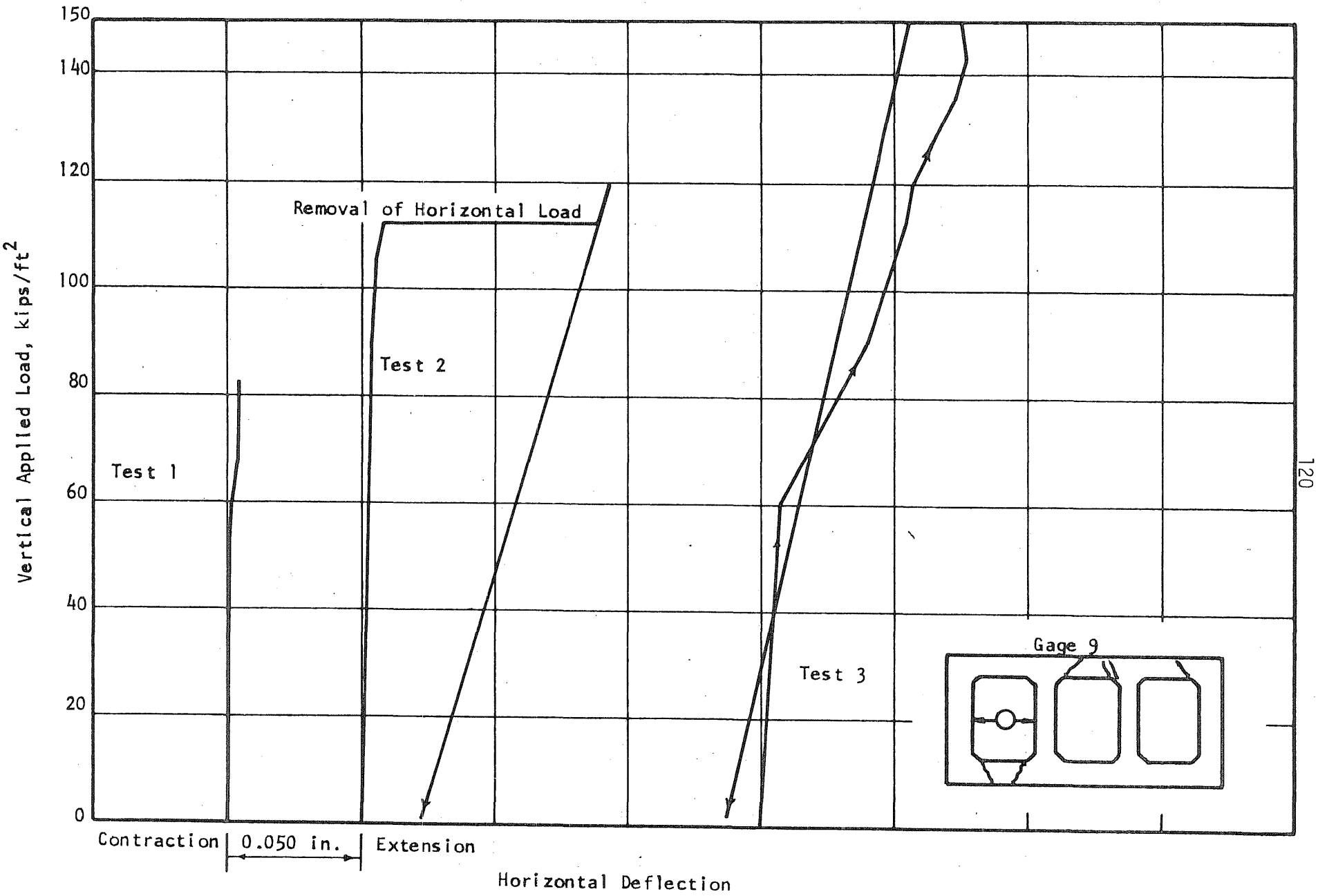

FIG. 7.19 LOAD-HORIZONTAL DEFLECTION CURVES, LEFT END SPAN, R1

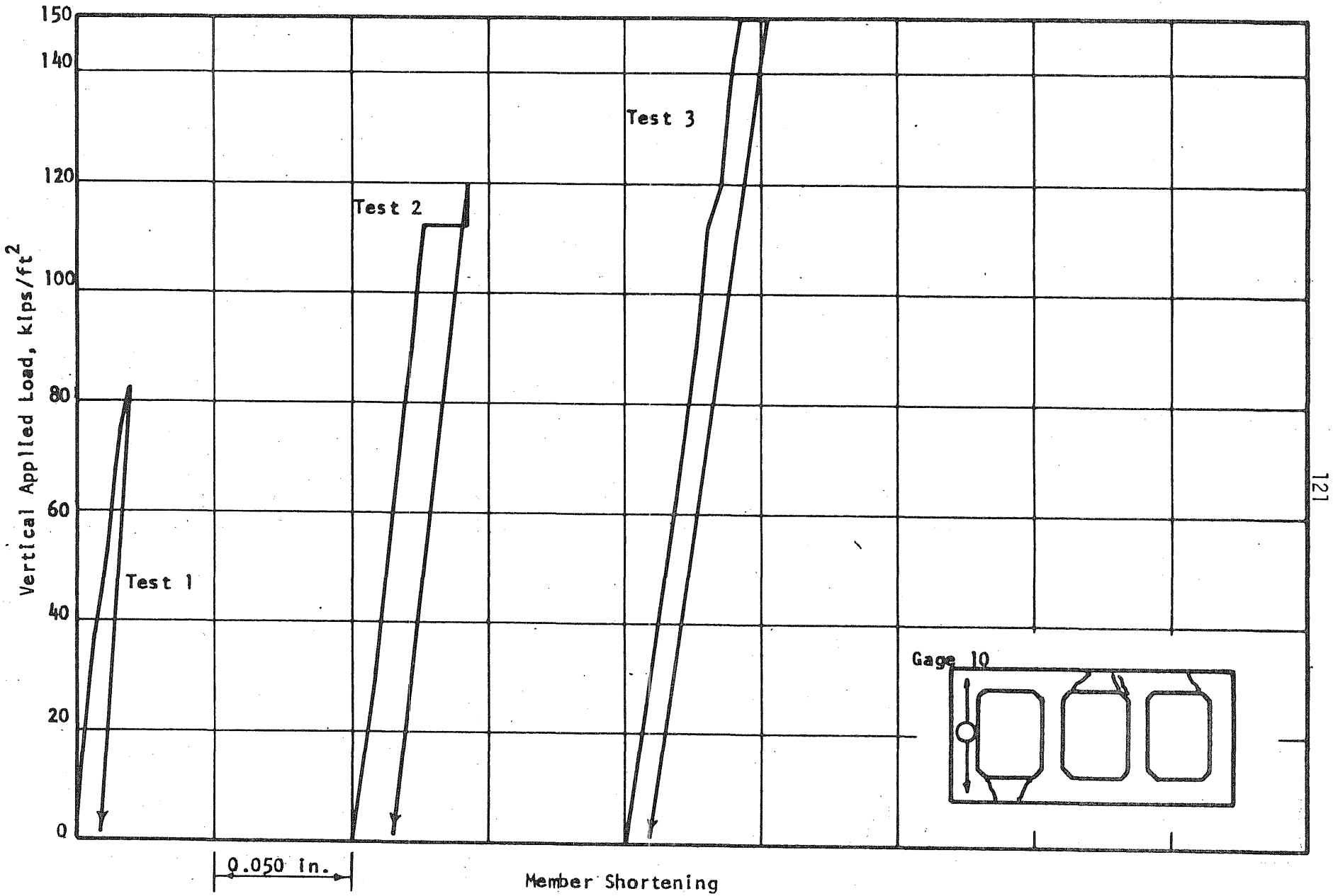

FIG. 7.20 LOAD-LENGTH CHANGE CURVES, EXTERIOR VERTICAL MEMBER, R1

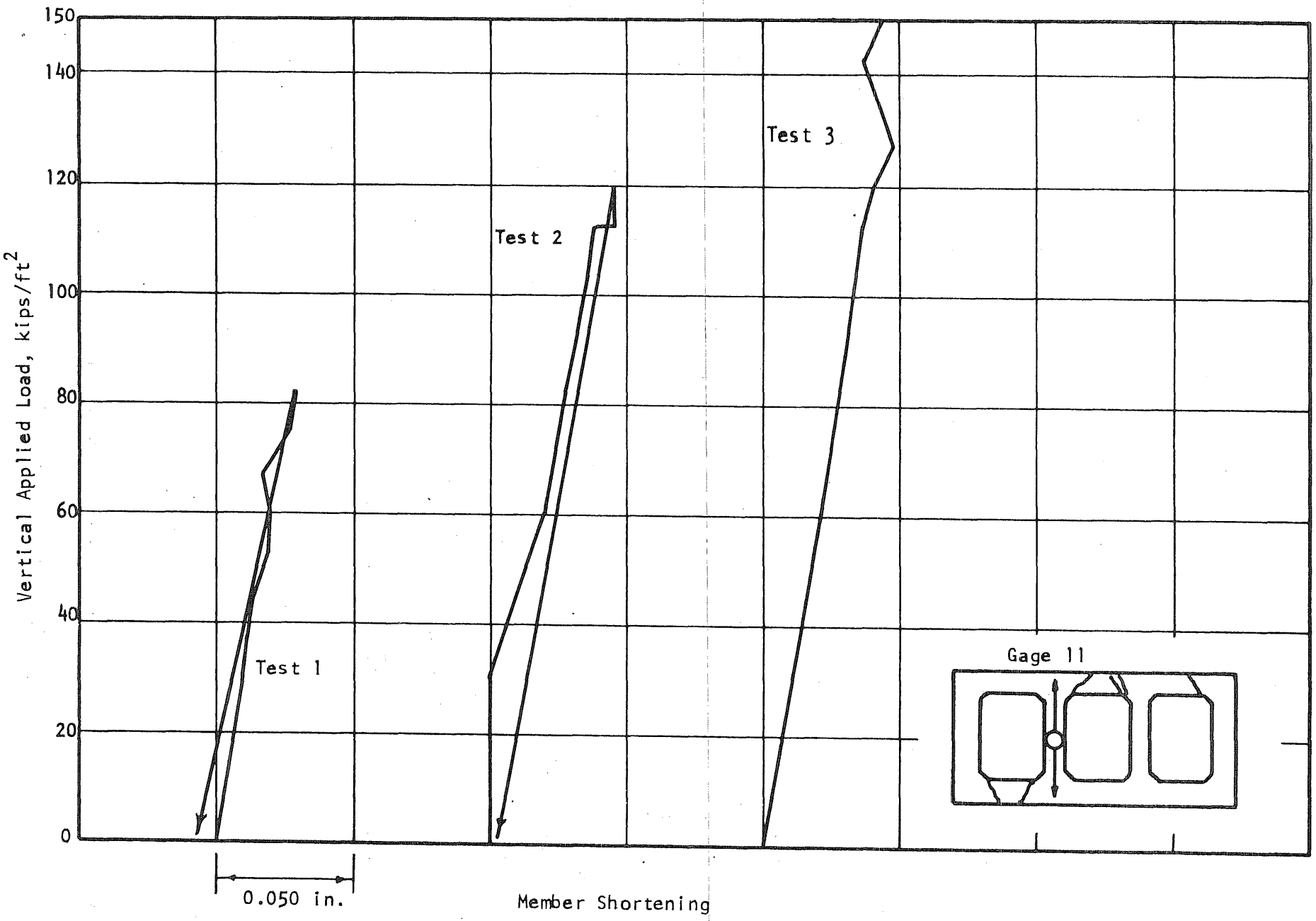

FIG. 7.21 LOAD-LENGTH CHANGE CURVES, INTERIOR VERTICAL MEMBER, R1

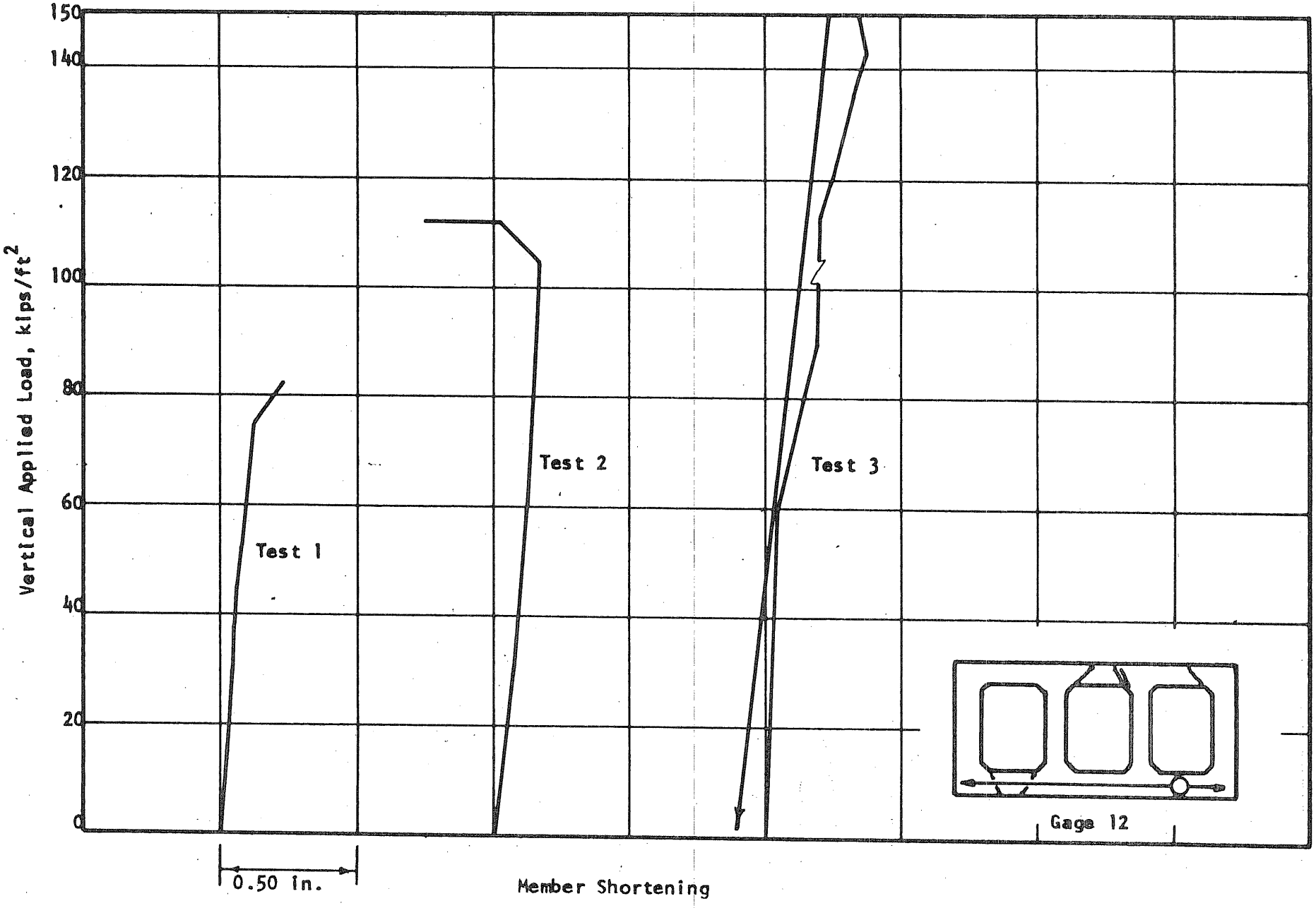

FIG. 7.22 LOAD-LENGTH CHANGE CURVES, LOWER HORIZONTAL MEMBER, R1

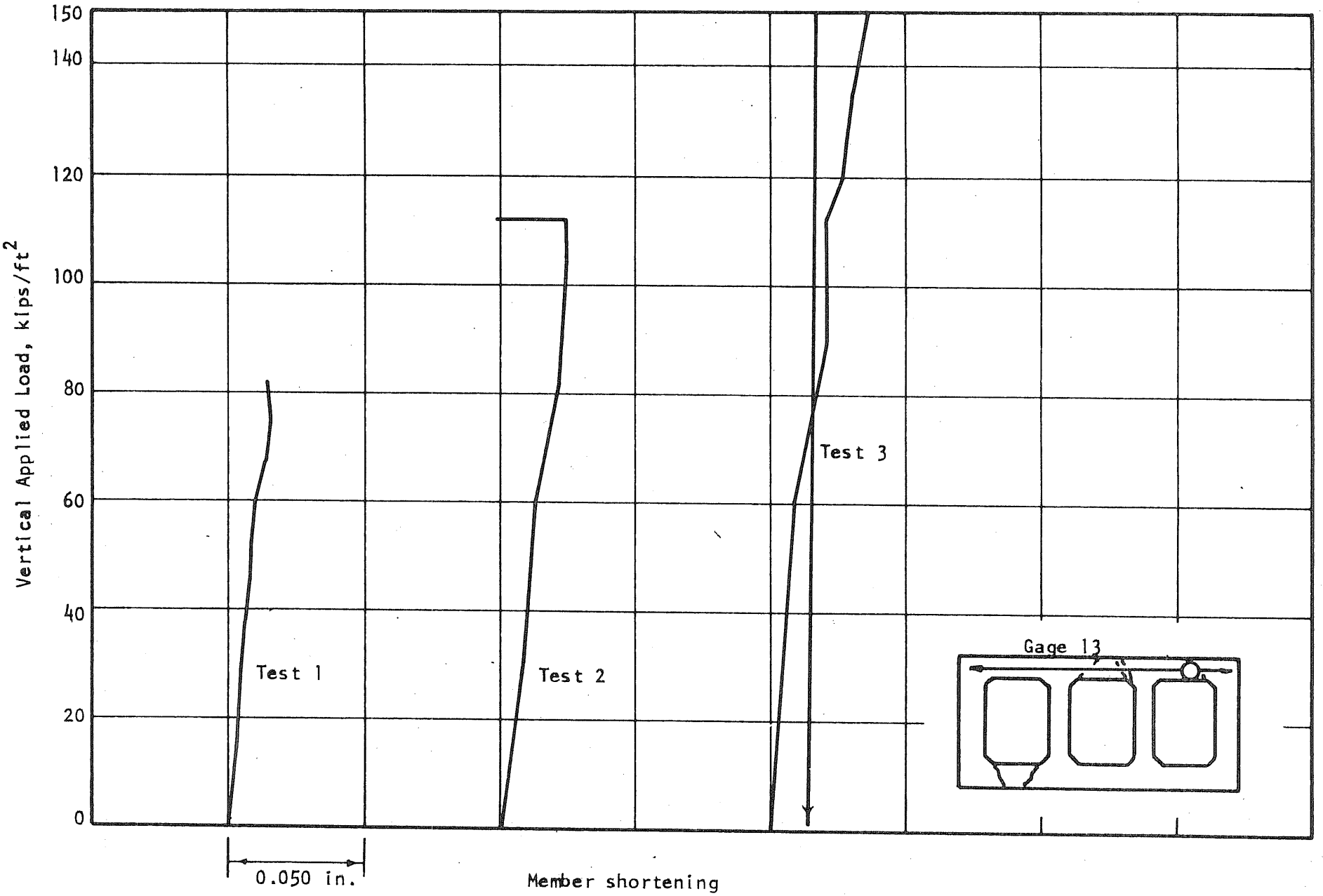

FIG. 7.23 LOAD-LENGTH CHANGE CURVES, UPPER HORIZONTAL MEMBER, R1

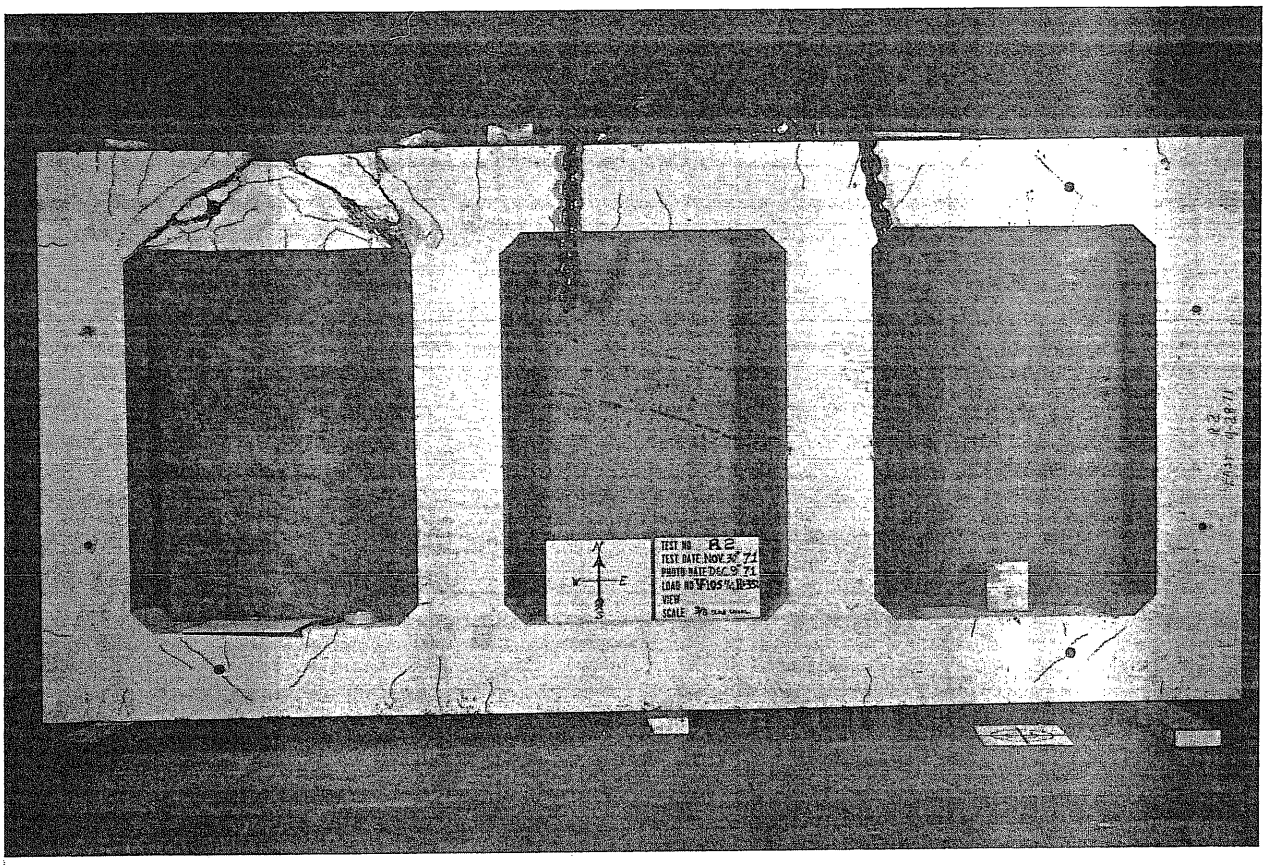

FIG. 7.24 SPECIMEN R2 AFTER TEST TO FAILURE

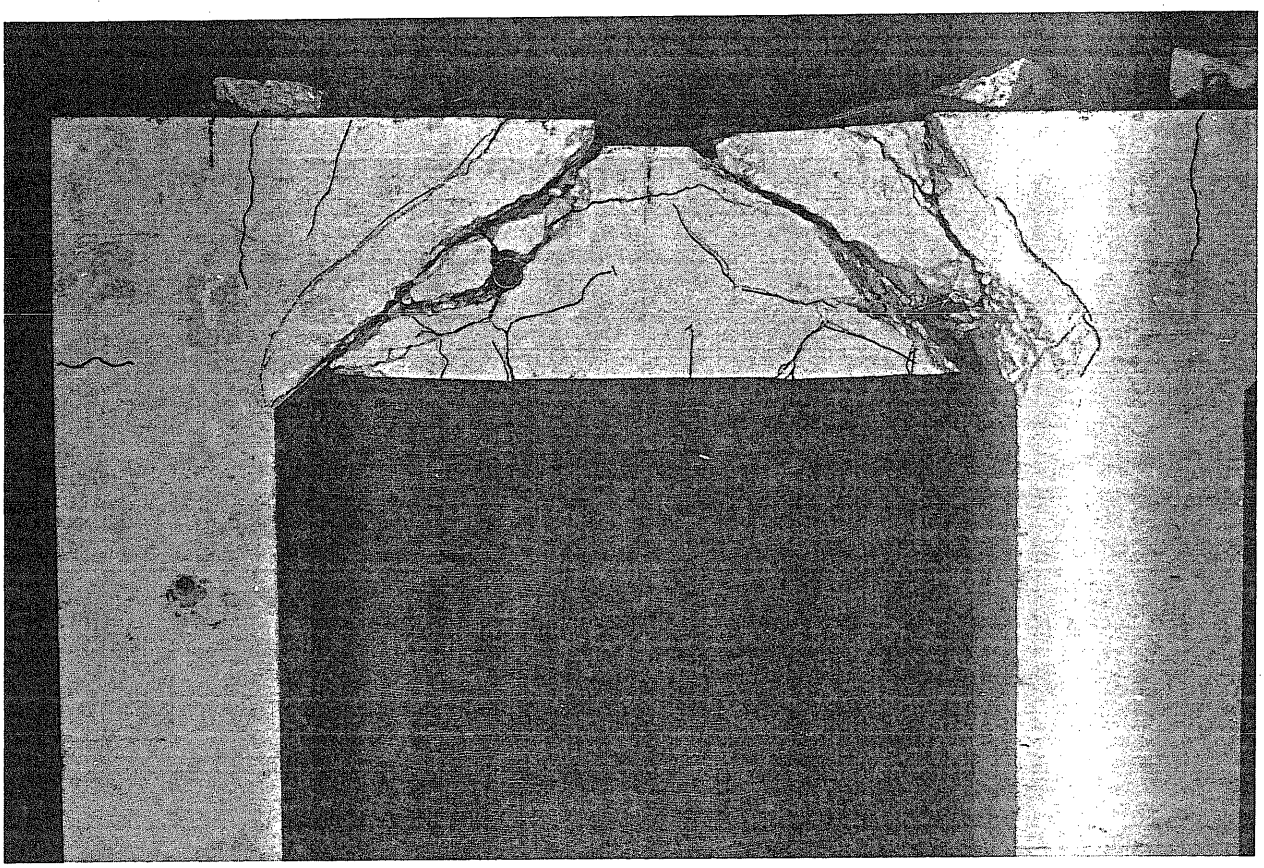

FIG. 7.25 FAILED END SPAN OF SPECIMEN R2

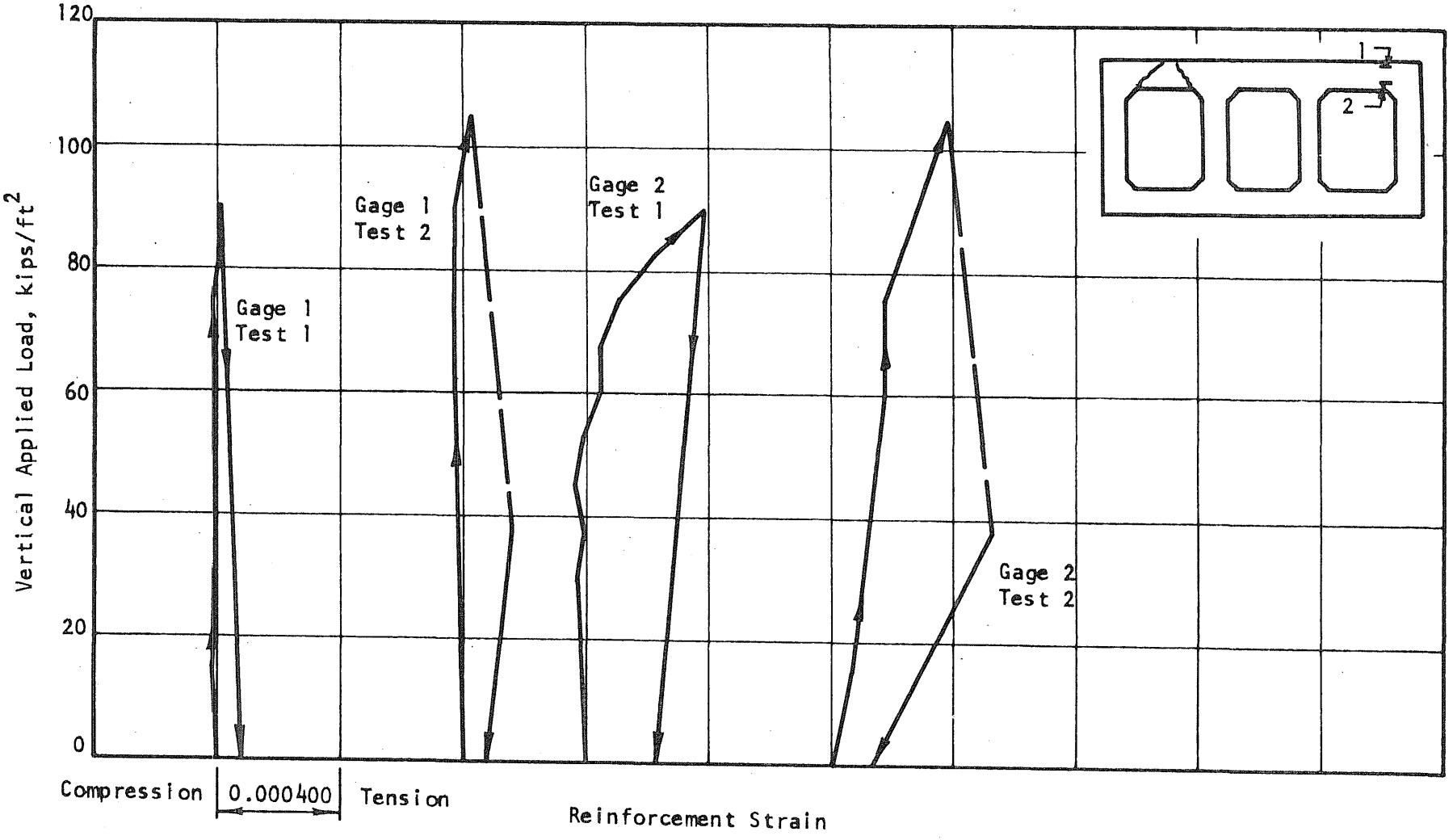

FIG. 7.26 LOAD-STRAIN CURVES, OUTER END OF END SPAN, R2

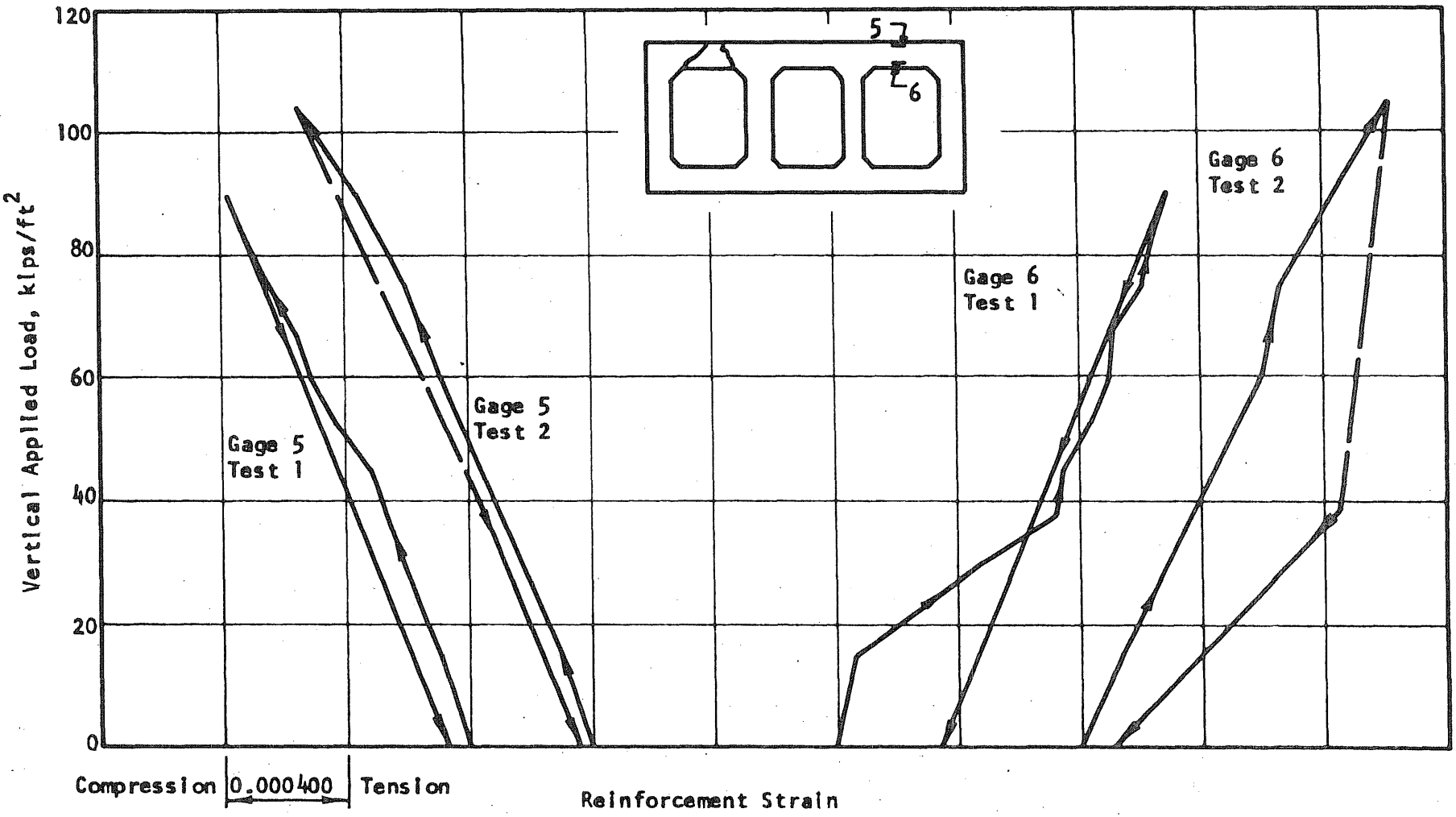

FIG. 7.27 LOAD-STRAIN CURVES, MIDSPAN OF END SPAN, R2

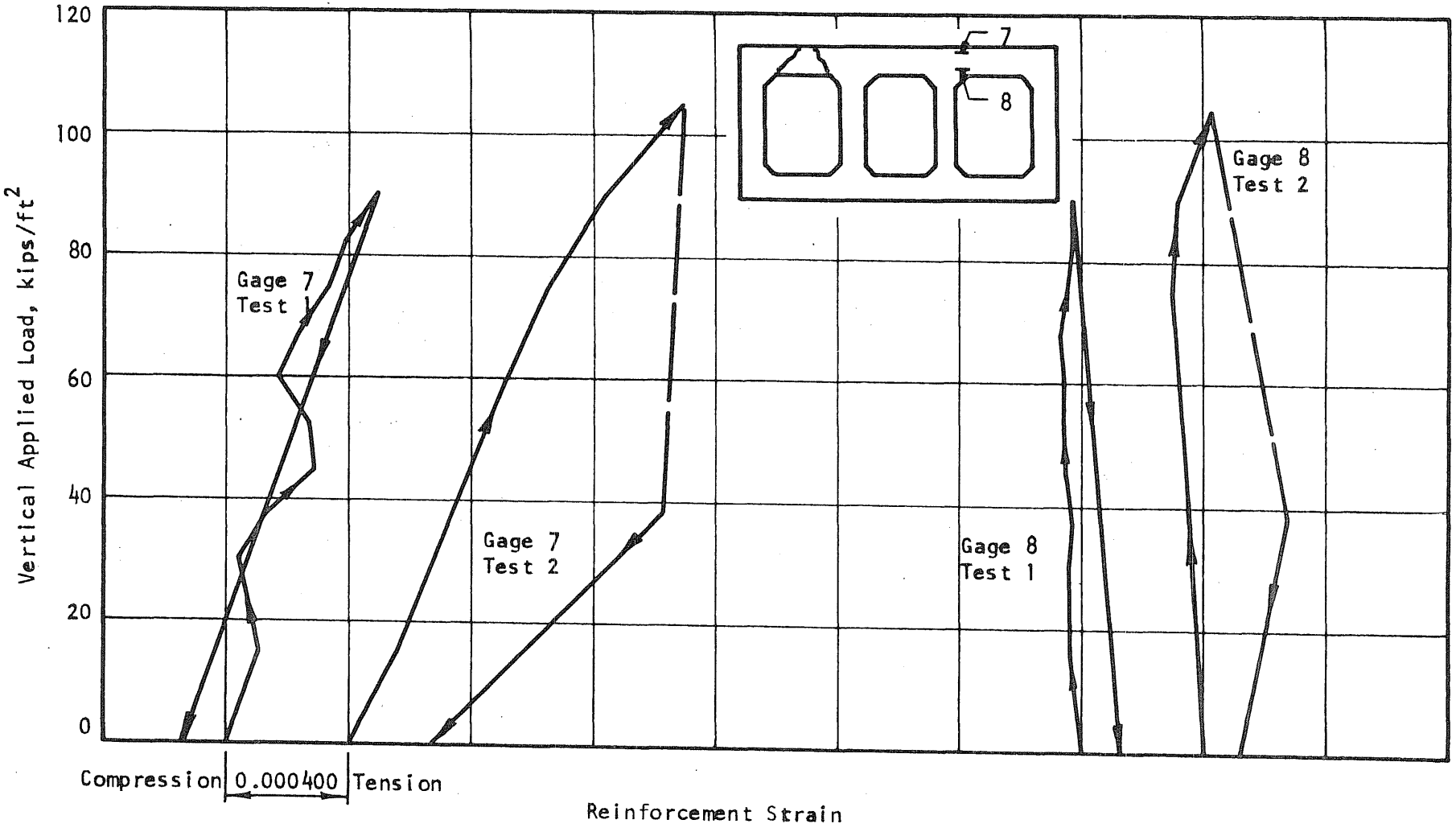

FIG. 7.28 LOAD-STRAIN CURVES, INTERIOR END OF END SPAN, R2

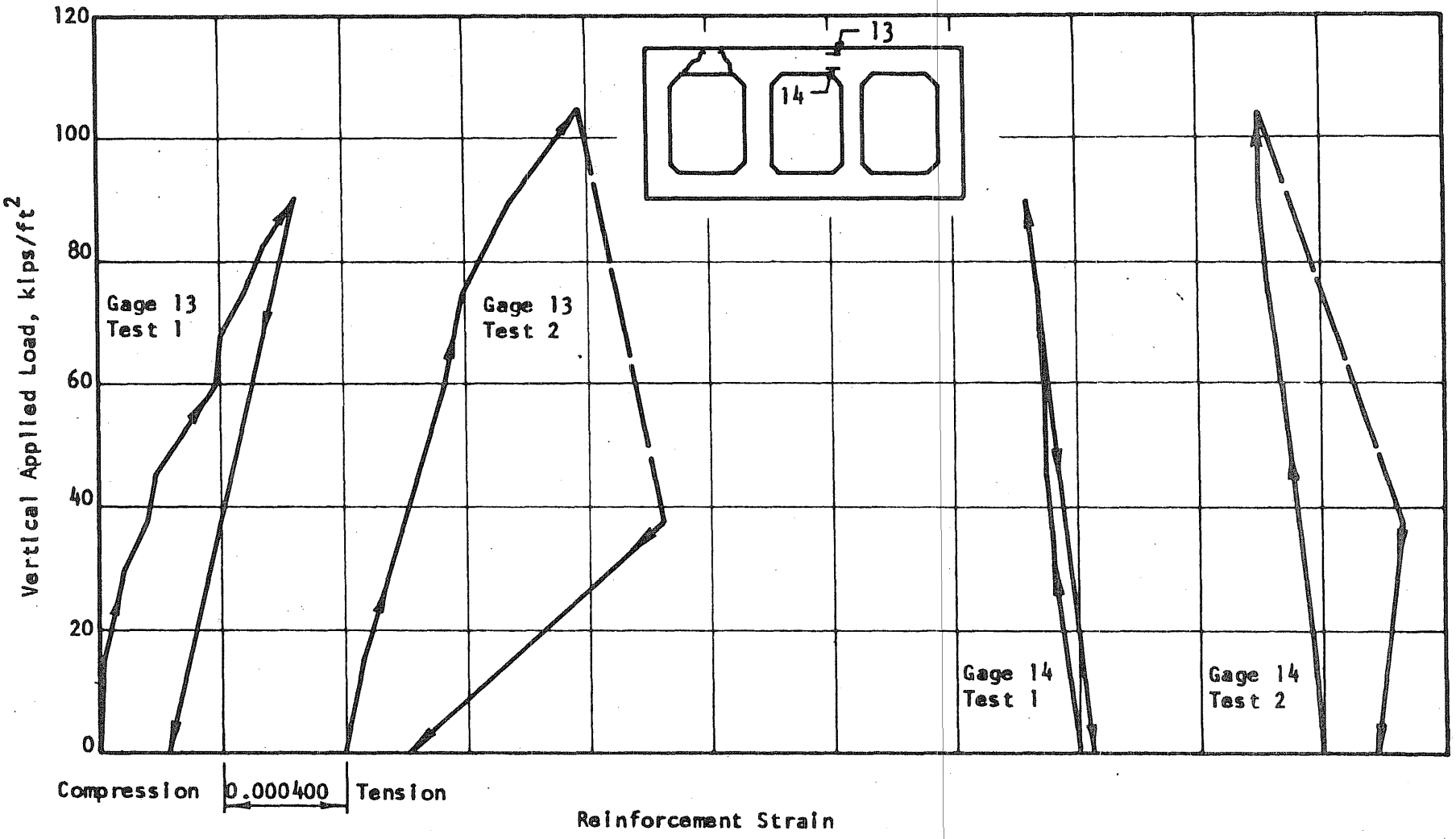

FIG. 7.29 -LOAD-STRAIN CURVES, END OF INTERIOR SPAN, R2

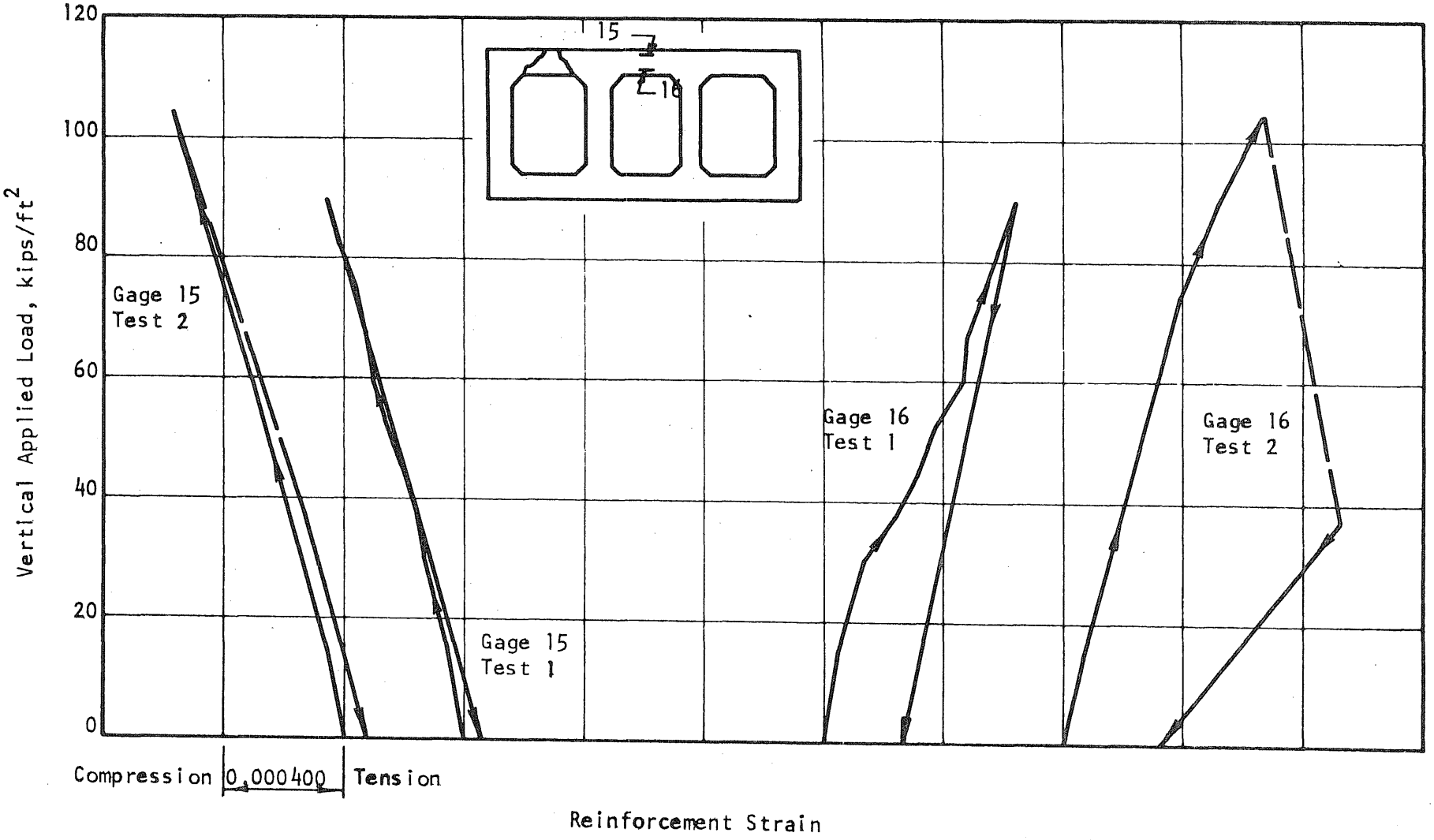

FIG. 7.30 LOAD-STRAIN CURVES, MIDSPAN OF INTERIOR SPAN, R2

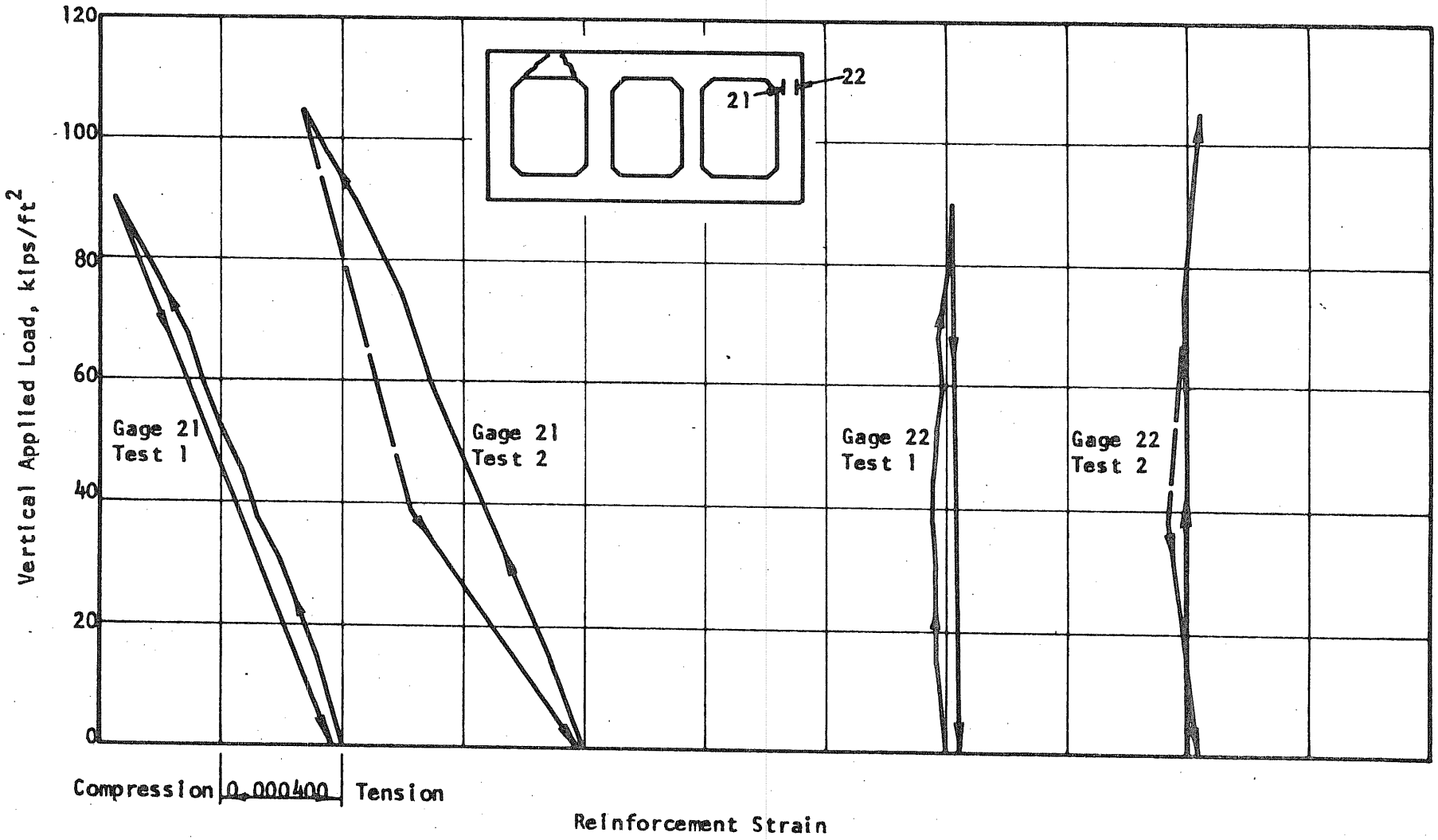

FIG. 7.31 LOAD-STRAIN CURVES, TOP OF END VERTICAL MEMBER, R2

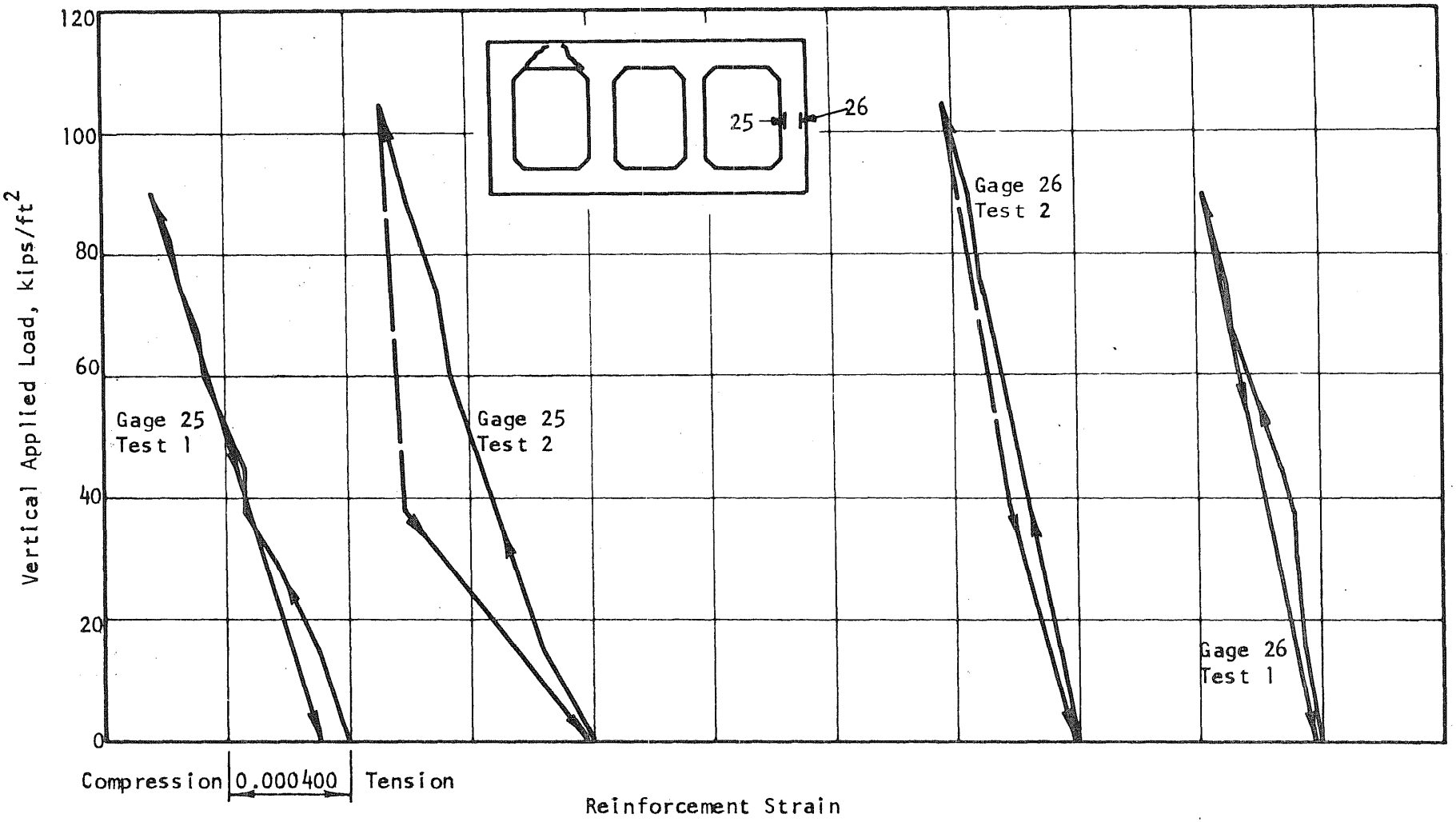

FIG. 7.32 LOAD-STRAIN CURVES, MIDHEIGHT OF END VERTICAL MEMBER, R2

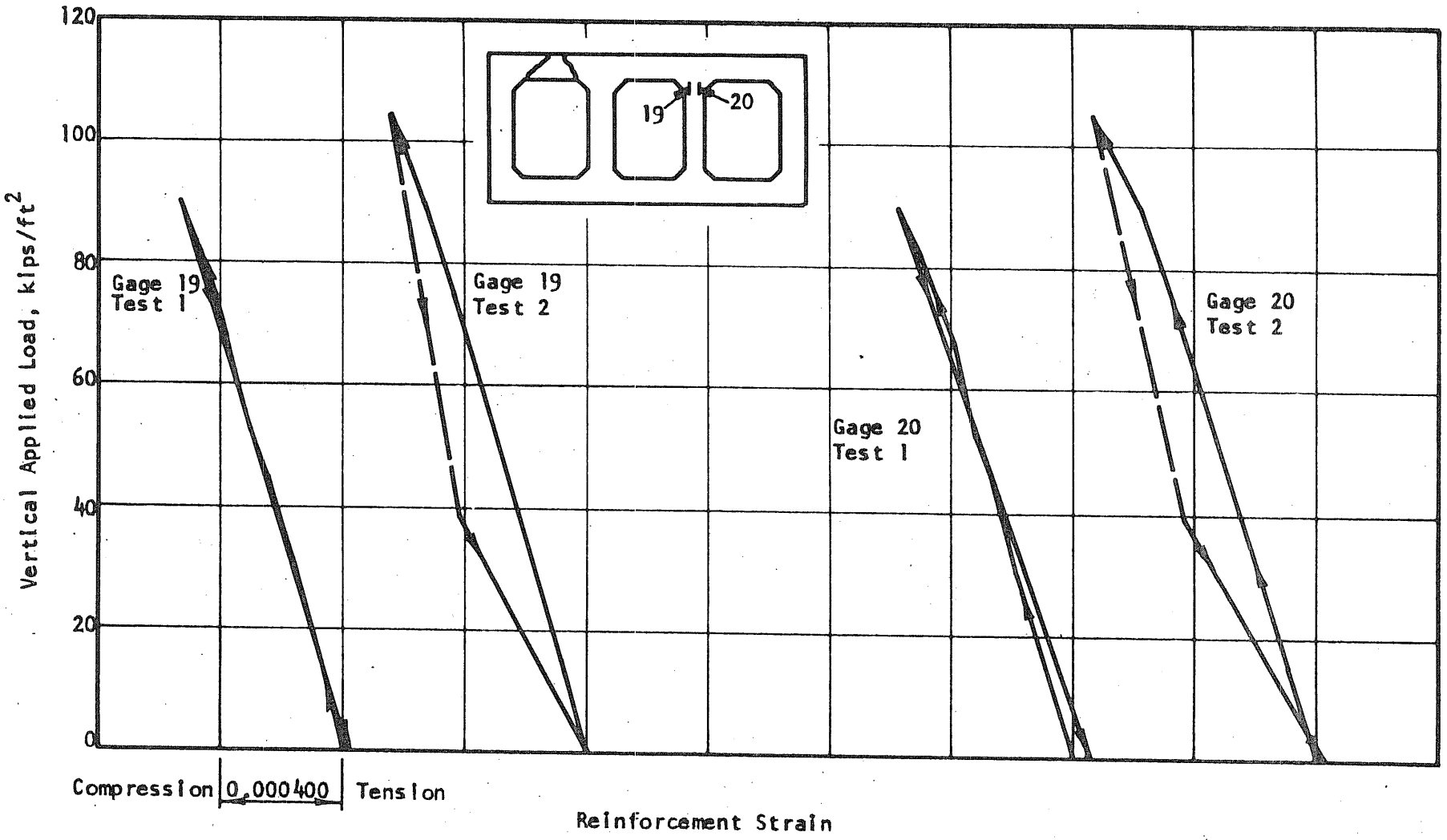

FIG. 7.33 LOAD-STRAIN CURVES, TOP OF INTERIOR VERTICAL MEMBER, R2

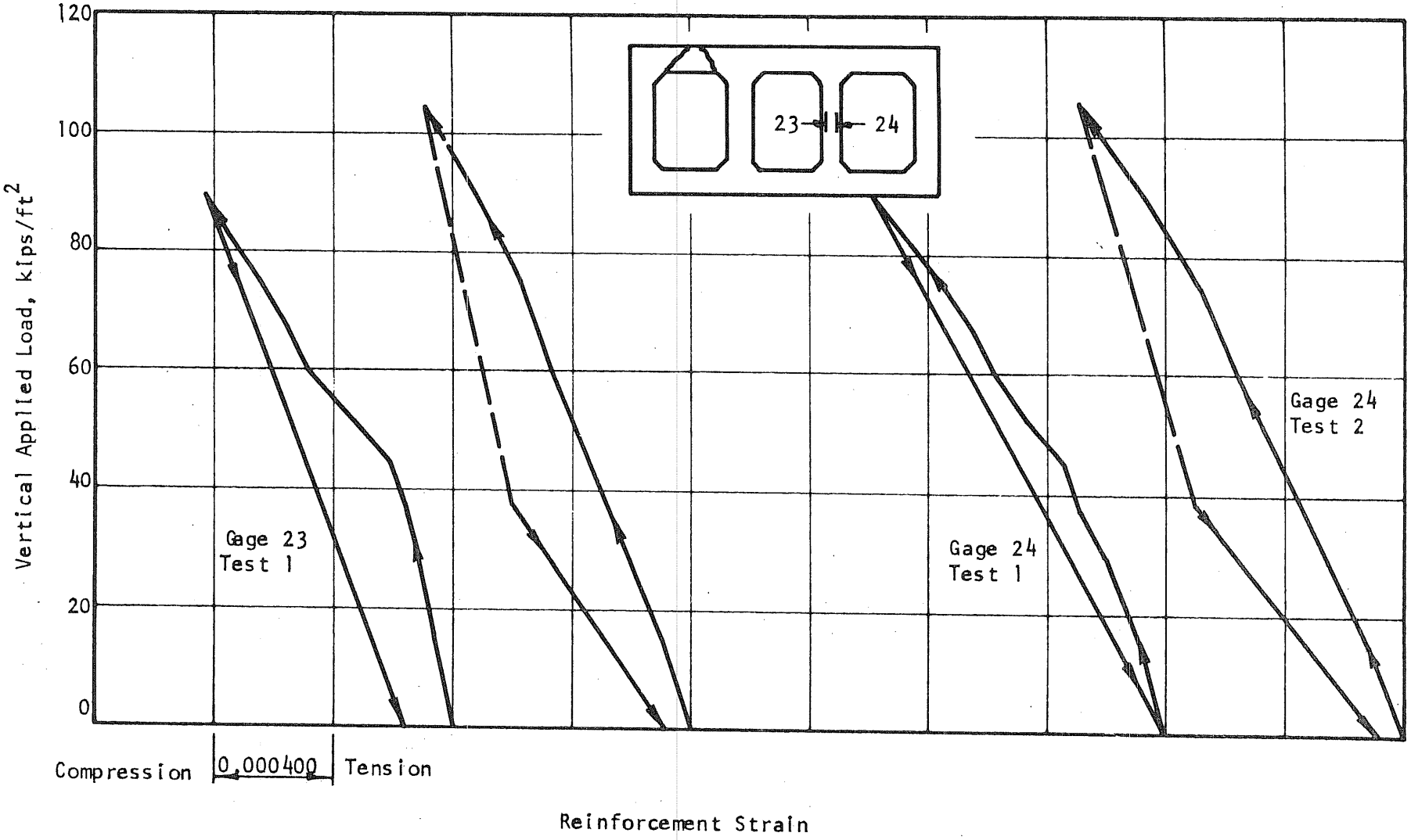

FIG. 7.34 LOAD-STRAIN CURVES, MIDHEIGHT OF INTERIOR VERTICAL MEMBER, R2

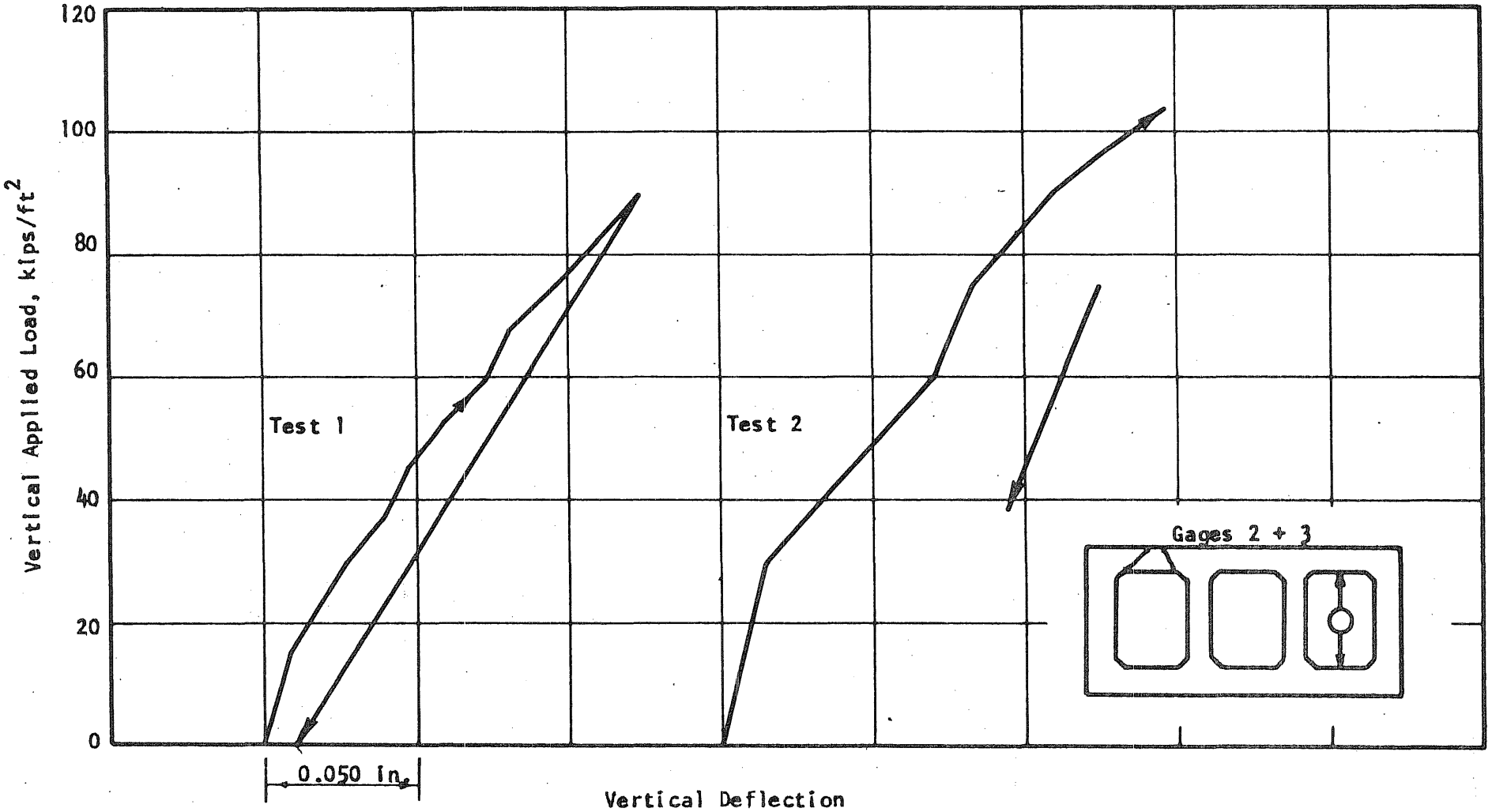

FIG. 7.35 LOAD-VERTICAL DEFLECTION CURVES, RIGHT END SPAN, R2

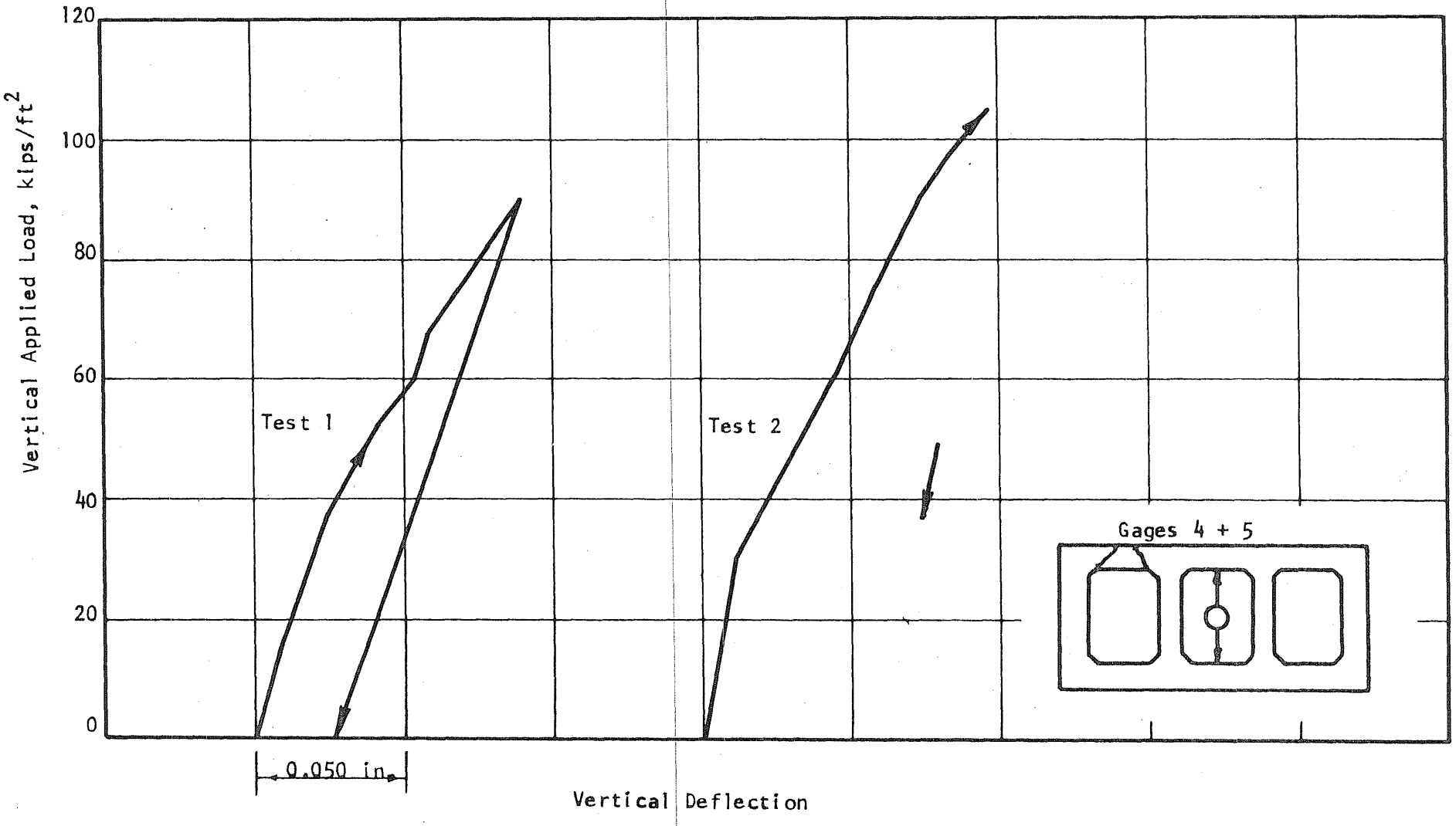

FIG. 7.36 LOAD-VERTICAL DEFLECTION CURVES, INTERIOR SPAN, R2

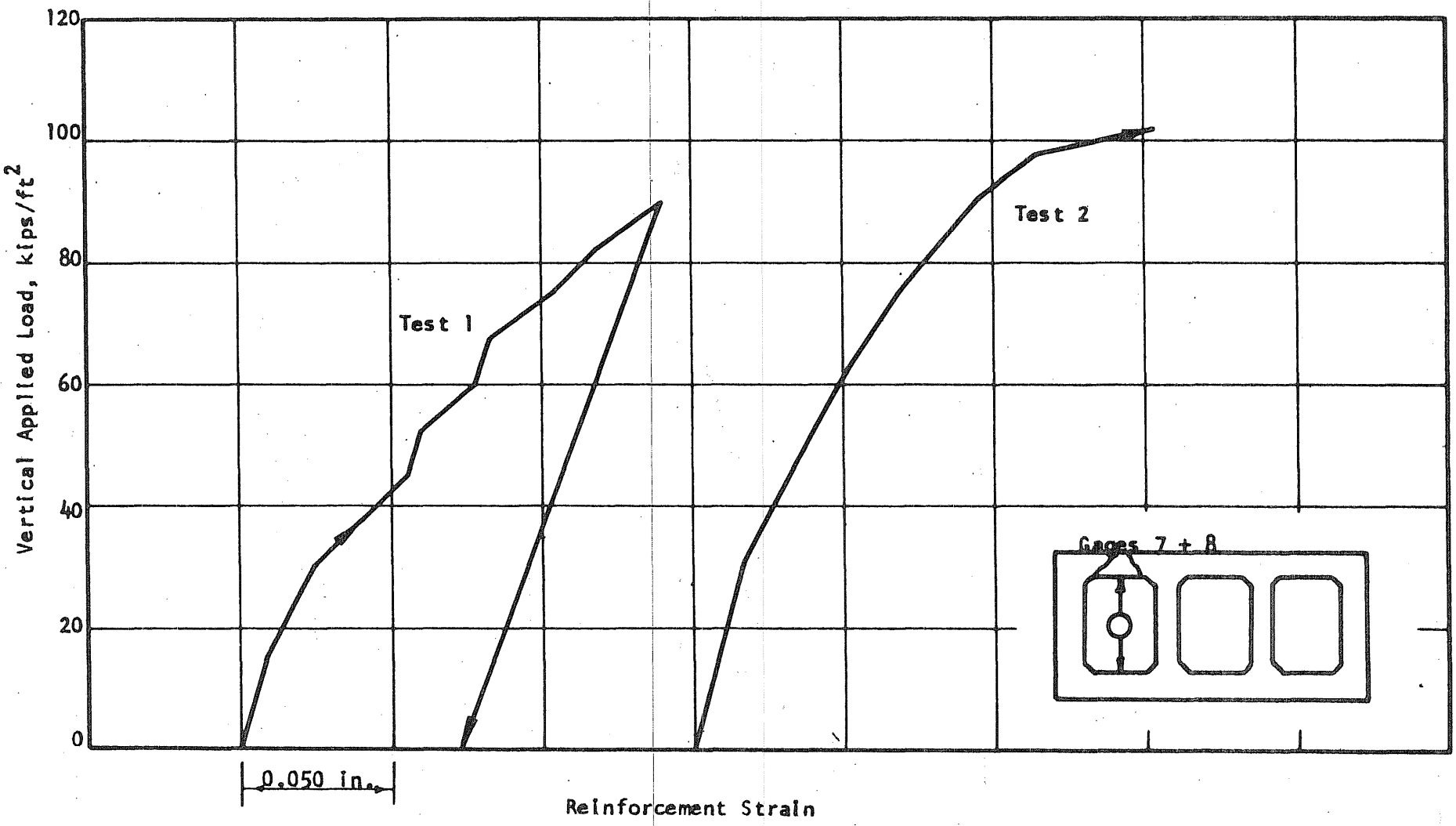

FIG. 7.37 LOAD-VERTICAL DEFLECTION CURVES, LEFT END SPAN, R2

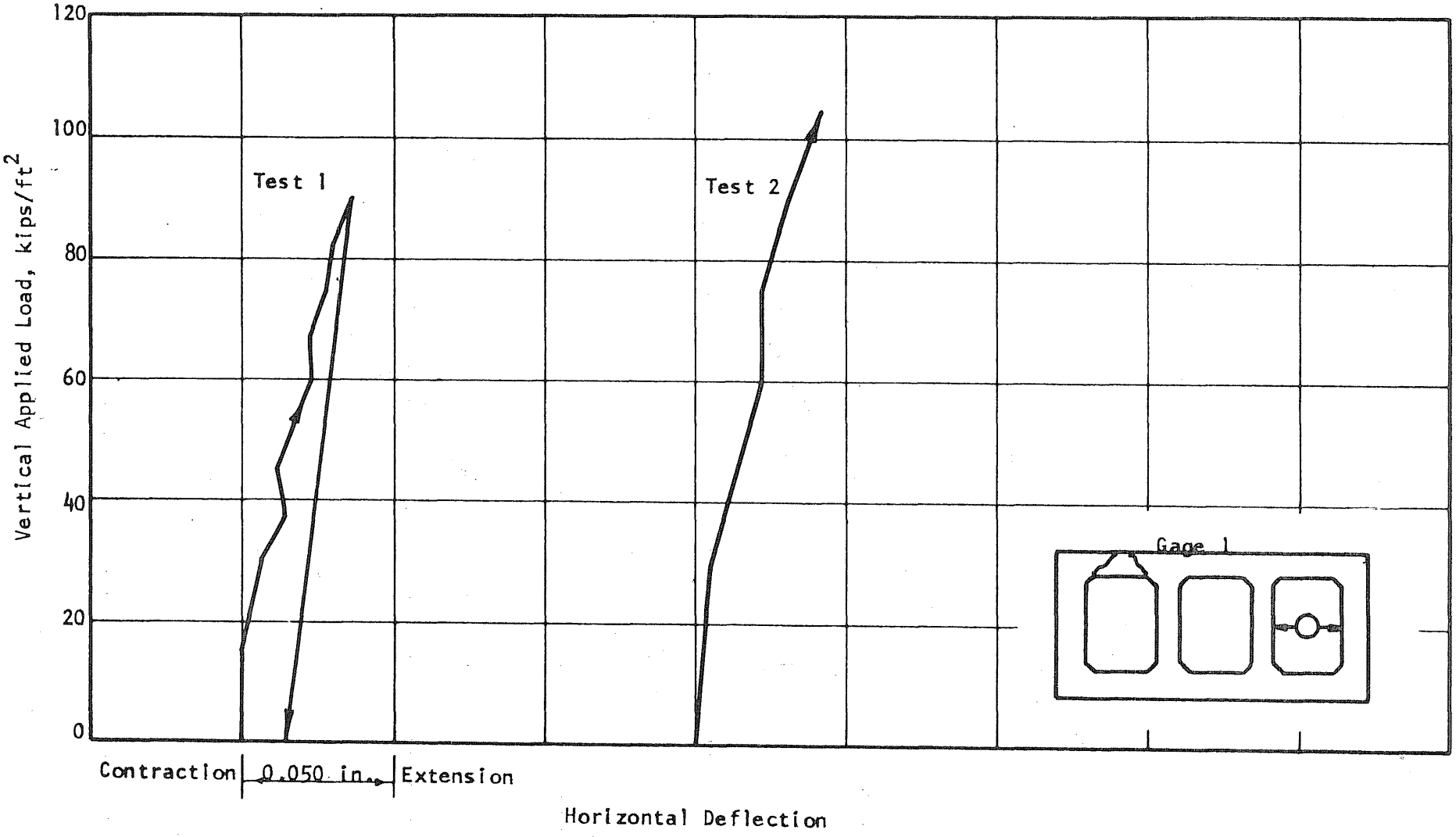

FIG. 7.38 LOAD-HORIZONTAL DEFLECTION CURVES, RIGHT END SPAN, R2

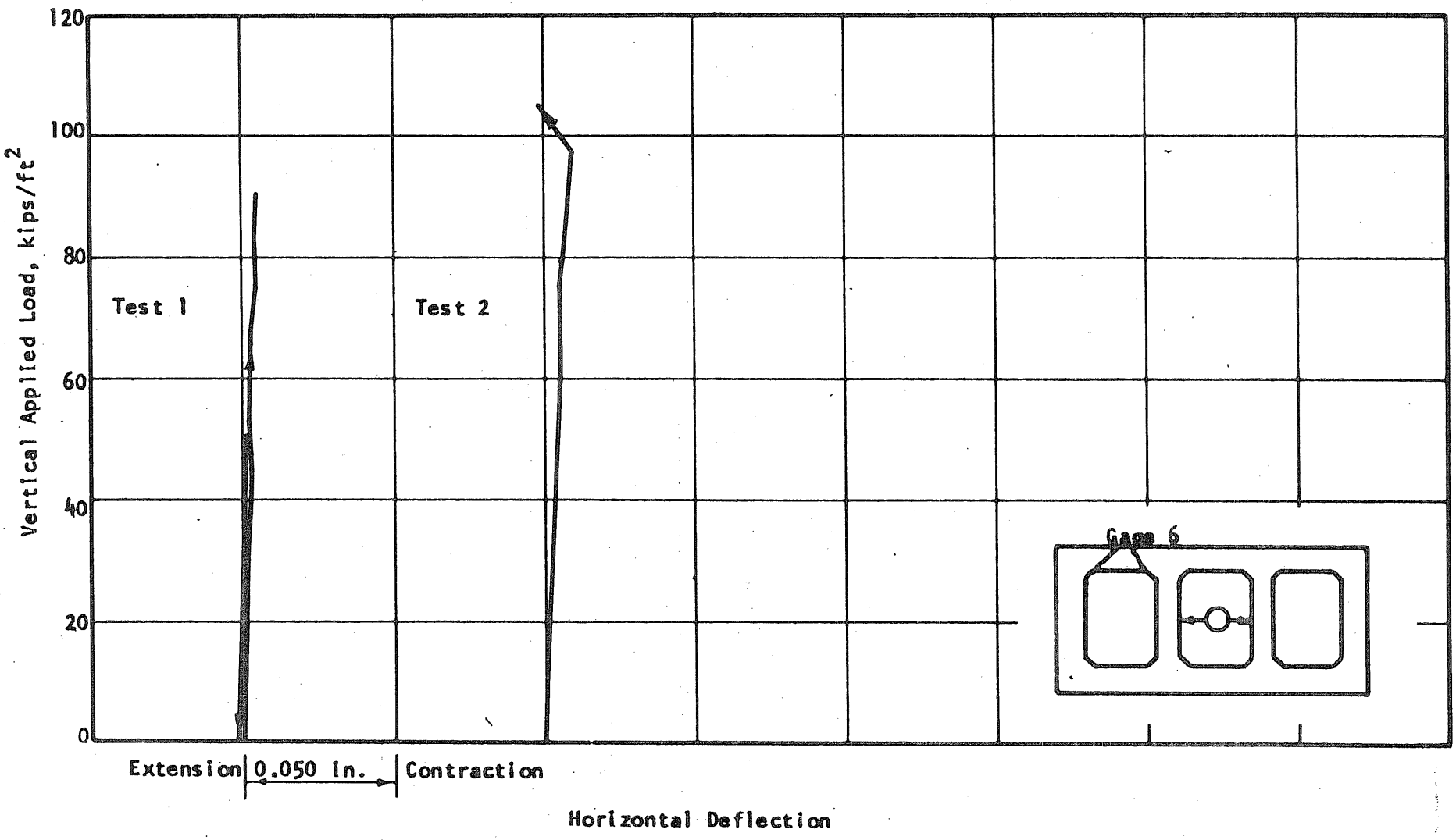

FIG. 7.39 LOAD-HORIZONTAL DEFLECTION CURVES, INTERIOR SPAN, R2

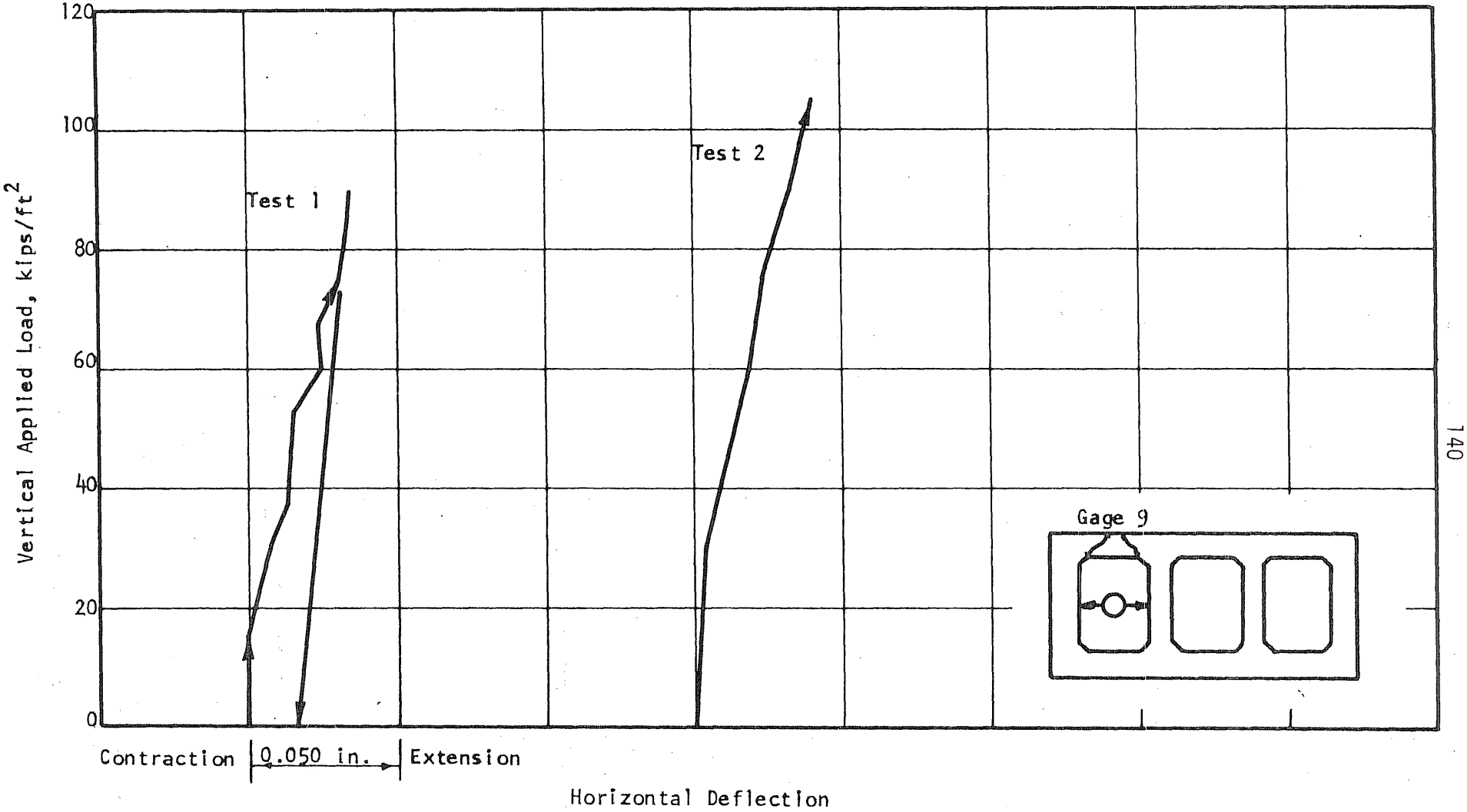

FIG. 7.40 LOAD-HORIZONTAL DEFLECTION CURVES, LEFT END SPAN, R2

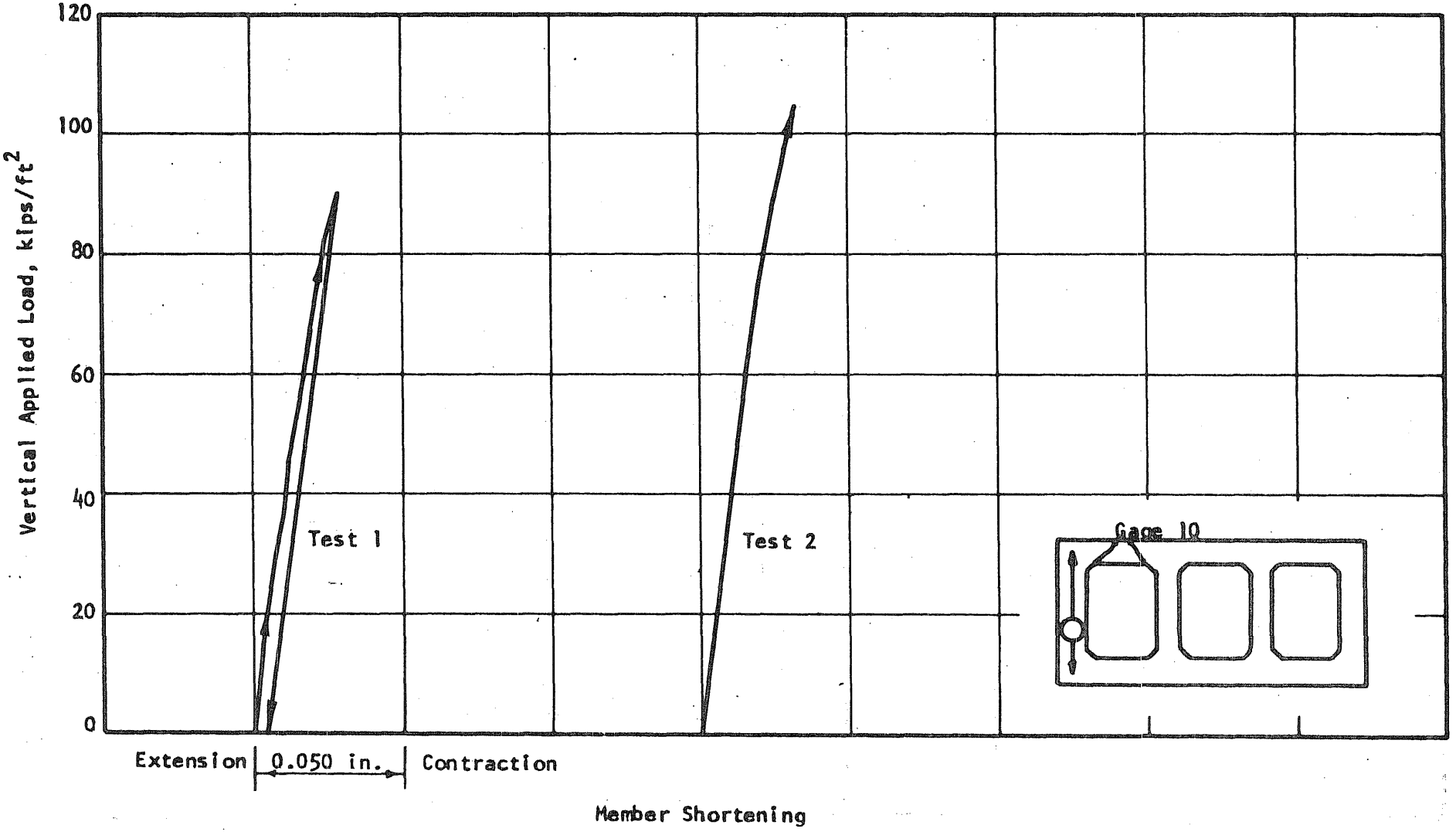

FIG. 7.41 LOAD-LENGTH CHANGE CURVES, EXTERIOR VERTICAL MEMBER, R2

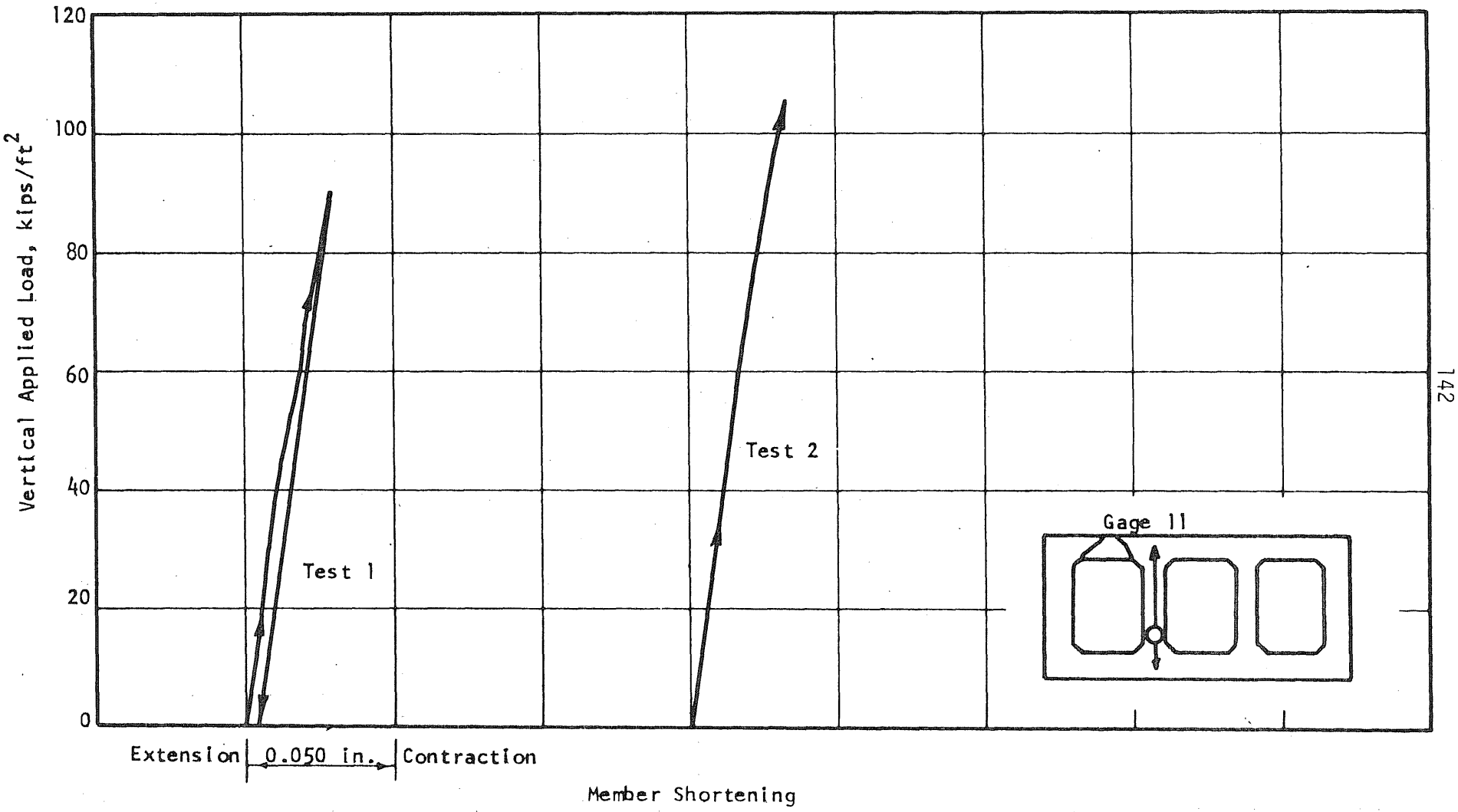

FIG. 7.42 LOAD-LENGTH CHANGE CURVES, INTERIOR VERTICAL MEMBER, R2

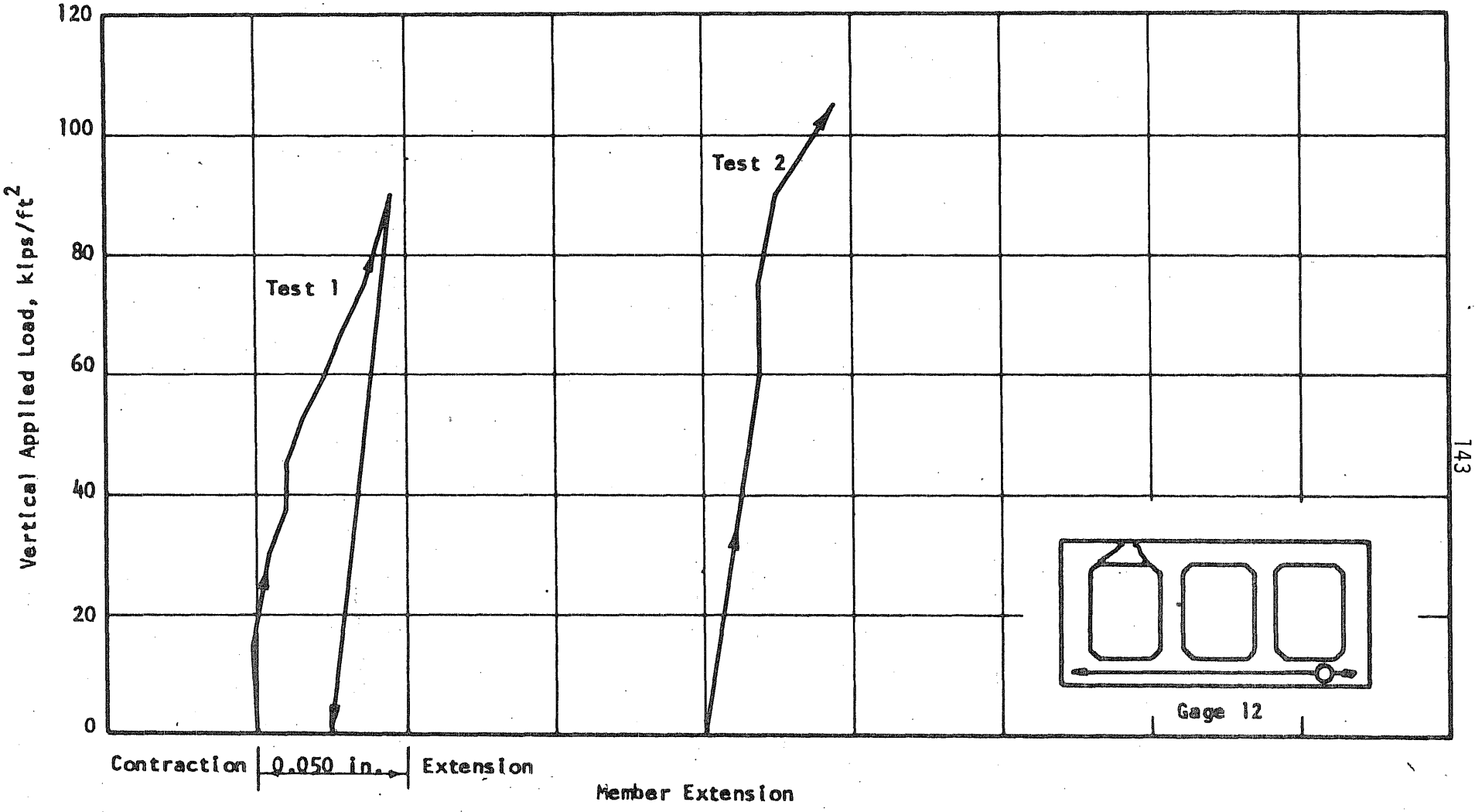

FIG. 7.43 LOAD-LENGTH CHANGE CURVES, LOWER HORIZONTAL MEMBER, R2

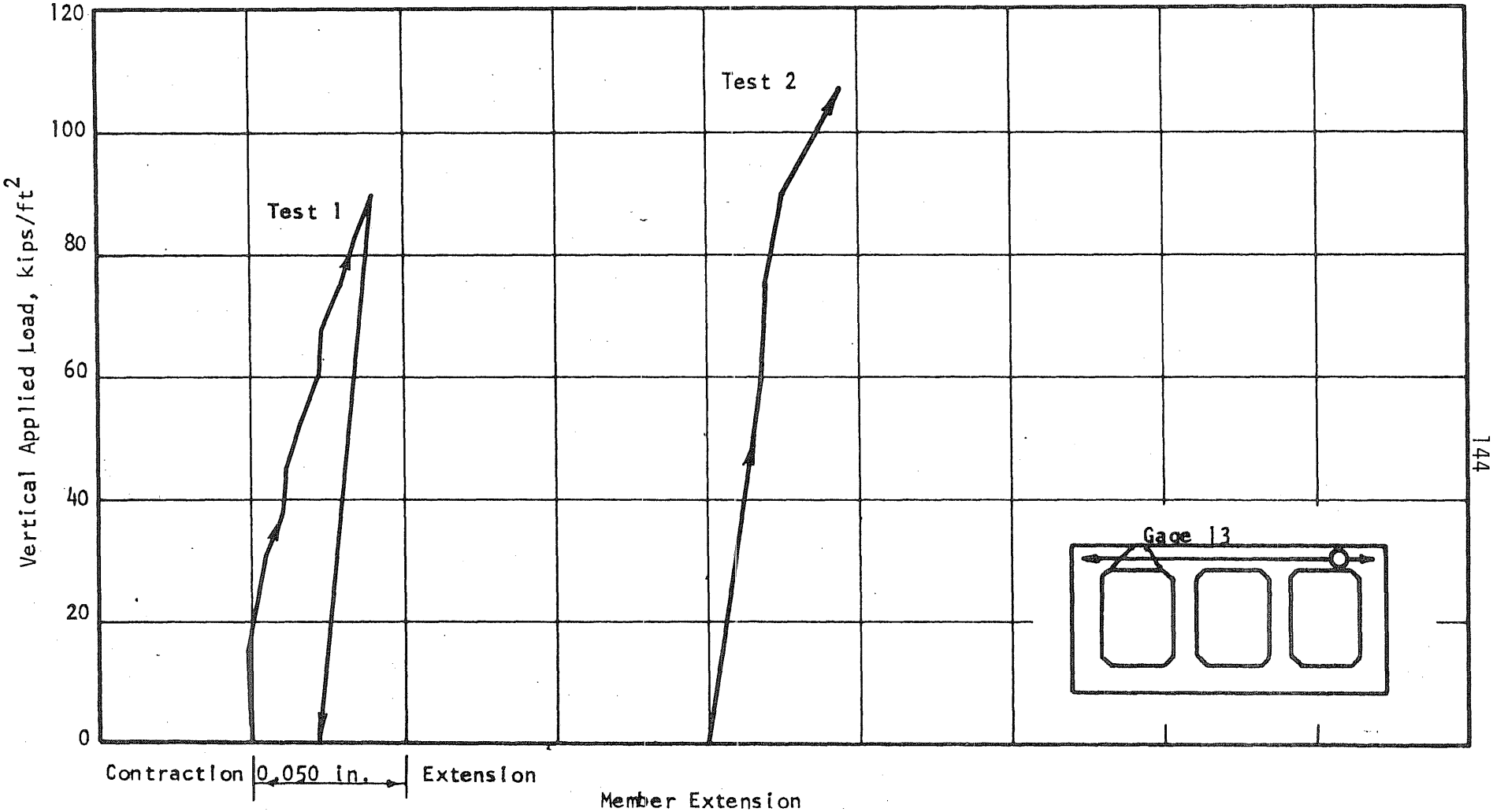

FIG. 7.44 LOAD-LENGTH CHANGE CURVES, UPPER HORIZONTAL MEMBER, R2

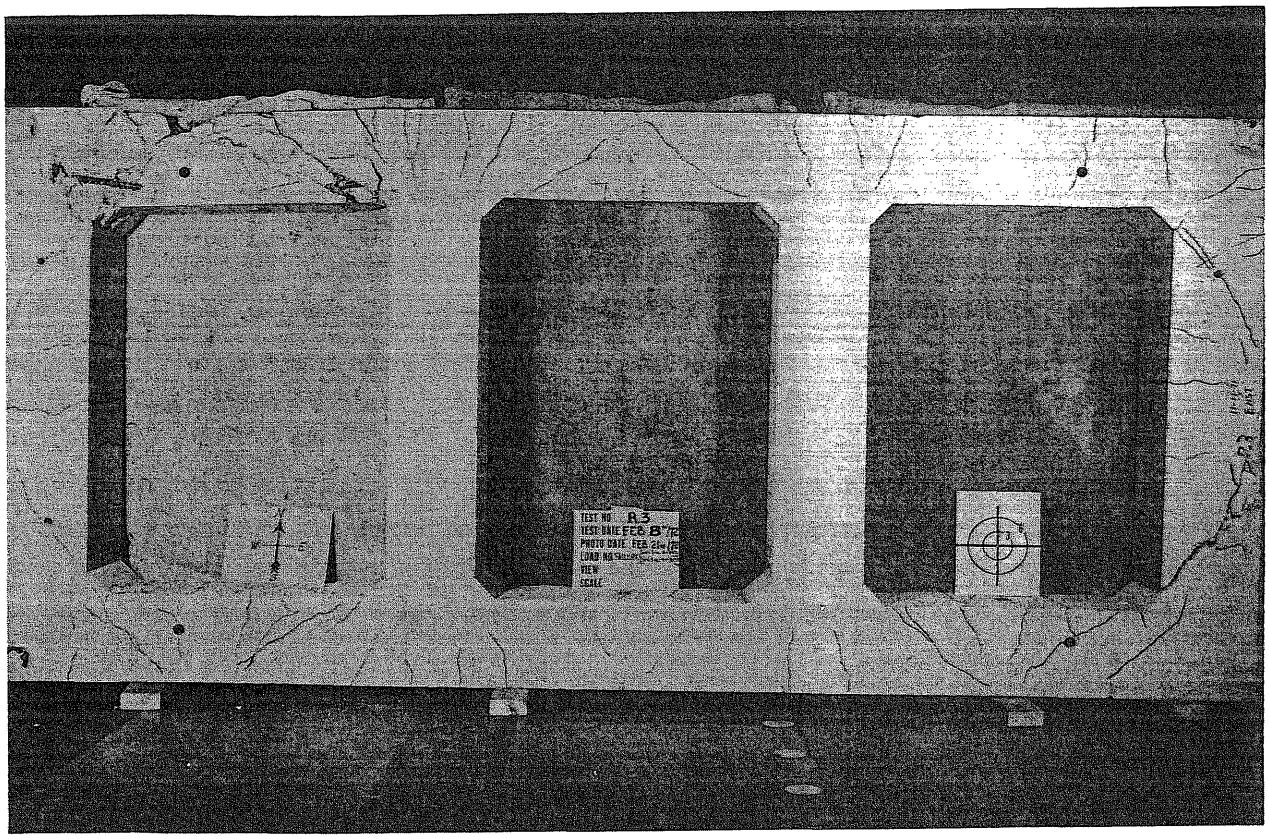

FIG. 7.45 SPECIMEN R3 AFTER TESTS TO FAILURE

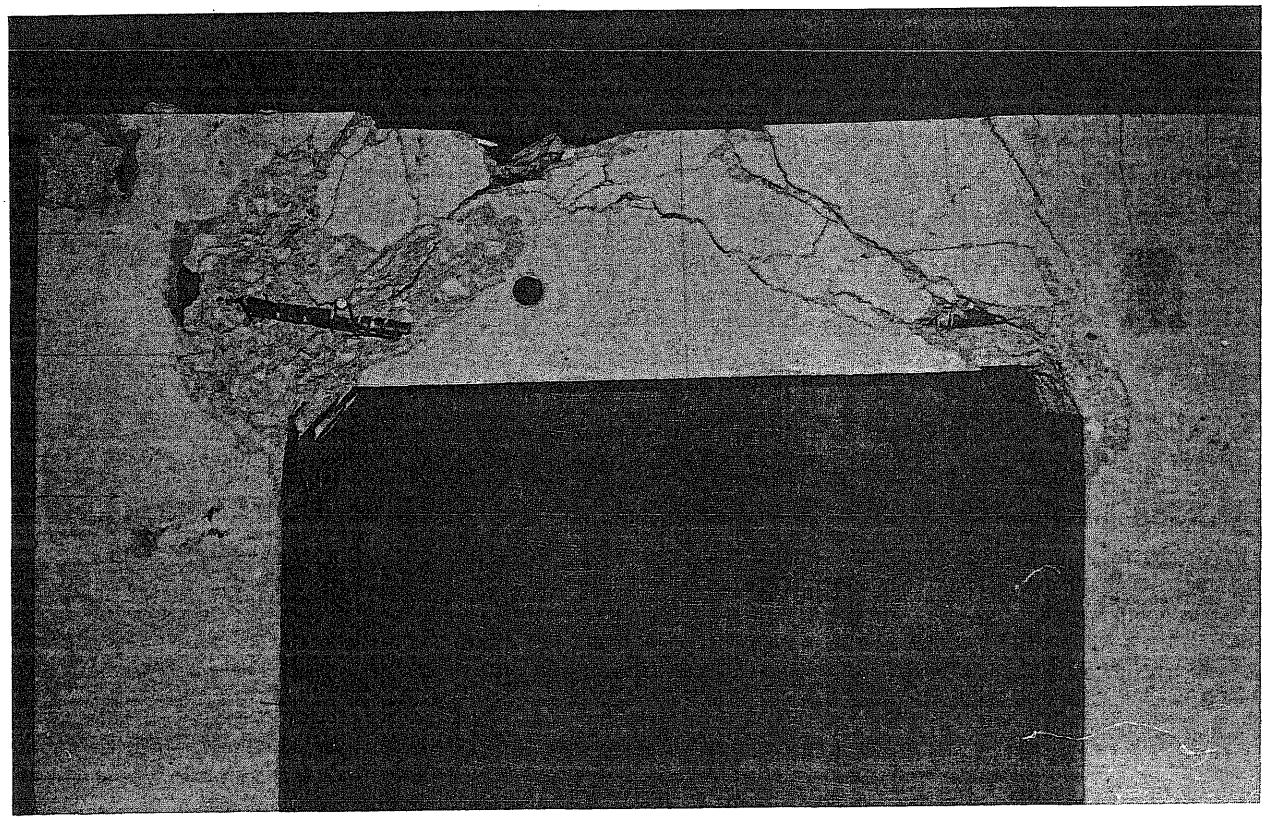

FIG. 7.46 FAILED HORIZONTAL MEMBER, SPECIMEN R3

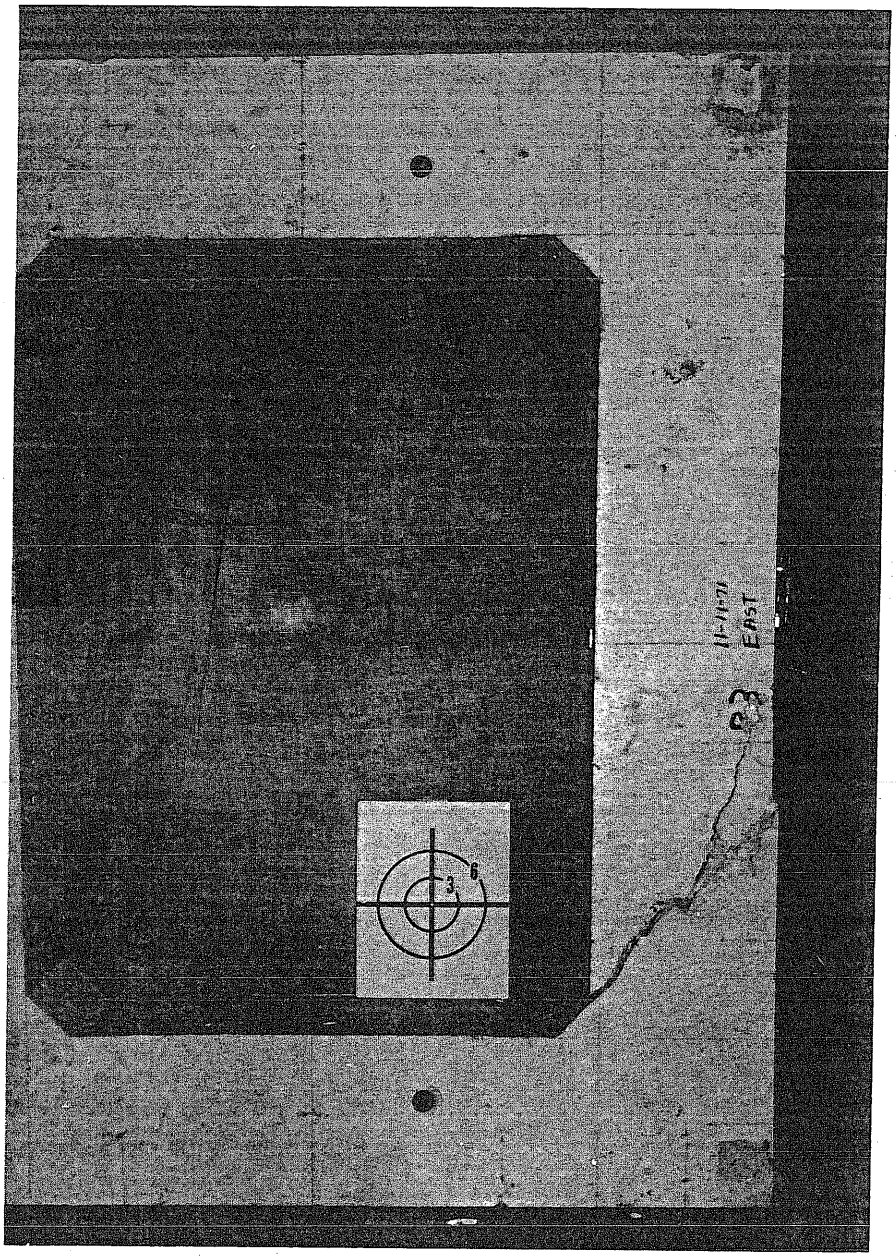

FIG. 7.47 FAILED VERTICAL MEMBER, SPECIMEN R3

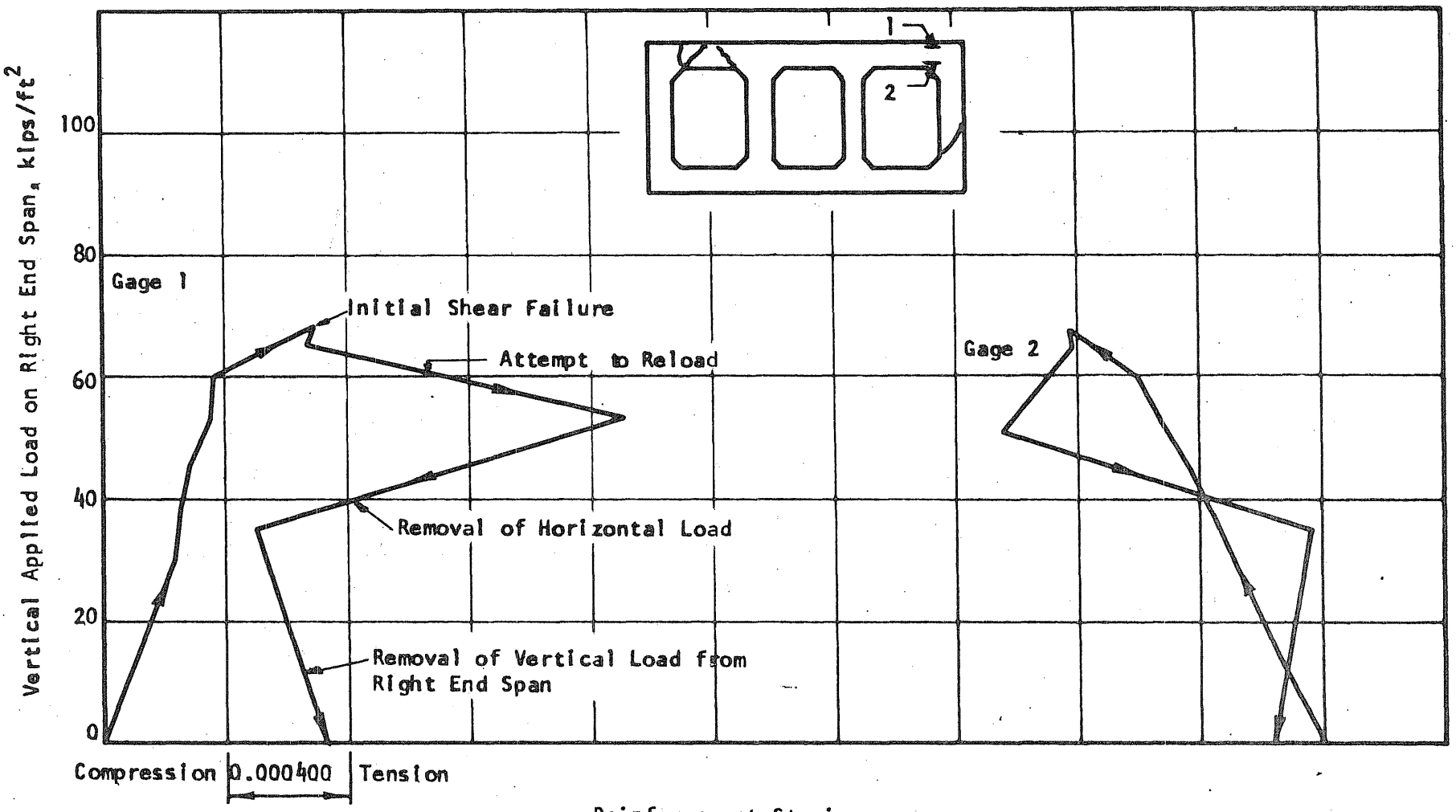

FIG. 7.48 LOAD-STRAIN CURVES, EXTERIOR END OF END SPAN, R3

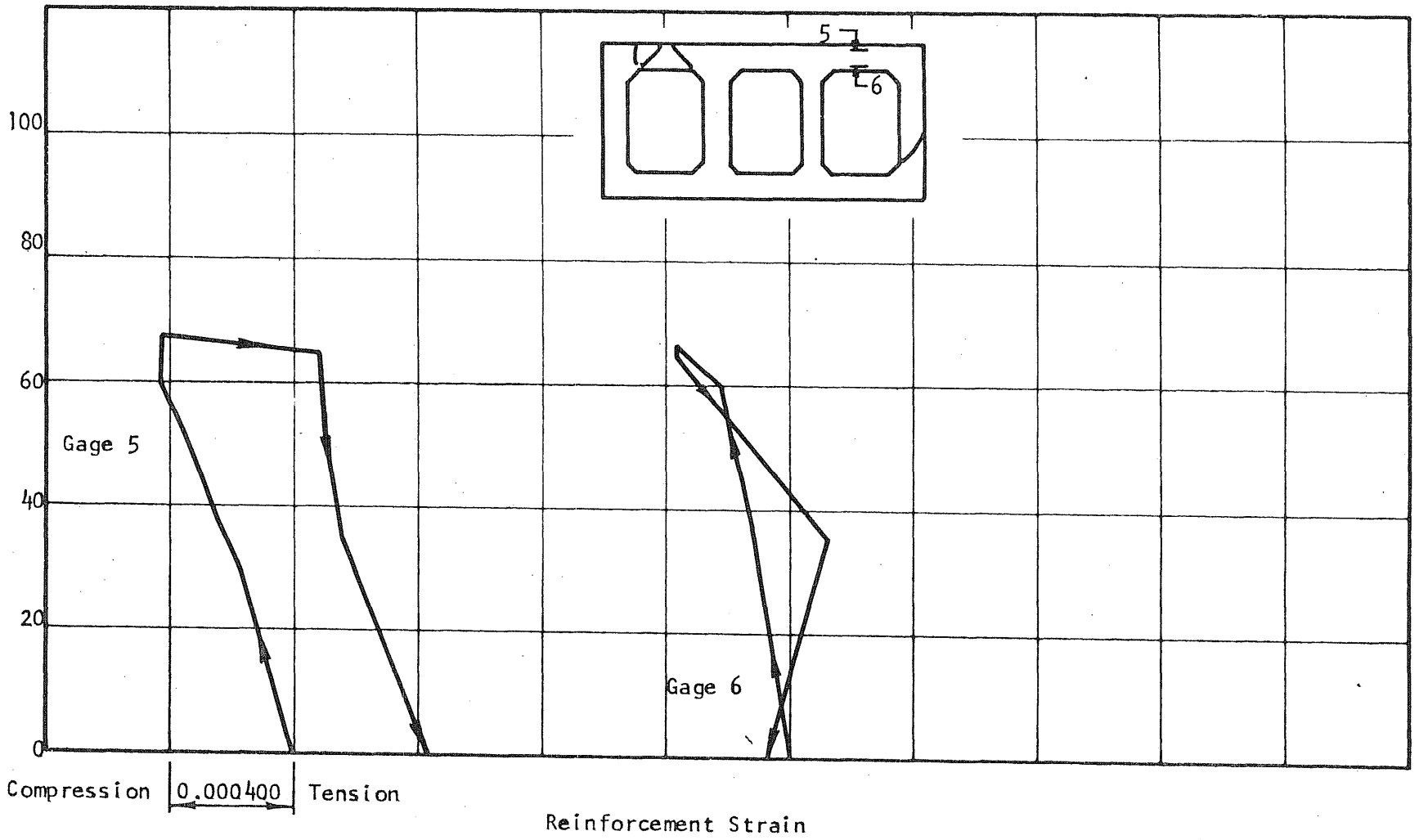

FIG. 7.49 LOAD-STRAIN CURVES, MIDSPAN OF END SPAN, R3

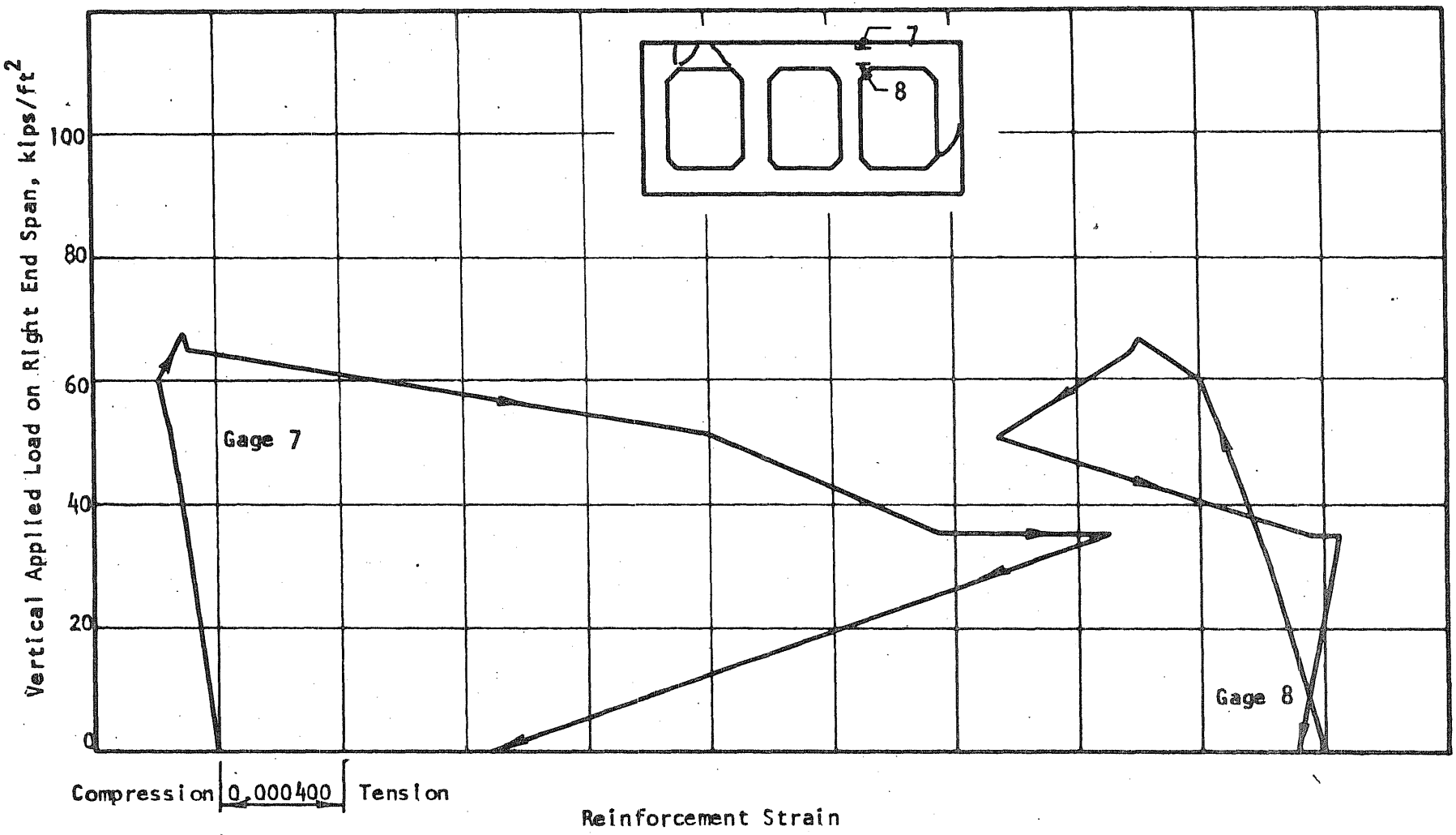

FIG. 7.50 LOAD-STRAIN CURVES, INTERIOR END OF END SPAN, R3

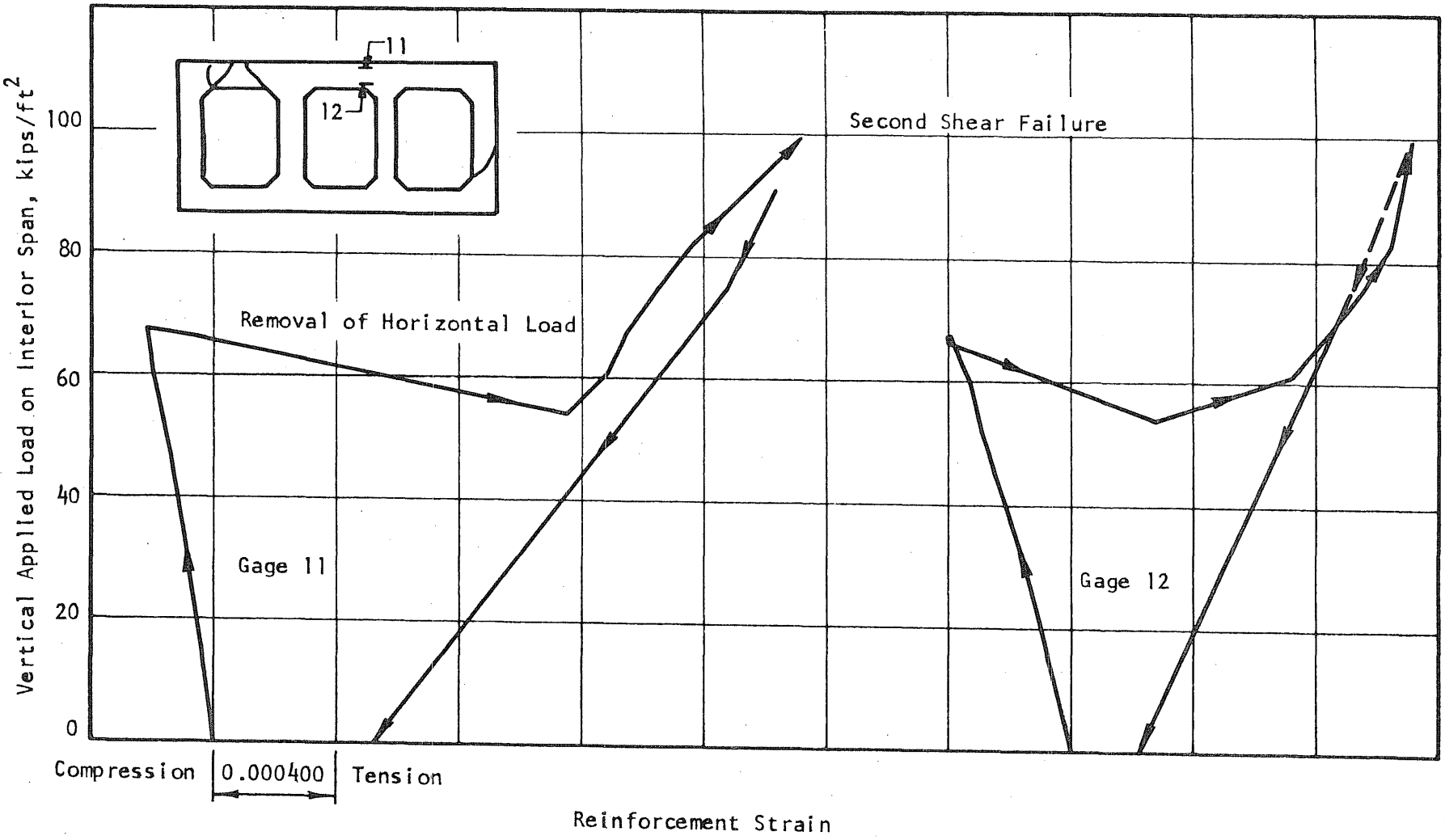

FIG. 7.51 LOAD-STRAIN CURVES, END OF INTERIOR SPAN, R3

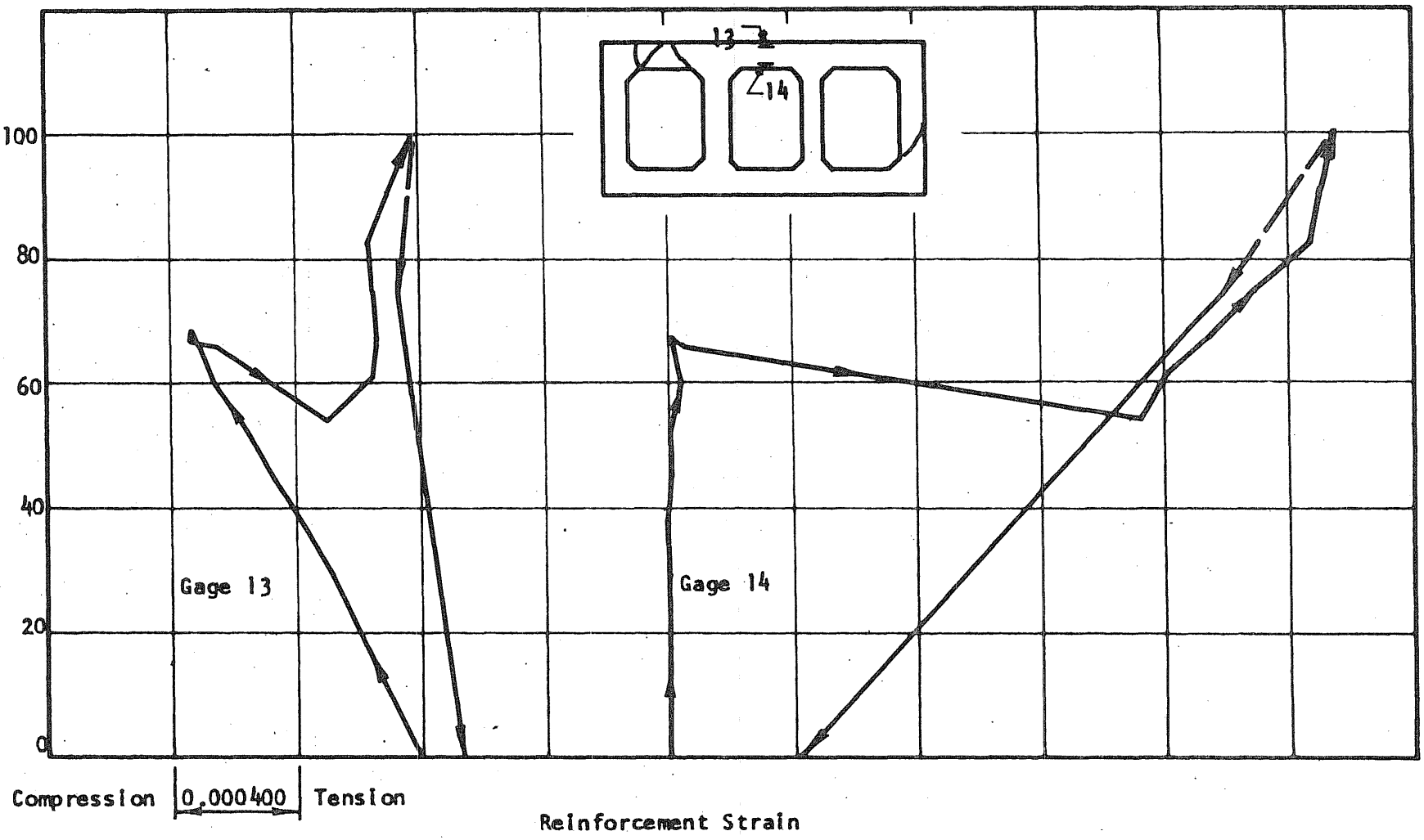

FIG. 7.52 LOAD-STRAIN CURVES, MIDSPAN OF INTERIOR SPAN, R3

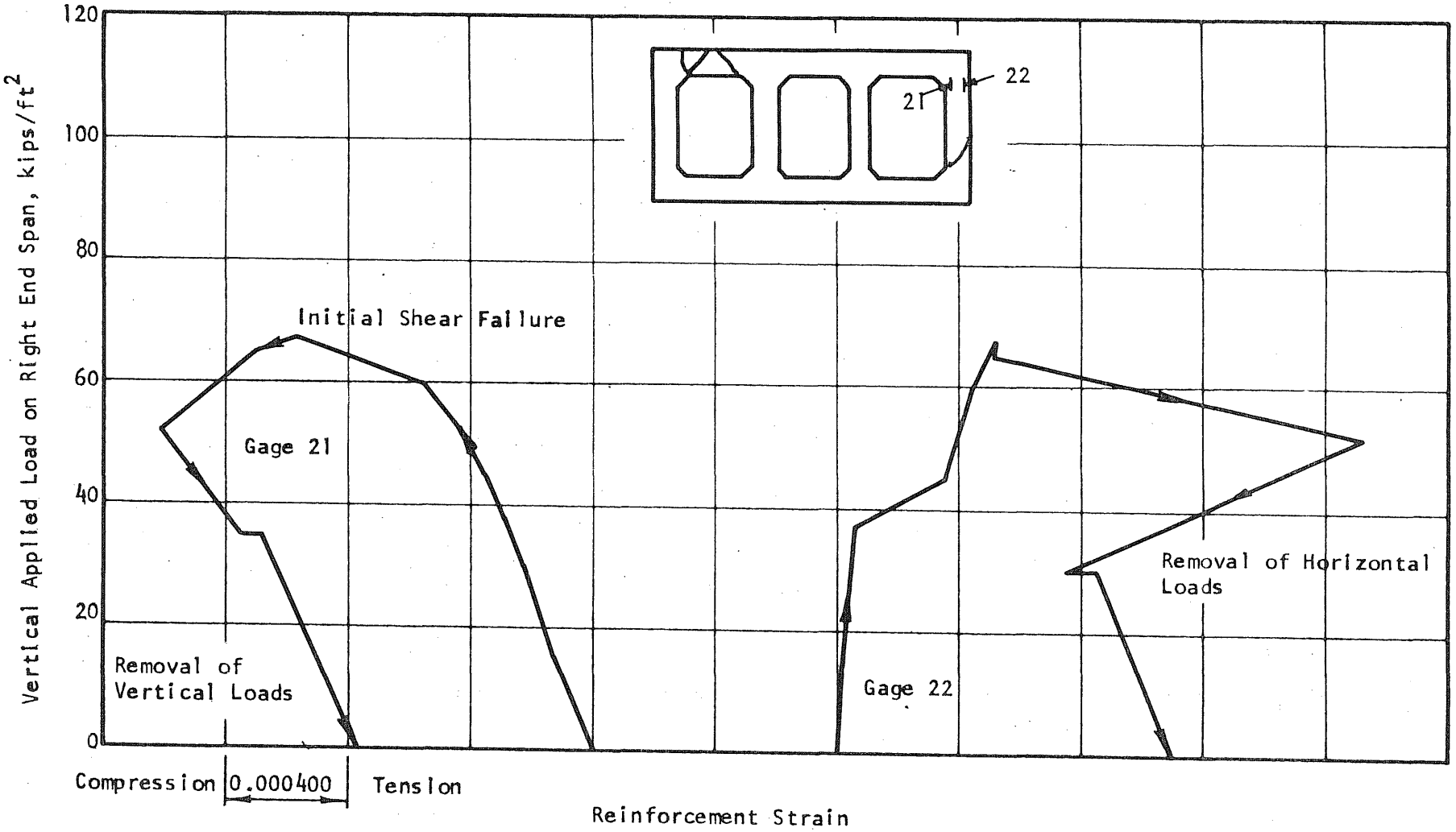

FIG. 7.53 LOAD-STRAIN CURVES, TOP OF EXTERIOR VERTICAL MEMBER, R3

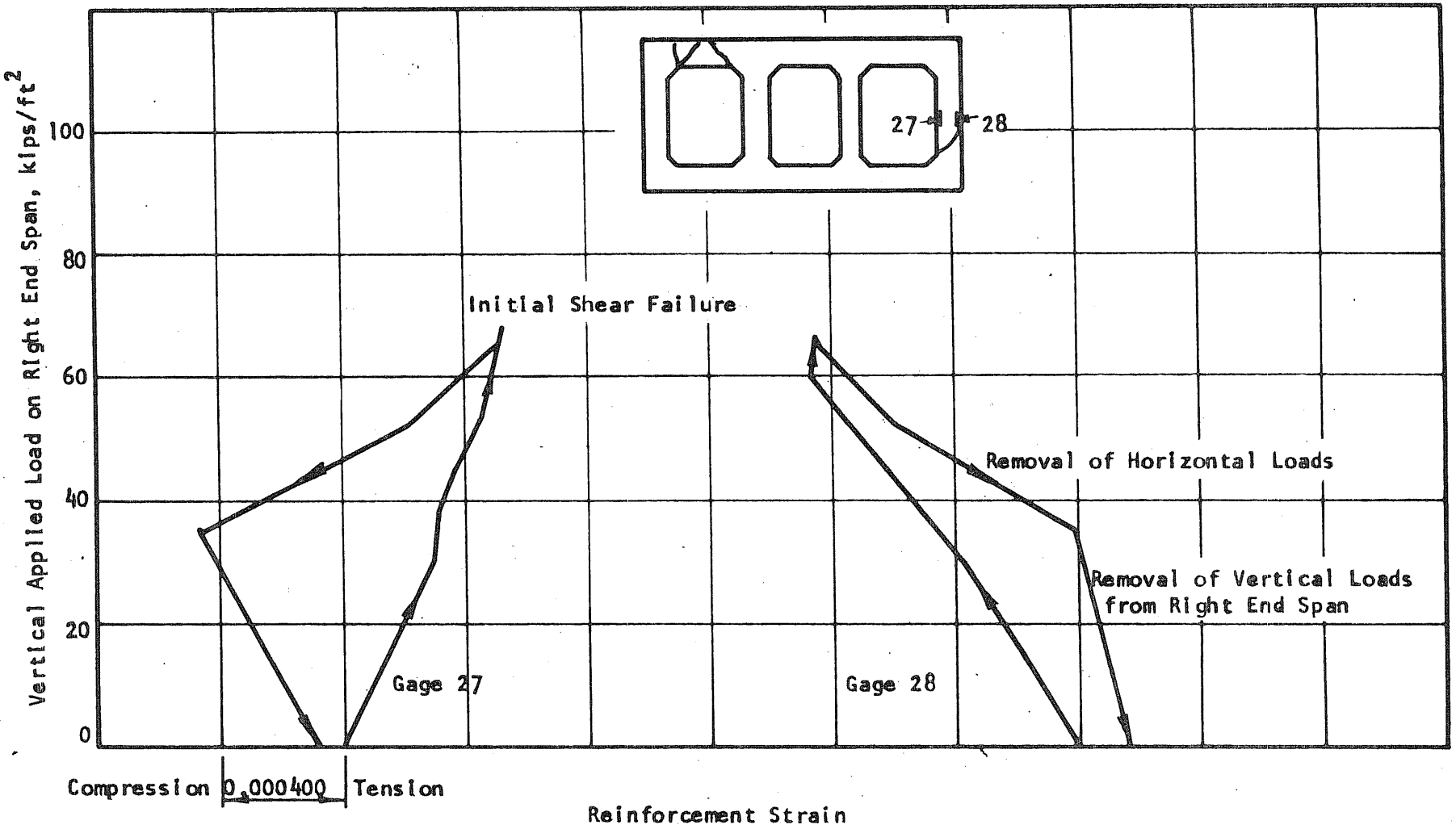

FIG. 7.54 LOAD-STRAIN CURVES, MIDHEIGHT OF END VERTICAL MEMBER, R3

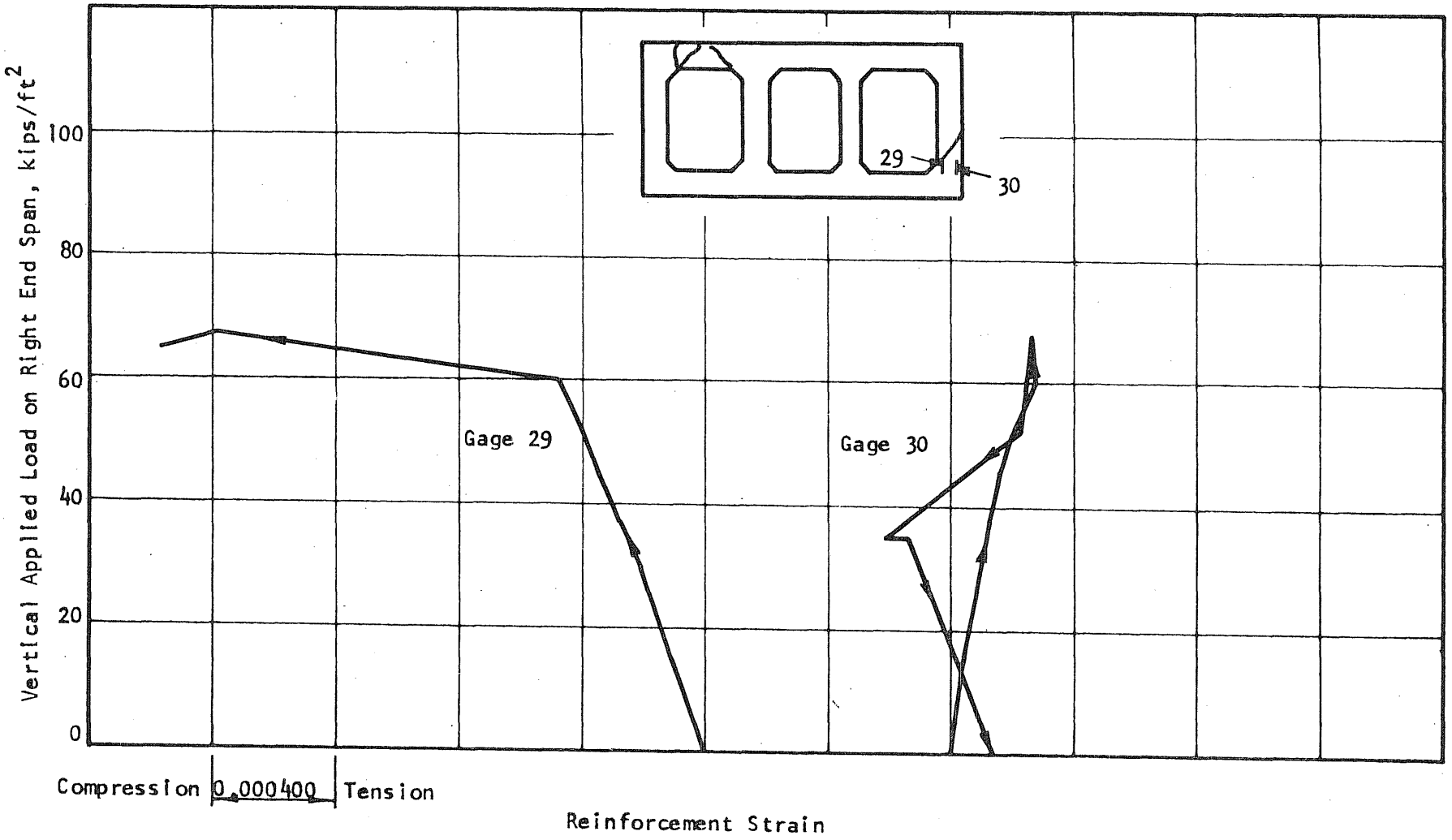

FIG. 7.55 LOAD-STRAIN CURVES, BOTTOM OF EXTERIOR END MEMBER, R3

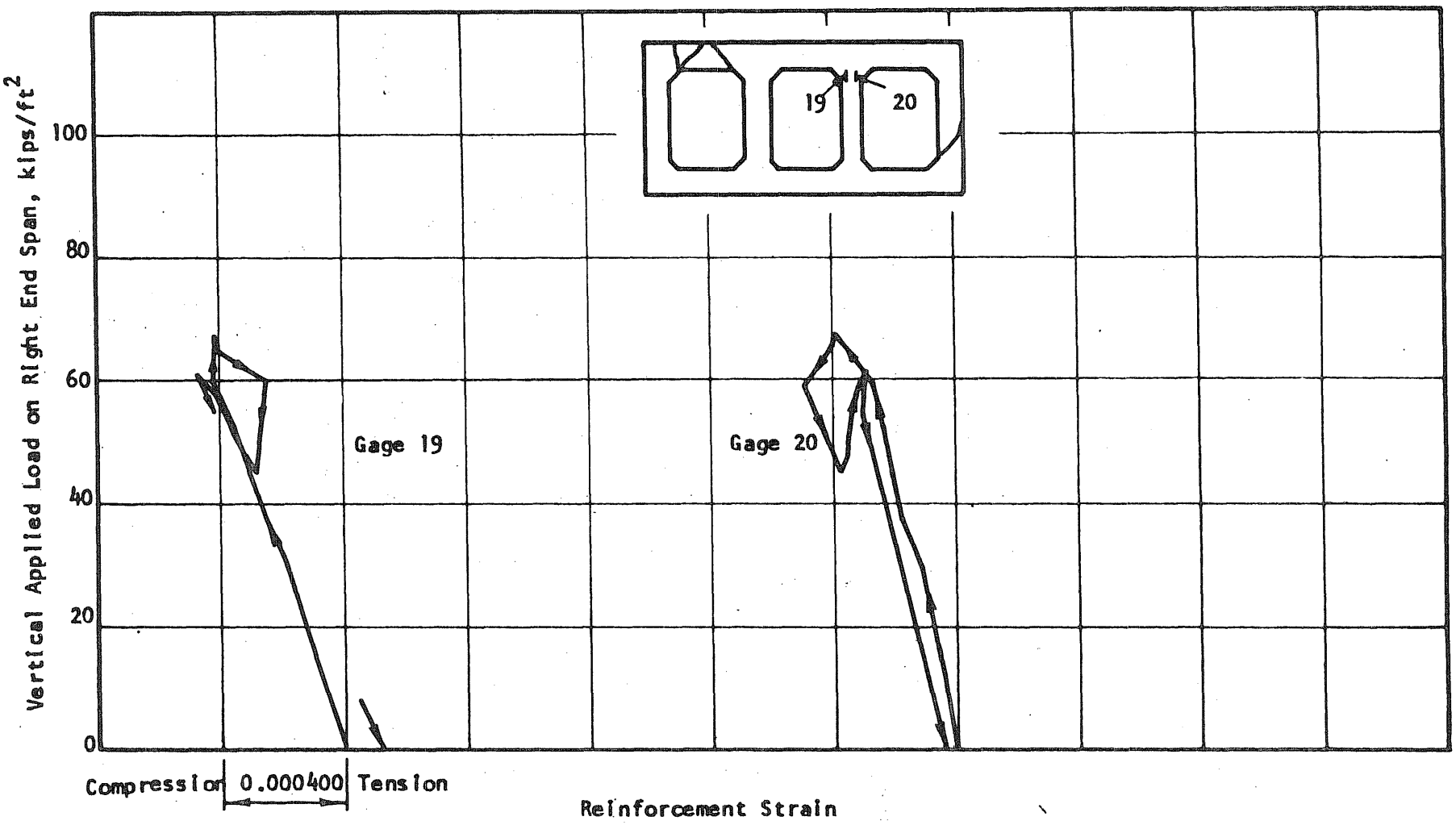

FIG. 7.56 LOAD-STRAIN CURVES, UPPER END OF INTERIOR VERTICAL MEMBER, R3

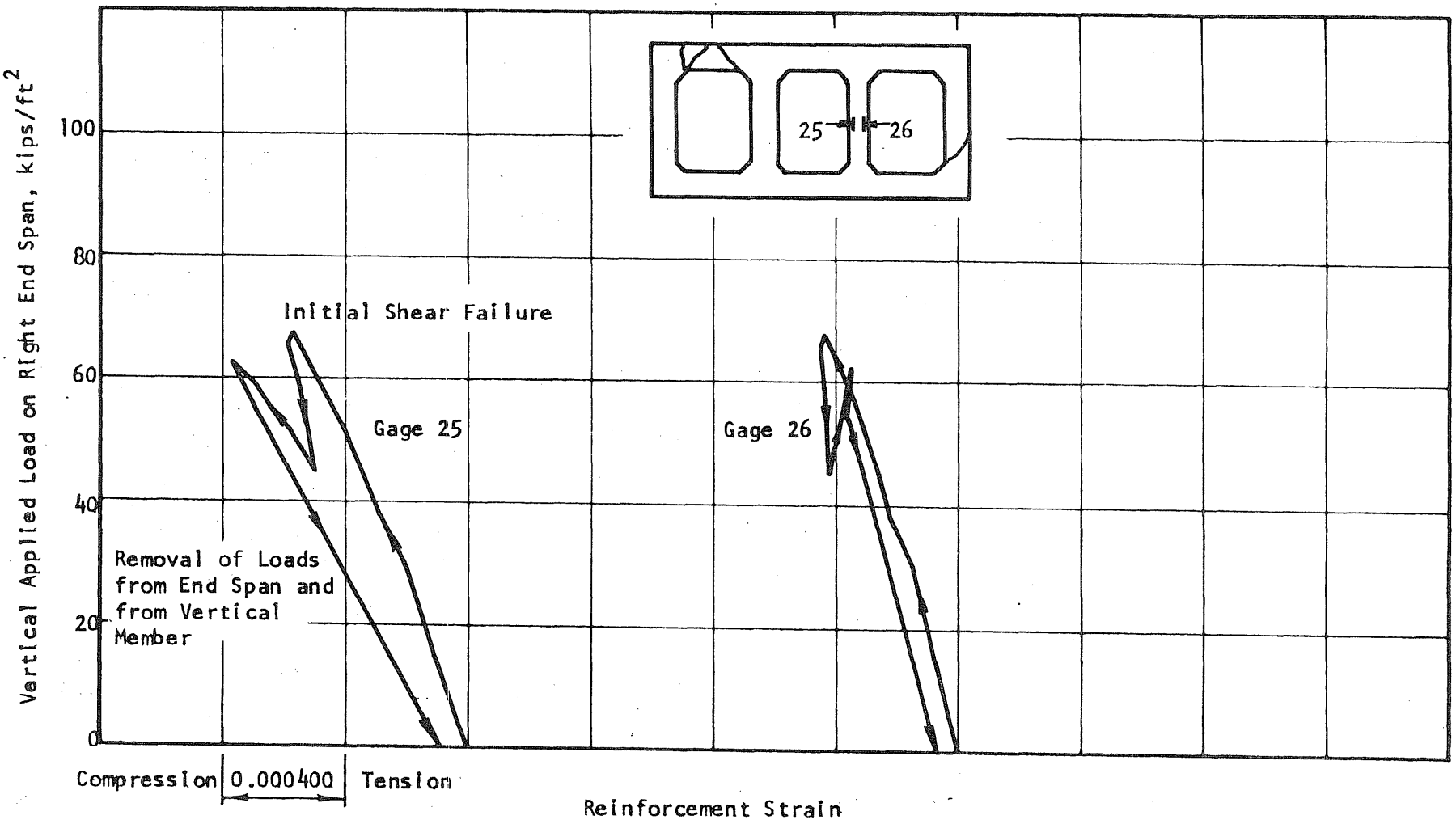

FIG. 7.57 LOAD-STRAIN CURVES, MIDHEIGHT OF INTERIOR VERTICAL MEMBER, R3

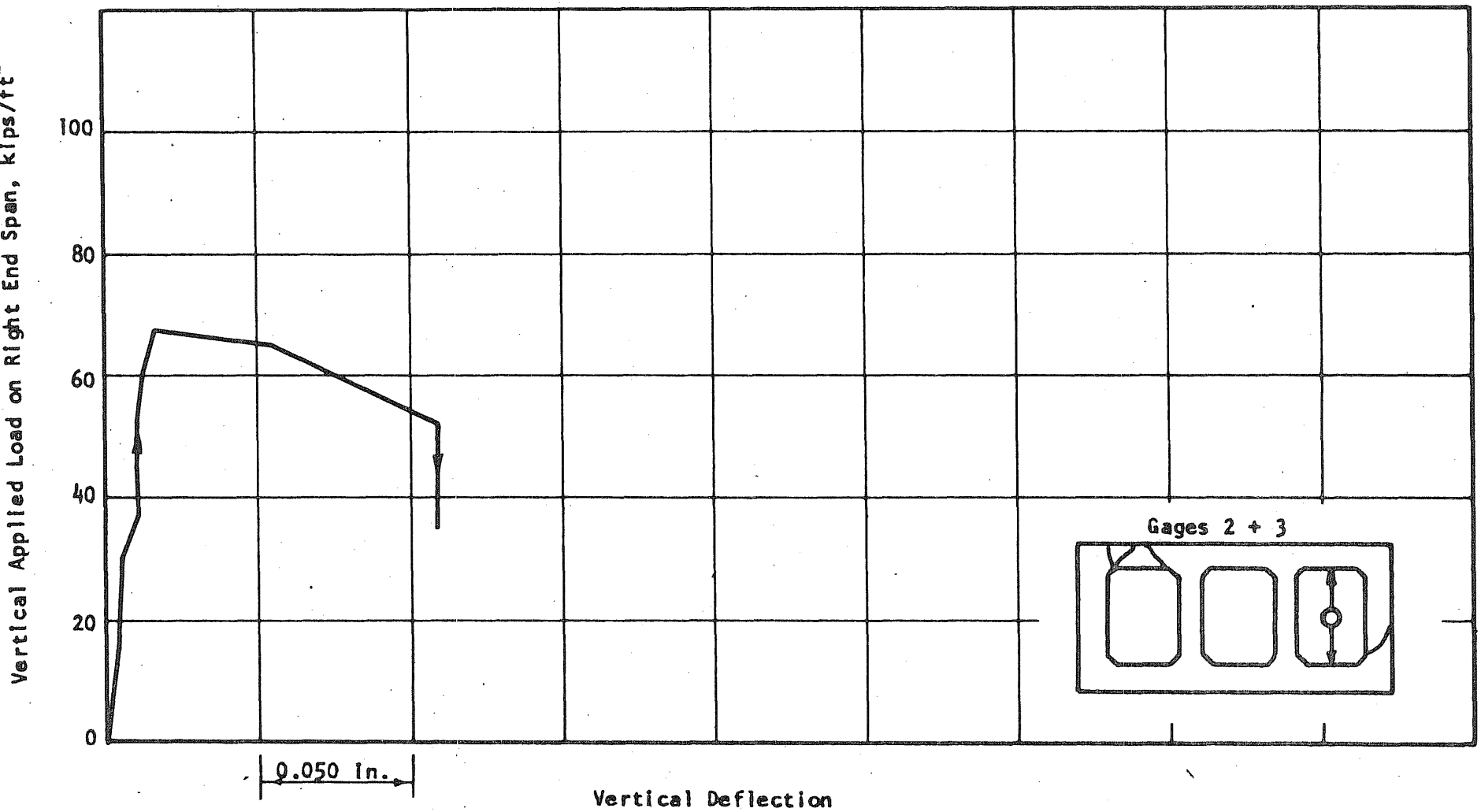

FIG. 7.58 LOAD-VERTICAL DEFLECTION CURVES, RIGHT END SPAN, R3

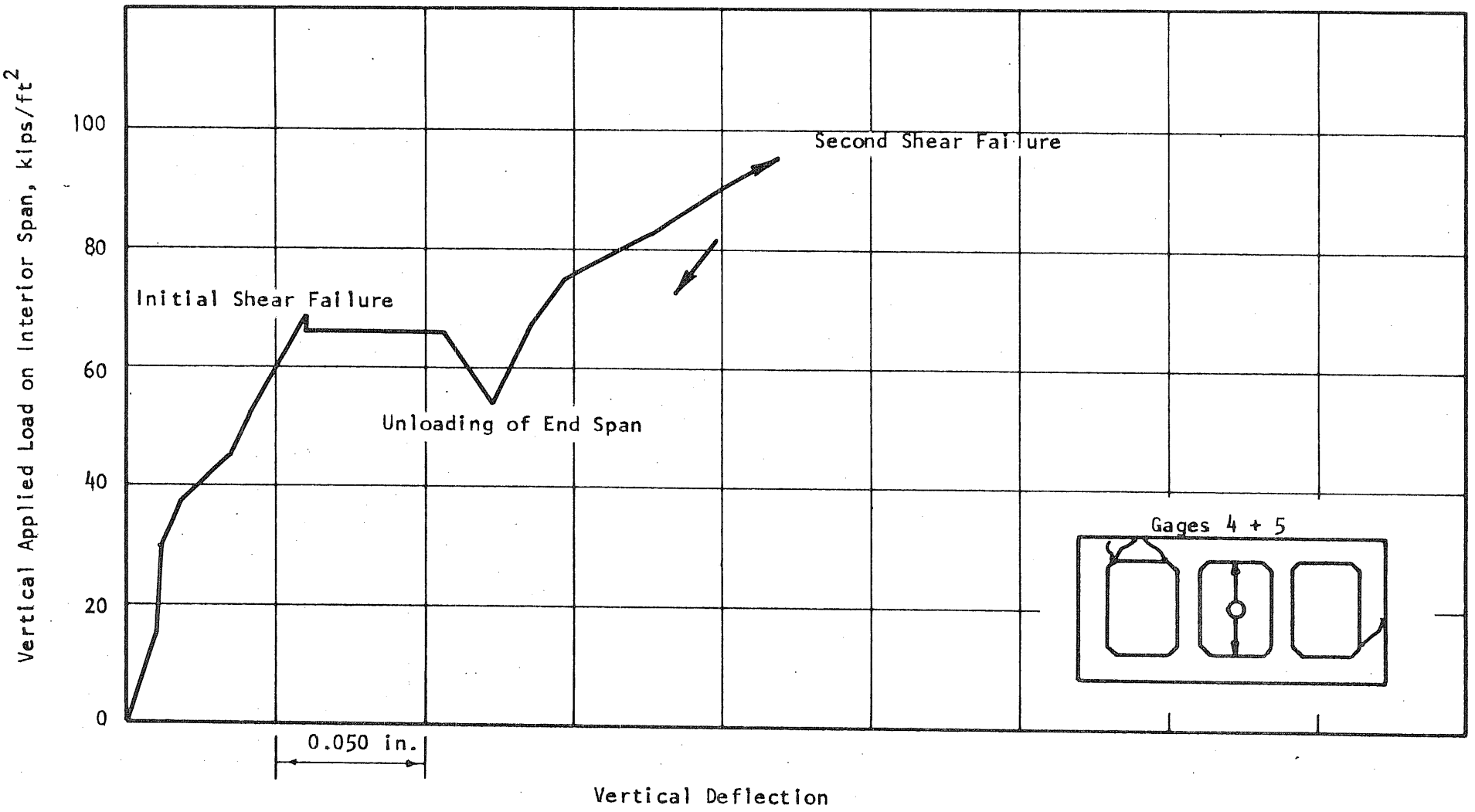

FIG. 7.59 LOAD-VERTICAL DEFLECTION, INTERIOR SPAN, R3

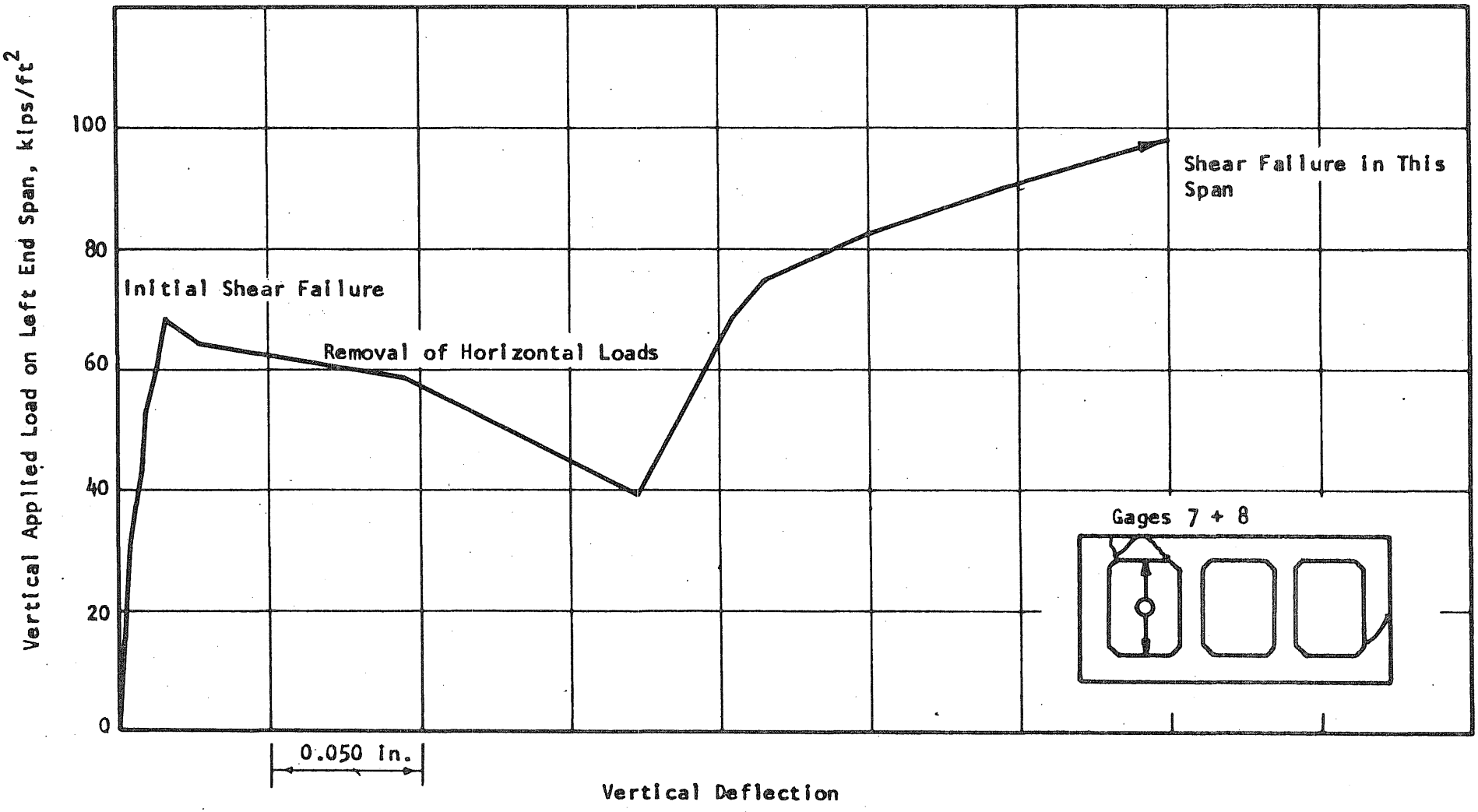

FIG. 7.60 LOAD-VERTICAL DEFLECTION, LEFT END SPAN, R3

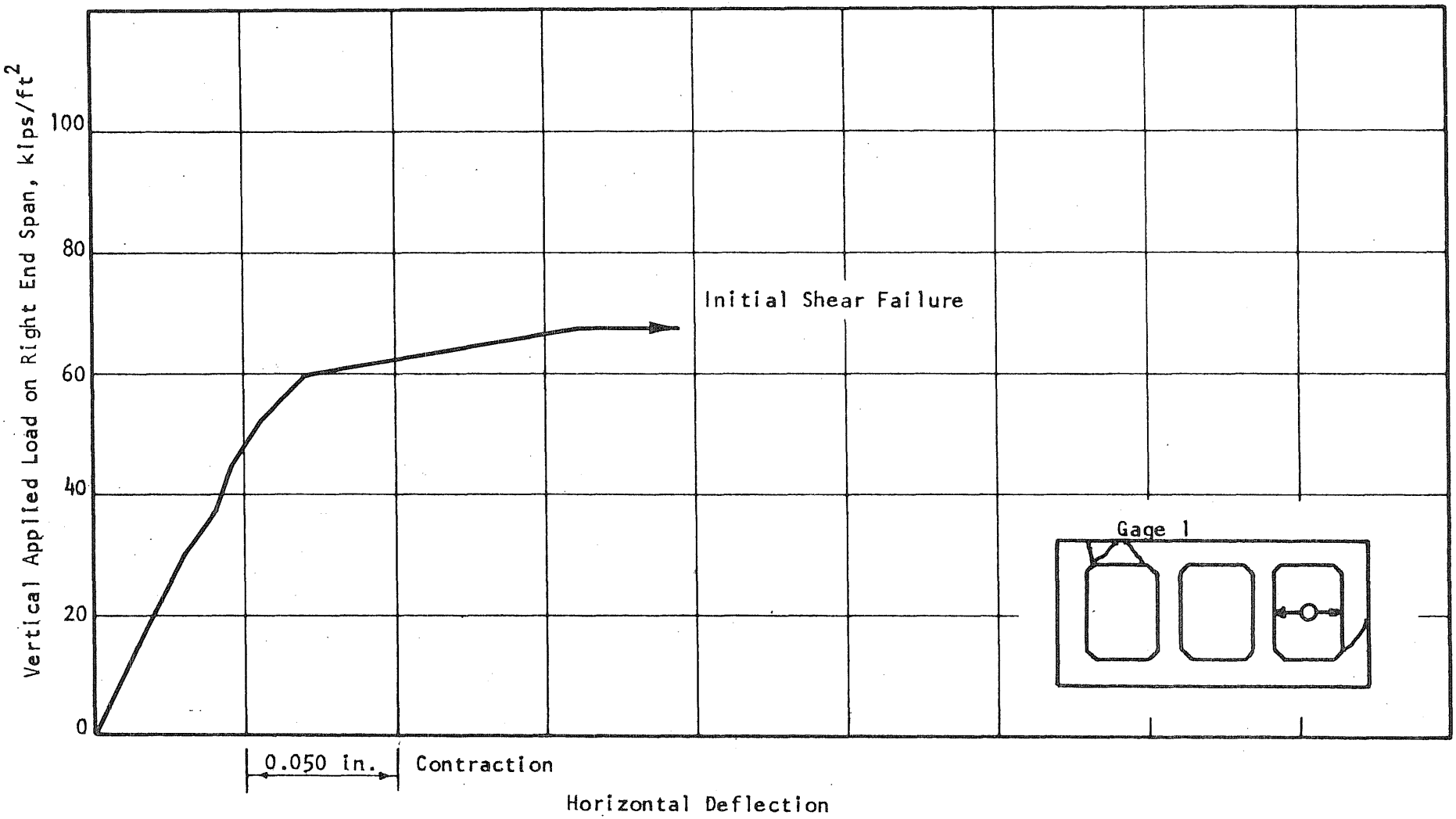

FIG. 7.61 LOAD-HORIZONTAL DEFLECTION CURVE, RIGHT END SPAN, R3

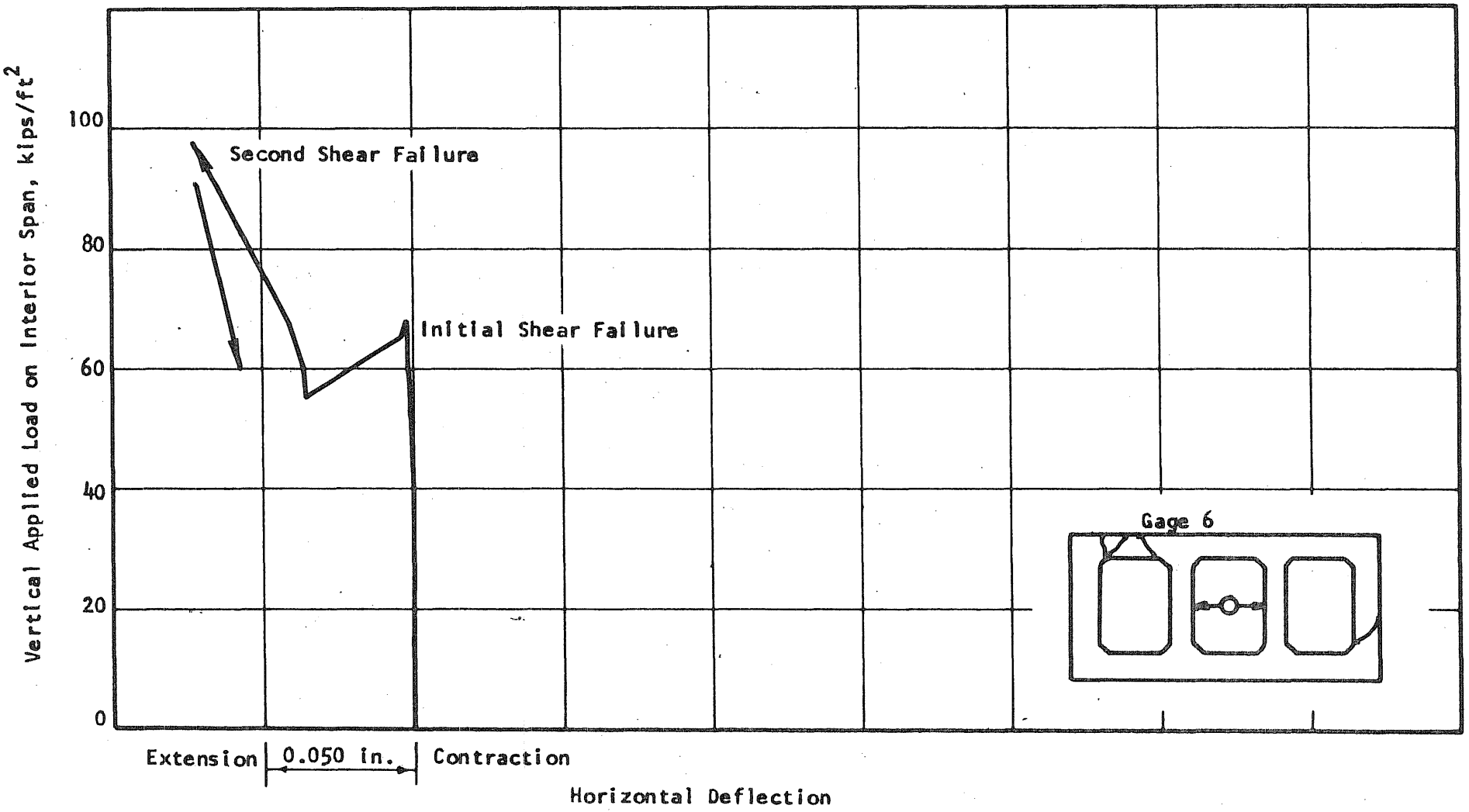

FIG. 7.62 LOAD-HORIZONTAL DEFLECTION CURVE, INTERIOR SPAN, R3

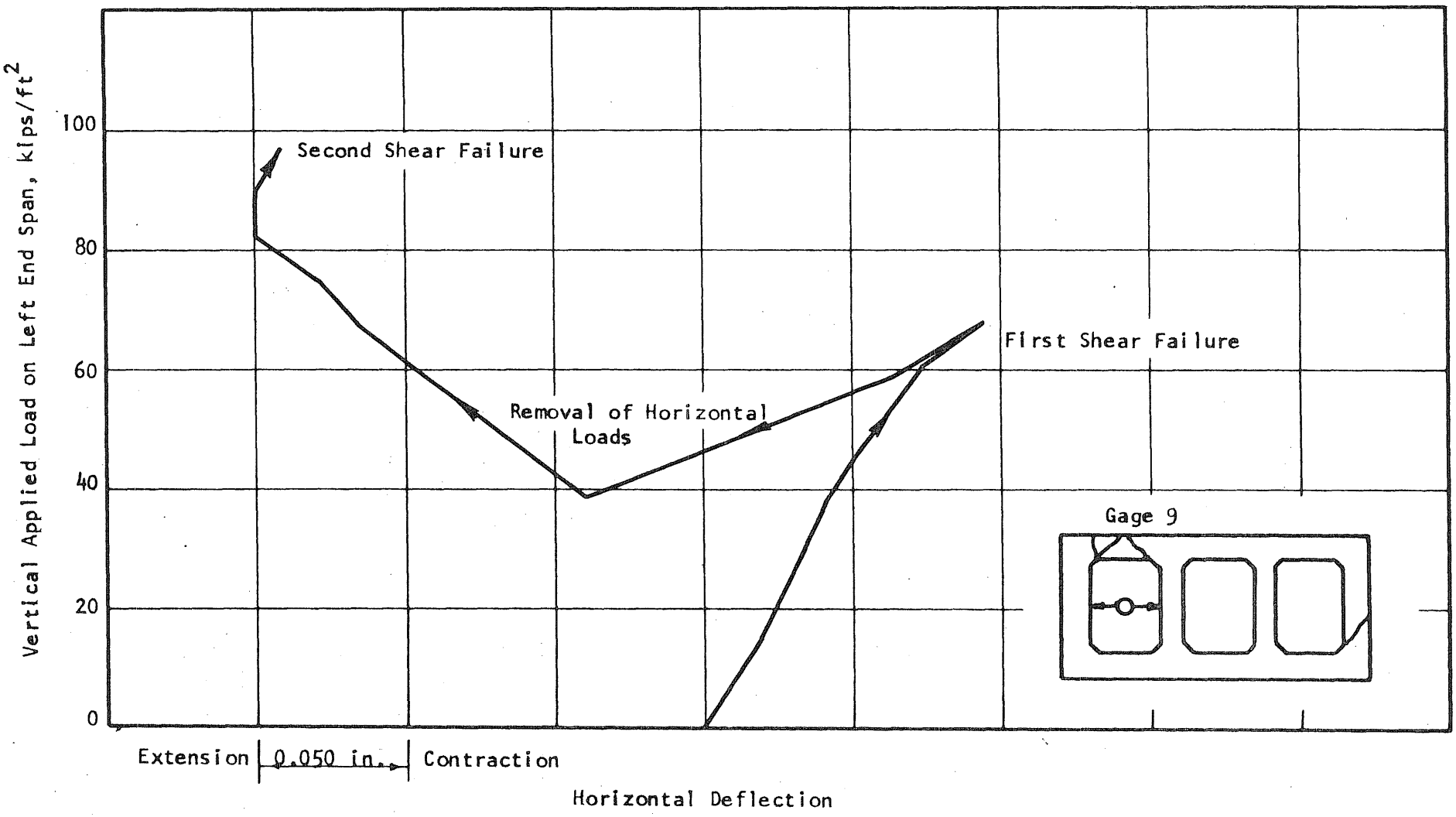

FIG. 7.63 LOAD-HORIZONTAL DEFLECTION CURVE, LEFT END SPAN, R3

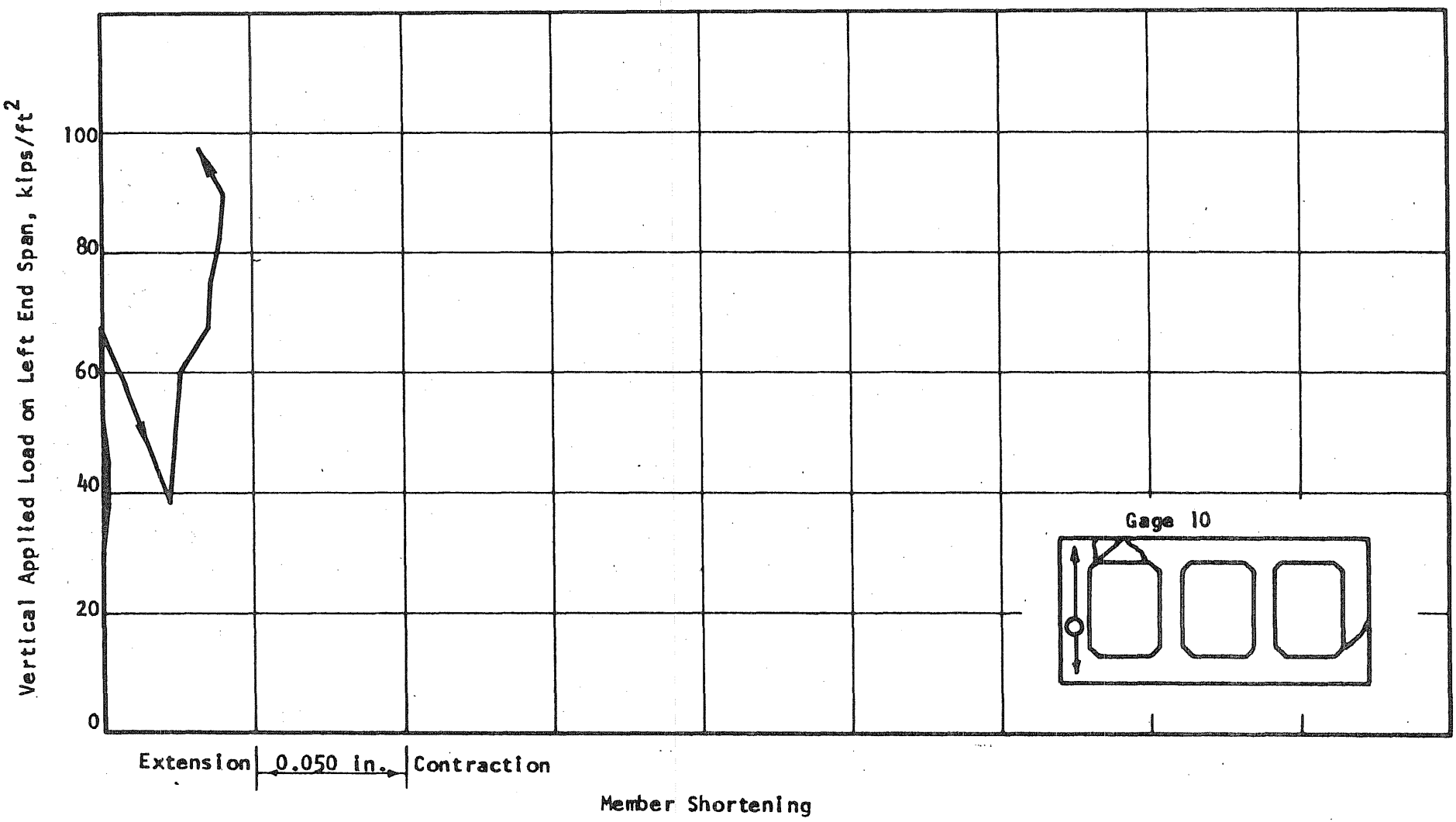

FIG. 7.64 LOAD-LENGTH CHANGE CURVE, EXTERIOR VERTICAL MEMBER, R3

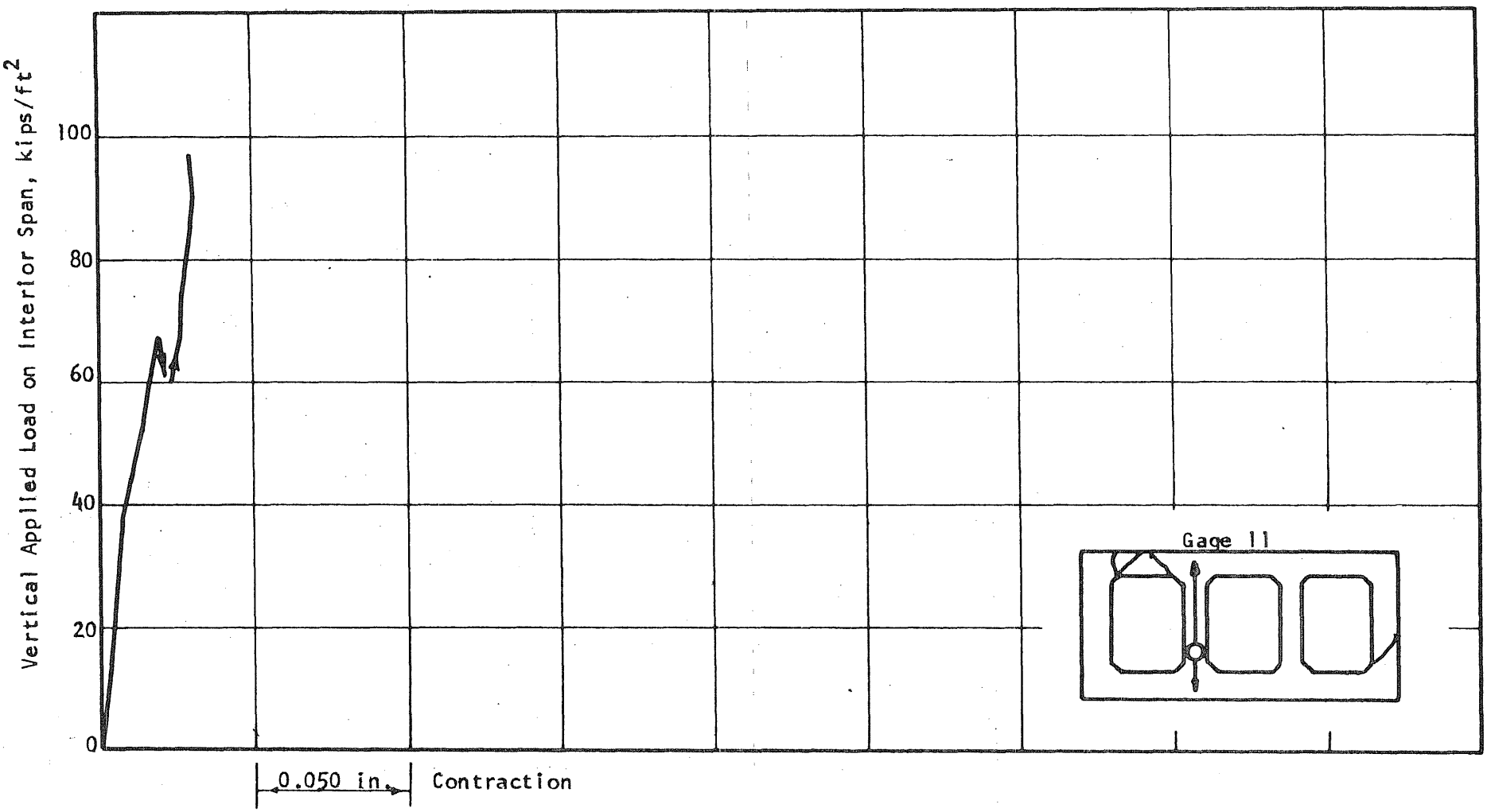

FIG. 7.65 LOAD-LENGTH CHANGE CURVE, INTERIOR VERTICAL MEMBER, R3

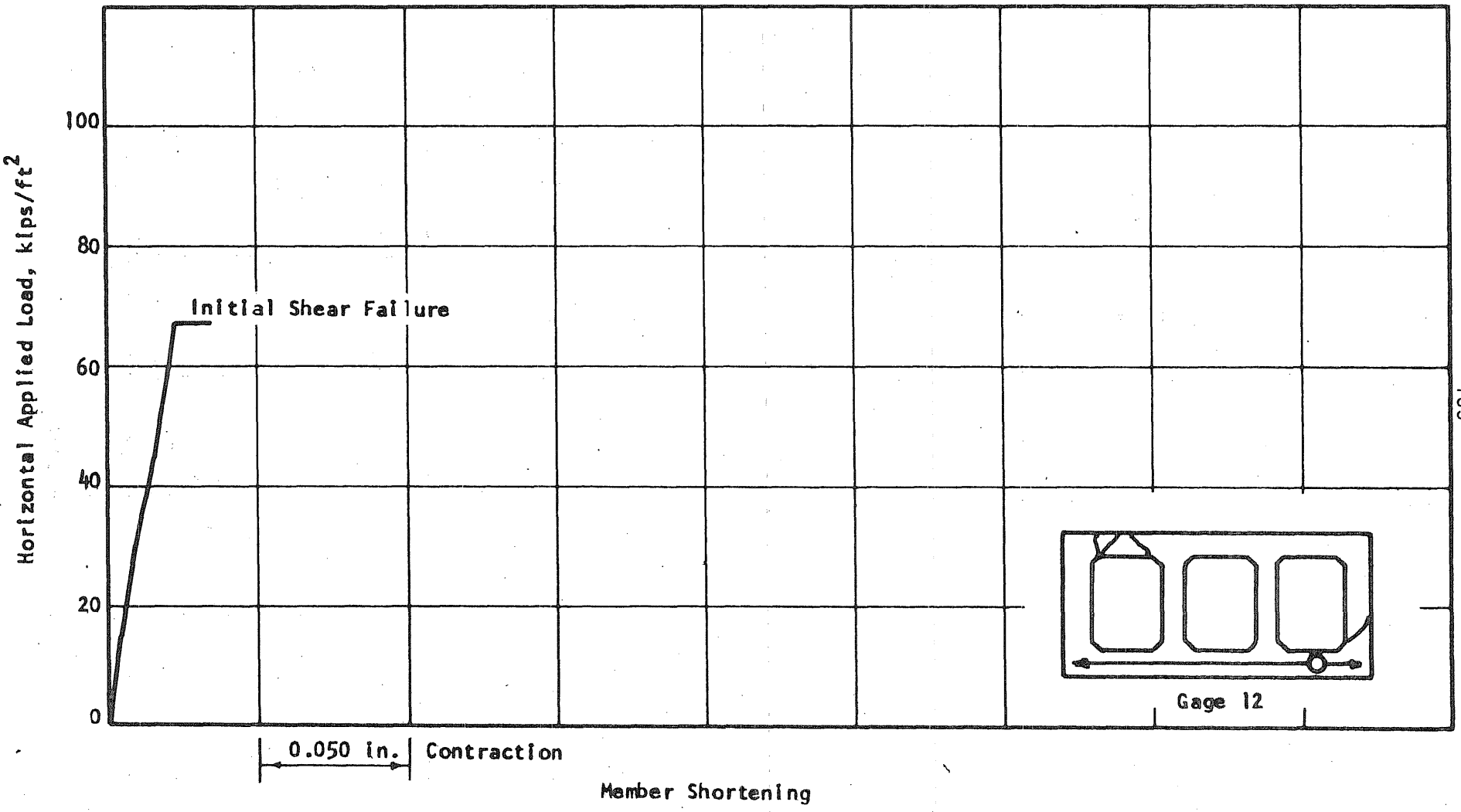

FIG. 7.66 LOAD-LENGTH CHANGE CURVE, LOWER HORIZONTAL MEMBER, R3

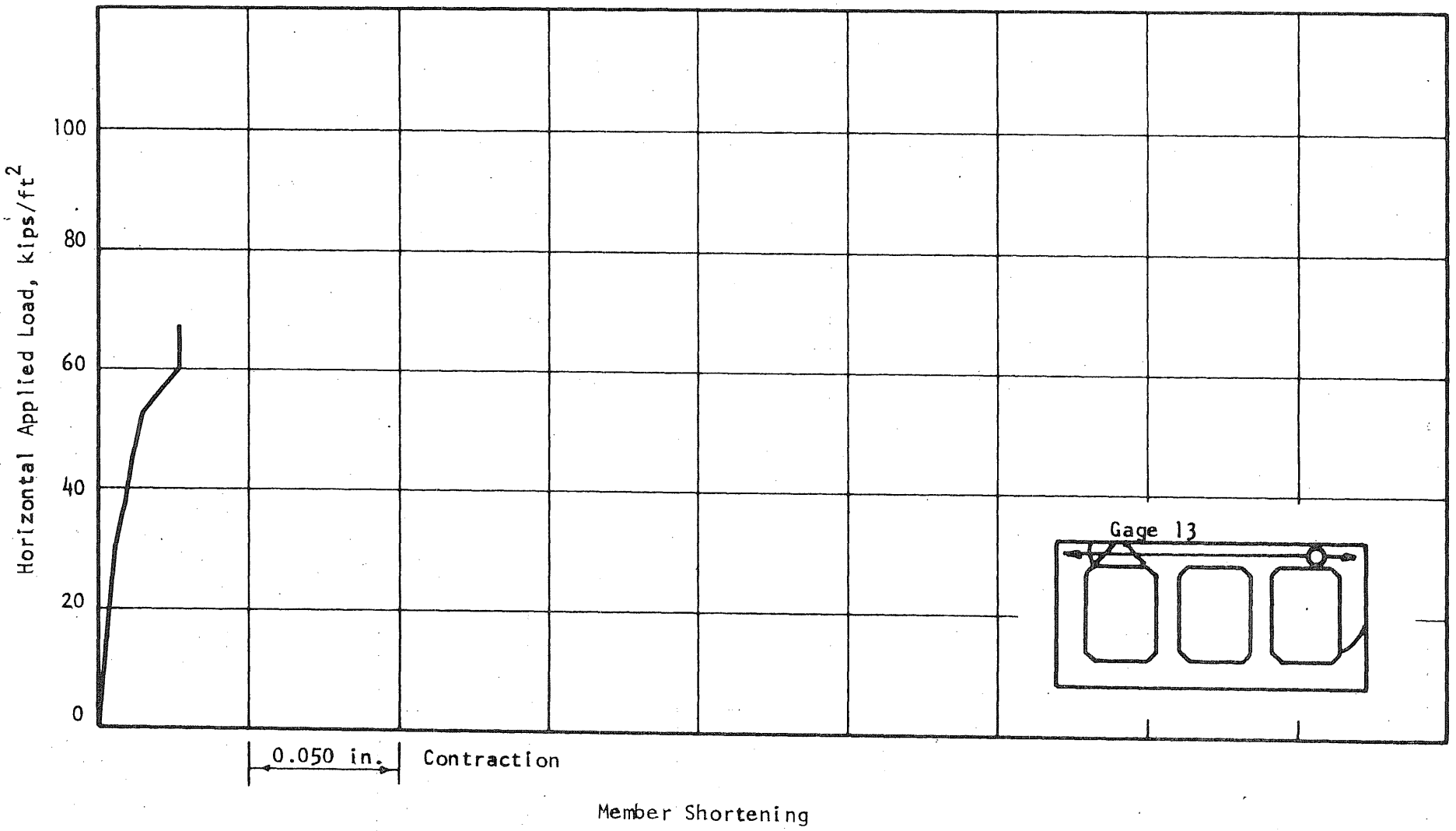

FIG. 7.67 LOAD-LENGTH CHANGE CURVE, UPPER HORIZONTAL MEMBER, R3

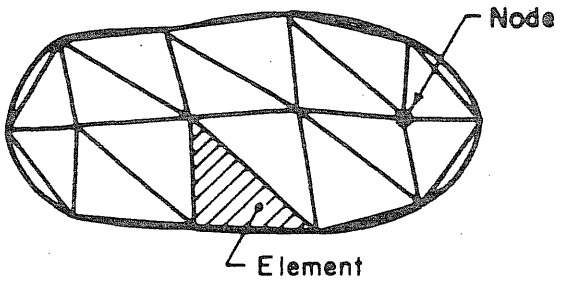

FIG. 8.1 FINITE-ELEMENT IDEALIZATION OF A TWO-DIMENSIONAL REGION

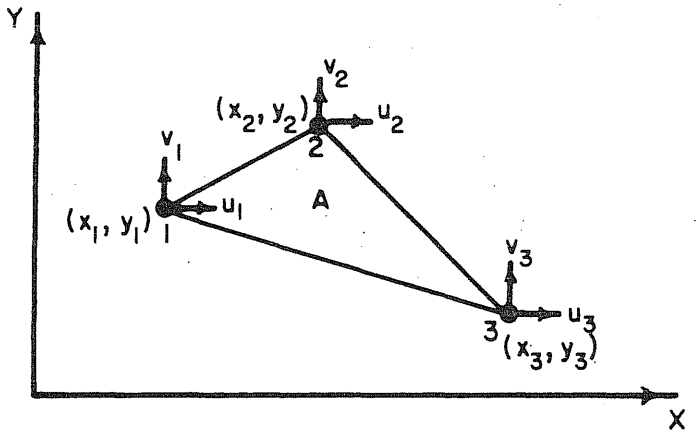

FIG. 8.2 CONSTANT STRAIN TRIANGULAR ELEMENT

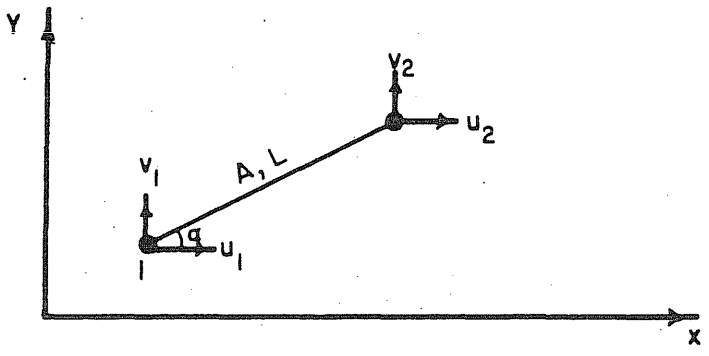

FIG. 8.3 STEEL BAR ELEMENT

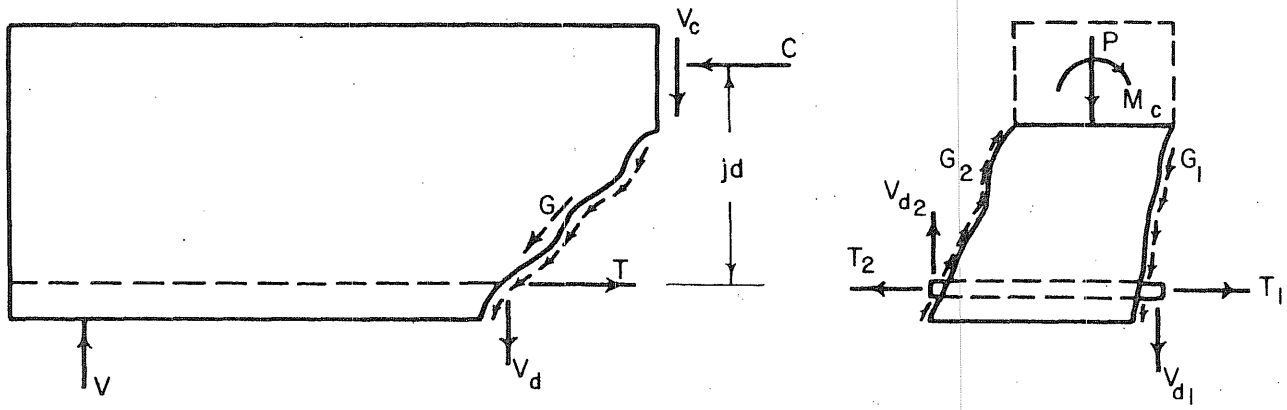

FIG. 8.4 SHEAR FORCES IN A REINFORCED CONCRETE BEAM

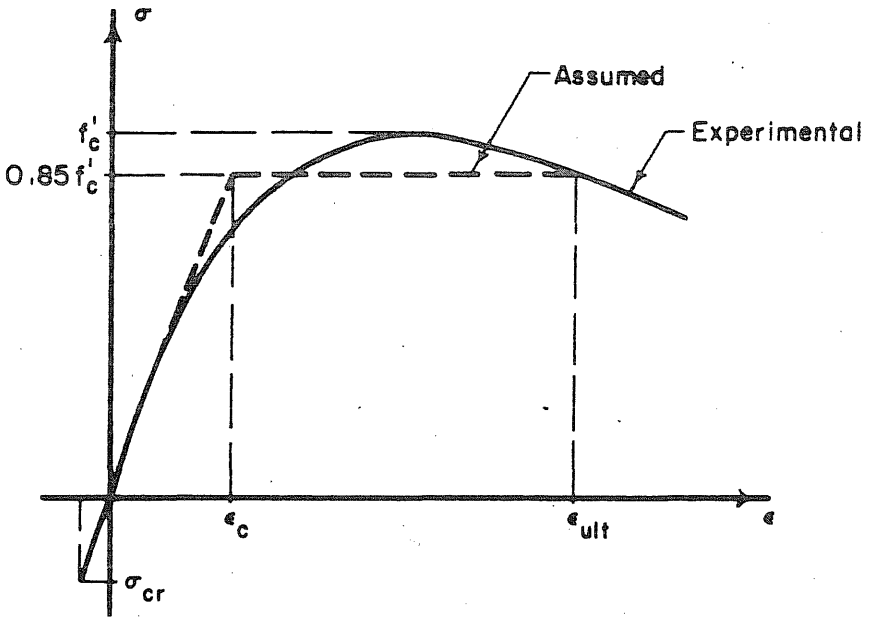

a) UNIAXIAL STRESS-STRAIN RELATIONSHIP FOR CONCRETE

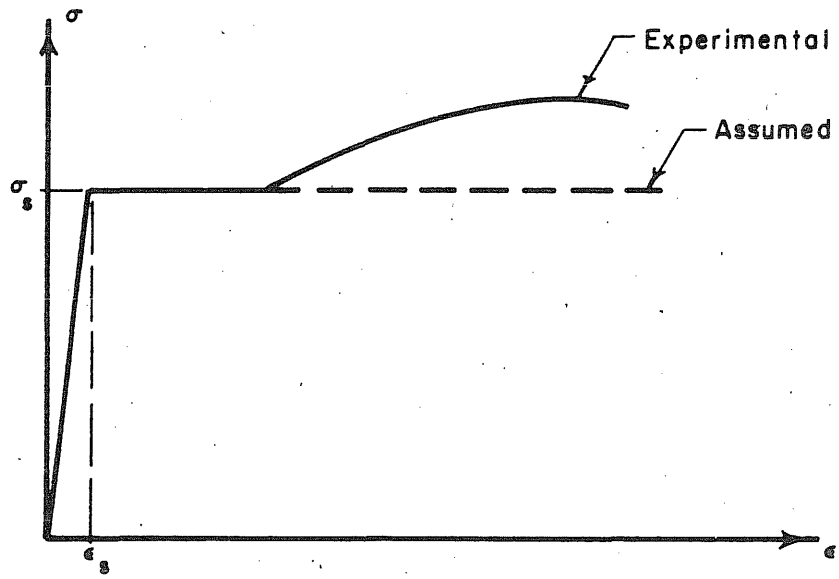

b) STRESS-STRAIN RELATIONSHIP FOR THE STEEL REINFORCEMENT

FIG. 8.5 UNIAXIAL STRESS-STRAIN MATERIAL BEHAVIOR

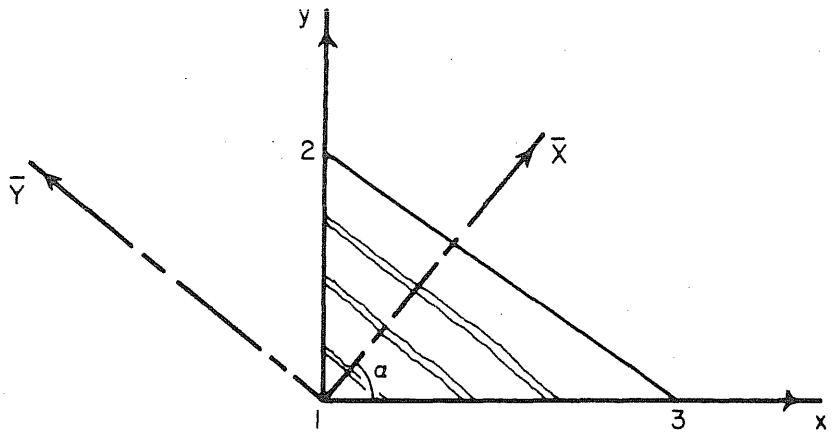

FIG. 8.6 CRACKED ELEMENT

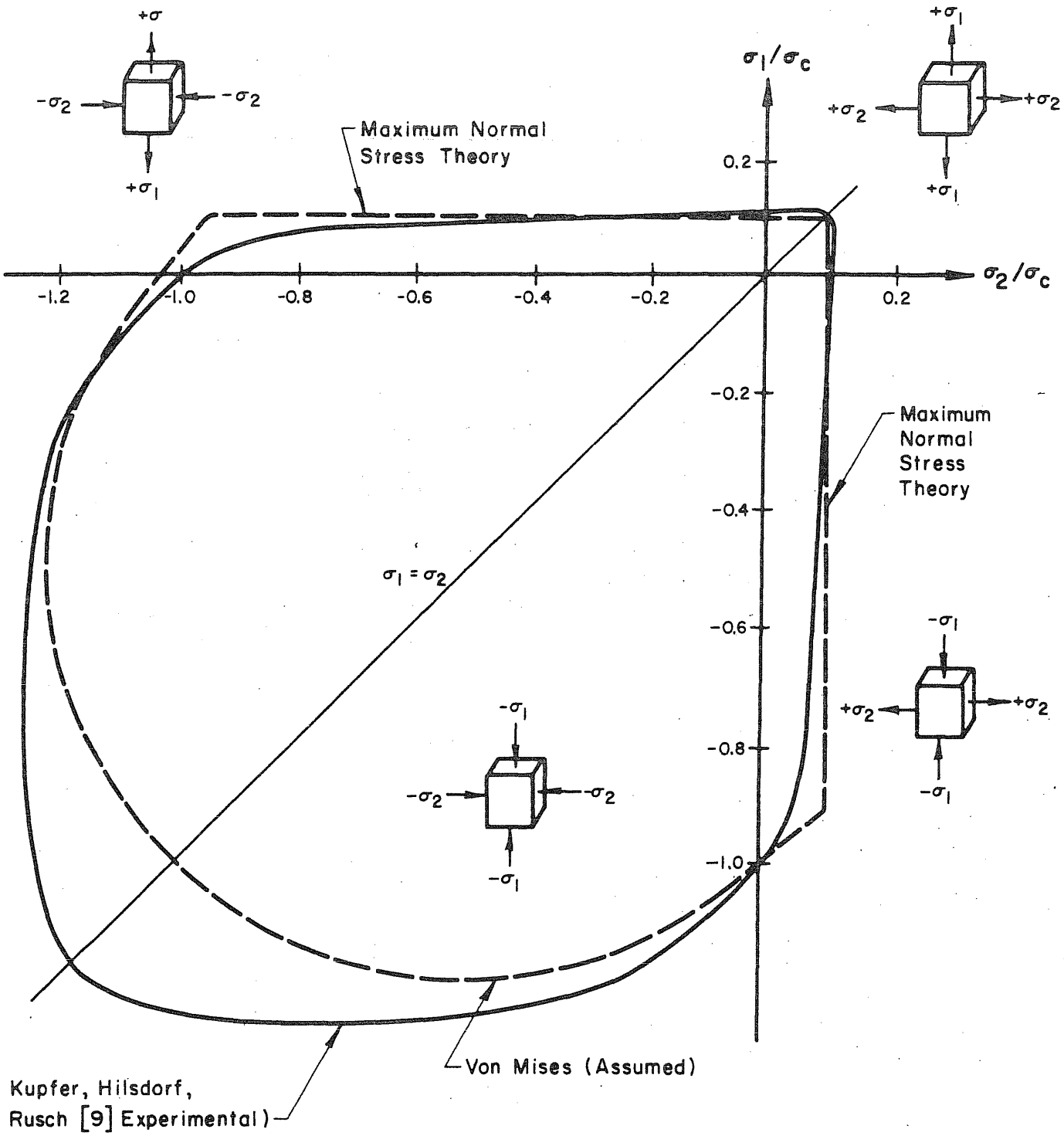

FIG. 8.7 FAILURE ENVELOPE FOR CONCRETE UNDER BIAXIAL STATE OF STRESS

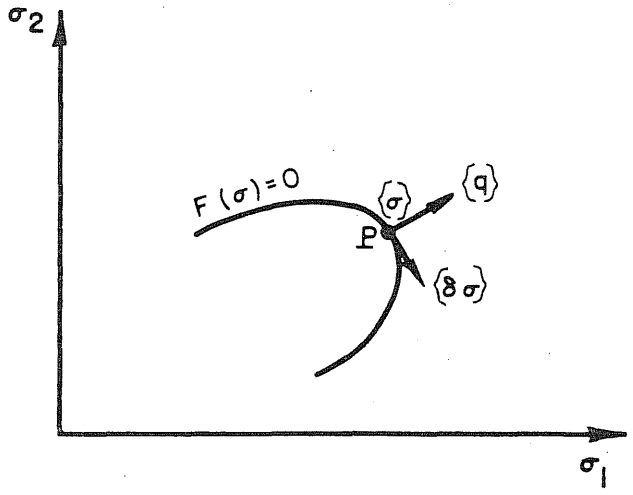

FIG. 8.8 YIELD SURFACE

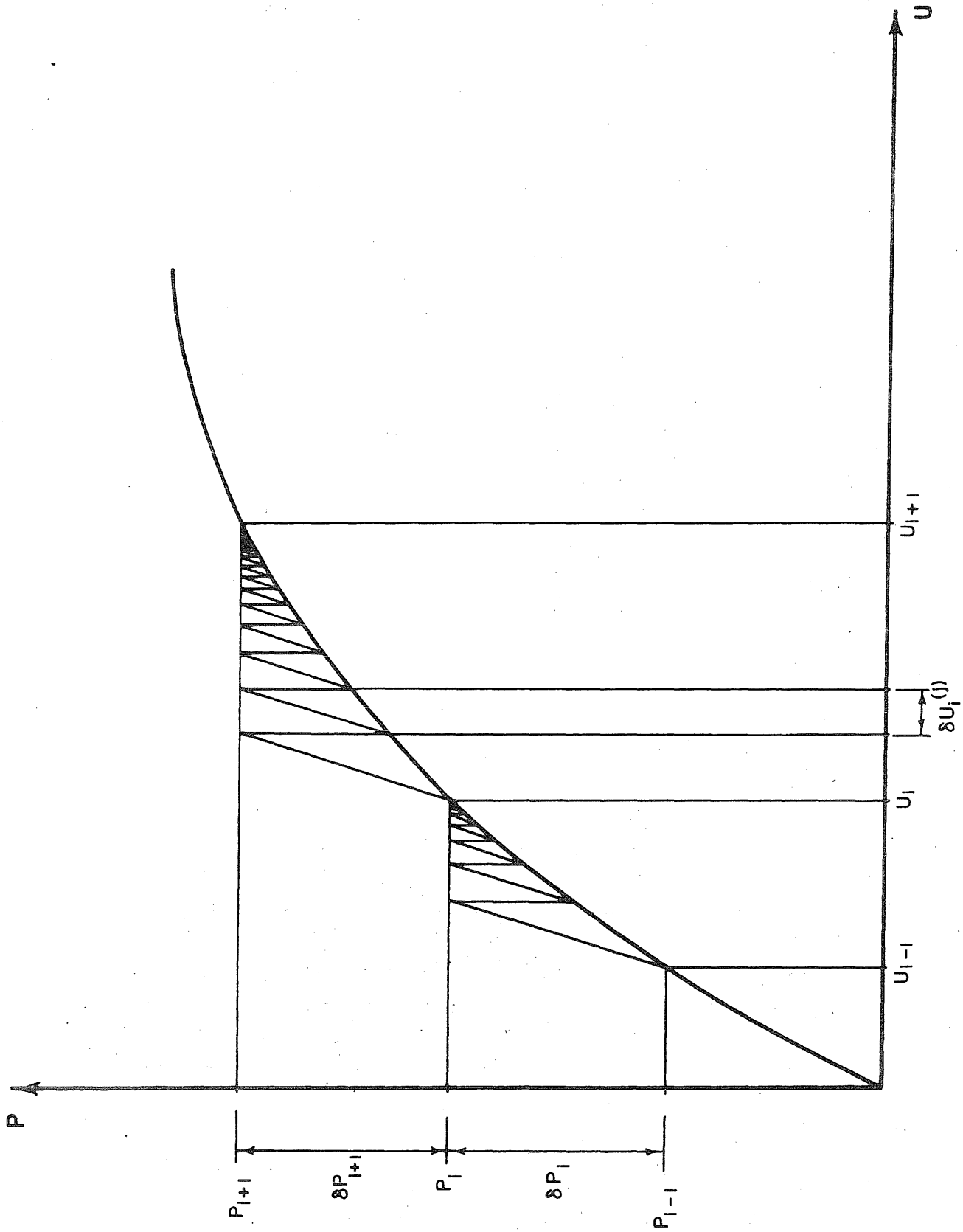

FIG. 8.9 METHOD OF SOLUTION (INITIAL STRESS METHOD)

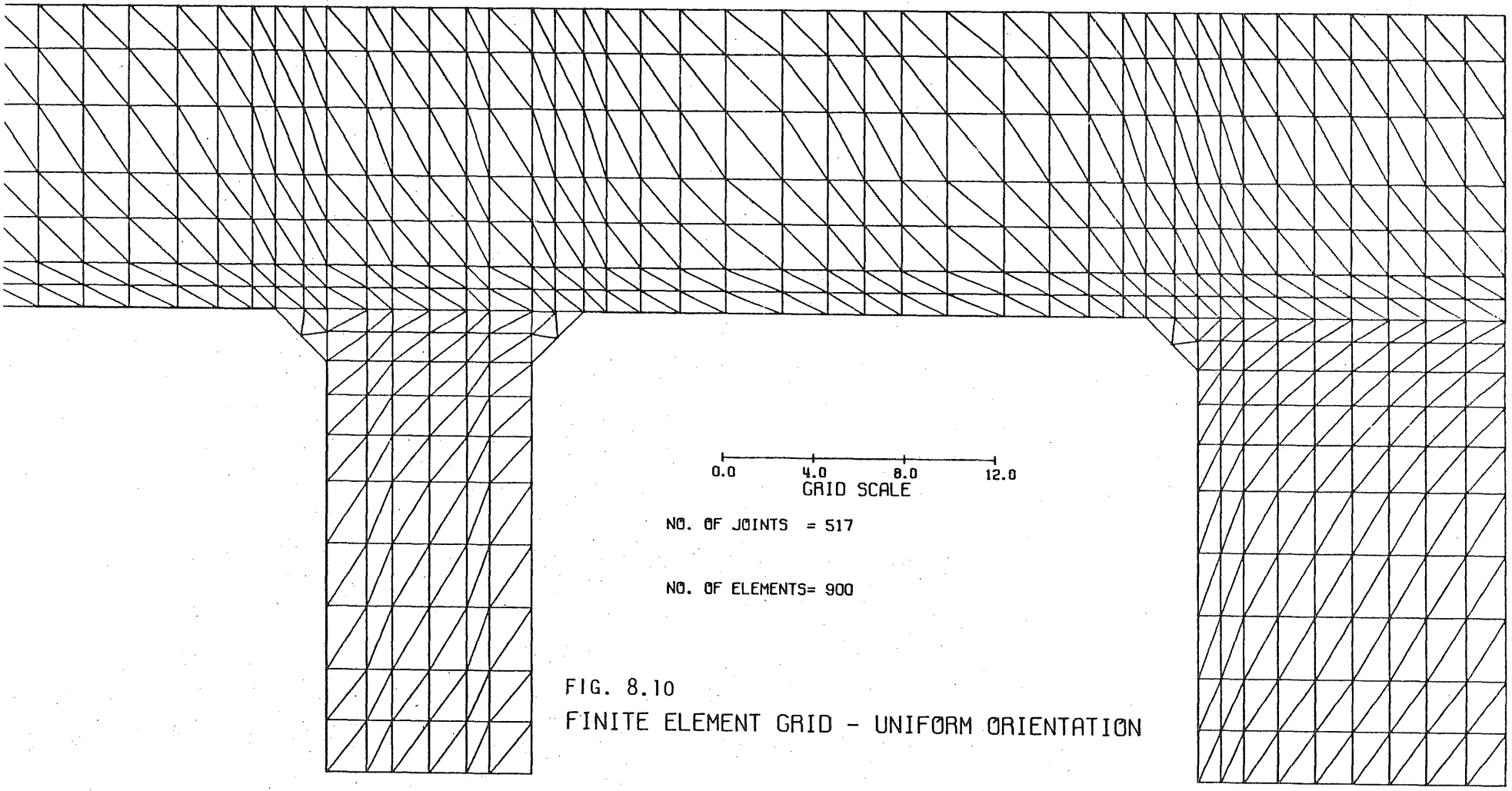

FIG. 8.10
FINITE ELEMENT GRID - UNIFORM ORIENTATION

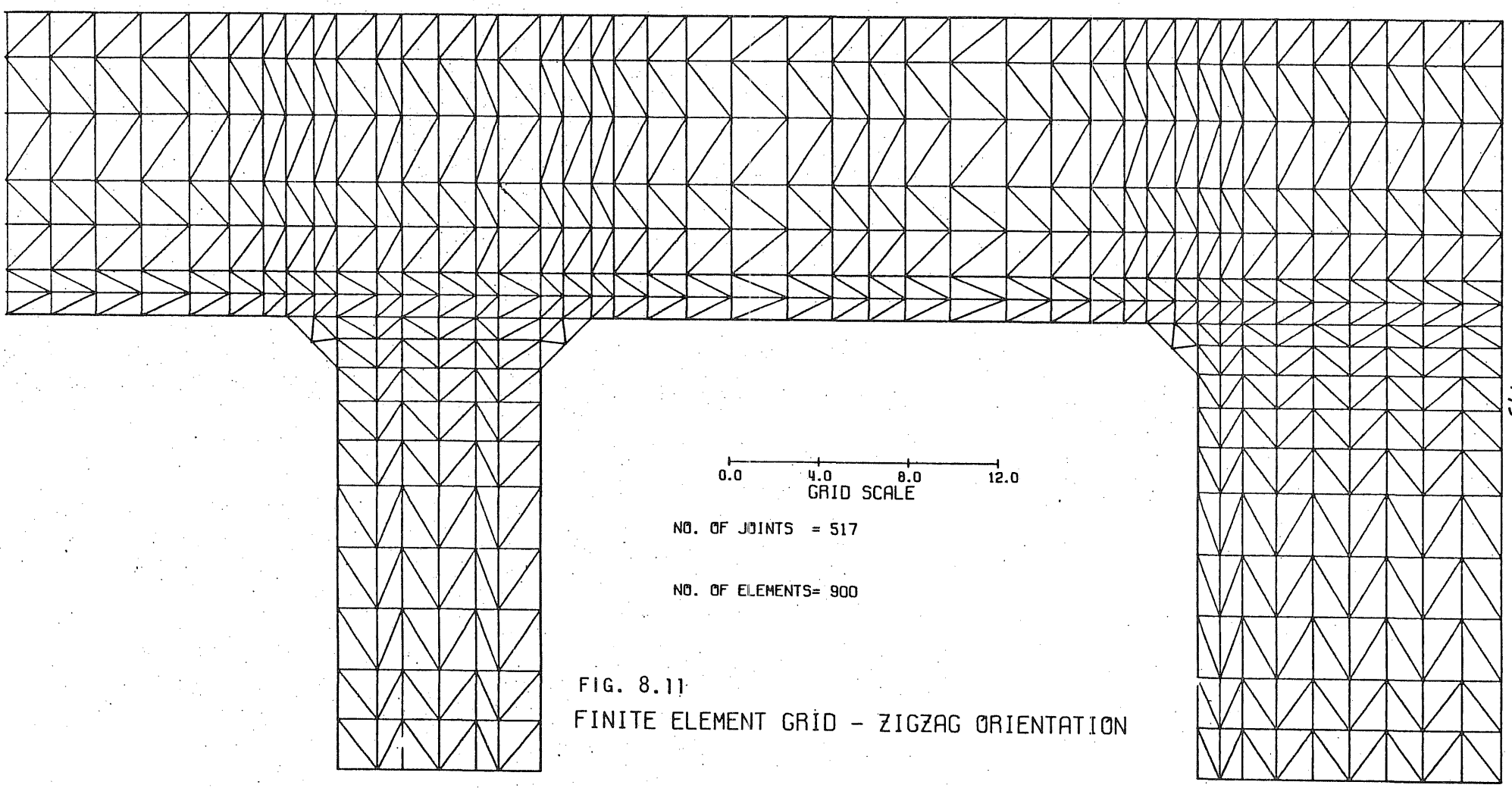

FIG. 8.11
FINITE ELEMENT GRID - ZIGZAG ORIENTATION

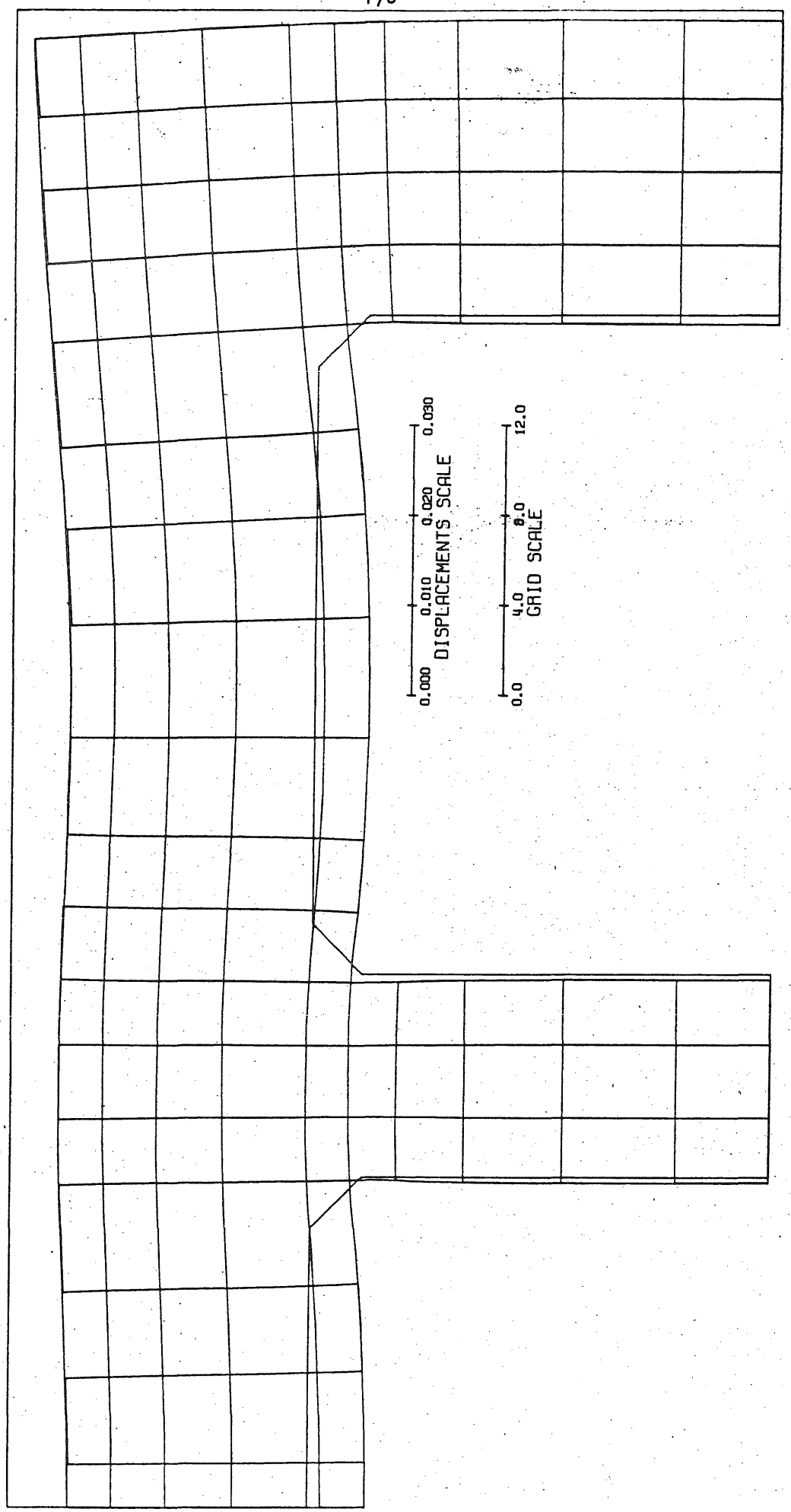

FIG. 8.12 DEFLECTED SHAPE OF SPECIMEN R1

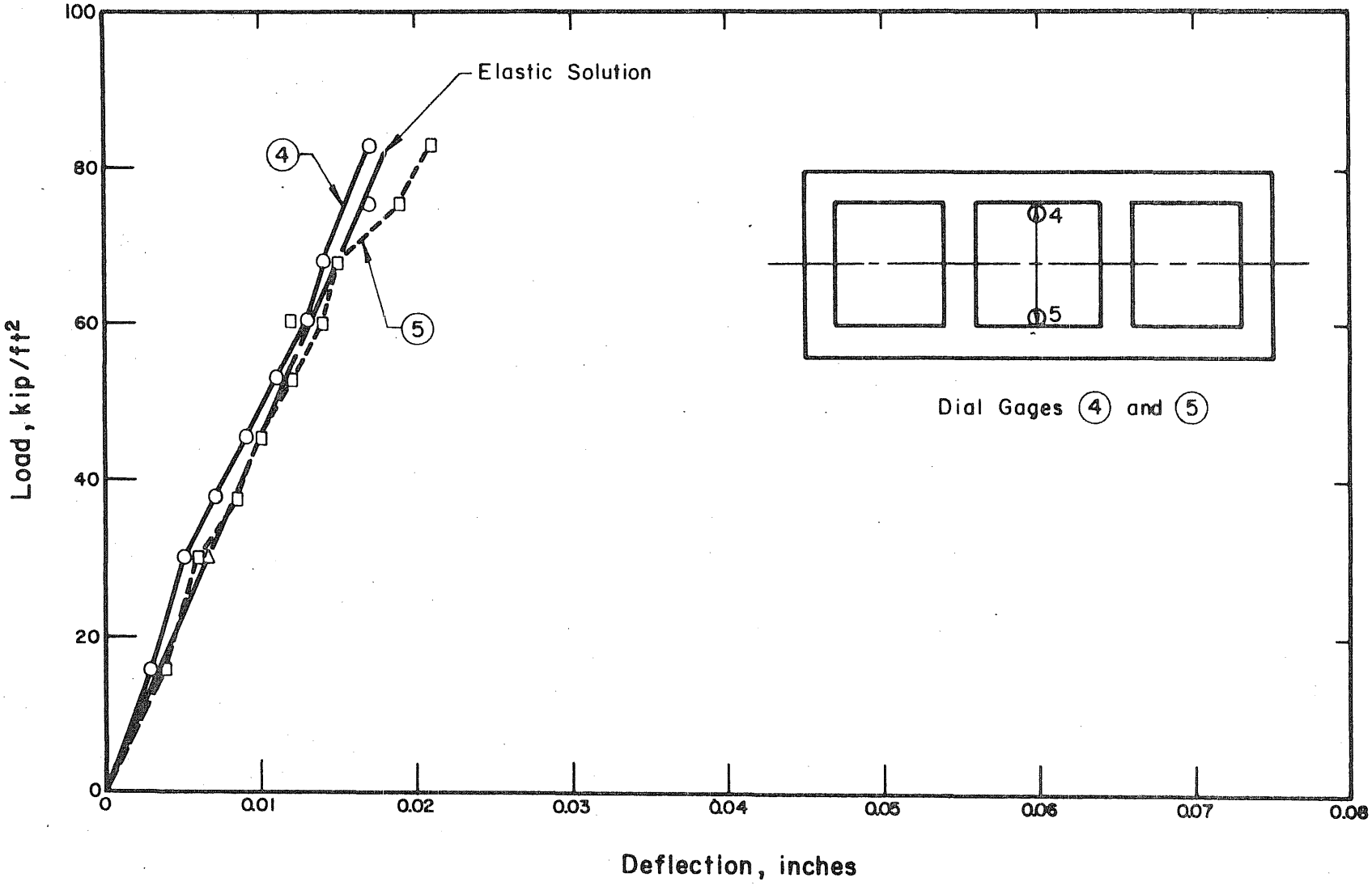

FIG. 8.13 LOAD DEFLECTION CURVES FOR SPECIMEN R1

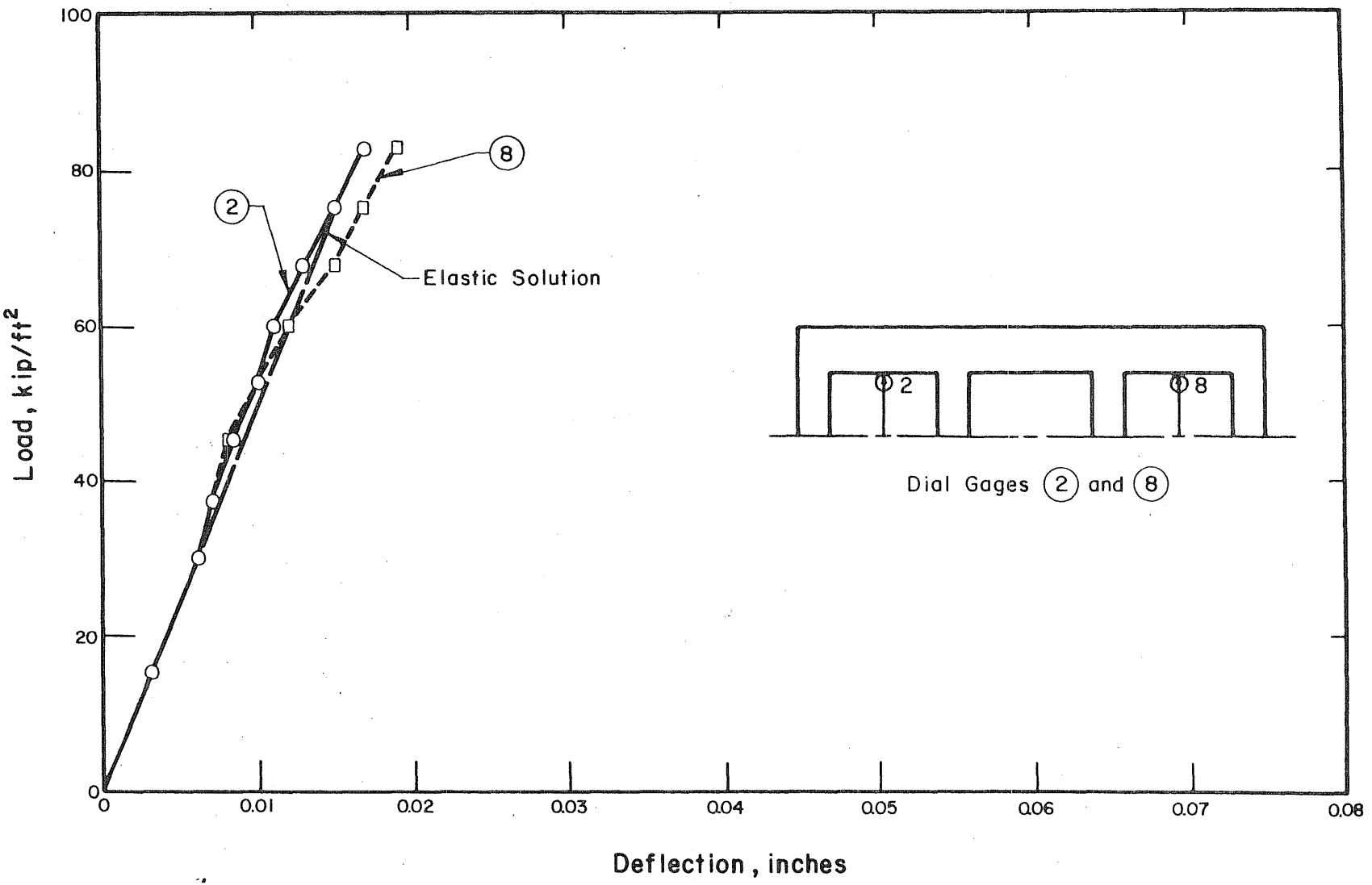

FIG. 8.14 LOAD DEFLECTION CURVES FOR SPECIMEN R1

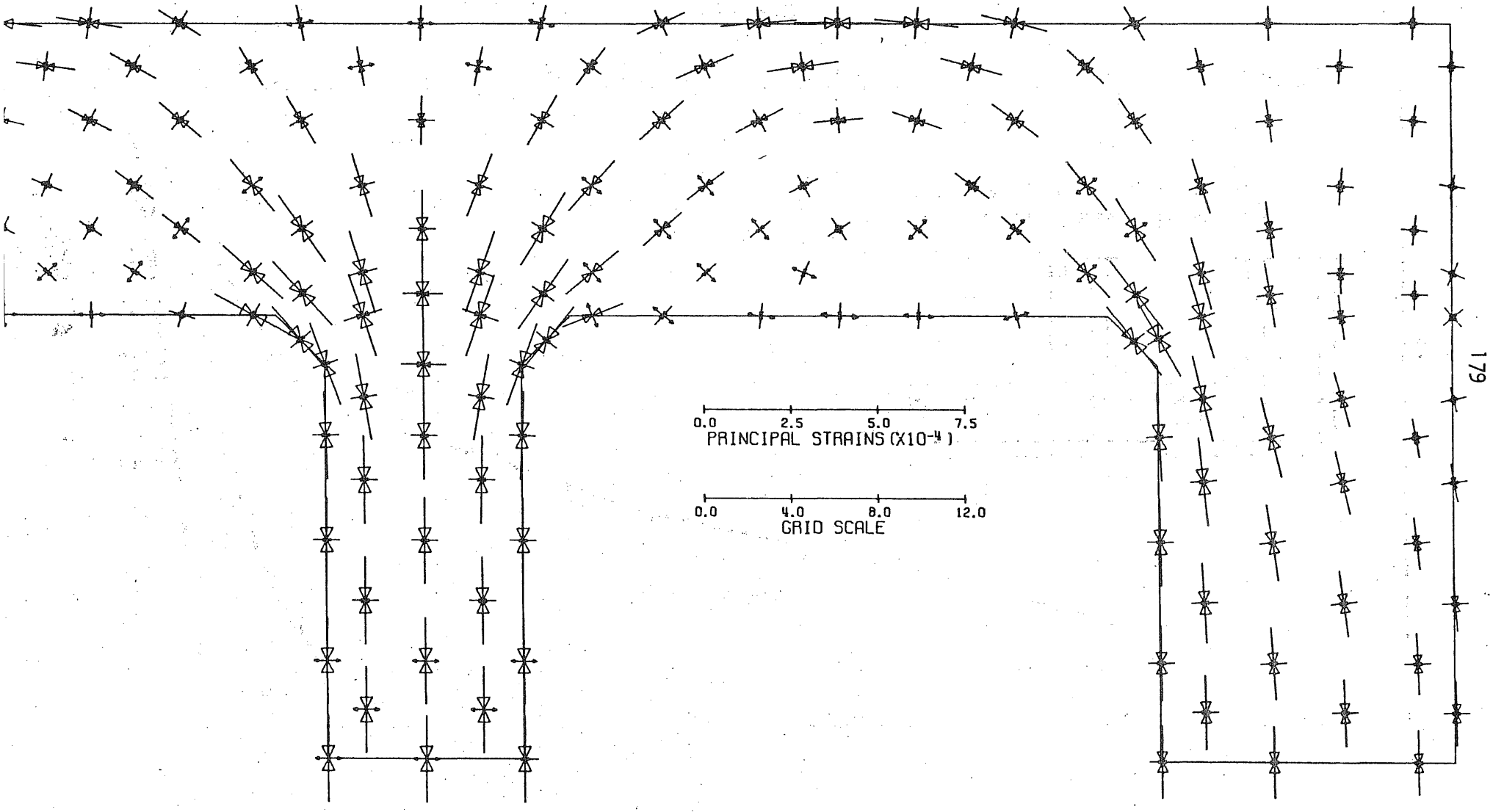

FIG. 8.15 PRINCIPAL STRAINS FOR SPECIMEN R1

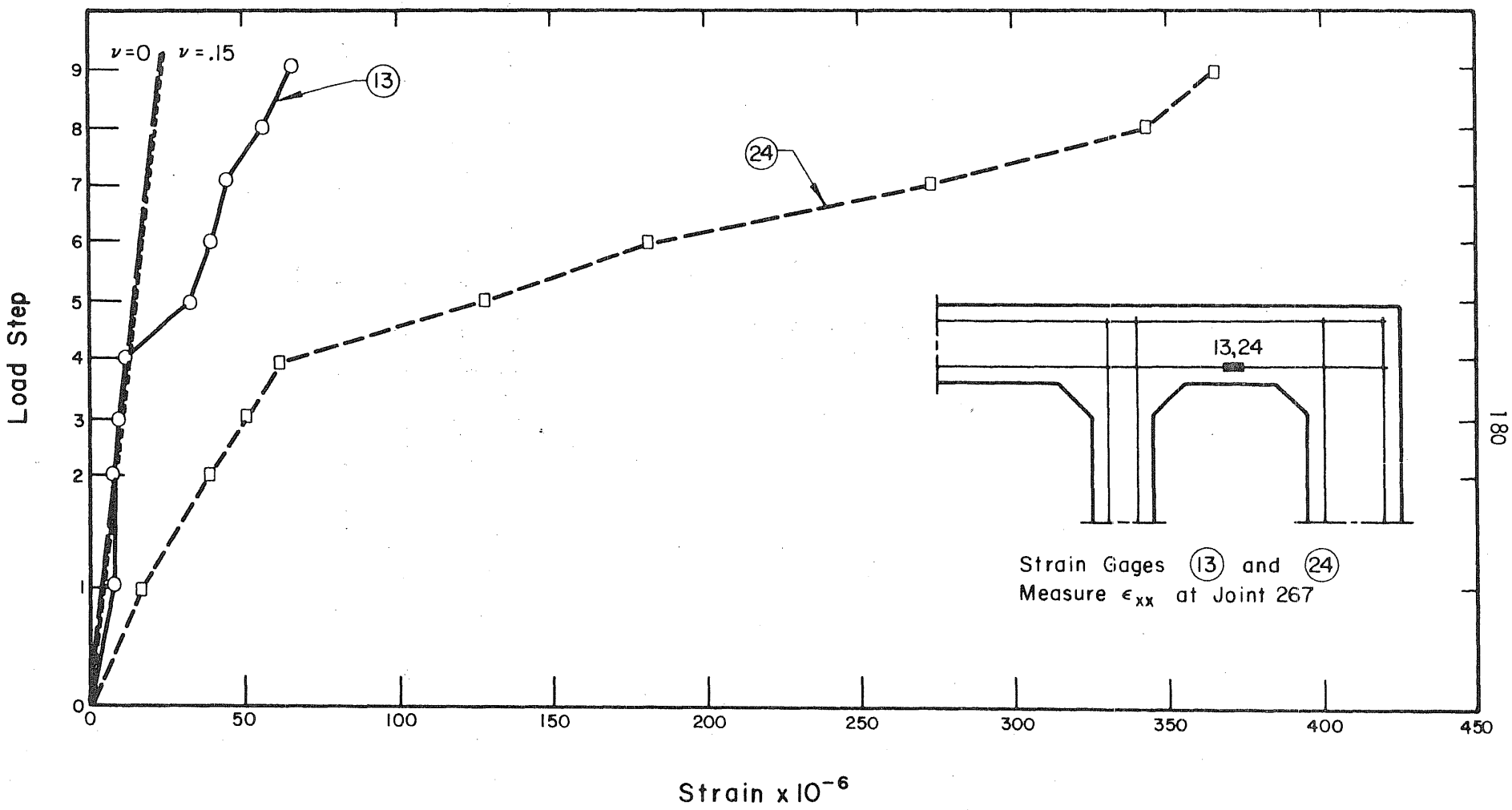

FIG. 8.16 LOAD-STRAIN CURVES FOR SPECIMEN R1

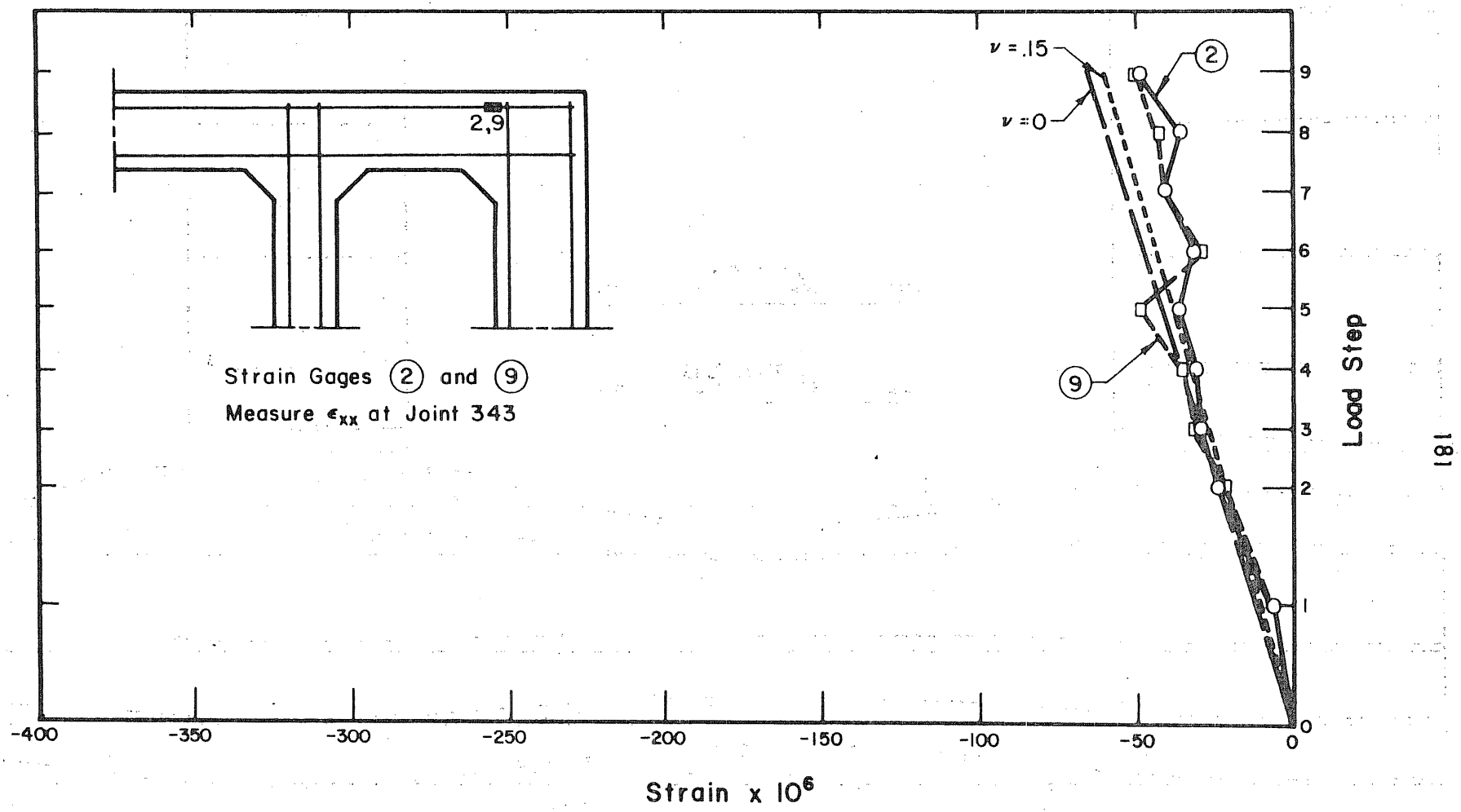

FIG. 8.17 LOAD-STRAIN CURVES FOR SPECIMEN R1

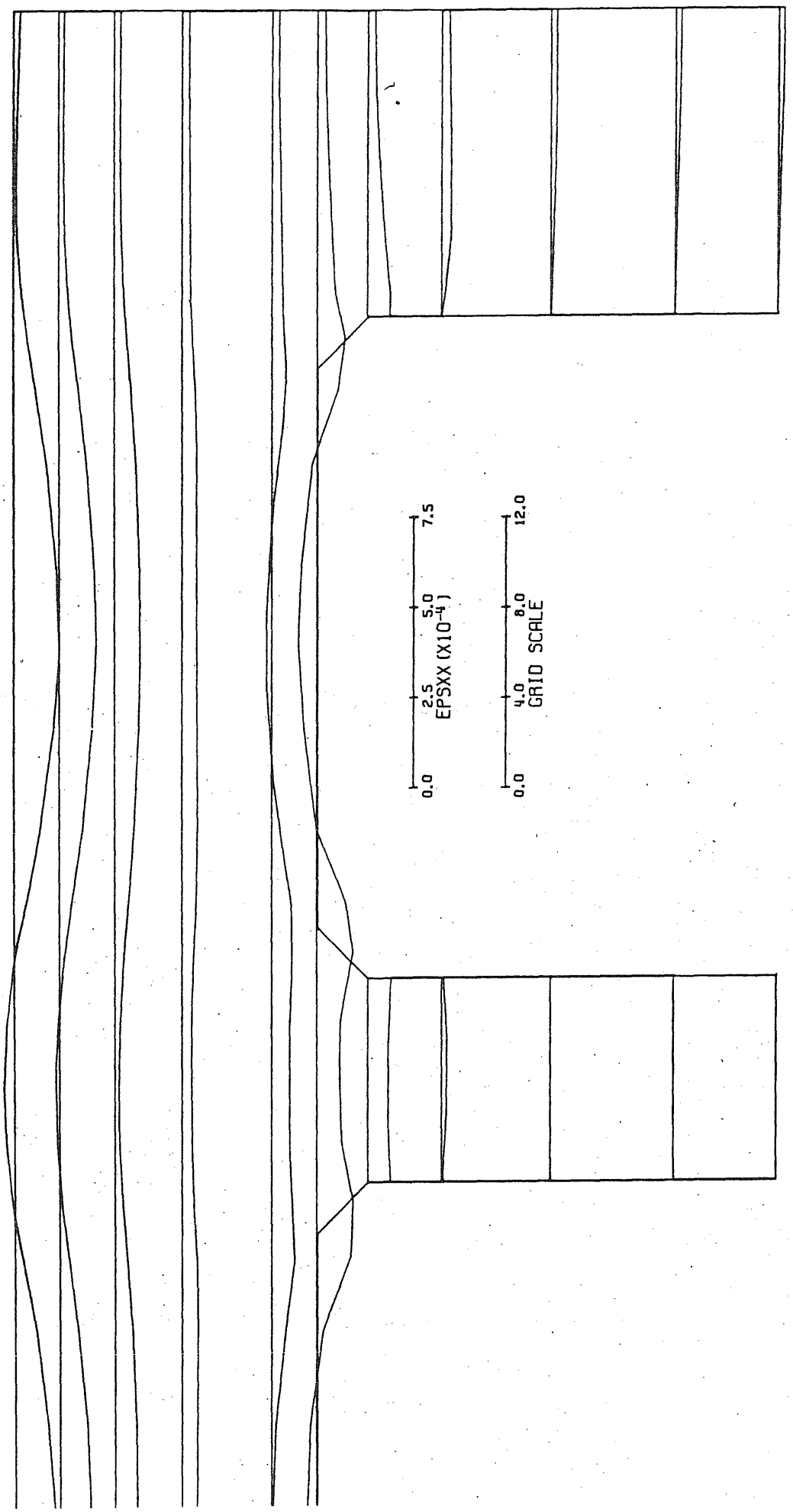

FIG. 8.18 STRAIN IN THE X-DIRECTION AT HORIZONTAL SECTIONS OF SPECIMEN R1

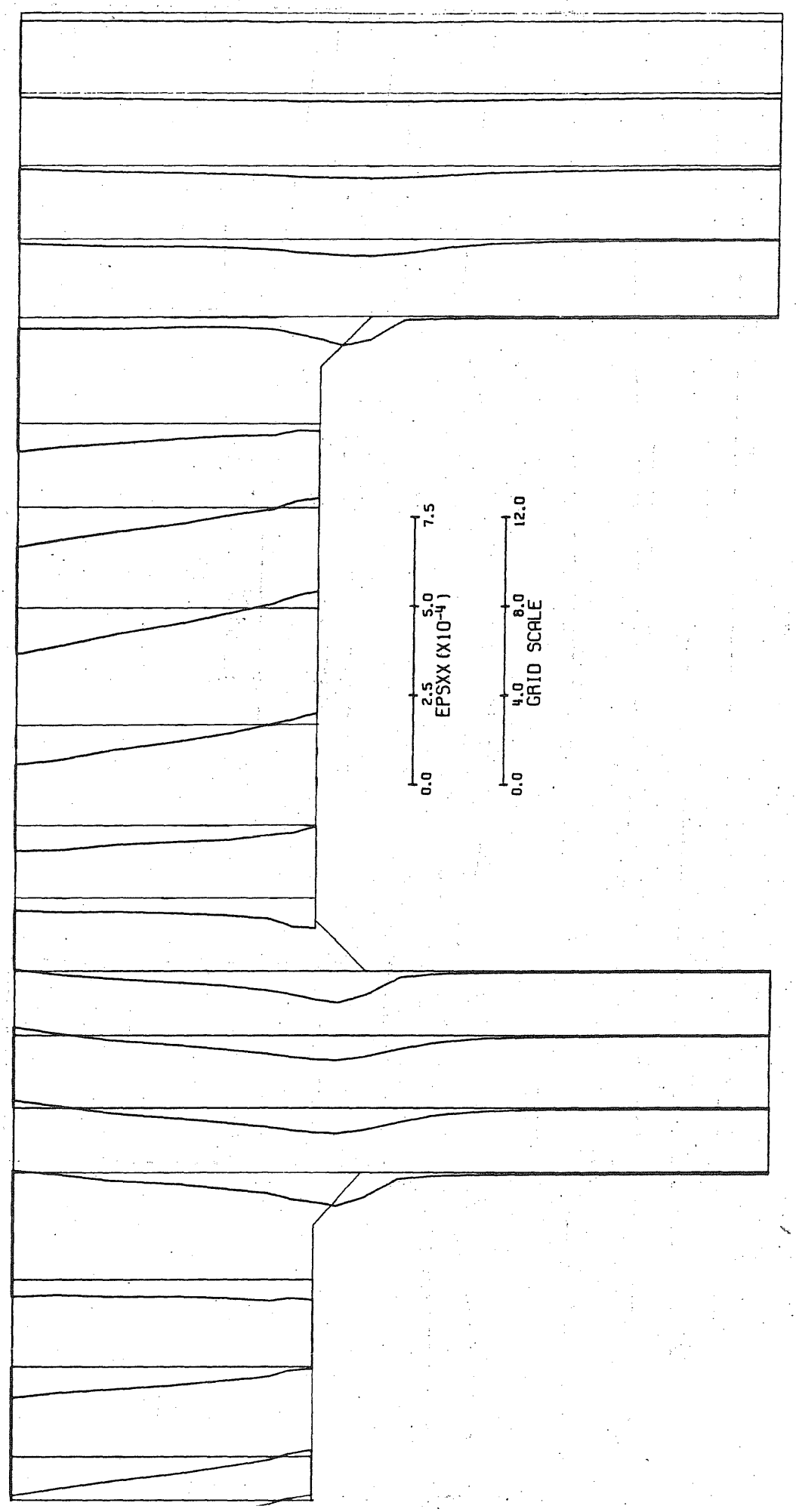

FIG. 8.19 STRAIN IN THE X-DIRECTION AT VERTICAL SECTIONS OF SPECIMEN R1

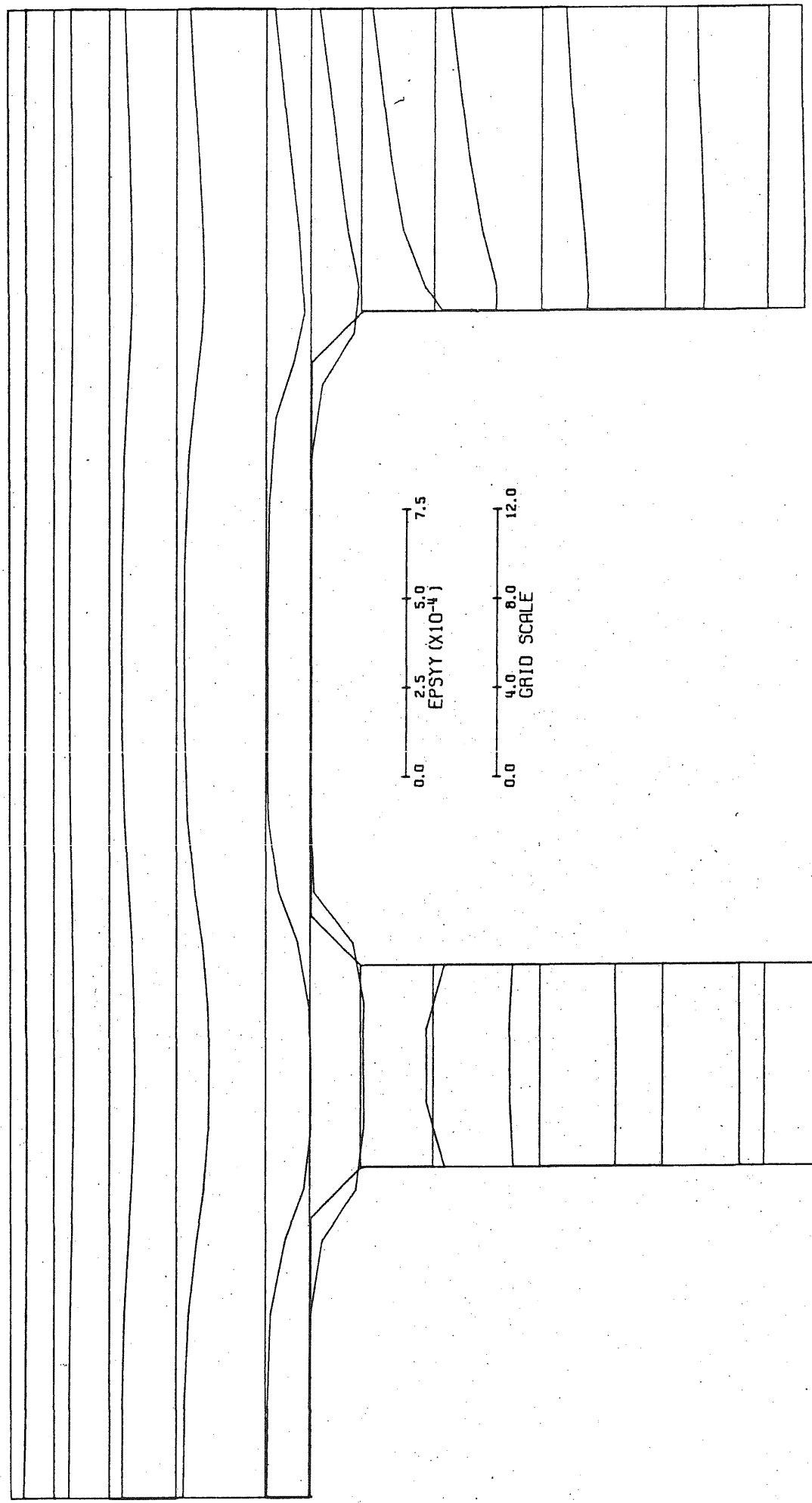

FIG. 8.20 STRAIN IN THE Y-DIRECTION AT HORIZONTAL SECTIONS OF SPECIMEN R1

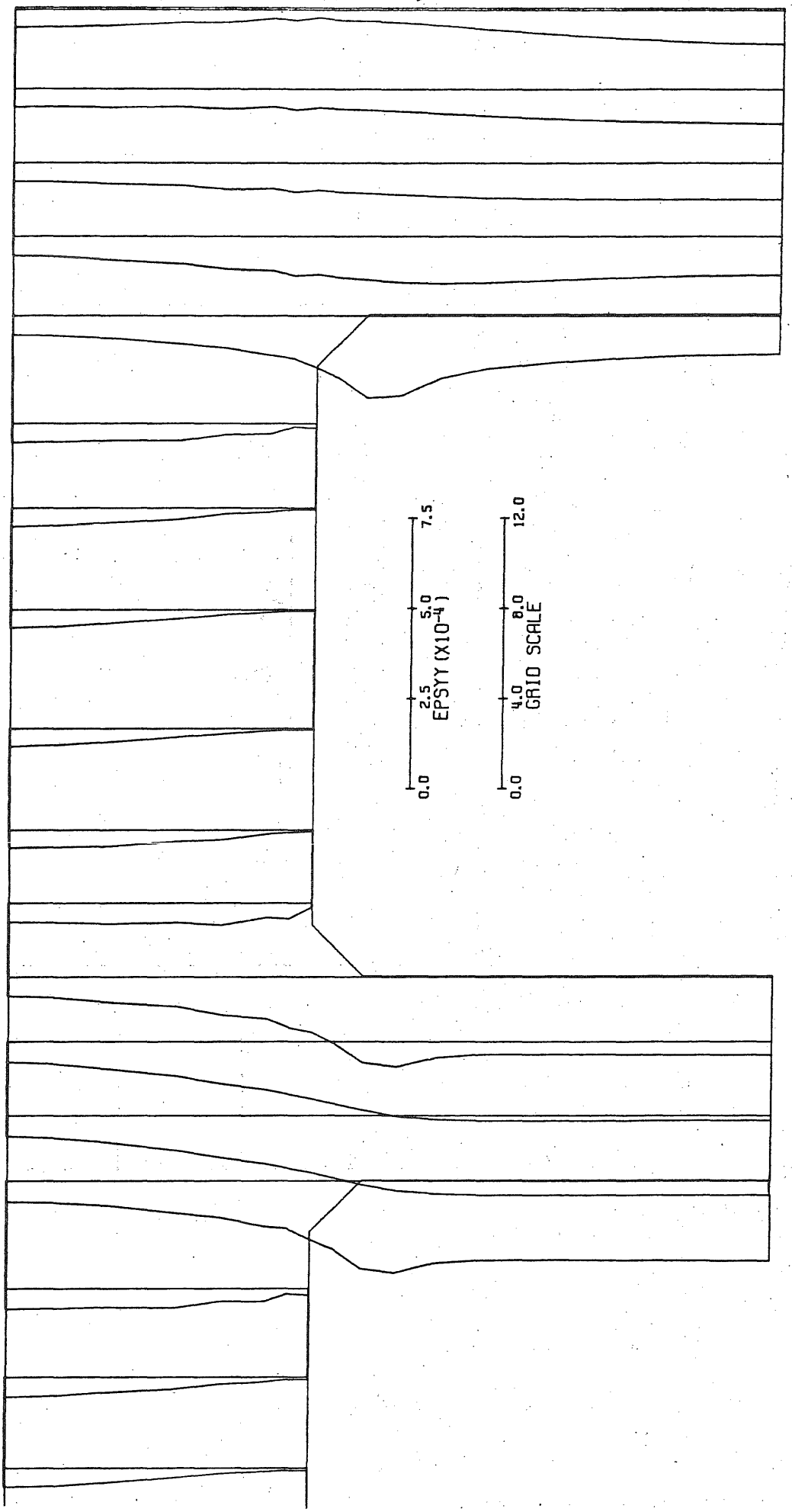

FIG. 8.21 STRAIN IN THE Y-DIRECTION AT VERTICAL SECTIONS OF SPECIMEN R1

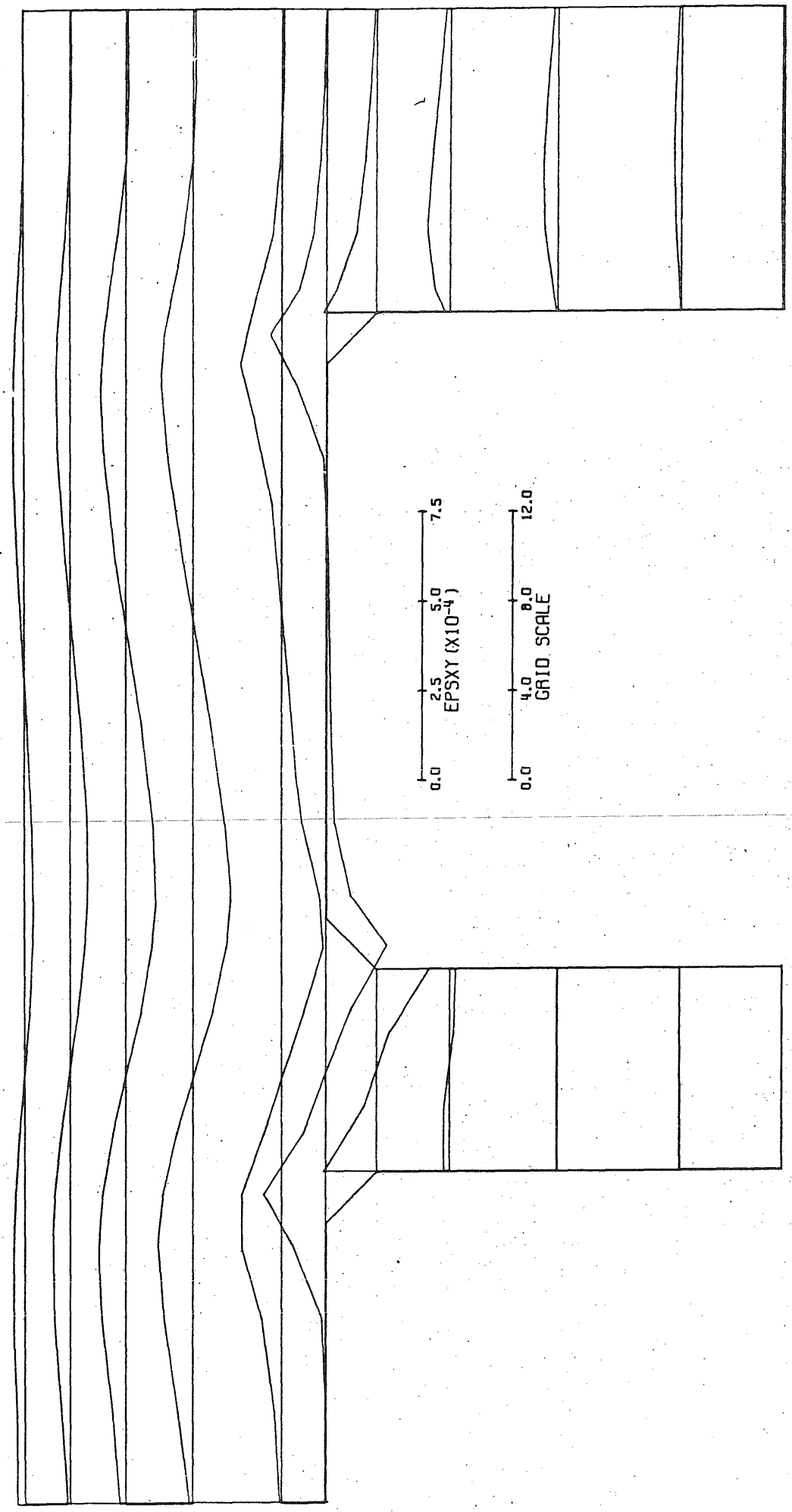

FIG. 8.22 SHEAR STRAIN AT HORIZONTAL SECTIONS OF SPECIMEN R1

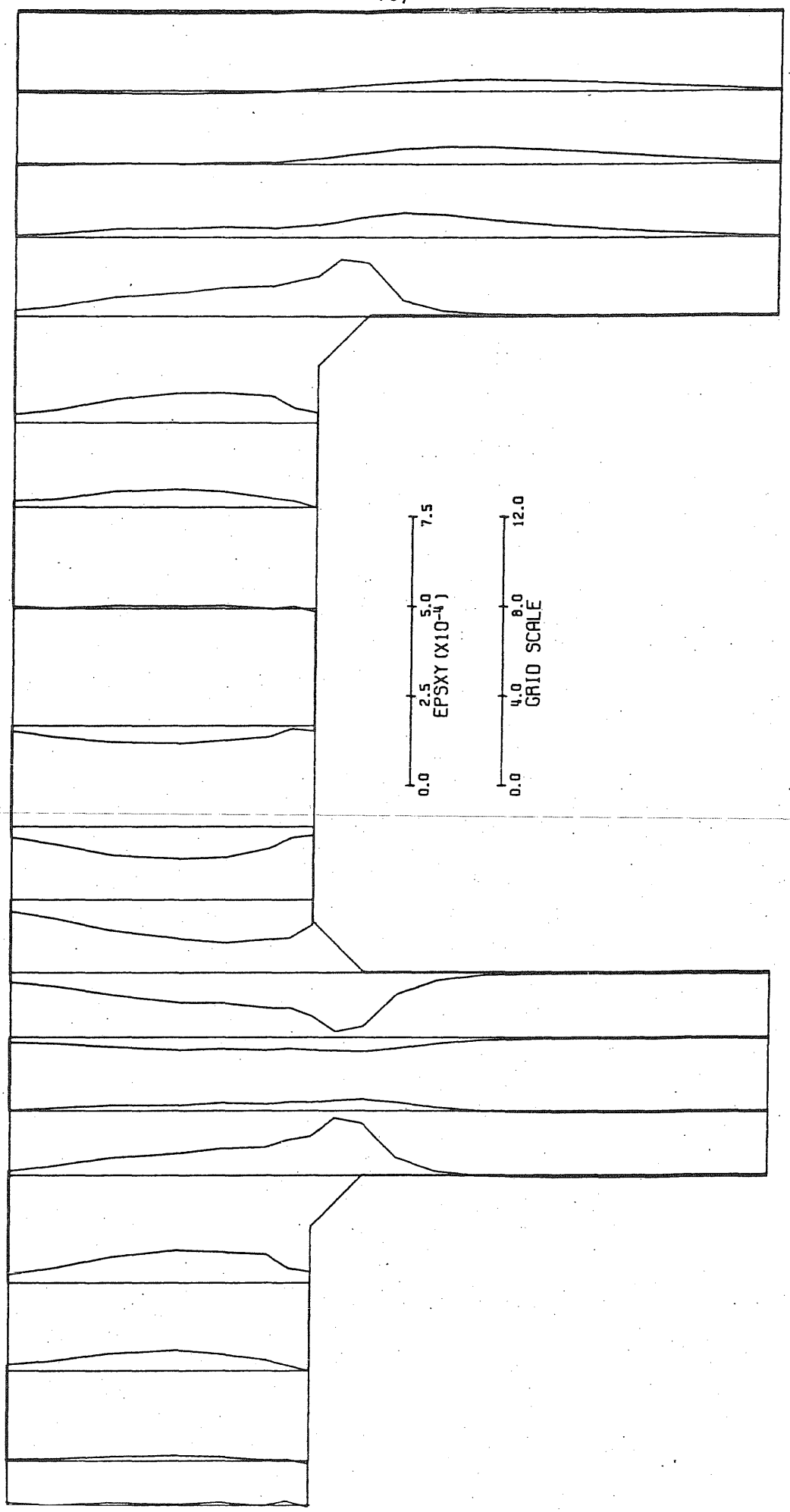

FIG. 8.23 SHEAR STRAIN AT VERTICAL SECTIONS OF SPECIMEN R1

UNCLASSIFIED
Security Classification

DOCUMENT CONTROL DATA - R & D

(Security classification of title, body of abstract and indexing annotation must be entered when the overall report is classified)

1. ORIGINATING ACTIVITY *(Corporate author)*

Department of Civil Engineering
University of Illinois at Urbana-Champaign

2a. REPORT SECURITY CLASSIFICATION
UNCLASSIFIED

2b. GROUP

3. REPORT TITLE

Thick Walled Multiple Opening Reinforced Concrete Conduits

4. DESCRIPTIVE NOTES *(Type of report and inclusive dates)*

Interim Progress Report July 1970-June 1972

5. AUTHOR(S) *(First name, middle initial, last name)*

M. O. Ryan, M. H. Salem, W. L. Gamble, and B. Mohraz

6. REPORT DATE	7a. TOTAL NO. OF PAGES	7b. NO. OF REFS
December 1972		18

8a. CONTRACT OR GRANT NO.	9a. ORIGINATOR'S REPORT NUMBER(S)
DACW-70-73-C-0037	UILU-ENG-72-20
b. PROJECT NO.	
c.	9b. OTHER REPORT NO(S) *(Any other numbers that may be assigned this report)*
d.	Structural Research Series No. 390

10. DISTRIBUTION STATEMENT

Distribution of this document is unlimited

11. SUPPLEMENTARY NOTES	12. SPONSORING MILITARY ACTIVITY
	U. S. Army Corps of Engineers Engineering Division, Civil Works

13. ABSTRACT

The construction and testing of three closed three span reinforced concrete frames representing slices of reinforced concrete conduits designed for loads up to 30,000 psf are described, as are the results of the tests.

The tests are the first known tests of complete frames made of deep reinforced concrete members, and the results of the tests indicate that the shear strength of such members may be much less than of simply supported members having similar geometry and loading conditions. Additional work is required in order to develop suitable design criteria for such structures.

The development of analytical techniques, using the finite element method, to predict the behavior of the structures is described. The analysis includes the effects of cracking, nonlinear stress-strain characteristics of the concrete, and yielding of the reinforcement. The results of an elastic analysis of one of the model structures is presented in the report, and there is good agreement between the predicted and initial measured slopes of various load-strain curves.

Recommendations about the parameters to be studied in the remainder of the program are made. Emphasis should be placed on determination of the effects of concrete strength and of reinforcement ratio first, with further investigations of the span-depth ratio effects secondary.

14. KEY WORDS	LINK A		LINK B		LINK C	
	ROLE	WT	ROLE	WT	ROLE	WT
Reinforced Concrete, Deep Beams, Conduits, Culverts, Shear Strength, Compression, Analysis, Finite Element, Cracking, Yielding, Nonlinear Analysis, Earth Pressures, Earth Dams						